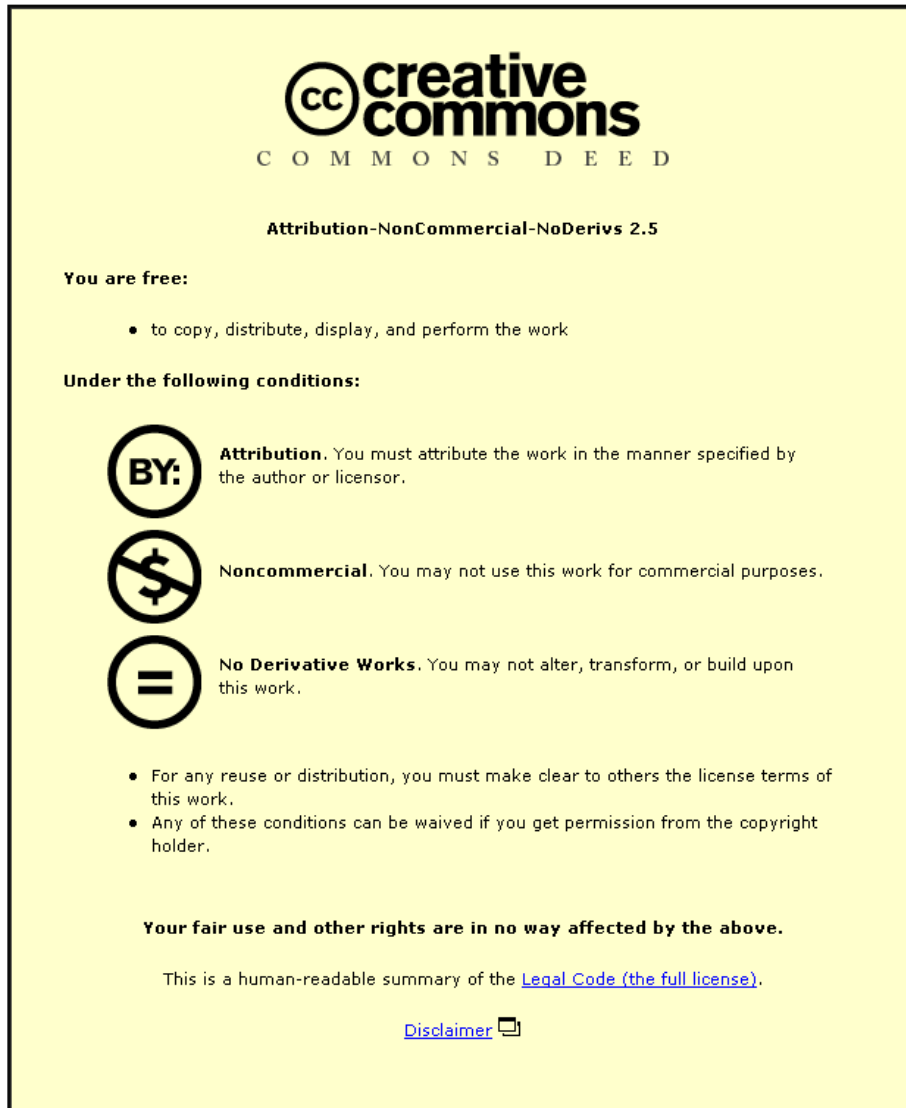


This item was submitted to Loughborough's Institutional Repository (<https://dspace.lboro.ac.uk/>) by the author and is made available under the following Creative Commons Licence conditions.



CC creative commons
COMMONS DEED

Attribution-NonCommercial-NoDerivs 2.5

You are free:

- to copy, distribute, display, and perform the work

Under the following conditions:

BY: **Attribution.** You must attribute the work in the manner specified by the author or licensor.

Noncommercial. You may not use this work for commercial purposes.

No Derivative Works. You may not alter, transform, or build upon this work.

- For any reuse or distribution, you must make clear to others the license terms of this work.
- Any of these conditions can be waived if you get permission from the copyright holder.

Your fair use and other rights are in no way affected by the above.

This is a human-readable summary of the [Legal Code \(the full license\)](#).

[Disclaimer](#) 

For the full text of this licence, please go to:
<http://creativecommons.org/licenses/by-nc-nd/2.5/>

Thesis access form

**Manganese Complexes with Biomimetic
Antioxidant Activity**

Manganese Complexes with Biomimetic Antioxidant Activity

By

Leanne James

Doctoral Thesis

Submitted in partial fulfillment of the requirements for the award of
Ph.D. of Loughborough University

Department of chemistry
Loughborough University
Loughborough
Leicestershire
LE11 3TU

© Leanne James 2010

III

Abstract

Several seven-coordinate manganese complexes have been synthesised, characterised and tested for both superoxide dismutase and catalase activity. Macrocyclic ring contractions have led to a series of new seven coordinate mononuclear manganese(II) macrocycles that have potential for their use as working superoxide dismutase mimics.

Numerous polynuclear seven coordinate manganese(II) macrocycles have been synthesised *via* Schiff base condensation. Subsequent reduction of the imine bonds has led to a variety of reduced amine analogues with varying axial ligands. The geometry has been compared about the manganese centres where possible. From the results of each complex tested for superoxide dismutase activity, the μ -chloro bridged tetranuclear complex $[\text{Mn}_2(\text{C}_{24}\text{H}_{29}\text{N}_6\text{O}_2)(\text{Cl})_2]_2(\text{ClO}_4)_2$ has proved to be the most efficient mimic with a calculated K_{MCCF} value of $7.7 \times 10^6 \text{ [M}^{-1} \text{ s}^{-1}]$.

A method for measuring catalase activity has been developed, and the most efficient catalase active compound was found to be $[\text{Mn}_5(\text{C}_{24}\text{H}_{29}\text{N}_6\text{O}_2)_2(\text{OAc})_2(\text{ClO}_4)_2](\text{ClO}_4)_2$ with one molecule of complex breaking down approximately 59000 molecules of hydrogen peroxide after one minute. Catalase testing showed that a reduction of the imine bonds produced an increase in activity overall for the complexes of H₂L1 ($\text{C}_{24}\text{H}_{29}\text{N}_6\text{O}_2$), but a decrease was observed for the reduced tripod complexes. An increase in the number of manganese centres resulted in a rise in catalase activity.

Many of the complexes tested for catalase activity showed an induction period prior to the activity being observed. This may suggest that the complexes undergo a change in structure, or that there is a rearrangement occurring before catalase activity may be observed. The results that are presented indicate that the axial ligands have an effect on the rate of catalase activity and the observed induction period.

Of the molecules that were tested for both superoxide dismutase and catalase activity, the pentanuclear complex $[\text{Mn}_5(\text{C}_{24}\text{H}_{29}\text{N}_6\text{O}_2)_2(\text{OAc})_2(\text{ClO}_4)_2](\text{ClO}_4)_2$

showed high activity for both analyses. This may be due to the extra manganese centre within the complex and the axial ligands that are present when compared with other tetranuclear complexes. The complex $[\text{Mn}_5(\text{HL1})(\text{OAc})_2(\text{ClO}_4)_2](\text{ClO}_4)_2$ may prove to be a good candidate for a working superoxide dismutase mimic.

Ring contracted complexes show high rates of superoxide dismutase activity but possess limited catalase activity.

Attempts have been made to produce a direct method of measuring superoxide dismutase activity using a stop-flow technique to complement the results using the indirect NBT (Nitro blue Tetrazoleum) method. This was carried out by analysing low concentration solutions of both complex and superoxide on a millisecond timescale. Progress has been made for this method with preliminary results being obtained.

Acknowledgements

I would like to thank my supervisor, Professor Vickie McKee for her support throughout this research project, providing many of the ideas along the way and encouragement throughout, particularly during the completion of this final thesis.

Thank you to Dr. Andrew Kellet and Professor Michael Devereux for allowing me to visit their laboratory at the Dublin Institute of Technology and providing the testing of complexes for superoxide dismutase activity, using the NBT assay.

Thank you to Soraya Sanchez-Ballester and Rebecca Dennet who synthesised several of the mononuclear compounds during their projects, and Sam Beckett for the initial set up of the catalase equipment.

Thank you to Mrs Pauline King who has provided support, advice and training throughout my research and has provided the elemental analysis for all of the samples. I would also like to thank all of the other researchers from the inorganic section, that is: – Raf, Anna, Muhammet, Chris, Simon, Tom, Lee, Jenna, Neil, Rachel, Joe, Andy B, Bansi, Noelia, Andy L, Gav, Stanny, Jo and Chris, Dr. Kelly, Dr. Smith, Dr. Dann, Dr. Kirk, Dr. Elsegood and our computer technician Stuart. We've had some fantastic curry nights and laughs along the way. Naga chilli's, schmoo and gallons of raspberry sambuca will remain a fond memory for years to come.

A huge thank you to Rob's family the Kings, who allow me visit them in sunny California every year.

I would like to give the biggest thanks to my family, firstly my brother and sister in law Chris and Liz, who have recently had their first very lucky child Isabella. To my Mom and dad who have always been a huge support throughout my degree and Ph.D. providing both valuable advice when I wasn't sure what to do next and providing the financial support when it was needed. I hope to repay you somehow.

Finally, a massive thankyou to Rob. I can't thank you enough for all your support and encouragement throughout all the ups and downs of working in the lab, despite having your own research which has come so far! We're all very proud of what you have achieved.

Abbreviations

DAP	2,6-Diacetylpyridine
DFP	2,6-Diformylpyridine
MeOH	Methanol
EtOH	Ethanol
Tren	Tris-(2-aminoethyl)-amine
SOD	Superoxide dismutase
NBT	Nitro blue tetrazoleum
IR	Infrared spectroscopy
cm	Centimetres
ν	Stretching mode (IR)
NMR	Nuclear magnetic resonance
δ	Chemical shift (NMR)
FAB	Fast Atom Bombardment
MS	Mass spectrometry
A	Absorbance
λ	Wavelength
s	Seconds
IC ₅₀	Half maximal inhibitory concentration
K _{cat}	Catalytic rate constant
K ^{obs}	Observed rate constant
CSD	Cambridge Structural Database
UV	Ultraviolet
Mins	Minutes
h	Hours
DMF	Dimethylformamide
DMSO	Dimethylsulfoxide
BAEP	3-Aminopropylbis(2-aminoethyl)amine
ABAP	2-Aminoethylbis(3-aminopropyl)amine
HPLC	High Performance Liquid Chromatography
His	Histidine
Asp	Aspartic acid
EDTA	Ethylenediamine tetraacetic acid

Table of Contents

Title Page	II
Abstract	IV
Acknowledgements	VI
Abbreviations	VIII
Table of Contents	IX
Table of Figures.....	XIII
1 Chapter One - Introduction	1
1.1 Macrocyclic chemistry	2
1.1.1 Schiff base reactions	5
1.1.2 Template synthesis	6
1.1.3 Macrocyclic ring contraction.....	12
1.2 Tripodal ligands	15
1.3 Superoxide dismutase activity	19
1.3.1 Methods of measurement.....	28
1.4 Catalase Activity.....	29
2 Chapter Two - Synthesis and Structure	36
2.1 Organic preparations	37
2.1.1 2,6-Diacetylpyridine.....	37
2.1.2 2,6-Diformylpyridine	38
2.2 Polynuclear complexes.....	39
2.2.1 [Ba(H ₂ L3)(ClO ₄) ₂](ClO ₄) ₂	41
2.2.2 [Ba(L5)(ClO ₄) ₂ (OH ₂)].(OH ₂)	44
2.2.3 [Mn ₂ (HL1)(Cl) ₂] ₂ (ClO ₄) ₂ .2DMF.....	48
2.2.4 [Mn ₂ (HL1)(N ₃) ₂] ₂ (ClO ₄) ₂ .2DMF	54
2.2.5 [Mn ₅ (L1) ₂ (OAc) ₂ (DMF) ₂](ClO ₄) ₄ .4DMF.....	59
2.2.6 [Mn ₂ (RedHL1)(Cl) ₂] ₂ [MnCl ₄].4DMF.EtOH	64
2.2.7 Complexes of H ₄ L2	69
2.3 Macrocyclic ring contractions	72
2.3.1 [Mn(H ₂ L4)(NCS) ₂].MeOH.DMF	74
2.4 Dinuclear complexes	78
2.4.1 [Mn ₂ (L6)(NCS) ₄].2DMF	78

2.4.2	[Pb ₂ (L8)(NCS) ₄]	82
2.5	[1+1] Mononuclear complexes	84
2.5.1	[Mn(L9)(OH ₂) ₂](ClO ₄) ₂	84
2.5.2	[Mn(L9)(Cl) ₂]	87
2.5.3	[Mn(L10)(OH ₂) ₂](ClO ₄) ₂	90
2.5.4	[Mn(RedL10)(OH ₂) ₂](Cl) ₂	93
2.5.5	[Mn(L10)(NCS) ₂].DMF	96
2.5.6	[Mn(L11)(Cl) ₂]	98
2.5.7	[Mn(L12)(OH ₂)(Cl)]ClO ₄	101
2.5.8	[Mn(L12)(OH ₂) ₂](ClO ₄) ₂	104
2.5.9	[Mn(L13)(OH ₂) ₂](ClO ₄) ₂	107
2.5.10	[Mn(L15)(Cl) ₂].MeOH	110
2.6	Tripodal ligands	112
3	Chapter Three – Biological testing	115
3.1	Electrochemistry	116
3.2	Superoxide dismutase activity	119
3.2.1	Indirect analysis	119
3.2.2	Experimental	122
3.2.3	Results	126
3.2.4	Direct analysis – Stopped-flow technique 1	132
3.2.5	Results	134
3.2.6	Direct analysis – Stopped-flow technique 2	139
3.2.7	Results	141
3.3	Catalase Activity	147
3.3.1	Results	148
	Expansion of Research	172
	Conclusions	175
4	Chapter Four - Experimental	179
4.1	General experimental conditions	180
4.2	Polynuclear complexes	180
4.2.1	2,6-Diacetylpyridine	180
4.2.2	[Ba(H ₂ L1)(H ₂ O) ₂](ClO ₄) ₂	182
4.2.3	[Mn ₂ (HL1)(Cl) ₂] ₂ (ClO ₄) ₂ .H ₂ O	183

4.2.4	[Mn ₂ (HL1)(N ₃) ₂] ₂ (ClO ₄) ₂ .H ₂ O.MeOH	184
4.2.5	[Mn ₄ (HL1)(L1)(NCS) ₄]NCS.H ₂ O.....	185
4.2.6	[Mn ₂ (HL1)(OAc)(ClO ₄) ₂] ₂ .2H ₂ O	186
4.2.7	[Mn ₅ (HL1) ₂ (OAc) ₂ (ClO ₄) ₂](ClO ₄) ₂ .2MeOH.....	187
4.2.8	[Mn ₂ (RedHL1)(Cl) ₂] ₂ [MnCl] ₄ .2H ₂ O	188
4.2.9	[Mn ₂ (RedHL1)(N ₃) ₂] ₂ (ClO ₄) ₂ .2H ₂ O	189
4.2.10	[Mn ₄ (L2)(ClO ₄) ₄](ClO ₄) ₂ .2EtOH	190
4.2.11	[Mn ₄ (L2)(NCS) ₂](ClO ₄) ₂	191
4.3	Ring contracted macrocycles	192
4.3.1	MnO ₂	192
4.3.2	2,6-Diformylpyridine	192
4.3.3	[Ba(H ₂ L3)(ClO ₄) ₂](ClO ₄) ₂	193
4.3.4	[Mn(L4)(NCS) ₂].MeOH	194
4.3.5	[Mn(L4)(Cl) ₂].MeOH.2H ₂ O	195
4.3.6	[Mn(L4)(N ₃) ₂].MeOH	196
4.3.7	[Mn(L4)(NCS) ₂].EtOH	197
4.3.8	[Ba(L5)(ClO ₄) ₂ (OH ₂) ₂]	198
4.3.9	[Mn(L5)(NCS) ₂].MeOH.H ₂ O	199
4.4	Dinuclear complexes	200
4.4.1	[Ba(L6)(ClO ₄) ₂].....	200
4.4.2	[Mn ₂ (L6)(NCS) ₄].MeOH	201
4.4.3	[Ba(L7)(ClO ₄) ₂].H ₂ O	202
4.4.4	[Pb ₂ (L8)(NCS) ₄].....	203
4.5	Mononuclear complexes	204
4.5.1	[Mn(L9)(Cl) ₂].H ₂ O.....	204
4.5.2	[Mn(L9)(OH ₂) ₂](ClO ₄) ₂ .MeOH.....	205
4.5.3	[Mn(L9)(NCS) ₂].....	206
4.5.4	[Mn(L10)(Cl) ₂].3H ₂ O.....	207
4.5.5	[Mn(L10)(OH ₂) ₂](ClO ₄) ₂	208
4.5.6	[Mn(RedL10)(OH ₂) ₂](Cl) ₂	209
4.5.7	[Mn(L10)(NCS) ₂].H ₂ O	209
4.5.8	[Mn(L11)(Cl) ₂].....	210
4.5.9	[Mn(L11)(OH ₂) ₂](ClO ₄) ₂ .H ₂ O.....	211

4.5.10	[Mn(L11)(NCS) ₂].2H ₂ O	212
4.5.11	[Mn(L12)(OH ₂)(Cl)](ClO ₄)	213
4.5.12	[Mn(L12)(OH ₂) ₂](ClO ₄) ₂	214
4.5.13	[Mn(L12)(Cl) ₂].H ₂ O	215
4.5.14	[Mn(L13)(OH ₂) ₂](ClO ₄) ₂ .2H ₂ O	215
4.5.15	[Mn(L13)(Cl) ₂]	216
4.5.16	[Mn(L13)(NCS) ₂].MeOH.H ₂ O	217
4.5.17	[Mn(L14)(NCS) ₂]	218
4.5.18	[Mn(L15)(Cl) ₂].MeOH.H ₂ O	219
4.5.19	[Mn(L16)(OH ₂) ₂](ClO ₄) ₂	220
4.6	Tripodal ligands	220
4.6.1	Saltren	221
4.6.2	[Mn(Saltren)](Cl) ₂ .2H ₂ O	222
4.6.3	[Mn ₄ (O) ₂ (Saltren) ₂](MnCl ₄) ₂	223
4.6.4	Reduced saltren	223
4.6.5	[Mn(RedSaltren)](Cl) ₂ .2H ₂ O	224
4.6.6	[Mn ₄ (O) ₂ (RedSaltren) ₂](MnCl ₄) ₂ .H ₂ O	225
4.6.7	N-(2-bromoethyl)phthalimide	226
4.6.8	2,2'-Diphthalimidoethylamine	226
4.6.9	2,2',3-Triphthalimidoethylpropylamine	227
4.6.10	- BAEP.6HCl	228
4.6.11	- BAEP-Sal.6H ₂ O	229
4.6.12	- [Mn(RedBAEP-Sal)](Cl) ₂ .4H ₂ O	229
4.6.13	- 3,3',2-Triphthalimidopropylethylamine	230
4.6.14	- ABAP.4HCl.H ₂ O	231
4.6.15	- [Mn(ABAP-Sal)]ClO ₄ .3H ₂ O	231
4.6.16	- [Mn ₄ (O) ₂ (ABAP-Sal)][MnCl ₄] ₂	232
	Single Crystal X-ray Data Tables.	234
	List of Publications and Poster Presentations.	255
	References.....	257

Table of Figures

Figure 1-1 – Ba^{2+} macrocyclic complex	2
Figure 1-2 – Macrocyclic complex with imposed geometry	3
Figure 1-3 – An example of a soft metal ion bound to soft donor ligands within a macrocyclic system.....	5
Figure 1-4 – Schiff base reaction	6
Figure 1-5 – Template reaction	7
Figure 1-6 – [2+2] macrocycle	8
Figure 1-7 – Routes for template reactions of Schiff base macrocycles	9
Figure 1-8 – Schematic illustration for a transamination reaction	10
Figure 1-9 – Transamination reaction for ring closure	11
Figure 1-10 – Excess barium during macrocyclic preparation	12
Figure 1-11 – Ring contraction mechanism	13
Figure 1-12 – Macrocyclic ring contraction	13
Figure 1-13 – Two separate attempts of a cyclocondensation reaction	14
Figure 1-14 – General structure of a tripodal ligand	15
Figure 1-15 – The structure of tren	16
Figure 1-16 – Hypodentate Cu(II) Complex	17
Figure 1-17 – Structure of the saltren ligand	17
Figure 1-18 – Products of reactions involving different ratios of manganese to saltren ligand.....	18
Figure 1-19 – Molecular orbital diagram of O_2	19
Figure 1-20 – Active site structure of human MnSOD.....	21
Figure 1-21 – Redox cycling in human MnSOD.....	22
Figure 1-22 – Mechanism for MnSOD as outlined by Bull et al.	22
Figure 1-23 - Generic structure of $[Mn([15]aneN_5)Cl_2]$	23
Figure 1-24 - Structure of M40403	24
Figure 1-25 – Proposed catalytic cycle of a SOD mimic	25
Figure 1-26 - Complexes analysed by Maroz et al.....	26
Figure 1-27 - Proposed catalytic cycle	26
Figure 1-28 - Hdapsox ligand complex.....	27
Figure 1-29 – Catalase active site of the <i>lactobacillus plantarum</i>	30

Figure 1-30 – Possible mechanism for catalase activity	31
Figure 1-31 – Dinuclear manganese catalase mimic.....	32
Figure 1-32 – Proposed mechanism for catalase activity of a dinuclear Manganese complex.....	33
Figure 1-33 – Structure of a manganese salen complex.....	34
Figure 1-34 – Ping pong mechanism for manganese salen complexes	34
Figure 2-1 – [2+2] macrocycles H_2L1 , $RedH_2L1$ and H_2L3	39
Figure 2-2 – Dimeric $[Ba(H_2L1)(H_2O)_2]^{4+}$ cation with perchlorate anions and hydrogens omitted for clarity.	40
Figure 2-3- Structure of $[Ba(H_2L3)(ClO_4)]_2^{2+}$ with perchlorate anions, and hydrogens omitted for clarity. Dashed lines represent hydrogen bonding.	41
Figure 2-4– Hydrogen bonding for $[Ba(H_2L3)(ClO_4)]_2 \cdot (ClO_4)$	43
Figure 2-5 - Structure of $[Ba(L5)(ClO_4)_2(H_2O)] \cdot H_2O$. with hydrogens omitted for clarity. Dashed lines represent hydrogen bonding.	44
Figure 2-6 – Packing diagram for $[Ba(L5)(ClO_4)_2(H_2O)] \cdot H_2O$ shown perpendicular to the <i>a</i> axis.	46
Figure 2-7 – Borohydride reduction	46
Figure 2-8 – Structure of $[Mn_2(HL1)(Cl)_2]^{2+}$ with perchlorate anions, hydrogens and solvent molecules omitted for clarity. Dashed lines represent hydrogen bonds.	49
Figure 2-9 – π - π stacking for $[Mn_2(HL1)(Cl)_2]_2(ClO_4)_2$	52
Figure 2-10 – Packing diagram for $[Mn_2(HL1)(Cl)_2]_2(ClO_4)_2$ as viewed down the <i>c</i> axis.	53
Figure 2-11 –Structure of $[Mn_2(HL1)(N_3)_2]^{2+}$ with perchlorate anions hydrogens and solvate DMF molecules omitted for clarity. Dashed lines represent hydrogen bonding.	54
Figure 2-12 – π - π stacking of $[Mn_2(HL1)(N_3)_2]^{2+}$	57
Figure 2-13 – Packing diagram for $[Mn_2(HL_2)(N_3)_2]_2(ClO_4)_2 \cdot 2DMF$ as viewed down the <i>a</i> axis.	58
Figure 2-14 – Structure of $[Mn_5(L1)_2(OAc)_2(DMF)_2]^{2+}$ with perchlorate anions, hydrogens and DMF solvate molecules omitted for clarity.	59
Figure 2-15 – Different binding modes for carboxylate ligands.....	61
Figure 2-16 – π - π Stacking in $[Mn_5(L1)(OAc)_2(DMF)_2]^{2+}$	62

Figure 2-17 - Packing diagram for $[Mn_5(L1)(OAc)_2(DMF)_2](ClO_4)_4 \cdot 4DMF$ as viewed down the <i>a</i> axis.	63
Figure 2-18 - Structure of $[Mn_2(RedHL1)(Cl)_2]^{2+}$ with the $[MnCl_4]^{2-}$ anion, hydrogens and solvent molecules omitted for clarity. Dashed lines represent hydrogen bonding.....	64
Figure 2-19 - π - π stacking for $[Mn_2(RedHL1)(Cl)_2]^{2+}$	67
Figure 2-20 - Packing diagram for $[Mn_2(RedHL1)(Cl)_2][MnCl_4] \cdot 4DMF \cdot MeOH$...	68
Figure 2-21 - H_4L2 Ligand.....	69
Figure 2-22-Structure of $[Mn_4L2](ClO_4)_4$	70
Figure 2-23 - Possible route for the formation of a [4+4] complex of L2.....	71
Figure 2-24- Ligand H_2L3	72
Figure 2-25 - Ring contracted ligand H_2L4	73
Figure 2-26 -Structure of $[Mn(H_2L4)(NCS)_2] \cdot MeOH \cdot DMF$ with solvate molecule and hydrogens omitted for clarity. Dashed line represents hydrogen bonding	74
Figure 2-27 - Ring contraction mechanism	75
Figure 2-28 - π - π stacking for $[Mn(H_2L4)(NCS)_2] \cdot MeOH \cdot DMF$	77
Figure 2-29 -Structure of $[Mn_2(L6)(NCS)_4]$ with solvent molecules and hydrogens omitted for clarity.....	78
Figure 2-30 - π - π stacking for $[Mn_2(L6)(NCS)_4]$	80
Figure 2-31 - Packing diagram for $[Mn_2(L6)(NCS)_4]$ as viewed down the <i>a</i> axis.	81
Figure 2-32 -Structure of $[Pb_2(L8)(NCS)_4]$ with hydrogens omitted for clarity.	82
Figure 2-33 -Structure of $[Mn(L9)(OH_2)_2]^{2+}$ with perchlorate anions and hydrogens omitted for clarity.....	84
Figure 2-34 - Packing diagram for $[Mn(L9)(OH_2)_2](ClO_4)_2$ as viewed down the <i>b</i> axis.	86
Figure 2-35 -Structure of $[Mn(L9)(Cl)_2]$ with hydrogens omitted for clarity.	87
Figure 2-36 - Hydrogen bonding in $[Mn(L9)(Cl)_2]$	89
Figure 2-37 - Packing diagram for $[Mn(L9)(Cl)_2]$ as viewed down the <i>c</i> axis	89
Figure 2-38 -Structure for $[Mn(L10)(OH_2)_2]^{2+}$ with perchlorate anions and hydrogens omitted for clarity	90
Figure 2-39 - Packing diagram for $[Mn(L10)(OH_2)_2](ClO_4)_2$ as viewed down the <i>b</i> axis	92

Figure 2-40 – Structure of $[Mn(RedL10)(OH_2)_2]^{2+}$ with chloride anions omitted for clarity	93
Figure 2-41 – Hydrogen bonding for $[Mn(RedL10)(OH_2)_2]2Cl$	95
Figure 2-42 - π - π stacking for $[Mn(RedL10)(OH_2)_2]2Cl$	95
Figure 2-43 –Structure for $[Mn(L10)(NCS)_2].DMF$ with solvate molecule and hydrogens omitted for clarity	96
Figure 2-44 – π - π stacking for $[Mn(L10)(NCS)_2]$	98
Figure 2-45 –Structure for $[Mn(L11)(Cl)_2]$	98
Figure 2-46 – π - π stacking for $[Mn(L11)(Cl)_2]$	100
Figure 2-47 –Structure for $[Mn(L12)(OH_2)(Cl)]^+$ with perchlorate anion omitted for clarity	101
Figure 2-48 – Hydrogen bonding on adjacent molecules of $[Mn(L12)(OH_2)(Cl)](ClO_4)$	103
Figure 2-49 - π - π stacking for $[Mn(L12)(OH_2)(Cl)](ClO_4)$	103
Figure 2-50 –Structure of $[Mn(L12)(OH_2)_2]^{2+}$ with perchlorate anions omitted for clarity	104
Figure 2-51 – Packing diagram for $[Mn(L12)(OH_2)_2](ClO_4)_2$ as viewed down the <i>b</i> axis	106
Figure 2-52 - Structure of $[Mn(L13)(OH_2)_2]^{2+}$ with perchlorate anions and hydrogens omitted for clarity	107
Figure 2-53 – Packing diagram for $[Mn(L13)(OH_2)_2](ClO_4)_2$ as viewed down the <i>a</i> axis	109
Figure 2-54 –Structure for $[Mn(L15)(Cl)_2].MeOH$	110
Figure 2-55 – π - π stacking for $[Mn(L15)(Cl)_2].MeOH$	112
Figure 3-1 – Cyclic voltammogram of ferrocene standard	117
Figure 3-2 – Cyclic voltammetry of seven-coordinate manganese complexes.....	118
Figure 3-3 – Reaction of NBT to blue formazan	120
Figure 3-4 – Schematic representation of the NBT indirect assay method	121
Figure 3-5 – Graph showing SOD activity of $[Mn_2(HL1)(Cl)_2]_2(ClO_4)_2$	123
Figure 3-6 – Calibration graph for NBT assay	124
Figure 3-7 - Graph of inhibition (%) versus concentration for complex $[Mn_2(HL1)(Cl)_2]_2(ClO_4)_2$	125
Figure 3-8 – Schematic representation of stopped-flow equipment.....	133

Figure 3-9 – Absorbance spectrum for a superoxide solution	135
Figure 3-10 – Absorbance spectrum of $[Mn_2(RedHL1)(Cl)_2]_2[MnCl_4]$ overlaid with superoxide.....	136
Figure 3-11 – Kinetic trace for stopped-flow analysis of superoxide and $1 \times 10^{-7} M$ $[Mn_2(RedHL2)(Cl)_2]_2[MnCl_4]$	137
Figure 3-12 – Overlay of superoxide with $[Mn(L10)(H_2O)_2](ClO_4)_2$	138
Figure 3-13 – Kinetic trace for stopped-flow analysis of superoxide and $1 \times 10^{-7} M$ $[Mn(L10)(H_2O)_2](ClO_4)_2$	138
Figure 3-14 – Stop-flow set up	139
Figure 3-15 – Pure DMSO.....	141
Figure 3-16 - Reaction of superoxide solution with $1 \times 10^{-4} M$ $[Mn_2(RedHL2)(Cl)_2]_2[MnCl_4]$	142
Figure 3-17 - Reaction of superoxide solution with $1 \times 10^{-5} M$ $[Mn_2(RedHL2)(Cl)_2]_2[MnCl_4]$	142
Figure 3-18 - Reaction of superoxide solution with $1 \times 10^{-6} M$ $[Mn_2(RedHL2)(Cl)_2]_2[MnCl_4]$	143
Figure 3-19 - Reaction of superoxide solution with $1 \times 10^{-7} M$ $[Mn_2(RedHL2)(Cl)_2]_2[MnCl_4]$	143
Figure 3-20 – Reaction of superoxide solution with $1 \times 10^{-4} M$ $[Mn(L10)(H_2O)_2](ClO_4)_2$	144
Figure 3-21 – Reaction of superoxide solution with $1 \times 10^{-5} M$ $[Mn(L10)(H_2O)_2](ClO_4)_2$	145
Figure 3-22 – Reaction of superoxide solution with $1 \times 10^{-6} M$ $[Mn(L10)(H_2O)_2](ClO_4)_2$	145
Figure 3-23 - Reaction of superoxide solution with $1 \times 10^{-7} M$ $[Mn(L10)(H_2O)_2](ClO_4)_2$	146
Figure 3-24 – Equipment used for measuring catalase activity.....	147
Figure 3-25 – Catalase activity of polynuclear complexes of H_2L1 and $RedH_2L1$..	150
Figure 3-26 – Induction periods for catalase activity of $L1$ complexes.....	153
Figure 3-27 - Catalase activity for polynuclear complexes of H_4L2	154
Figure 3-28 – Catalase activity for $[Mn_5(HL1)_2(OAc)_2](ClO_4)_2$ without the addition of base	156
Figure 3-29 – Catalase activity for ring contracted species	158

Figure 3-30 – <i>Catalase activity for dinuclear complex $[Mn_2(L6)(NCS)_4]$</i>	160
Figure 3-31 – <i>Catalase activity for mononuclear complexes with a diacetylpyridine head unit</i>	161
Figure 3-32 – <i>Catalase activity for mononuclear complexes with a diformylpyridine head unit</i>	162
Figure 3-33 - <i>Delay observed for catalase activity of mononuclear complexes with a diacetyl pyridine head unit</i>	166
Figure 3-34 - <i>Delay observed for catalase activity of mononuclear complexes with a diformyl pyridine head unit</i>	166
Figure 3-35 – <i>Catalase activity of tripodal complexes</i>	168
Figure 3-36 – <i>Delay for catalase activity observed for the tripodal complexes</i>	171

1 Chapter One - Introduction

1.1 Macrocyclic chemistry

A macrocycle is a cyclic organic compound; and a macrocyclic ligand must have at least nine atoms in the ring and a minimum of three potential donor atoms that can coordinate to a metal ion. The introduction of varying donor atoms and aromatic rings within a macrocyclic system can potentially provide control over some aspects of geometry and donors. An example of a macrocyclic complex is shown below in Figure 1-1 as reported by Harding *et al.*¹

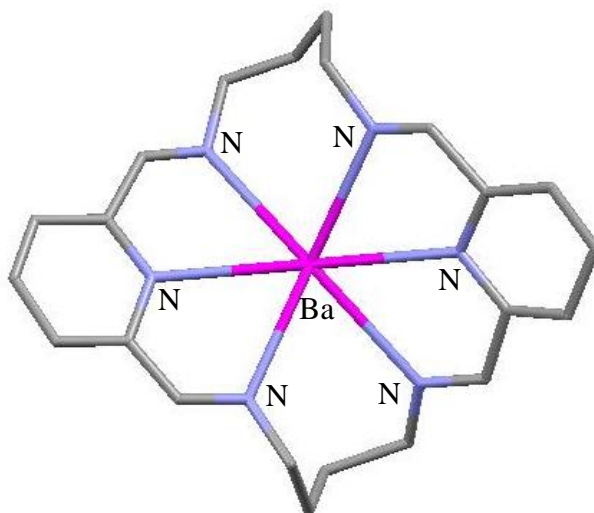


Figure 1-1 – Ba^{2+} macrocyclic complex

The denticity of the ligand is the number of atoms through which a ligand coordinates to a metal. Polydentate ligands can impose an unlimited range of three dimensional geometric constraints and properties upon the metal ion. A macrocycle can be designed to impose a certain stereochemistry and potentially give tighter control over some aspects of geometry around a metal centre and the donors within the system can be altered according to the metal it is desired to bind into the macrocyclic system. A macrocyclic ligand that imposes pentagonal geometry onto the metal centre is shown in Figure 1-2.² In this system, the pyridinediimine head unit has a bite angle of 70.2° (N1-Mn-N2), imposed onto the metal ion creating a slight distortion from the ideal geometry of 72° which would be expected for a pentagonal bipyramidal geometry.

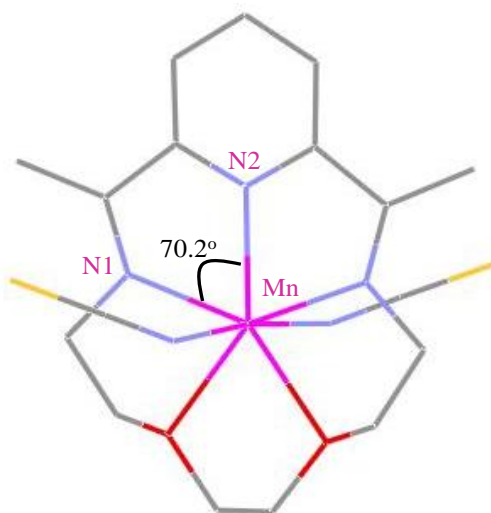


Figure 1-2 – *Macrocyclic complex with imposed geometry*

Macrocyclic complexes are more stable than complexes of non-cyclic ligands, and this is due to both kinetic and thermodynamic stability effects. The kinetic and thermodynamic effects together, are referred to as the ‘Macrocyclic effect’.³⁻⁵

Macrocyclic complexes are more kinetically inert than non-macrocyclic ligands because there are no terminal donors and therefore they do not dissociate readily. It is not possible to break a single M-L bond and move the donor away, there has to be additional bond breakage or extensive rearrangement of the coordination sphere, therefore higher activation energy is needed to dissociate the ligand from the metal ion than for an open chain analogue.

For the thermodynamic component, both entropy and enthalpy are involved:⁴

$$\Delta G = \Delta H - T\Delta S$$

Due to entropy effects, as the denticity of the ligand increases, so does the stability constant of the complex formed. The entropy factor (ΔS) is more favourable for macrocyclic ligands because there is less rearrangement of the molecule on coordination. The enthalpy factor (ΔH) however, can be either favourable or unfavourable.

A macrocyclic ligand is less solvated than that of a monodentate ligand, and so a macrocycle has less amine hydrogen bonded water molecules to be displaced upon the formation of a complex creating a negative effect in terms of entropy for a macrocyclic ligand. For a macrocyclic ligand, there is a limitation of internal rotation during complex formation and less hydrogen bonded solvent molecules to be displaced during the formation of the complex.^{5,6}

The most important factor for the stability constant of a macrocyclic complex is the relative size of the metal ion and the macrocyclic hole, and this is important when designing a macrocyclic host for a particular metal ion. A complex is most stable when the macrocyclic cavity is a good fit for the central ion. If the cavity is too small for the metal ion, then the ion may become displaced from the plane of the ring and if the ion is too small then the bonds that coordinate the metal to the ligand are longer and also weaker. By introducing variations into a macrocycle it is possible to selectively chelate certain metal ions depending upon the number, type and position of the donor atoms in the system.

In a coordination complex, the central metal ion acts as a Lewis acid and is coordinated to the donor atoms in the ligand that act as Lewis bases. According to the hard soft acid base theory, hard cations will form more stable complexes with hard ligands and soft cations will form more stable complexes with soft ligands.^{7, 8} Hard donor ligands will also favour the higher oxidation states of a metal ion and a softer donor will favour the lower oxidation states of a metal ion. An example of a complex that contains a soft silver ion which is bound to soft sulfur donor atoms is illustrated in Figure 1-3⁹

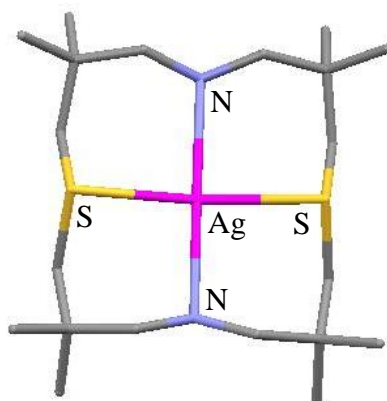


Figure 1-3 – *An example of a soft metal ion bound to soft donor ligands within a macrocyclic system*

The ligand illustrated in Figure 1-3 can be used for the synthesis of a silver complex but binding would not occur in the same fashion with a harder manganese 2^+ ion which does not bind to sulfur donor atoms. All of these factors need to be taken into account when designing a ligand for a particular metal ion.

The properties associated with macrocycles have stimulated much interest in their chemistry.^{4, 10} They have the ability to mimic some properties of proteins such as the transport of oxygen in mammalian and other respiratory systems. In nature, proteins can hold a metal centre in a transitional geometry that is critical for the chemical activity of the protein this is known as an entactic state. Similarly, a macrocyclic ligand may tune the properties of a metal ion (e.g. redox potential) by imposing a particular geometry.³

1.1.1 Schiff base reactions

Schiff base condensation has been of great importance in macrocyclic chemistry,^{11, 12} and has been used in the formation of many macrocyclic systems. This type of reaction involves the synthesis of an imine bond by reacting a carbonyl group with a primary amine, losing water in the process (Figure 1-4).¹³⁻¹⁵

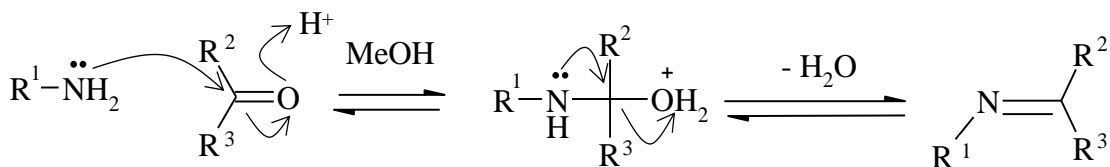


Figure 1-4 – Schiff base reaction

The size of the metal ion and the coordination properties of the counter ions are also important in the design of a Schiff base macrocycle.^{12, 16} An isolated imine bond as shown in Figure 1-4 is susceptible to hydrolysis, However, upon coordination to a metal ion, the stability of the bond is increased and less likely to undergo hydrolysis.

A Schiff base macrocycle can be altered by the reduction of the imine bonds to form amines, in this system the complex becomes less susceptible to hydrolysis. This process renders the nitrogen donors harder, again altering and influencing the binding properties of the macrocycle and the stability of a given complex.

1.1.2 Template synthesis

A basic problem in all macrocyclic synthesis is the formation of polymers rather than cyclic products. To avoid the polymerisation reaction, high dilution conditions are sometimes used, requiring large volumes of solvent to reduce the chances of the molecules reacting with each other. An alternative way to overcome the polymerisation reaction is to use a metal ion in a template reaction.

Schiff base condensation reactions are commonly used for macrocyclic template reactions. A template reaction is one where a metal ion directs the cyclisation of a ligand. During this *in situ* reaction, the metal ion coordinates to the donor atoms and organises the intermediates into the conformation that is required to give the desired cyclic product. The presence of a metal ion template preferentially leads to a cyclic product, whereas attempts at formation of a macrocyclic ligand without a metal template can lead to oligomeric oils or gums.¹⁷ The bite angle can change slightly depending on the size of the metal that is bound to the ligand. A larger metal ion would decrease the bite angle and a smaller ion would increase the bite angle.

Limitations may exist when designing a macrocyclic complex, as not all metal ions will fit into a specific macrocyclic cavity or the favoured geometry of the metal ion may be different to that imposed by the ligand.

During a template reaction, the metal ion can have two possible roles; firstly, the thermodynamic template effect is when the presence of the metal ion promotes the formation of the macrocycle as its metal complex and so the ion may shift the position of equilibrium between products and reactants for example. Secondly, the kinetic template effect is when the metal ion may direct the steric course of a condensation so that formation of the required cyclic product is facilitated.^{3, 15}

An example of such a reaction is where 2,6-diacetylpyridine (DAP), which contains a pyridyl nitrogen donor for the metal ion to bind, reacts with a diamine, in the presence of Mn(II), forming two imine bonds^{18, 19} as shown in Figure 1-5.

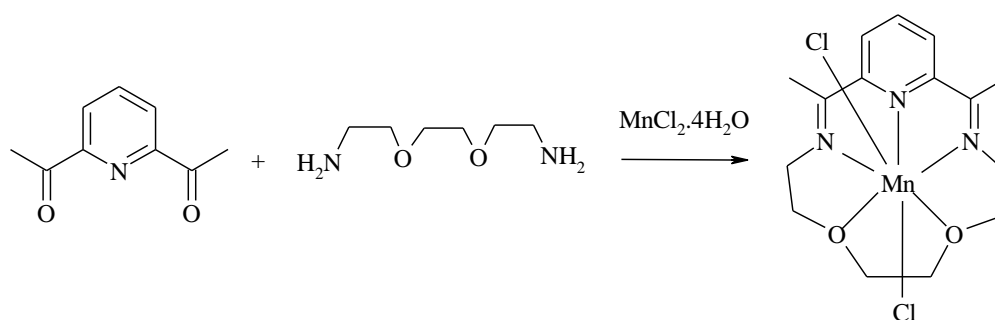


Figure 1-5 – *Template reaction*

Template reactions tend to be metal ion specific, therefore, certain desired metal complexes may not be directly accessible using the template synthesis, and this may be because the metal ion does not favour the desired geometry for the ligand to form.

A change in metal ion can have a profound effect on the nature of a templated product, this is because different metal ions may have preferences for different geometries, for example, a d⁸ ion such as Ni(II) has a stereochemical preference for a tetragonal geometry and will not form a seven coordinate compound, however a d⁵ ion such as Mn(II) has no stereochemical preferences and readily adopts the geometry imposed by the ligand. The kinetic template effect can be used to direct the

geometry of the product via organisation of the reacting components.²⁰ There are two factors that can contribute to the formation of a seven coordinate Mn(II) complex. Firstly, a pyridinediimine section with three planar nitrogen donors sits rigid with an arc of approximately 138°, this leaves ample room for two further donors in the same plane. Secondly, the length of the alkyl chain and the number of donors is important in defining the geometry of the complex.^{18, 21}

A possible route for introducing a target metal ion into a ligand system, would be to firstly form the macrocyclic ligand in the presence of a metal ion which allows formation of the macrocycle. This can then be followed with a transmetallation reaction in which one metal ion is displaced for a more strongly bound metal ion of interest and the geometry of the ligand may be imposed onto the new metal ion.

For a Schiff base template reaction, a macrocycle may form as a [1+1] macrocycle, which is the reaction of one dicarbonyl head unit with one molecule of diamine in the presence of a metal ion, (see Figure 1-1 and Figure 1-5) or as a [2+2] macrocycle which is the reaction of two dicarbonyl head units with two molecules of amine in the presence of a metal ion. A [1+1] macrocycle will form in the presence of a smaller ion and a [2+2] macrocycle will form in the presence of a large ion. For example an amine chain is not long enough to form as [1+1] macrocycle. An example of a [2+2] macrocycle can be seen in Figure 1-6²²

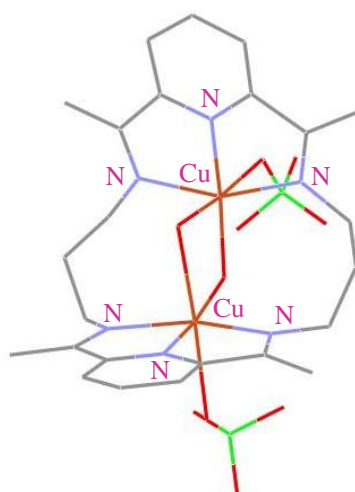


Figure 1-6 – [2+2] macrocycle

The general considerations of possible mechanisms for the routes of formation of both [1+1] and [2+2] Schiff base macrocycles were outlined by Nelson *et al.* as shown in Figure 1-7²³

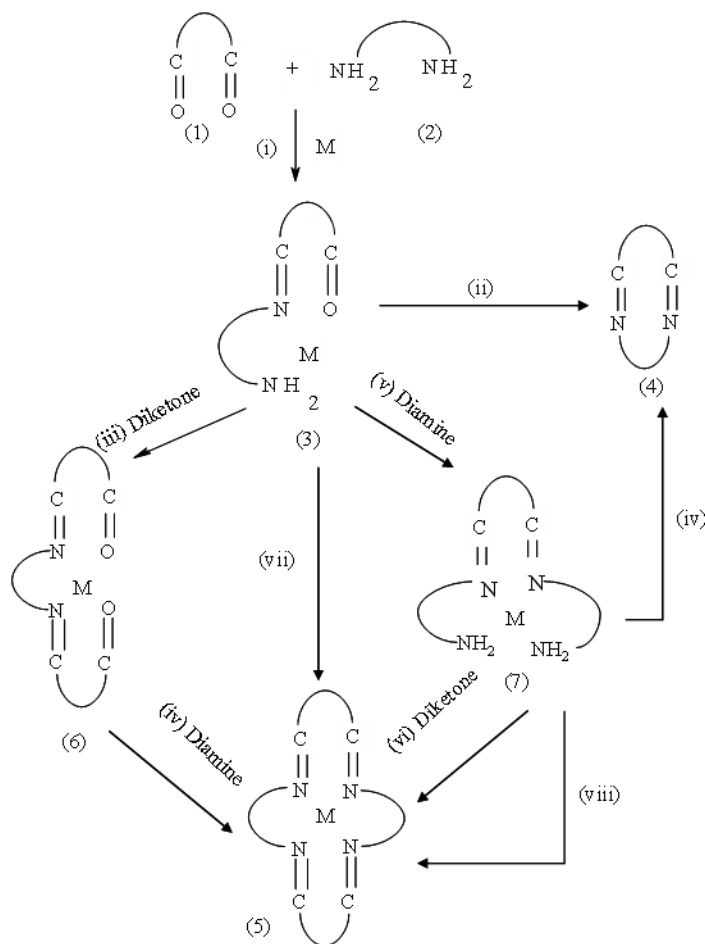


Figure 1-7 – Routes for template reactions of Schiff base macrocycles

The scheme shows that firstly, the intermediate (3) may undergo condensation with a dicarbonyl (1) to form the new species (6), this can then further react with a diamine (2) to give a [2+2] product (5). Secondly, a reverse sequence of condensation steps can occur to form the product via the diimino species (7) (v+vi). Thirdly, the intermediate (3) can undergo a bimolecular self condensation (step vii) to produce the product (5). The fourth route involves self condensation between two molecules of the diamine-diimine species (7) undergoing a transamination reaction. A transamination reaction involves the transfer of an amine group from one molecule to another via nucleophilic substitution of the primary amine, which can be used as a

route to form new imines.(step viii). A scheme for a transamination reaction can be seen in Figure 1-8.²³

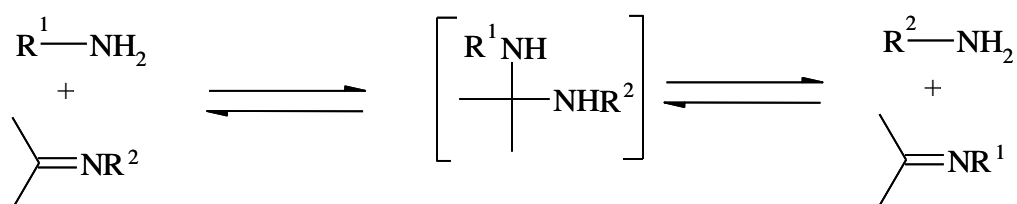


Figure 1-8 – Schematic illustration for a transamination reaction

The mechanism for a ring closure reaction of a macrocyclic complex was proposed to involve one intramolecular, and one intermolecular transamination²³ as illustrated in Figure 1-9.

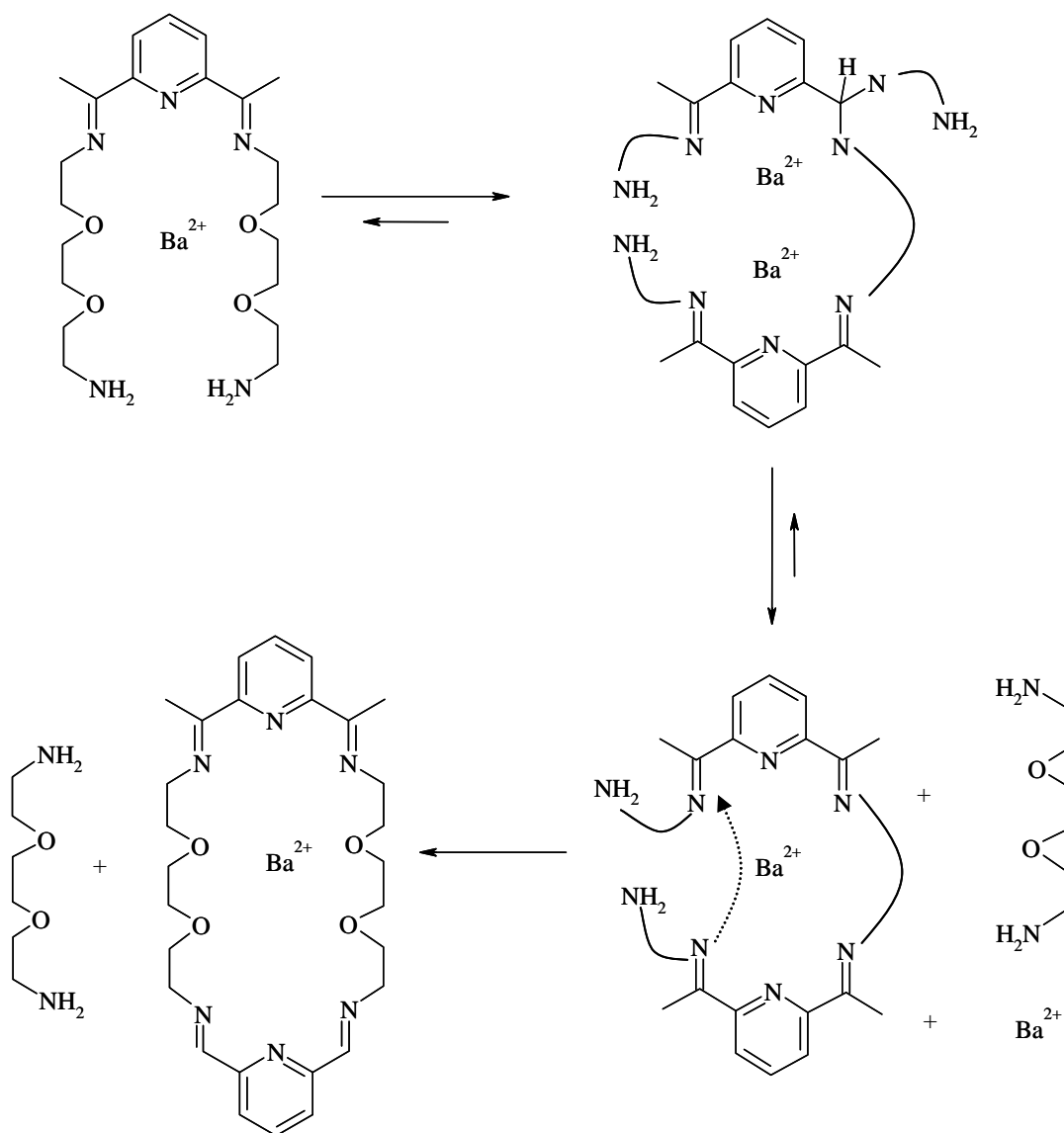


Figure 1-9 – Transamination reaction for ring closure

The mechanism for the reaction shown in Figure 1-9 involves a bimolecular reaction between two molecules of the initial complex. An intermolecular transamination reaction occurs *via* nucleophilic attack from one NH_2 group upon the imino carbon of the second molecule. The imine is then reformed with elimination of the amine. Next an intramolecular transamination reaction occurs from the uncoordinated NH_2 at the neighbouring imine group of the second molecule. Nelson *et al.*²³ observed that an excess of amine or Ba^{2+} suppressed the macrocycle formation. It is possible that an excess of amine provides free NH_2 groups which are available for nucleophilic attack of the imino-carbon groups of the initial molecule shown in Figure 1-9. The extra NH_2 groups that are available due to excess amine, can then introduce competition

for the self-condensation reaction of macrocyclic formation. In the presence of excess Ba^{2+} it is possible that an equilibrium can exist between the initial complex as shown in Figure 1-7, and a binuclear species as illustrated in Figure 1-10, where the primary amines become bound to the free Ba^{2+} and are then not available for nucleophilic attack.²³

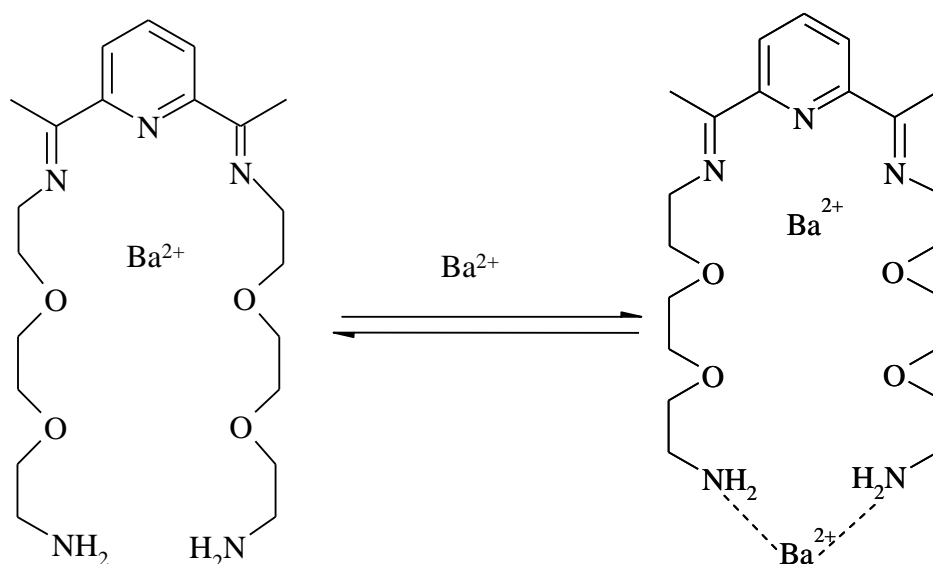


Figure 1-10 – *Excess barium during macrocyclic preparation*

1.1.3 Macrocyclic ring contraction

Macrocyclic ring contractions may occur when there is a functional group available such as $-\text{OH}$ or $=\text{NH}$ and if there is a mismatch in size for the metal and the cavity in which it sits.¹⁵ Several Schiff base macrocycles have been shown to undergo ring contractions as a result of nucleophilic addition of a secondary amine across an adjacent imine bond. An example can be seen in Figure 1-11²⁴⁻²⁷ in which the transamination reaction is observed.

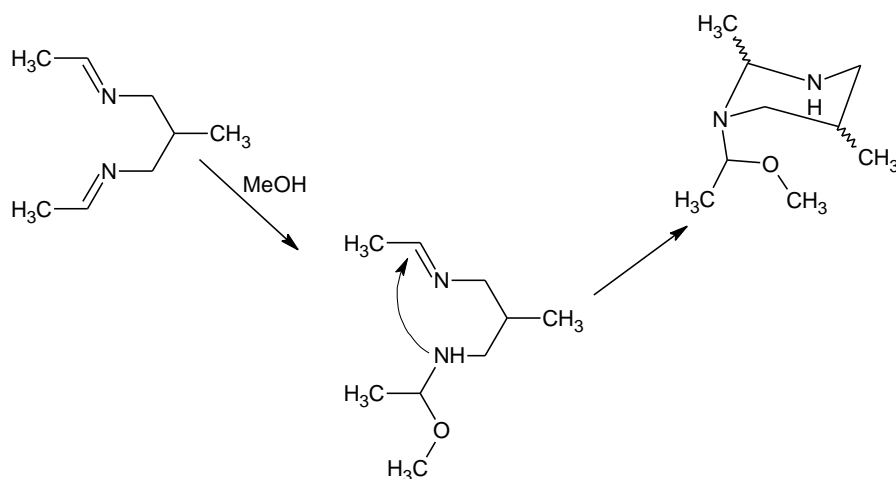


Figure 1-11 –Ring contraction mechanism

Nelson *et al.*²³ describe the formation of a ring contracted Ba^{2+} macrocycle as shown below in Figure 1-12.

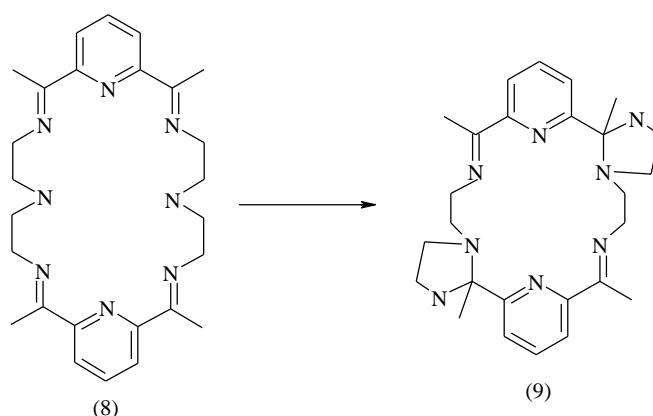


Figure 1-12 – Macrocyclic ring contraction

The macrocycle contains an 18 membered inner ring (9) rather than the expected 24 membered ring (8) reducing the denticity of the macrocycle from eight to six. The unexpected macrocycle formed due to the mismatch in cavity size of the macrocycle and the barium metal ion forming two five-membered imidazolidine rings as illustrated in Figure 1-12.²⁵

Fenton and co workers²⁸ showed that two separate attempts at a cyclocondensation reaction involving *N,N*-bis(2-aminoethyl)-2-phenylethylamine and 2,6-diformylpyridine in the presence of a barium ion yielded different products. These

were the expected 24 membered Schiff base macrocycle and a macrocycle with an unexpected ring contraction at one side arm producing an 18 membered macrocycle with an imidazolidine ring. The two products that were formed are illustrated in the reaction²⁸ shown in Figure 1-13.

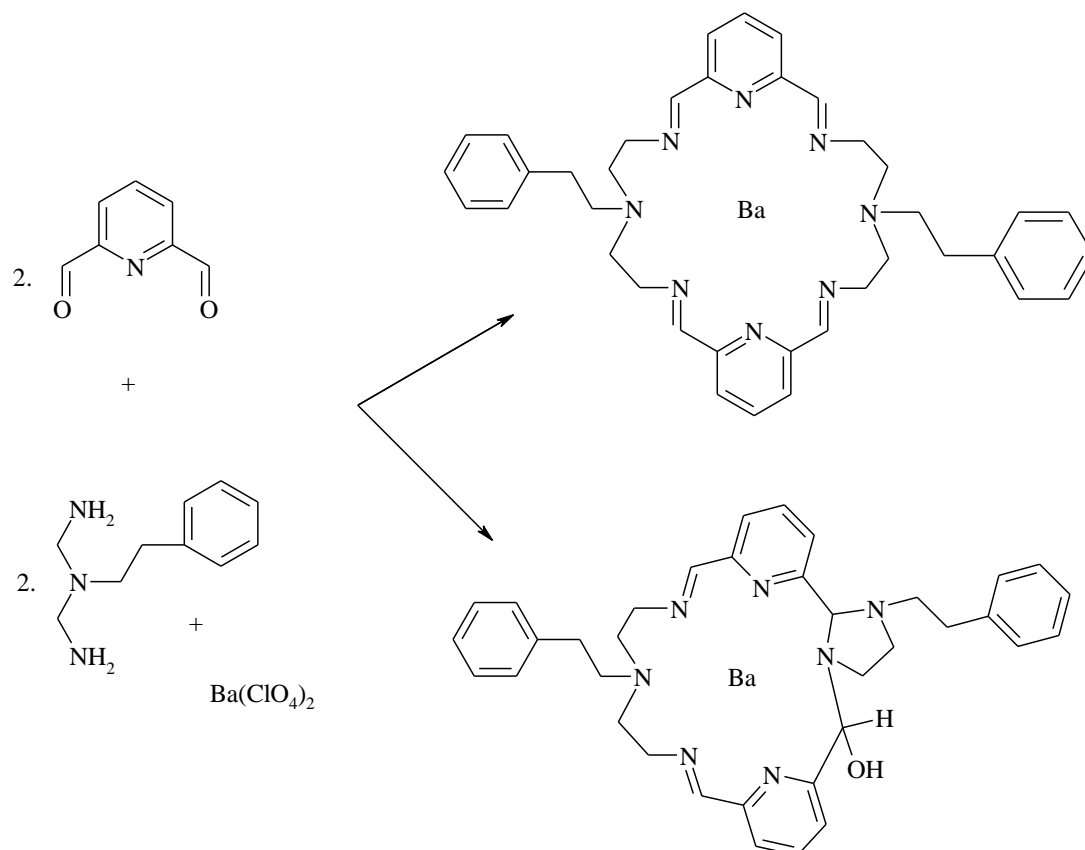


Figure 1-13 – Two separate attempts of a cyclocondensation reaction

The reaction scheme shown in Figure 1-13 shows that when the imidazolidine ring is formed as a result of the ring contraction, the number of donor atoms available to the barium ion is reduced from eight to six. The macrocyclic hole becomes reduced in size as a result of the ring contraction and there is an addition of a hydroxy group onto the ligand.

The non-contracted [2+2] tetraimine species would be the expected result for this type of reaction as shown by Nelson *et al*²³ and Fenton and co workers evidently found it difficult to reproduce the conditions to form the ring contracted species. The

size of the barium ion was the driving force for the ring contraction, to produce a macrocyclic cavity with a size more suited to the ion that is present.

In this thesis, design and synthesis of several different types of manganese macrocyclic complexes will be described. The complexes were prepared for biological testing, to analyse the effects that different ligands and geometries may produce on the observed activity.

1.2 Tripodal ligands

Tetradentate tripodal ligands contain a central tertiary nitrogen atom that is attached to three arms, each of which contains a donor atom Y as illustrated in Figure 1-14:²⁹

30

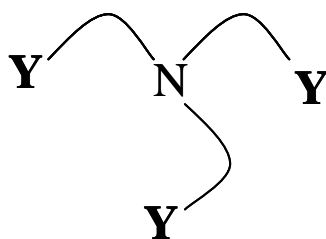


Figure 1-14 – *General structure of a tripodal ligand*

During the course of this work, a particular focus on the synthesis of tripods with nitrogen as the donor atom has been adopted. Multidentate nitrogen donor ligands are interesting due to their potential applications in areas such as catalysis, transport processes and modelling of several biological compounds.²⁹ Several tripods have been synthesised and are known by a four letter abbreviation of the full name of the ligand, for example, N,N-bis(2-aminoethyl)ethane-1,2-diamine is better known as tren, the structure of which is shown in Figure 1-15.³¹

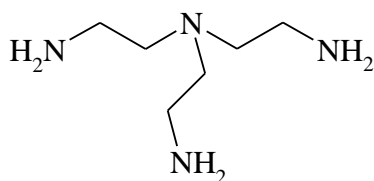


Figure 1-15 – *The structure of tren*

In these tripodal systems, the tertiary nitrogen caps the ligand and differences can be introduced by altering the length of the arms and the nature of the nitrogen donor atoms. All routes of synthesis use the alkylation of a nitrogen atom from either an ammonium ion or a primary or secondary amine precursor to form the tertiary nitrogen of the tripod.

When a tripod is symmetrical, then all three arms are the same and this usually has C_{3v} symmetry about the central nitrogen atom. However, when differences are introduced into the arm lengths of the ligand, the tripod becomes asymmetric and the symmetry is usually C_s or lower. Only more recently have ligands of lower symmetry been prepared.³¹

Crystal structures of the free ligand have shown both a splayed conformation as well as an internally hydrogen bonded system where all three arms are folded to form a cavity into which a metal ion can bind. This is usually seen in ligands that are protonated.³⁰

A tripodal ligand will usually bind to a transition metal using all four nitrogen atoms, although examples exist where the ligand binds to a metal using less than the number of full donor atoms available to it. An example of this can be seen with a tripod containing a long arm when bound to a copper ion as seen in Figure 1-16.^{31, 32}

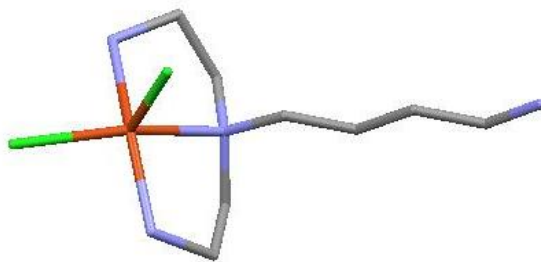


Figure 1-16 – *Hypodentate Cu(II) Complex*

The reason that some tripodal ligands bind in this way, may be due to the stability of the complexes formed, usually explained in terms of the chelate effect. Chelation can become less entropically favoured when the chelate ring contains six or more atoms as the ring can become strained, so tripods with a long pendant arm may coordinate in this hypodentate fashion.^{32, 33}

A tripodal amine ligand is able to undergo a Schiff base reaction to form a wider variety of ligands that are available for complexation. A Schiff base ligand prepared from tren and salicylaldehyde, known as the saltren ligand, has previously been prepared and its coordination chemistry with various metal ions has also been investigated (Figure 1-17).^{24, 34, 35}

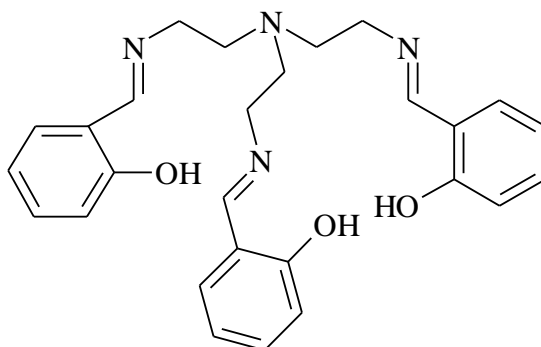


Figure 1-17 – *Structure of the saltren ligand*

McKee and co-workers^{36, 37} have illustrated that by varying the ratio of manganese ion to saltren ligand, different complexes can be prepared. Crystallographic data were obtained for two forms of tripodal complex to form both the mononuclear

manganese complex A)³⁷ $[\text{Mn}(\text{L})]^{2+}$ and the tetranuclear complex B)³⁶ $[\text{Mn}_4\text{O}_2(\text{L})_2]^{2+}$ both illustrated below in Figure 1-18.

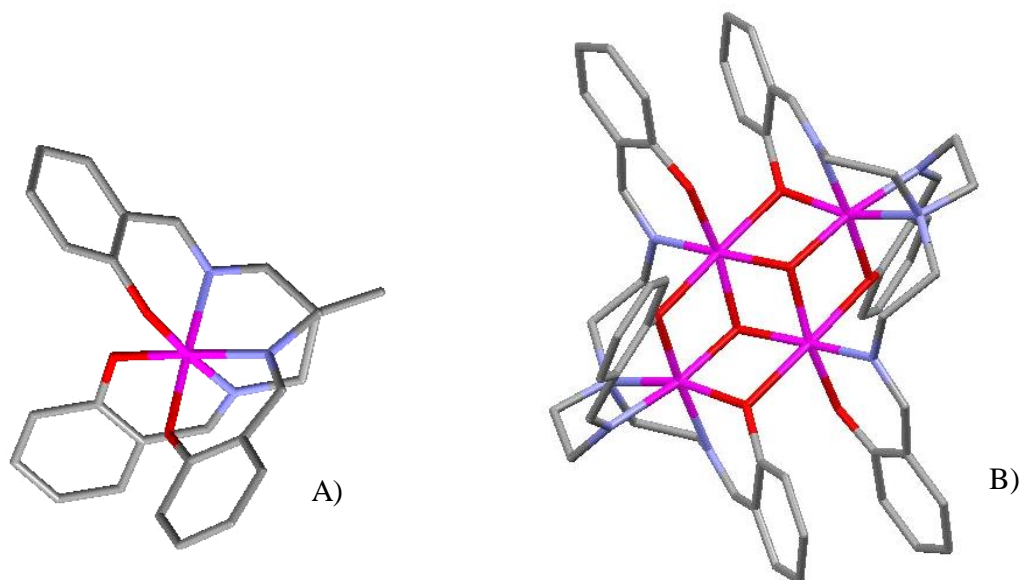


Figure 1-18 – *Products of reactions involving different ratios of manganese to saltren ligand*

To form complex A), the reaction was carried out as a 1:1 molar ratio of manganese ion to saltren ligand. To form complex B), a 2:1 ratio was required and this complex exists as a tetranuclear system with two tripodal ligands forming two independent, centrosymmetric cations within the unit cell. For each complex, the manganese ion is in a six coordinate geometry, with each donor atom from the saltren ligand, except for the two oxo ions present in complex B).

In this thesis, the attempted synthesis of various asymmetric tripodal ligands will be described. These were reacted with a salicylaldehyde ligand to form Schiff base ligands that can be used for the synthesis of various complexes in different molar ratios. Different arm lengths should provide a wider variety of geometries about the manganese ion; this may be directly related to the biological activity of the complexes.

1.3 Superoxide dismutase activity

The superoxide anion (O_2^-) formed by a one electron reduction of O_2 , is an example of a free radical due to the presence of its unpaired electron.³⁸ The molecular orbital diagram for oxygen is shown in Figure 1-19:

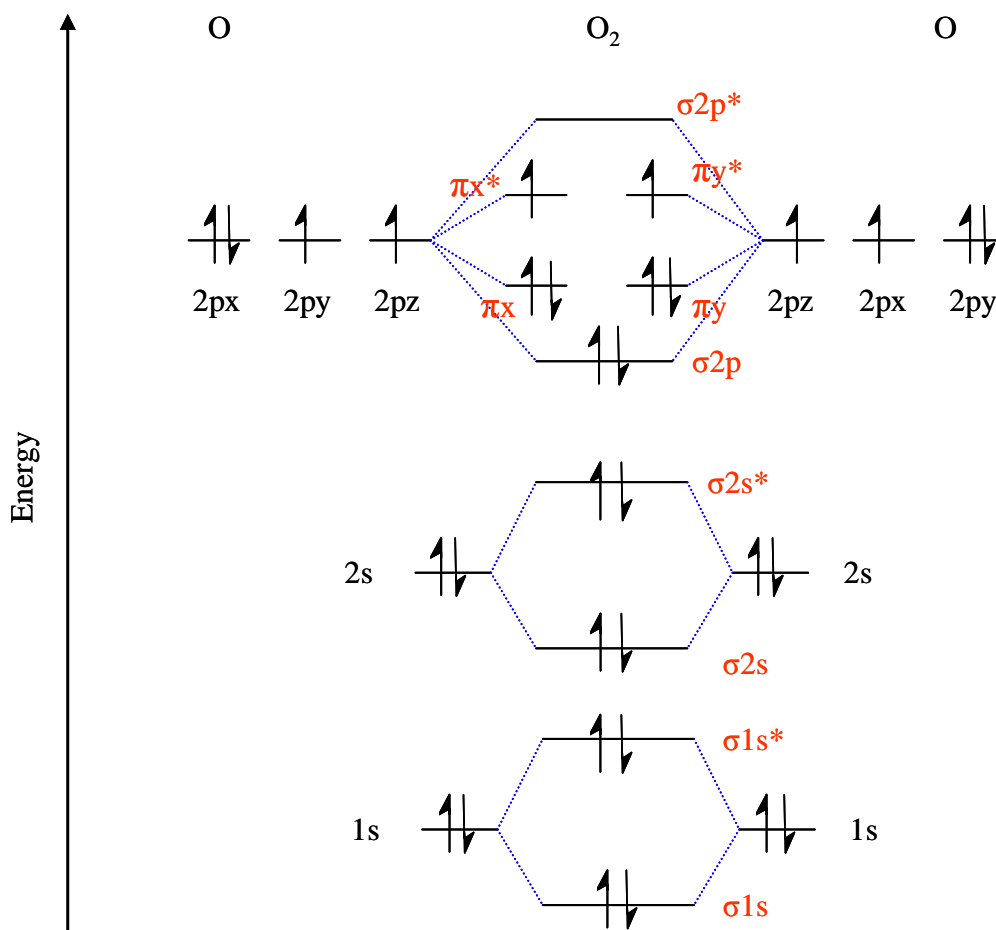


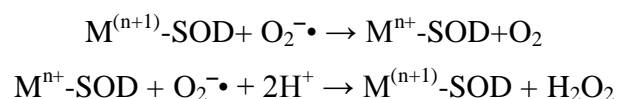
Figure 1-19 – Molecular orbital diagram of O_2

From the molecular orbital diagram shown in Figure 1-19, the bond order of molecular oxygen can be calculated as 2, however, once the oxygen undergoes a one electron reduction, the bond order is reduced to 1.5 with the extra electron placed in the π_x^* or the π_y^* antibonding orbitals. The superoxide molecule then has a longer bond length due to the existence of the extra electron that is present. Due to the unpaired electron, superoxide exists as a very reactive free radical,^{39,40} its

decomposition produces further undesired harmful species such as the hydroxyl radical and hydrogen peroxide.⁴¹

In living cells, low levels of the superoxide radical anions are produced in the mitochondria as a by-product of aerobic respiration that is essential for cell function. However, a fine balance exists between the reactive oxygen species produced and the amount of superoxide scavengers (antioxidants) present in the cells, which protect tissues from oxidative damage. Oxidative stress may develop when this balance is disrupted.^{42, 43} In acute inflammation, for example, the production of superoxide is increased at a rate that overwhelms the capacity of the superoxide dismutase (SOD) enzyme to remove it,⁴⁴ and oxidative stress is responsible for contributing to the symptoms of the ageing process, arthritis and degenerative diseases such as Alzheimer's and Parkinson's diseases. Manganese SODs are a class of oxidoreductases⁴⁴ which play a critical role in scavenging intramitochondrial free radicals as a defence against oxidative stress.^{40, 45-47}

Different types of superoxide dismutase enzymes exist within living cells and all are important antioxidants,⁴⁵ There are four major classes of SOD which are Mn, Fe, Cu/Zn and Ni.^{41, 46, 48-50} In humans, there are three different types of superoxide dismutase enzymes, these are SOD 1 which is a Cu/Zn enzyme and is found in the cytoplasm of the cell, SOD 2 is a manganese SOD and is found in the mitochondria and SOD 3 is an extracellular Cu/Zn enzyme. Superoxide dismutase protects the cells from its damaging and uncontrolled reactions by catalysing the dismutation of superoxide ($O_2^{\cdot-}$) into oxygen and hydrogen peroxide, preventing the formation of dangerous $OH\cdot$ radicals^{51, 52} (see Equation 1). Once this reaction is complete, the hydrogen peroxide is then either broken down to water and oxygen via a catalase enzyme, or it may reduce the $M^{(n+1)}$ -SOD enzyme⁵³



Where M=Cu (n=1), M=Mn (n=2), M = Fe (n=2), M = Ni (n=2)

Equation 1 - *Dismutation of superoxide into oxygen and hydrogen peroxide*

Mn(SOD) was discovered in 1970 and is a redox active manganese enzyme which has a mononuclear core at the active site.³⁸ Cu/Zn SOD enzymes have shown to possess catalytic rates in excess of $2 \times 10^9 \text{ M}^{-1} \text{ s}^{-1}$ ⁵⁴ with Mn and Fe SODs possessing rates of an order of magnitude slower than the Cu/Zn enzymes depending upon the source of the enzyme present.⁵⁵

Natural SOD enzymes have been shown to have promising therapeutic properties but suffer as drug candidates due to immunogenic responses.⁵⁶ Their large molecular weights also prevent the molecules passing through cell membranes.⁵⁷ The active site of the human MnSOD can be seen in Figure 1-20 below.⁵⁸

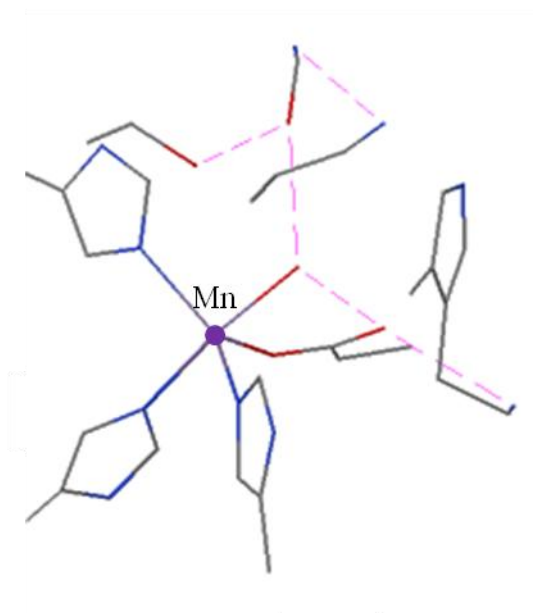


Figure 1-20 –*Active site structure of human MnSOD*

The diagram in Figure 1-20 shows that the active site of the native human MnSOD contains a five coordinate manganese centre with distorted trigonal bipyramidal geometry. The manganese is coordinated to three nitrogen atoms from the His

residues (26, 74 and 163) an oxygen atom from Asp (159) and one oxygen from a bound OH₂ (water) molecule. The mechanism for the reaction with superoxide involves cycling between oxidised Mn³⁺ and reduced Mn²⁺. In the reduced form, MnSOD is thought to react with superoxide through two pathways involving Mn³⁺SOD-O₂²⁻ and Mn³⁺SOD which is often called the inhibited complex.⁵⁹⁻⁶¹ The redox cycling is illustrated in Figure 1-21 below.

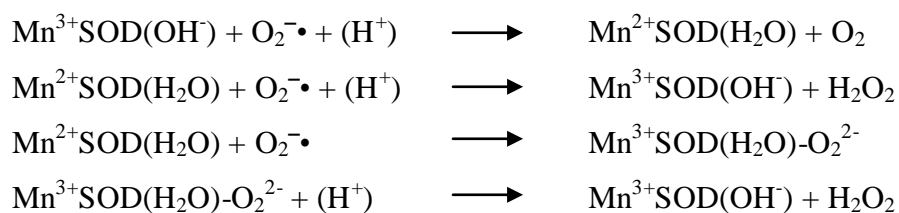
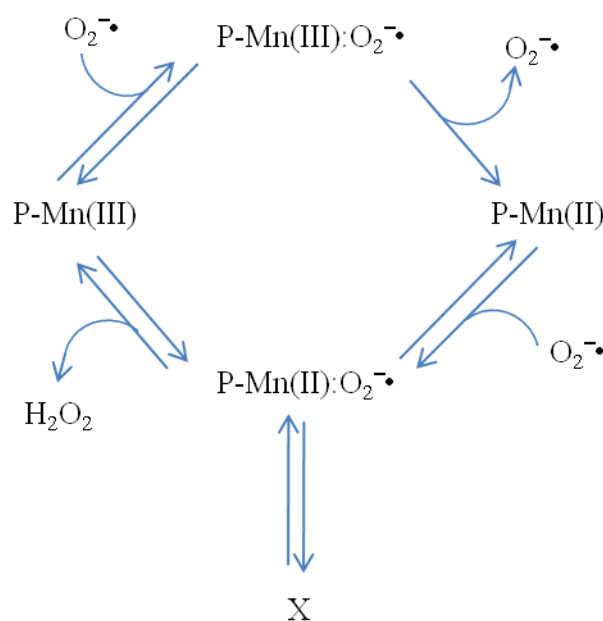


Figure 1-21 – Redox cycling in human MnSOD

A more detailed mechanism was proposed by Bull *et al.* as shown in Figure 1-22, which allows for the reversibility of steps:



P = Protein; X = Inactive enzyme

Figure 1-22 – Mechanism for MnSOD as outlined by Bull *et al.*

In the mechanism shown in Figure 1-22, the inactive enzyme arises by an internal rearrangement of the P-Mn²⁺: O₂^{·-} to yield the inactive enzyme X.

Considerable interest is being shown in the development of low molecular weight synthetic therapeutic SOD mimetics which provide a low energy reaction pathway⁶². These types of compounds may be important for the treatment of rheumatoid and osteoarthritis, which are conditions that are associated with oxidative stress.^{45, 48, 53}

Riley *et al.* developed the very active SOD mimics that are manganese(II) complexes incorporating the macrocyclic ligand 1,4,7,10,13-pentazacyclopentadecane [Mn([15]aneN₅)Cl₂]. All of the complexes are seven-coordinate high spin d⁵ Mn(II) dichloro complexes and can effectively catalyse the dismutation of superoxide.^{55, 63,}
⁶⁴ The generic structure of this macrocycle is shown below.

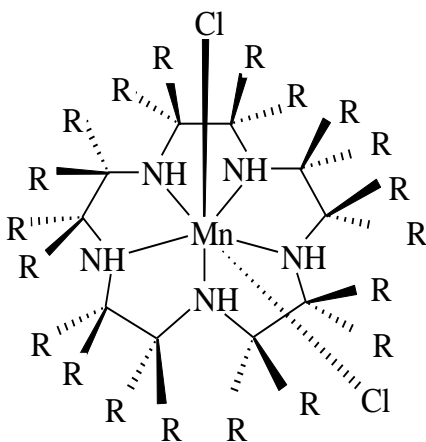


Figure 1-23 - Generic structure of [Mn([15]aneN₅)Cl₂]

This class of molecule was investigated by altering the number of substituents, their placement, and their stereochemistry with two key features thought necessary for improvement:

- Increase the kinetic stability of the complex by increasing the rigidity of the molecule.
- Increase SOD activity, resulting in lower dosage, diminishing exposure to the metal.

Riley *et al.* found that an increase in the number of carbon substituents increased the stability of the complex non-linearly. The stereochemistry of the R groups, however,

had a large effect on SOD activity, but little effect on stability assuming the number of constituents remain constant.

Riley *et al.*³⁹ with the aid of computer modelling, synthesised the complex M40403, the structure of which is shown below in Figure 1-24. The complex M40403 was derived from the 1,4,7,10,13-pentaazacyclopentadecane containing the added pyridine functionality. This complex was shown to exceed the catalytic rate of the native human MnSOD enzyme and has the advantage of being a much smaller molecule. The complex M40403 has successfully completed phase I safety clinical trials in healthy human subjects,^{44, 64} and has more recently entered phase II clinical trials.⁶⁵

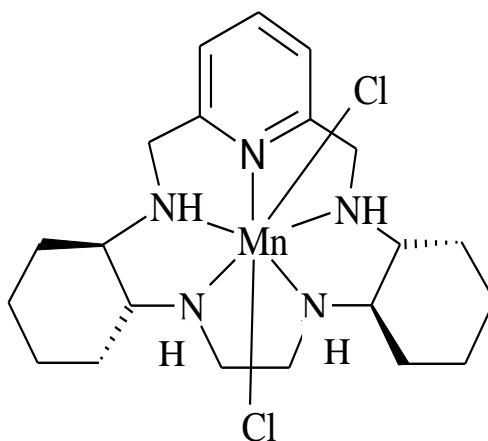


Figure 1-24 - Structure of M40403

The catalytic cycle for the SOD mimics as prepared by Riley *et al.* was proposed and is illustrated below in Figure 1-25.^{63, 64, 66} A detailed understanding of the mechanism is important for designing a synthetic, low molecular weight MnSOD complex.

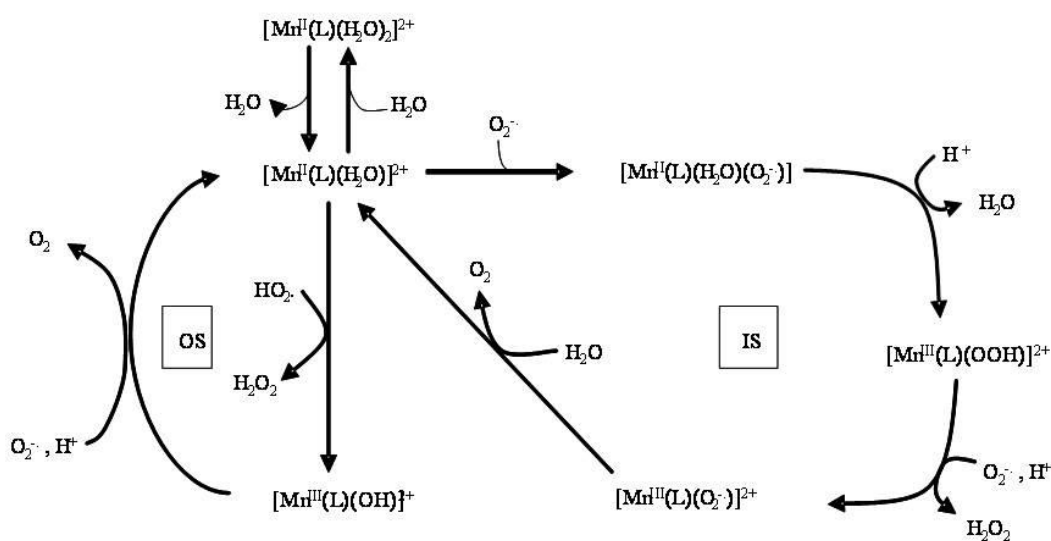


Figure 1-25 – Proposed catalytic cycle of a SOD mimic

The catalytic cycle consists of two reaction pathways:

- A pH independent inner sphere (IS) pathway
- A pH dependent outer sphere (OS) pathway

Riley *et al.* claimed that where the inner sphere binding of the superoxide radical to a vacant coordination site at the manganese centre occurs, the rate of the formation of the vacant site is the rate determining step of the reaction and for the outer sphere pathway, the proton coupled electron transfer step was rate limiting.

However, Dees *et al.*⁴¹ have suggested that the water exchange mechanism is an interchange dissociative (I_d) mechanism where the incoming superoxide anion also plays a role in the overall substitution process. Water exchange rate constants and activation parameters were assessed to come to this conclusion. Firstly the activation entropies and volumes gave positive values. Secondly, the water exchange rate constants decreased with an increase of π acceptor ability of the ligand. They also found that for the inner sphere pathway, the second order rate constants were significantly higher than the values for the water exchange rate suggesting that the release of H_2O cannot be the rate determining step.

Maroz *et al.*⁶⁷ suggested that the oxidation of the metal centre is not the rate determining step. Three complexes that were analysed are shown below in Figure 1-26.

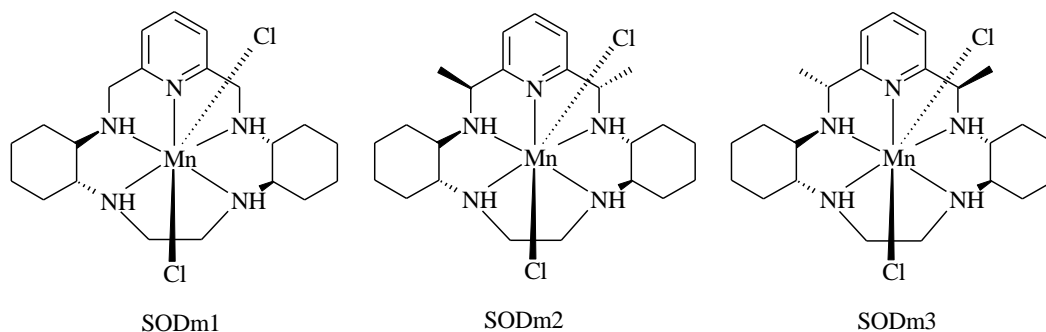


Figure 1-26 - Complexes analysed by Maroz *et al*

The moderately active catalyst SODm1 reacted with superoxide at a similar rate as the ineffective catalyst SODm3. Cyclic voltammetry showed that the redox potential of the Mn(III)/Mn(II) couple is similar for two complexes with very different SOD activities. Maroz *et al.* suggested that the $[\text{Mn}^{\text{III}}(\text{L})\text{O}_2]^+$ intermediate oxidizes the next molecule of superoxide and that this is the crucial point in the catalytic cycle. Maroz *et al.* proposed the following reaction mechanism:

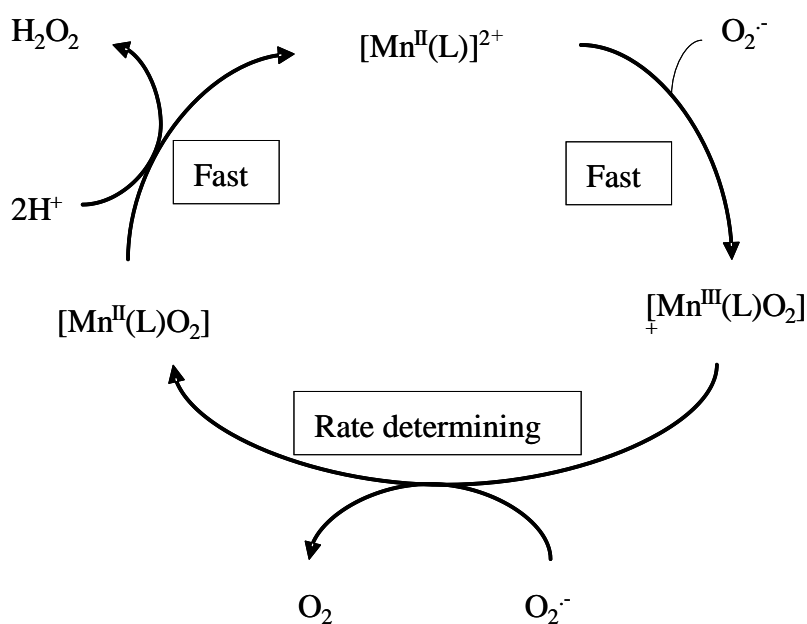
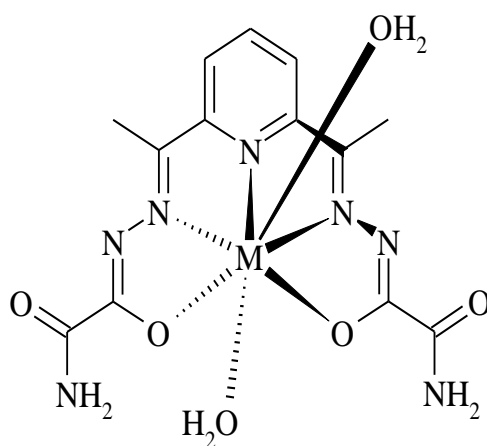


Figure 1-27 - Proposed catalytic cycle

The mechanism illustrated in Figure 1-27 involves three steps:⁶⁷

- Activation of the complex by reaction with superoxide to form the deprotonated Mn(III) intermediate.
- Reduction of the intermediate with a second superoxide, influenced by its structure. The metal centre is reduced back to the initial Mn(II) maintaining a pseudooctahedral geometry.
- Hydrogen peroxide is released and the complex returns to its original conformation.

Riley *et al.* postulated that only ligands with conformational flexibility could possess SOD activity.⁶⁴ Conversely, Liu *et al.*⁵⁶ synthesised seven coordinate iron and manganese complexes with the acyclic and rigid Hdapsox ligand, shown below in Figure 1-28, which demonstrated catalytic activity similar to that found for macrocyclic pentadentate ligands. This suggests that the water release and conformational rearrangement of the ligand are not the rate limiting step in the overall inner sphere SOD pathway of the SOD mimics.⁵⁶



M = Mn(II), Fe(II), Fe(III)

Figure 1-28 - Hdapsox ligand complex

For a SOD mimic to be effective *in vivo* as well as *in vitro*, it should be non-toxic, non-immunogenic and inexpensive. They should also have a high metabolic half-life and be able to penetrate into the cells as well as having a high stability constant.⁶⁸

Manganese-containing systems are preferred due to the lower toxicity of the free aquated manganese ion *in vivo*, it is also the least likely to react with hydrogen peroxide to produce hydroxyl radicals.^{64, 69}

Devereux *et al.*⁷⁰ suggested that there is possibly significant cytotoxic activity in these complexes. Where a molecule possesses superoxide dismutase activity and no catalase activity, the cytotoxic hydroxyl radical does not become broken down. This may be considered as a potential anticancer compound where high levels of superoxide may exist in cancerous growths.

1.3.1 Methods of measurement

The indirect analysis of superoxide dismutase relies on a spectrophotometric change of a redox indicator. This was first carried out by McCord and Fridovich in their development of a Cytochrome c assay.⁷¹ Since then, many indirect assays have been developed where the amount of superoxide is estimated by reaction of the superoxide with a redox indicator such as NBT (Nitro blue tetrazolium) which is often used in the xanthine/xanthine oxidase system.

In the xanthine/xanthine oxidase system, the xanthine oxidase aerobically oxidises the xanthine to urate, producing a constant flux of superoxide in the process. During this reaction, the yellow indicator NBT^{2+} scavenges the superoxide causing NBT^{2+} to be reduced to the blue formazan (MF^+) which produces a spectral change. Inhibition of the reduction of the indicator in the presence of the superoxide dismutase mimic is taken as a measure of superoxide dismutase activity.⁷¹⁻⁷³ There are underlying assumptions that the SOD mimic has removed superoxide from the system and that this is the only reason for the decrease in the formazan production. However, the indirect methods cannot kinetically distinguish between a catalytic and a stoichiometric dismutation and are prone to giving false positives when the superoxide dismutase mimic oxidises the indicator or reacts stoichiometrically with the superoxide.⁷⁴ To determine if a complex is truly catalytically active, a result

obtained using an indirect method should ideally be complemented with the results from a direct method of analysis to support the results obtained.

One example of a direct method is the stop-flow technique, in which a solution of the putative catalyst is rapidly mixed with superoxide solution. This method allows the precise measurement of the decay of superoxide to be visually measured spectrophotometrically. For the direct methods, if there is a first order decay of superoxide observed then the reaction is a truly catalytic reaction. If however the reaction is found to be second order, then the reaction is deemed to be a non-catalytic decay.⁷⁵

1.4 Catalase Activity

Catalase is a metalloenzyme that removes the potentially harmful hydrogen peroxide (H_2O_2) of which, some is produced during the disproportionation of the superoxide radical as shown in Equation 1. Catalase helps to protect living organisms from the reactive oxygen species (ROS) that are responsible for oxidative stress.⁵³ Most catalases are heme-containing enzymes, however, a manganese containing catalase was first isolated and purified from the *Lactobacillus plantarum* in 1983.⁷⁶ Since then, various other manganese catalases have been purified and isolated from other organisms.

The crystal structure of the manganese catalase from a *Lactobacillus plantarum* showed that the active site contained a dimanganese core linked with a μ -glutamate carboxylate and two μ -oxygen atoms as illustrated in Figure 1-29.^{77, 78}

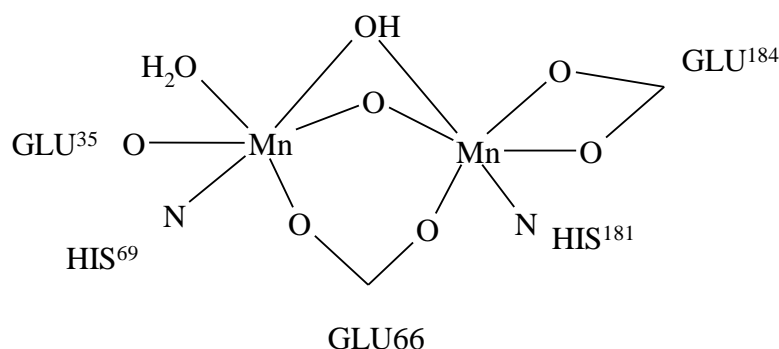
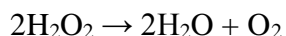


Figure 1-29 – Catalase active site of the *lactobacillus plantarum*

Hydrogen peroxide can be produced at increased levels in different pathological situations and when the level of H_2O_2 is too high for the catalase enzymes, cellular damage can arise due to the production of the mutagenic $\text{OH}\cdot$ radical that is formed when H_2O_2 reacts with Fe^{2+} or Cu^{2+} . Due to the toxicity of H_2O_2 , organisms have developed methods to aid in its fast decomposition which requires a two electron catalyst. Naturally occurring manganese catalases contain two manganese centres,⁷⁹ carboxylate bridges, and their binding mode can alter the observed activity.^{78, 80, 81} Nitrogen containing heterocyclic bases known as histidines exist in the vicinity of the active site of manganocatalases. The addition of base during the testing of catalase models has often been shown to increase catalytic activity and Pecoro *et al.*⁸² suggested that base was needed to deprotonate the hydrogen peroxide to initiate the reaction for binding to the manganese ions. During decomposition, one molecule of catalase can convert millions of molecules of H_2O_2 per second.⁸³⁻⁸⁵

H_2O_2 is decomposed by catalase to molecular oxygen and water according to Equation 2 shown below:^{43, 80, 86, 87}



Equation 2 – Removal of hydrogen peroxide

A possible mechanism for the catalase activity is shown below in Figure 1-30:⁷⁸

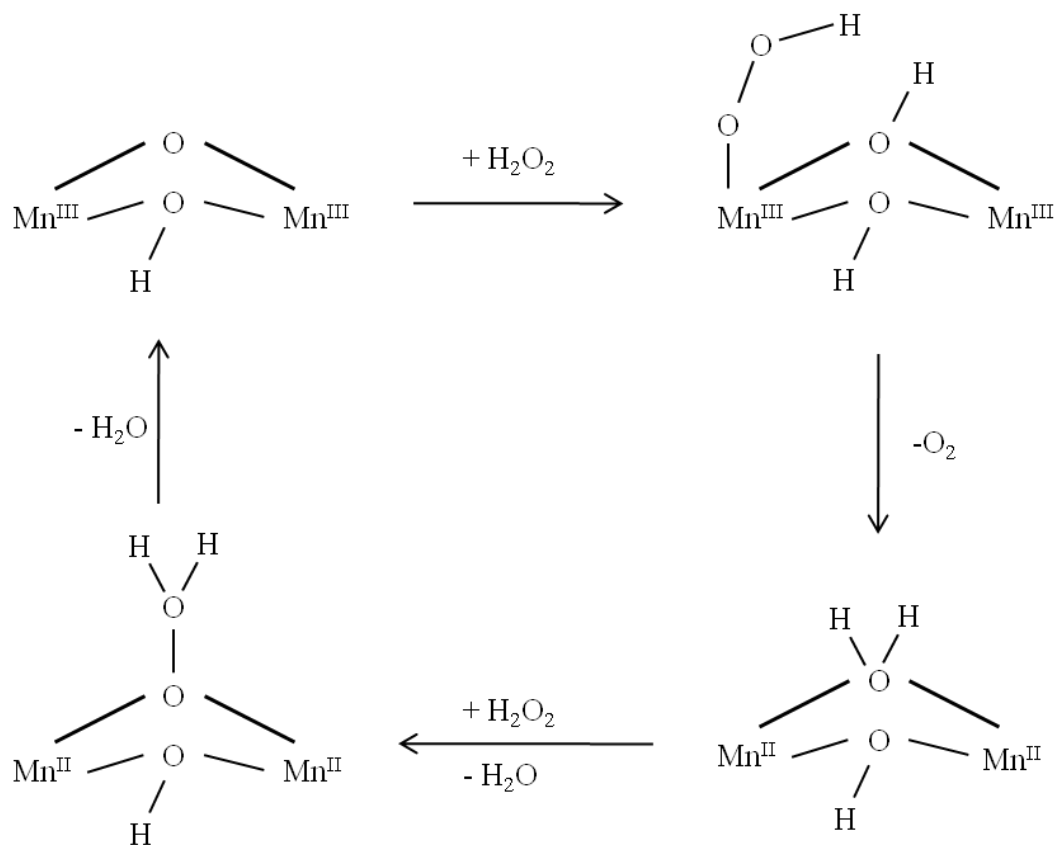


Figure 1-30 – Possible mechanism for catalase activity

During catalysis, the manganese centres cycle between $\text{Mn}_2^{(\text{III})}$ and $\text{Mn}_2^{(\text{II})}$ and one molecule of H_2O_2 is oxidised to oxygen while another is reduced to H_2O . During the oxidative reaction, H_2O_2 replaces the terminal H_2O ligand from one of the $\text{Mn}(\text{III})$ centres and protonates the μ -oxo bridge. Reduction of the manganese dimer results in the formation and release of O_2 . The second molecule of H_2O_2 binds to the manganese(II) as a bridging hydroperoxo ligand. O-O bond cleavage followed by reoxidation to $\text{Mn}_2^{(\text{III})}$ with loss of H_2O completes the cycle.^{78, 79, 88, 89}

When designing manganese catalase mimics, it is important to explore how changes in geometry of the manganese centre and the nature of the complexes can affect reaction rates and provide suggestions for increasing catalase activity. This in turn may lead to a more detailed understanding of the mechanisms involved in the catalytic cycle.

Early examples of manganese catalase mimics were based on porphyrin manganese dimer complexes. However, the dimeric units would dissociate during catalysis, and although efforts were made to stabilise the complex *via* addition of rigid linkers, the rate of catalase activity was slow compared to the natural enzyme.⁷⁹ Since then, porphyrin derivatives have been prepared that show increased rates of catalytic activity.^{79, 90}

Dismukes *et al.* later synthesised a family of dinuclear complexes with varying coordination environments and oxidation states, an example of this type of complex is illustrated below in Figure 1-31⁸⁸

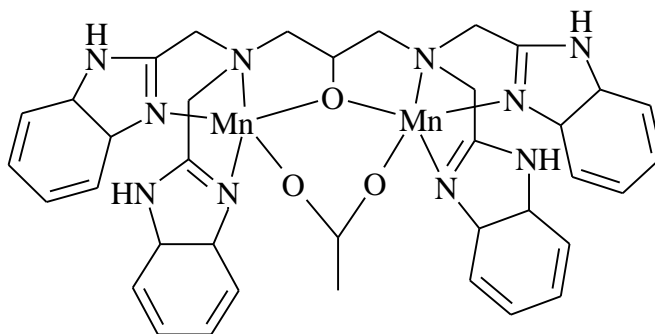


Figure 1-31 – *Dinuclear manganese catalase mimic*

Following their studies, they proposed a mechanism of catalase activity for a hydroxide derivative of the complex shown in Figure 1-31, this was a ping pong mechanism as shown below in Figure 1-32.

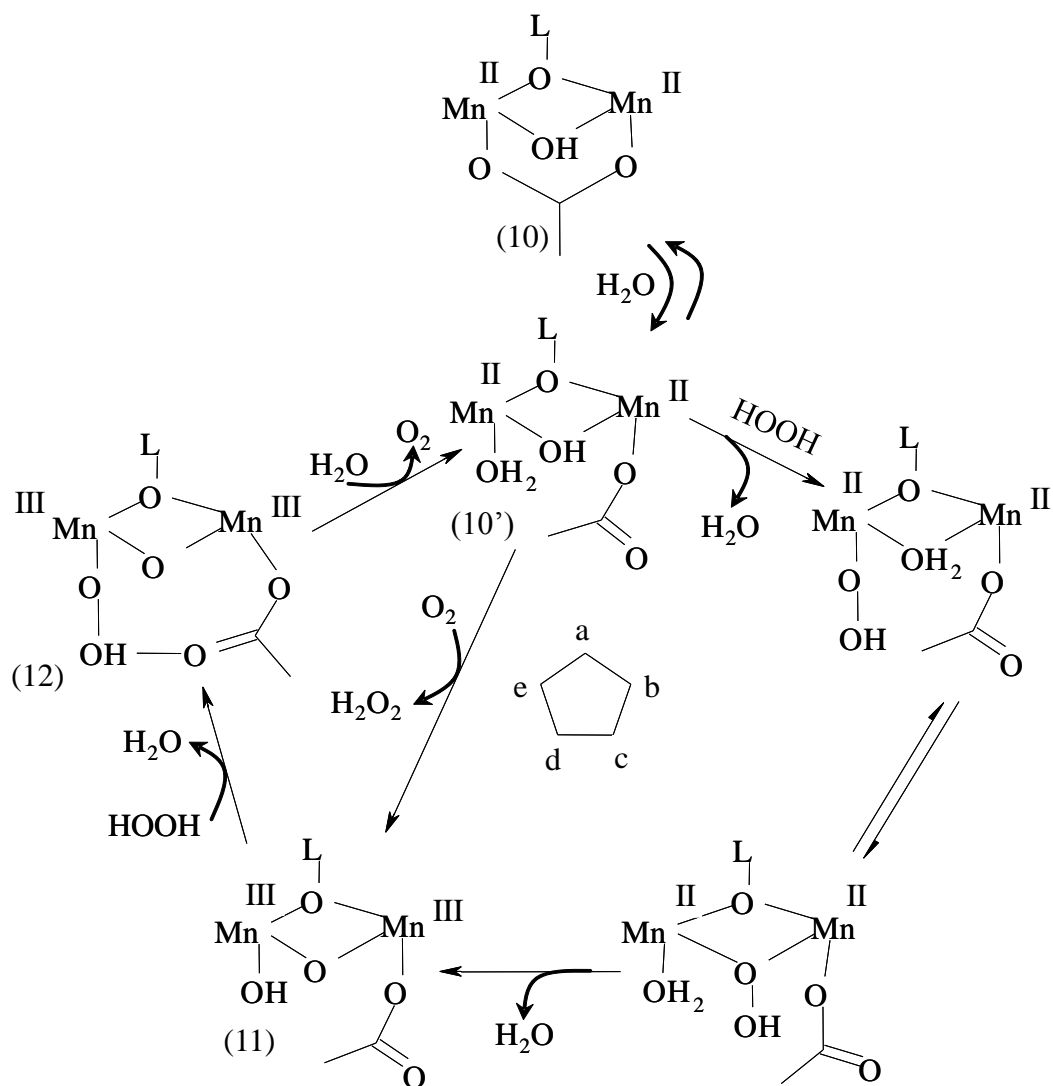


Figure 1-32 – Proposed mechanism for catalase activity of a dinuclear Manganese complex

For the mechanism shown in Figure 1-32, the substrate binds to the μ -hydroperoxide to (10') by exchange of the hydroxide bridge ($\mu\text{-OH}^- + \text{H}_2\text{O}_2 \longrightarrow \mu\text{O}_2\text{H}^- + \text{H}_2\text{O}$) this is steps $\text{A} \longrightarrow \text{B} \longrightarrow \text{C}$. Steps $\text{D} \longrightarrow \text{E}$ follow formation of the oxidised complex 6A and precedes its reduction $\text{E} \longrightarrow \text{A}$. Dismukes *et al.* suggested that substrate binding to the oxidised complex (11) or reduction to (10') is accelerated by excess hydroxide and the step that is accelerated by excess hydroxide may involve the reduction of 11 to form complex 12 ($\text{D} \longrightarrow \text{E}$).⁸⁸

Mn-Salen complexes have been shown to be particularly promising catalase mimics. These complexes have also shown to possess superoxide dismutase activity as well as

catalase activity, with catalase activity varying significantly with ligand substituents. A ping pong mechanism was suggested by Abashkin and Burt⁸⁶ for a Mn Salen complex as shown in Figure 1-33.

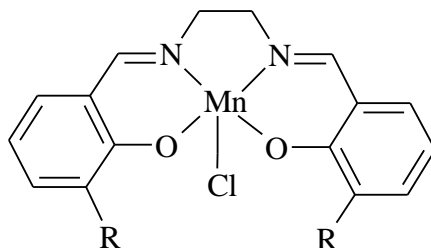


Figure 1-33 – Structure of a manganese salen complex

It was suggested that the H_2O_2 molecule binds to the Mn(III) metal centre, which then becomes oxidised releasing a molecule of water. In the second step, a peroxide molecule approaches the oxo manganese(V) intermediate, transforming the oxygen back to peroxide forming O_2 and H_2O (see Figure 1-34).

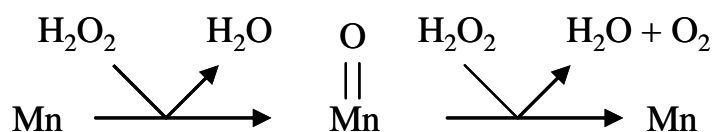


Figure 1-34 – Ping pong mechanism for manganese salen complexes

Throughout his thesis, various manganese complexes have been investigated for their catalase and superoxide dismutase activity; this is with the intention of helping to identify key differences and geometric constraints that may induce higher rates of activity. The observed changes may help to facilitate the understanding of the catalytic activity.

Model compounds that may be successful for both superoxide dismutase activity and catalase activity may be of interest for the role of both antioxidant actions in one potential pharmaceutical compound however, in the case where a compound shows only superoxide dismutase activity or only catalase activity, then there may be scope for further developments and testing of that compound. The absence of either superoxide dismutase activity or catalase activity may be an essential feature for the

treatment of specific conditions, for example, where a compound shows high superoxide dismutase activity, the potentially harmful $\text{OH}\cdot$ radical may be produced which in the absence of a catalase mimic may survive long enough to show significant cytotoxicity, thus providing a potential scope for their use against cancerous cells which may have heightened levels of superoxide present. Catalase mimics which show no superoxide dismutase activity may be required for conditions which produce harmful hydrogen peroxide at a rate which overwhelms the natural enzyme's capacity at which it is able to deal with.

The aims of this thesis were to develop a wide range of low molecular weight seven coordinate manganese(II) complexes with slight geometric alterations introduced around the metal centres. This type of complex was expected to show both superoxide dismutase and/or catalase activity. Structure activity relationships may improve the understanding of the catalytic cycle involved in these two important reactions which may prevent oxidative stress.

2 Chapter Two - Synthesis and Structure

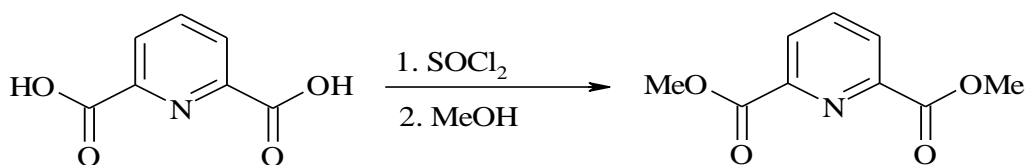
2.1 Organic preparations

The pyridine head units for the macrocyclic complexes of H₂L1, H₄L2 and H₂L3 were prepared in house as described below. The head units of the complexes contain the carbonyl functional group (C=O) which is able to undergo a Schiff base condensation reaction with the appropriate amines to form the desired macrocyclic complexes. The two head units differ slightly with 2,6-diacetylpyridine containing two methyl groups where these are not present in the 2,6-diformylpyridine head unit. This was with the intention of forming complexes with slight differences in geometry around the metal centre, with the notion that without the methyl groups, there would be more flexibility in the macrocycle around the metal centre. Two different types of complex have been synthesised due to macrocyclic ring contractions that occur with the use of the diformylpyridine head unit.

2.1.1 2,6-Diacetylpyridine

2,6-Diacetylpyridine was prepared in two stages, firstly, 2,6-pyridinedicarboxylic acid undergoes an esterification reaction to form the product 2,6-dimethylpyridine dicarboxylate as illustrated.¹⁰⁰

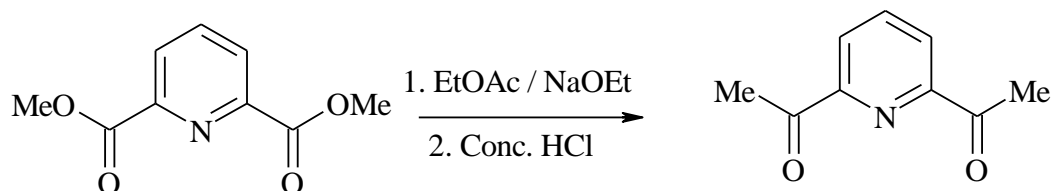
Step 1:



The ¹H NMR data were used to confirm the presence of the methyl groups which were found as a singlet at δ (H) 3.96 ppm, this was not present in the NMR found for the start material 2,6-pyridinedicarboxylic acid, confirming that the reaction was successful.

The second stage of the reaction is the formation of 2,6-diacetylpyridine from 2,6-dimethylpyridine dicarboxylate in a Claisen condensation reaction as illustrated below.¹⁰⁰

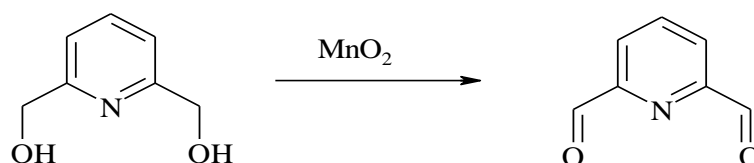
Step 2:



Analysis of the ^1H NMR for the product formed in this reaction showed that the signal for the methyl group has shifted to δ (H) 2.73 ppm, this is due to the removal of the electron density on the oxygen atom from the OMe group of the 2,6-dimethylpyridine dicarboxylate. Fine crystals of 2,6-diacetylpyridine were formed during this reaction. Crystals of the macrocyclic complexes further verified the success of this reaction.

2.1.2 2,6-Diformylpyridine

Activated manganese dioxide (MnO_2) which is an oxidant, was freshly prepared in house and used for the oxidation of the precursor to 2,6-diformylpyridine which was formed in good yield and purity. This was then used as the head unit for the macrocyclic complexes of $\text{H}_2\text{L3}$.



During the preparation of 2,6-diformylpyridine, a $\nu_{\text{C=O}}$ stretch at 1700 cm^{-1} in the infrared spectrum proved that the reaction had taken place. Crystals of the macrocyclic complexes further verified the success of this reaction.

2.2 Polynuclear complexes

The [2+2] macrocycle H_2L1 shown in Figure 2-1 was prepared via Schiff base template condensation of 2,6-diacetylpyridine (DAP) with 1,3-diamino-2-hydroxypropane, utilising a Ba^{2+} ion from barium perchlorate. Borohydride reduction was then carried out to form the [2+2] macrocycle $RedH_2L1$ as illustrated in Figure 2-1. The [2+2] macrocycle H_2L3 shown in Figure 2-1 was prepared via Schiff base template condensation of 2,6-diformylpyridine (DFP) with 1,3-diamino-2-hydroxypropane, utilising a Ba^{2+} ion from barium perchlorate.¹⁰⁰

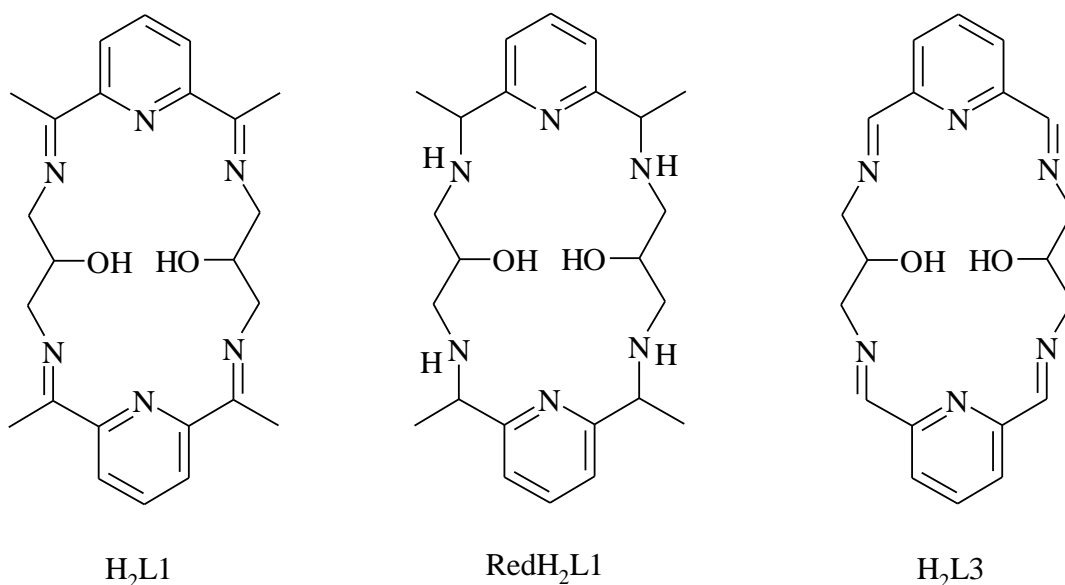


Figure 2-1 – [2+2] macrocycles H_2L1 , $RedH_2L1$ and H_2L3

The use of barium as the template ion produces the [2+2] macrocycles of H_2L1 , $RedH_2L1$ and H_2L3 in good yield and purity. Once the barium complex is formed, the complex can be transmetallated by manganese(II) ions forming a complex which is more stable than the barium complex. The manganese ions have a higher affinity for the donors within the ligand system. The transmetallation reaction will not work with all transition metal ions due to the geometry that is imposed by the macrocyclic ligand and the nature of the donors within the system, however manganese(II) has no preferred geometry and readily adopts the pentagonal bipyramidal geometry that is imposed upon it, whilst having a high affinity for the donors in accordance with HSAB theory, which states that a hard acid will coordinate more strongly with a hard

base and a soft acid will coordinate more strongly with a soft base. A hard species is generally small in size with a high charge and a soft species tends to be large in size with a low charge. Nitrogen is a medium soft donor, which is made slightly softer within the macrocyclic system that has an imine bond, however, the barium ion is hard and so is easily displaced for the more softer manganese ion. The barium macrocycle then acts as a precursor for a transmetalation reaction with manganese allowing synthesis of a range of tetranuclear and pentanuclear manganese(II) macrocycles with differing axial ligands.

When the mononuclear barium macrocyclic complex $[\text{Ba}(\text{H}_2\text{L1})(\text{H}_2\text{O})](\text{ClO}_4)_2$ is formed, the charge on the barium is +2, therefore, two negatively charged perchlorate anions are present to maintain electric neutrality.

The structure of a barium complex of $\text{H}_2\text{L1}$ has previously been reported by Adams *et al*⁹¹ and the structure of the cation is shown in Figure 2-2.

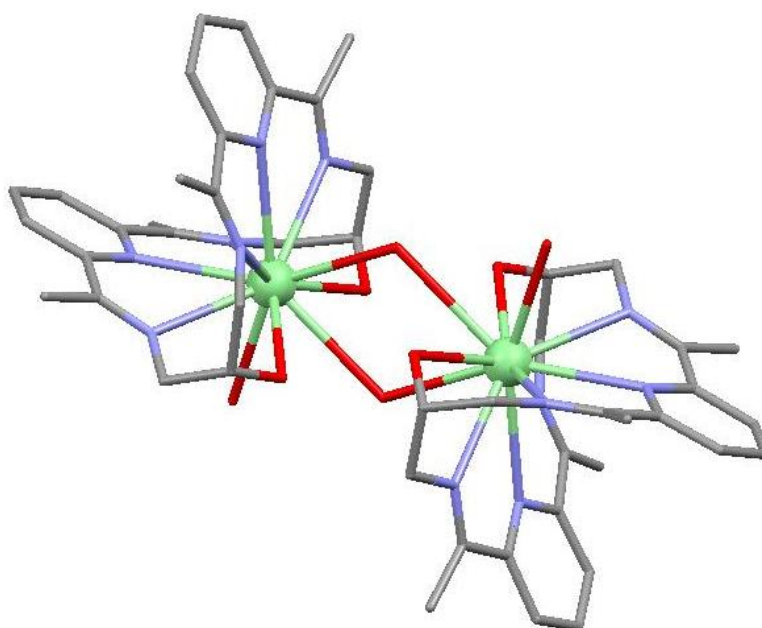


Figure 2-2 – Dimeric $[\text{Ba}(\text{H}_2\text{L1})(\text{H}_2\text{O})_2]_2^{4+}$ cation with perchlorate anions and hydrogens omitted for clarity

The complex was found to crystallise in the triclinic space group $P\bar{1}$. The macrocycle shows substantial folding between the pyridyl fragments and a dimerisation *via* two bridging water molecules. Two perchlorate anions are not directly coordinated to the complex but are involved in extended hydrogen bonding to the coordinated water molecules.⁹¹

2.2.1 $[\text{Ba}(\text{H}_2\text{L3})(\text{ClO}_4)]_2(\text{ClO}_4)_2$

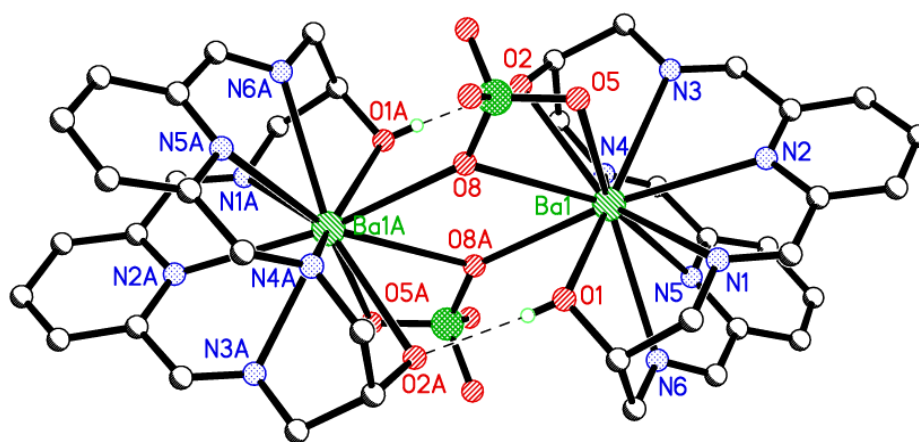


Figure 2-3- Structure of $[\text{Ba}(\text{H}_2\text{L3})(\text{ClO}_4)]_2^{2+}$ with perchlorate anions, and hydrogens omitted for clarity. Dashed lines represent hydrogen bonding

A Schiff Base condensation reaction was used for the preparation of the barium complex yielding either large clear crystals or a white powder that crystallises as clear blocks under slow diffusion of ether into a DMF solution.

$[\text{Ba}(\text{H}_2\text{L3})(\text{ClO}_4)]_2(\text{ClO}_4)_2$ crystallised as large clear block shaped crystals in the triclinic space group $P\bar{1}$ with $R1 = 0.0374$. The details of the crystal structure and refinement can be found in Table 27 in appendix 1.

The metric parameters for this type of compound were as expected. The macrocycle shows substantial folding between the pyridyl fragments as seen for the published structure for the barium complex of $\text{H}_2\text{L1}$ previously described and a dimerisation

due to the coordinated perchlorate ions. The dimerisation is then strengthened by hydrogen bonds that form between the alcohol units on adjacent macrocyclic units.

The structure of the $[\text{Ba}(\text{H}_2\text{L3})(\text{ClO}_4)]_2^{2+}$ cation as shown in Figure 2-3 shows that each macrocycle binds a single eleven coordinate barium ion. Selected bond lengths and angles for $[\text{Ba}(\text{H}_2\text{L3})(\text{ClO}_4)]_2(\text{ClO}_4)_2$ are given Table 1.

Table 1 - Selected bond lengths [\AA] and angles [$^\circ$] for $[\text{Ba}(\text{H}_2\text{L3})(\text{ClO}_4)]_2(\text{ClO}_4)_2$

Ba(1)–O(1)	2.783(3)	Ba(1)–O(5)	2.876(3)
Ba(1)–N(5)	2.918(3)	Ba(1)–N(4)	2.933(3)
Ba(1)–N(1)	2.935(3)	Ba(1)–N(6)	2.949(3)
Ba(1)–N(2)	2.958(3)	Ba(1)–O(2)	2.976(2)
Ba(1)–N(3)	3.004(3)	Ba(1)–O(8)	3.090(3)

O(1)–Ba(1)–O(8A)	72.96(8)	O(1)–Ba(1)–N(5)	113.53(8)
O(8A)–Ba(1)–N(5)	96.46(8)	O(8A)–Ba(1)–N(4)	78.97(8)
O(1)–Ba(1)–N(4)	148.42(8)	N(5)–Ba(1)–N(4)	55.28(8)
O(1)–Ba(1)–N(1)	57.21(8)	O(8A)–Ba(1)–N(1)	127.35(8)
N(4)–Ba(1)–N(1)	140.10(8)	N(5)–Ba(1)–N(1)	89.14(8)
O(8A)–Ba(1)–N(6)	83.80(8)	O(1)–Ba(1)–N(6)	58.86(8)
N(5)–Ba(1)–N(6)	54.76(8)	N(4)–Ba(1)–N(6)	104.45(8)
N(1)–Ba(1)–N(6)	57.62(8)	O(1)–Ba(1)–N(2)	112.70(8)
O(8A)–Ba(1)–N(2)	166.22(8)	N(4)–Ba(1)–N(2)	91.85(8)
N(5)–Ba(1)–N(2)	69.79(8)	N(6)–Ba(1)–N(2)	88.64(8)
N(1)–Ba(1)–N(2)	55.65(8)	O(8A)–Ba(1)–O(2)	73.64(7)
O(1)–Ba(1)–O(2)	124.42(7)	N(5)–Ba(1)–O(2)	113.27(7)
N(4)–Ba(1)–O(2)	58.07(8)	N(1)–Ba(1)–O(2)	148.74(8)
N(6)–Ba(1)–O(2)	153.42(8)	N(2)–Ba(1)–O(2)	110.29(7)
O(1)–Ba(1)–N(3)	154.48(8)	O(8A)–Ba(1)–N(3)	124.68(8)
N(4)–Ba(1)–N(3)	56.63(8)	N(5)–Ba(1)–N(3)	84.67(8)
N(6)–Ba(1)–N(3)	134.43(8)	N(1)–Ba(1)–N(3)	107.95(8)
O(2)–Ba(1)–N(3)	56.07(7)	N(2)–Ba(1)–N(3)	55.09(8)

Symmetry operations for equivalent atoms A $x, y-1, z$

The $[\text{Ba}(\text{H}_2\text{L3})(\text{ClO}_4)]_2^{2+}$ cation is centrosymmetric and each barium ion binds to all 6 nitrogen donors and two oxygen donors within the macrocycle. The bite angle of the pyridine diimine head unit $107.95(8)^\circ$ (for N1–Ba1–N3), and $104.45(8)^\circ$ (for N4–Ba1–N6) is much smaller than those of the manganese bound complexes of L1 due to the larger size of the barium ion. Each barium ion also binds to two oxygen atoms from one bridging perchlorate and one oxygen atom from the second bridging perchlorate.

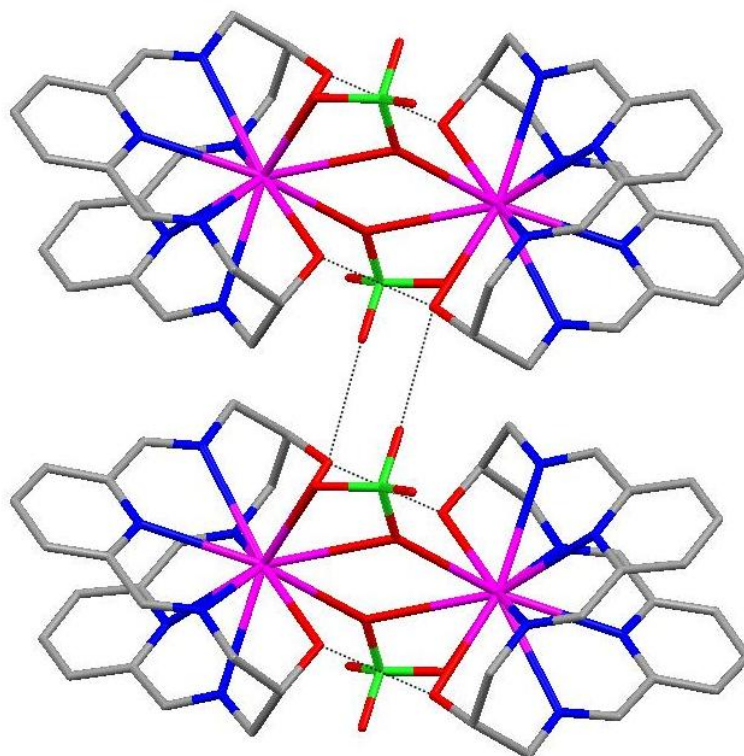


Figure 2-4– *Hydrogen bonding for $[\text{Ba}(\text{H}_2\text{L3})(\text{ClO}_4)]_2 \cdot (\text{ClO}_4)$*

Hydrogen bonding exists between the two alcohol units strengthening the dimerisation, with further hydrogen bonding observed between one alcohol unit from the macrocyclic unit to a perchlorate ion on a second dimeric macrocyclic unit as illustrated in Figure 2-4.

At this stage, there is no ring contraction observed for the barium precursor $[\text{Ba}(\text{H}_2\text{L3})(\text{ClO}_4)]_2 \cdot (\text{ClO}_4)_2$ which crystallises as a dimeric molecule. When the barium complex is used in a transmetallation reaction to form a manganese complex,

one imine bond undergoes a nucleophilic attack from the solvent molecule forming a ring contracted species to accommodate the size of the manganese ion.

2.2.2 [Ba(L5)(ClO₄)₂(OH₂)].(OH₂)

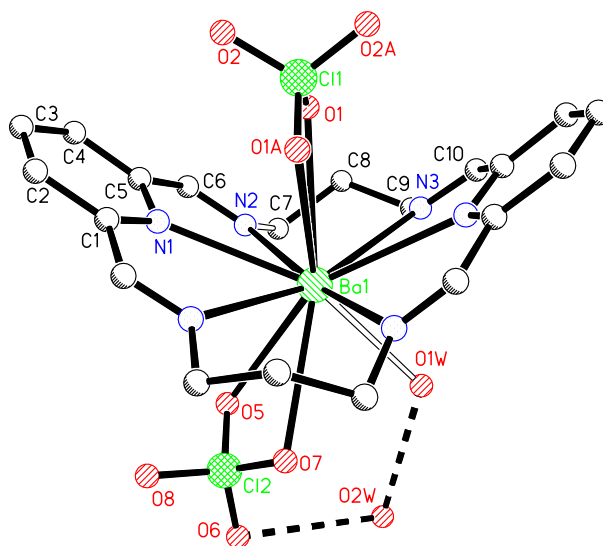


Figure 2-5 - Structure of [Ba(L5)(ClO₄)₂(H₂O)].H₂O. with hydrogens omitted for clarity. Dashed lines represent hydrogen bonding

Large colourless crystals of [Ba(L5)(ClO₄)₂(H₂O)].H₂O, the structure of which is shown in Figure 2-5⁹² were formed from the reaction mixture of 2,6-diformylpyridine, 1, 3-diaminopropane and barium perchlorate in a methanolic solvent by Rebecca Dennett as part of a BSc honours project.

The crystals obtained as described above crystallised in the monoclinic space group C2/c with R1 = 0.0227. The details of the crystal structure and refinement can be found in Table 29 in appendix 1.

The molecule described here crystallises differently to that of the complex [Ba(H₂L3)(ClO₄)₂](ClO₄)₂ described earlier and illustrated in Figure 2-3 due to there being no alcohol groups in the macrocyclic ligand. Here, there is a two fold axis which runs through Ba1-Cl1, the asymmetric unit contains a single eleven coordinate barium ion that is bonded to all six nitrogen donors of the macrocycle which is

folded to accommodate the metal. Two bidentate perchlorate anions are coordinated with one on each side of the macrocycle. A water molecule is coordinated on the convex side of the macrocycle to complete the coordination sphere. A non-coordinated water molecule (O2W) is hydrogen bonded to O1W and to the perchlorate ion. The perchlorate anion and the water molecules on the convex side of the macrocycle are all disordered and was modelled with equal occupancy of the two positions about a two fold axis running through Ba1 and C11 within the complex.

The selected bond lengths and angles for [Ba(L5)(ClO₄)₂(H₂O)].H₂O are reported in Table 2:

Table 2 - Selected bond lengths [Å] and angles [°] for [Ba(L5)(ClO₄)₂(H₂O)].H₂O

Ba(1)–O(1W)	2.836(4)	Ba(1)–N(2)	2.9217(16)
Ba(1)–N(1)	2.8856(16)	Ba(1)–N(3)	3.0002(15)
Ba(1)–O(5)	2.893(4)	Ba(1)–O(1)	3.0253(14)

N(1)–Ba(1)–O(5)	77.19(8)	O(1W)–Ba(1)–N(1)	148.48(11)
O(5A)–Ba(1)–O(5)	75.11(15)	O(1W)–Ba(1)–O(5)	73.93(10)
N(1A)–Ba(1)–N(2)	118.24(4)	O(1W)–Ba(1)–N(2)	100.79(12)
O(5)–Ba(1)–N(2)	71.63(8)	O(1W)–Ba(1)–N(3)	67.18(9)
N(1)–Ba(1)–N(3)	115.02(5)	O(1W)–Ba(1)–O(1)	130.24(8)
O(5A)–Ba(1)–N(3)	80.34(9)	N(1)–Ba(1)–O(1)	65.68(4)
N(2)–Ba(1)–N(3)	66.22(5)	N(2)–Ba(1)–O(1)	66.01(4)
O(5)–Ba(1)–O(1)	134.03(7)	N(3)–Ba(1)–O(1)	63.66(4)
O(5)–Ba(1)–N(3)	113.95(9)	N(2)–Ba(1)–N(3A)	112.35(5)

Symmetry operations for equivalent atoms A $-x, y, -z+3/2$

The angle of the pyridine diimine head unit 112.35(5)^o (for N2–Ba1–N3A) is much smaller than that of the manganese bound complexes of L1 due to the larger size of the barium ion but is larger than the angle observed for the complex [Ba(H₂L3)(ClO₄)₂](ClO₄)₂. Longer bond lengths are also observed for the Ba-donor ligand than for the manganese bound complexes previously described.

[Ba(L5)(ClO₄)₂(H₂O)].H₂O packs as a two dimensional sheet as shown in Figure 2-6 where only one portion of the disorder is shown. The complex molecules are linked *via* hydrogen bonding from the water molecules. The disorder of the groups coordinated on the convex side of the macrocycle gives rise to two possible hydrogen bonding nets related by a two fold axis.

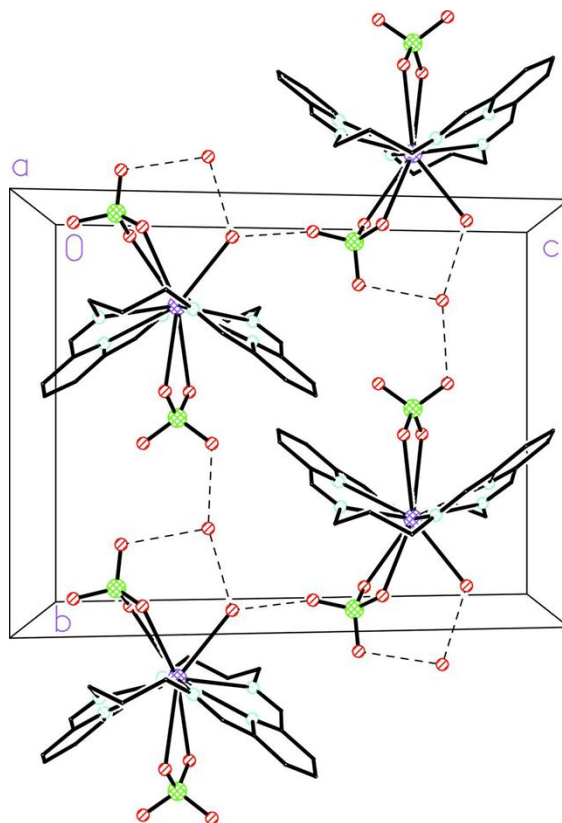


Figure 2-6 – Packing diagram for [Ba(L5)(ClO₄)₂(H₂O)].H₂O shown perpendicular to the *a* axis

The reduced analogue of H₂L1, named RedH₂L1, was prepared using sodium borohydride to reduce the imine bonds of the barium macrocycle as illustrated Figure 2-7.

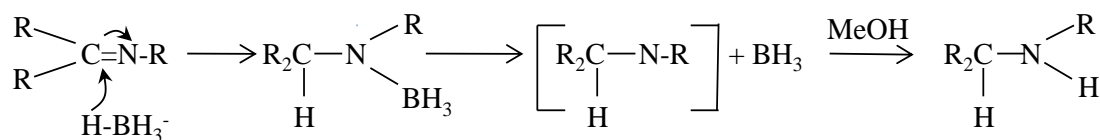


Figure 2-7 – Borohydride reduction

During the reduction, borohydride donates a hydrogen to the imine bond and the residual BH₃ then complexes with the nitrogen atom. The second hydrogen is from

the hydroxyl group of the alcoholic solvent which forms a hydrogen bond to the nitrogen of the imine bond. At this stage, the H-BH₂OMe borate molecule is formed and there are three remaining B-H bonds available for the reduction of further imines.

After extraction of the ligand, transmetallation reactions with various manganese salts were completed. Reduction was carried out in this way to form the complex in a high yield. IR analysis of the reduced macrocycle confirmed that a reduction had taken place due to the disappearance of the imine stretch at 1639 cm⁻¹ observed for the complex of H₂L1. In principle, it is possible to form any combination of the R,R', S,S' and R,S isomers with regard to the dimethylhead units of the macrocycle following reduction of the imine bonds, however, due to the folding of the macrocycle that is observed for both complexes of H₂L1 and H₂L3, there are likely to be less isomers formed as the folding may restrict the position that the borohydride can approach the imine bonds. Riley *et al*³⁹ found that when borohydride was used for the reduction of M40403, only the R,R-dia stereoisomer was formed, as monitored by HPLC. This result is expected due to being the least stereochemically restricted approach to the imine bond with each borohydride approaching from opposite sides of the macrocyclic plane.

Table 3 - Key IR data

Ligand	Key IR data (cm ⁻¹)
H ₂ L1	3431 $\nu_{(O-H)}$, 1639 $\nu_{(C=N)}$, 1584 $\nu_{(C=C)}$
RedHL1	3299 $\nu_{(O-H)}$, 1574 $\nu_{(C=C)}$, 1095
H ₂ L3	3380 $\nu_{(O-H)}$, 1654 $\nu_{(C=N)}$, 1586 $\nu_{(C=C)}$
L5	1642 $\nu_{(C=N)}$, 1586 $\nu_{(C=C)}$

Each complex was analysed using infrared (IR) spectroscopy, elemental analysis, FAB mass spectrometry and, where possible, X-ray crystallography. The IR data were initially used to confirm the absence of an amine and carbonyl stretches associated with the reactant materials and the presence of an imine bond at 1643 – 1658 cm⁻¹ confirming that the reaction had taken place. A band at 1565 – 1598 cm⁻¹ is associated with the pyridyl ring of the two head units. Where perchlorate ions were

present, a broad peak was observed at $\sim 1100\text{ cm}^{-1}$ with a sharp peak at 625 cm^{-1} , the first of which is due to the ν_3 asymmetric stretch and the latter being a symmetrical bend.

On formation of the barium precursor, a transmetallation reaction was carried out to form the manganese complexes of $\text{H}_2\text{L1}$ $\text{RedH}_2\text{L1}$ and HL3 . During formation of the $\text{H}_2\text{L1}$ and $\text{RedH}_2\text{L1}$ complexes, there can be a monodeprotonation of one of the alcohol groups for each macrocyclic ligand due to the formation of a dimeric species in which the hydrogen sits between the two oxygens of the macrocycle with hydrogen bonding. The monodeprotonation introduces a negative charge into each of the two macrocyclic units, so for a complex which contains for example, negatively charged chloride axial ligands, there remain two uncoordinated negatively charged counter ions such as perchlorate. In the case where there is a chloride ligand present for example, these will bind in the axial position in favour of the perchlorate anions due to the chloride having a stronger ligand field, and possessing a higher affinity for the manganese. Complexes of $\text{H}_2\text{L3}$ were found to undergo a macrocyclic ring contraction. IR peaks confirming the axial ligand were observed, for example, azide and isothiocyanate ligands showed sharp peaks at 2046 and 2037 cm^{-1} respectively.

2.2.3 $[\text{Mn}_2(\text{HL1})(\text{Cl})_2]_2(\text{ClO}_4)_2 \cdot 2\text{DMF}$

$[\text{Mn}_2(\text{HL1})(\text{Cl})_2]_2(\text{ClO}_4)_2$ was prepared *via* transmetallation of the barium precursor with $\text{MnCl}_2 \cdot 4\text{H}_2\text{O}$ under reflux in dry methanol solvent. During the synthesis a colour change was observed from colourless to orange on addition of manganese chloride. The solid product was collected via filtration from the cooled reaction vessel however, more product could be recovered from the filtrate thereafter by reducing the volume of the solvent to approximately 5 ml under reduced pressure. FAB ms analysis suggested that a dimer was present as indicated by the fragmentation pattern with m/z of 1327 which corresponds to the fragment $[\text{Mn}_2(\text{HL2})(\text{Cl})_2]_2(\text{ClO}_4)^+$. Suitable crystals for X-ray diffraction were grown from DMF by slow diffusion of ether. The structure of the cation is shown in Figure 2-8.

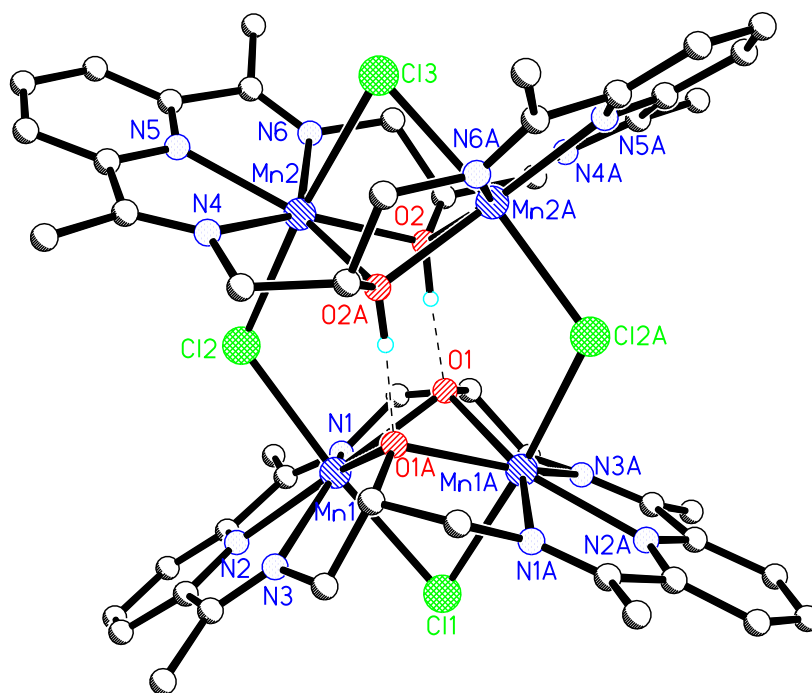


Figure 2-8 – Structure of $[Mn_2(HL1)(Cl)_2]_2^{2+}$ with perchlorate anions, hydrogens and solvent molecules omitted for clarity. Dashed lines represent hydrogen bonds

The crystal structure of $[Mn_2(HL1)(Cl)_2]_2(ClO_4)_2$ was previously reported by McKee and co-workers;⁹³ it crystallised in the orthorhombic space group *Pbcn* with $R1 = 0.0706$.

The complex prepared here was found to crystallise in the same space group but the refinement has been improved with $R1 = 0.0375$. The details of the crystal structure and refinement can be found in Table 23 in Appendix 1.

The $[Mn_2(HL1)(Cl)_2]_2^{2+}$ cation lies on a crystallographic 2-fold axis passing through Cl1 and Cl3. Each macrocycle binds two Mn(II) ions and the cation is dimeric with the two macrocyclic units linked by bridging chloride ions thus creating a tetramanganese system. During the synthesis of the molecule, two of the four pendant alcohol groups are deprotonated. The diagram shown in Figure 2-8 indicates that there is one macrocycle which is fully protonated and one macrocycle which is fully deprotonated, however this is probably an artefact and occurs because the hydrogen that is present was freely refined and located on O2, this was then symmetry generated on O2A under $-x, y, 0.5-z$. Hydrogen bonds exist between the

alcohol groups of the adjacent macrocycles with a bond distance of 2.491(2) Å. Each manganese ion is seven-coordinate with each metal centre having pentagonal bipyramidal geometry. Selected bond lengths and angles for [Mn₂(HL1)(Cl)₂]₂(ClO₄)₂.2DMF are given in Table 4 below.

Table 4-Selected bond lengths [Å] and angles [°] for [Mn₂(HL1)(Cl)₂]₂(ClO₄)₂.2DMF

Mn(1)–N(2)	2.225(2)	Mn(1)–N(3)	2.261(2)
Mn(1)–O(1)	2.2670(16)	Mn(1)–N(1)	2.284(2)
Mn(1)–Cl(2)	2.5419(7)	Mn(1)–Cl(1)	2.6008(8)
Mn(2)–N(5)	2.218(2)	Mn(2)–O(2)	2.2710(15)
Mn(2)–N(6)	2.281(2)	Mn(2)–N(4)	2.2963(19)
Mn(2)–Cl(2)	2.5358(7)	Mn(2)–Cl(3)	2.5944(8)

N(2)–Mn(1)–N(3)	70.30(7)	N(2)–Mn(1)–O(1)	143.05(7)
N(3)–Mn(1)–O(1)	144.60(7)	N(2)–Mn(1)–N(1)	70.28(7)
N(3)–Mn(1)–N(1)	138.88(8)	O(1)–Mn(1)–N(1)	72.83(7)
N(2)–Mn(1)–Cl(2)	90.16(5)	N(3)–Mn(1)–Cl(2)	103.69(6)
O(1)–Mn(1)–Cl(2)	90.38(4)	N(1)–Mn(1)–Cl(2)	87.67(6)
N(2)–Mn(1)–Cl(1)	94.82(5)	N(3)–Mn(1)–Cl(1)	79.25(6)
O(1)–Mn(1)–Cl(1)	84.89(4)	N(1)–Mn(1)–Cl(1)	92.81(6)
Cl(2)–Mn(1)–Cl(1)	174.87(2)	N(5)–Mn(2)–O(2)	142.57(7)
N(5)–Mn(2)–N(6)	70.40(7)	O(2)–Mn(2)–N(6)	72.82(6)
N(5)–Mn(2)–N(4)	70.24(7)	O(2)–Mn(2)–N(4)	147.18(7)
N(6)–Mn(2)–N(4)	139.30(7)	N(5)–Mn(2)–Cl(2)	90.50(6)
O(2)–Mn(2)–Cl(2)	89.17(4)	N(6)–Mn(2)–Cl(2)	100.05(6)
N(4)–Mn(2)–Cl(2)	90.24(6)	N(5)–Mn(2)–Cl(3)	94.14(5)
O(2)–Mn(2)–Cl(3)	84.48(4)	N(6)–Mn(2)–Cl(3)	77.46(6)
N(4)–Mn(2)–Cl(3)	95.45(5)	Mn(1A)–Cl(1)–Mn(1)	73.76(3)
Mn(2A)–O(2)–Mn(2)	86.59(5)		

Symmetry operations for equivalent atoms A $-x+1, y, -z-3/2$

The pentagonal plane contains three nitrogen donors from a pyridinediimine unit with a bite angle of 138.88(8)^o (N3-Mn1-N1) and two oxygen donors from the

macrocycle. The coordination sphere is completed by a bridging chloride ion that sits in the axial position and serves to link the two macrocyclic units and a further axial chloride ligand which bridges the two manganese ions within each macrocyclic unit. The bridge angles between the manganese centres within the macrocyclic units are considerably smaller [Mn1A-Cl1-Mn1, $73.76(3)^\circ$] and [Mn(2A)-O(2)-Mn(2), $86.59(5)^\circ$] than the equivalent bridge angles which link the macrocyclic units [Mn2-Cl2-Mn1, $115.67(3)^\circ$]. The bond distances observed for the bridge angles between the manganese centres within the macrocyclic units are [Mn1-Cl1, $2.6008(8) \text{ \AA}$], and [Mn2-Cl3, $2.5944(8) \text{ \AA}$]. The bond distances observed for the equivalent bridge angles which link the macrocyclic units are $2.5419(7) \text{ \AA}$ for Mn1-Cl2, and $2.5358(7) \text{ \AA}$ for Mn2-Cl2.

The principal interaction between adjacent cations is π - π stacking between the pyridinediimine head units of two adjacent molecules this is observed between the overlapping sections as illustrated in Figure 2-9 below. The centroid - centroid distance is 3.760 \AA and the centroid of the ring is $3.707(1) \text{ \AA}$ from the mean plane of the second ring under symmetry operation $-0.5-x+2, -0.5+y+1, z$. The π - π stacking continues between adjacent molecules of the complex and can be seen in the packing diagram as viewed down the c axis shown in Figure 2-10 below.

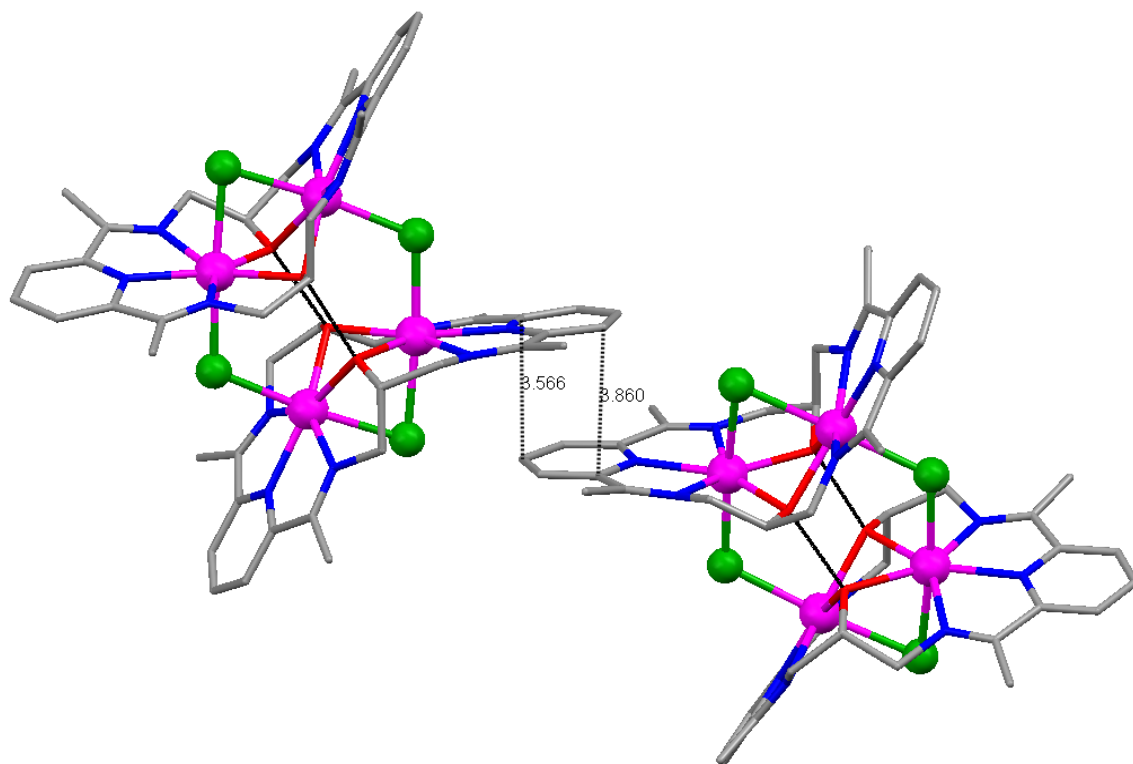


Figure 2-9 – π - π stacking for $[Mn_2(HLI)(Cl)_2]_2(ClO_4)_2$

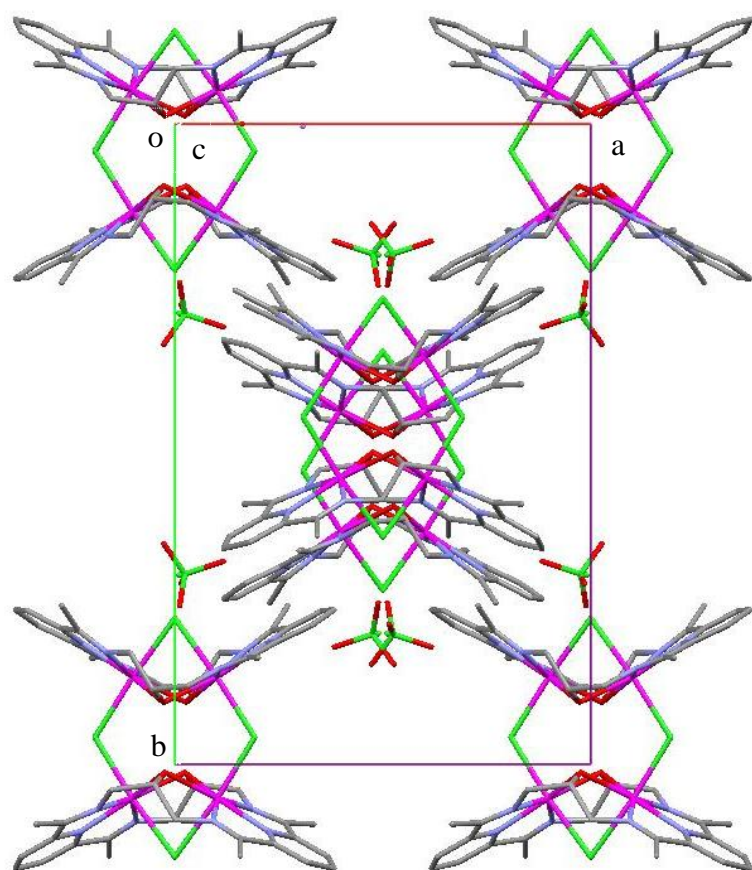


Figure 2-10 – Packing diagram for $[Mn_2(HL1)(Cl)_2]_2(ClO_4)_2$ as viewed down the *c* axis

2.2.4 $[\text{Mn}_2(\text{HL1})(\text{N}_3)_2]_2(\text{ClO}_4)_2 \cdot 2\text{DMF}$

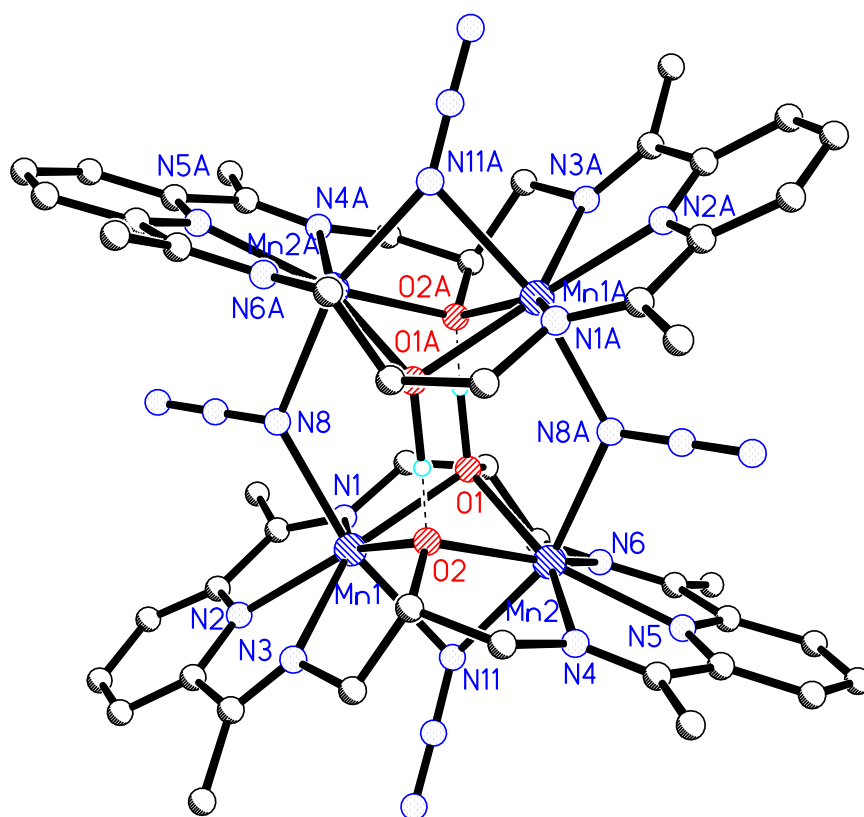


Figure 2-11 –Structure of $[\text{Mn}_2(\text{HL1})(\text{N}_3)_2]^{2+}$ with perchlorate anions hydrogens and solvate DMF molecules omitted for clarity. Dashed lines represent hydrogen bonding

The crystal structure of $[\text{Mn}_2(\text{HL1})(\text{N}_3)_2]^{2+}$ is illustrated in Figure 2-11. $[\text{Mn}_2(\text{HL1})(\text{N}_3)_2]_2(\text{ClO}_4)_2 \cdot 2\text{DMF}$ crystallises in the monoclinic spacegroup $P2_1/c$ and was refined to $R1 = 0.0399$. The details of the crystal structure and refinement can be found in Table 24 in Appendix 1.

The structure of a different solvate, $[\text{Mn}_2(\text{C}_{24}\text{H}_{29}\text{N}_6\text{O}_2)(\text{N}_3)_2]_2(\text{ClO}_4)_2 \cdot 3\text{MeCN}$, has previously been published by McKee and coworkers⁹³. The published structure crystallised in the triclinic spacegroup $P\bar{1}$ with $R1 = 0.0667$. The published structure was crystallised from an acetonitrile solution by vapour diffusion of diethylether and the complex prepared here was crystallised from a DMF solution by vapour diffusion

of diethylether and was found to crystallise with two uncoordinated molecules of DMF, however the structures of the cations are similar.

The $[\text{Mn}_2(\text{HL1})(\text{N}_3)_2]_2^{2+}$ cation is broadly similar to the structure of $[\text{Mn}_2(\text{HL1})(\text{Cl})_2]_2(\text{ClO}_4)_2$. As before, the macrocycle binds two Mn(II) ions and the molecule is dimeric with two macrocyclic units linked by the bridging azide ligands forming a tetramanganese system. Each macrocycle is mono deprotonated with the hydrogen freely refined on O1 and symmetry generated on O1A under $-x+1, -y+1, -z+4$ and so hydrogen bonds exist between the alcohol groups of the adjacent macrocycles. The hydrogen bonding as illustrated in Figure 2-11 appears different to that for the previous complex which is shown in Figure 2-8, this is because second macrocyclic unit is symmetry generated for the complex described here.

Each manganese ion is seven-coordinate with pentagonal bipyramidal geometry. Selected bond lengths and angles are shown in Table 5 below.

Table 5 -Selected bond lengths [\AA] and angles [$^\circ$] for $[\text{Mn}_2(\text{HL1})(\text{N}_3)_2]_2(\text{ClO}_4)_2 \cdot 2\text{DMF}$

N(1)–Mn(1)	2.3079(14)	N(2)–Mn(1)	2.2430(14)
N(3)–Mn(1)	2.2962(13)	Mn(1)–O(2)	2.2587(11)
Mn(1)–N(8)	2.2803(14)	Mn(1)–O(1)	2.2883(11)
Mn(1)–N(11)	2.3127(15)	Mn(1)–Mn(2)	3.1122(4)
O(2)–Mn(2)	2.2514(11)	N(4)–Mn(2)	2.2736(14)
N(5)–Mn(2)	2.2407(15)	N(6)–Mn(2)	2.2705(13)
Mn(2)–O(1)	2.2775(11)	Mn(2)–N(11)	2.3209(15)
Mn(2)–N(8A)	2.3223(14)	N(8)–Mn(2A)	2.3223(14)

N(2)–Mn(1)–O(2)	141.71(5)	N(2)–Mn(1)–N(8)	95.30(5)
O(2)–Mn(1)–N(8)	91.50(5)	N(2)–Mn(1)–O(1)	140.28(5)
O(2)–Mn(1)–O(1)	77.36(4)	N(8)–Mn(1)–O(1)	88.69(5)
N(2)–Mn(1)–N(3)	69.69(5)	O(2)–Mn(1)–N(3)	72.31(5)
N(8)–Mn(1)–N(3)	107.38(5)	O(1)–Mn(1)–N(3)	145.76(5)
N(2)–Mn(1)–N(1)	69.31(5)	O(2)–Mn(1)–N(1)	148.62(5)
N(8)–Mn(1)–N(1)	88.94(5)	O(1)–Mn(1)–N(1)	71.28(4)
N(3)–Mn(1)–N(1)	136.94(5)	N(2)–Mn(1)–N(11)	98.34(5)
O(2)–Mn(1)–N(11)	79.36(5)	N(8)–Mn(1)–N(11)	166.12(5)
O(1)–Mn(1)–N(11)	79.18(5)	N(3)–Mn(1)–N(11)	79.95(5)
N(1)–Mn(1)–N(11)	93.47(5)	N(2)–Mn(1)–Mn(2)	146.25(4)
O(2)–Mn(1)–Mn(2)	46.27(3)	N(8)–Mn(1)–Mn(2)	118.41(4)
O(1)–Mn(1)–Mn(2)	46.88(3)	N(3)–Mn(1)–Mn(2)	99.45(4)
N(1)–Mn(1)–Mn(2)	107.29(4)	N(5)–Mn(2)–O(2)	142.67(5)
N(5)–Mn(2)–N(6)	69.48(5)	O(2)–Mn(2)–N(6)	146.29(5)
N(5)–Mn(2)–N(4)	70.05(5)	O(2)–Mn(2)–N(4)	72.63(5)
N(6)–Mn(2)–N(4)	137.03(5)	N(5)–Mn(2)–O(1)	139.43(5)
O(2)–Mn(2)–O(1)	77.73(4)	N(6)–Mn(2)–O(1)	72.21(5)
N(4)–Mn(2)–O(1)	150.21(5)	N(5)–Mn(2)–N(11)	106.63(5)
O(2)–Mn(2)–N(11)	79.33(5)	N(6)–Mn(2)–N(11)	80.39(5)
N(4)–Mn(2)–N(11)	97.95(5)	O(1)–Mn(2)–N(11)	79.23(5)
N(5)–Mn(2)–N(8A)	91.75(5)	O(2)–Mn(2)–N(8A)	87.96(5)
N(6)–Mn(2)–N(8A)	103.91(5)	N(4)–Mn(2)–N(8A)	91.11(5)
O(1)–Mn(2)–N(8A)	84.80(5)	N(11)–Mn(2)–N(8A)	161.35(5)
Mn(1)–N(11)–Mn(2)	84.39(5)	Mn(1)–N(8)–Mn(2A)	127.76(6)

Symmetry operations for equivalent atoms A $-x+1, -y+1, -z+4$

The pentagonal plane contains three nitrogen atoms from a pyridinediimine unit with a bite angle of $136.94(5)^\circ$ (for N3–Mn1–N1) and $137.03(5)^\circ$ (for N6–Mn2–N4) and two oxygen donors from the macrocycle. The coordination sphere is completed by two exogenous bridging azide ligands, one in the axial position bridging the two macrocyclic units, and a further axial azide ligand which bridges the two manganese ions within the macrocyclic unit. The bridge angles between the manganese centres

within the macrocyclic units are considerably smaller [Mn1-N11-Mn2, 84.38(5)] than the equivalent bridge angles which link the macrocyclic units [Mn1-N8-Mn2, 127.76(6)] and all equivalent bridging angles are larger than those observed for the complex $[\text{Mn}_2(\text{HL1})(\text{Cl})_2]_2(\text{ClO}_4)_2$. The bond distances observed for the bridge angles between the manganese centres within the macrocyclic units are 2.3127(15) Å for Mn1-N11, and 2.3209(15) Å Mn2-N11. The bond distances observed for the equivalent bridge angles which link the macrocyclic units are 2.2803(14) Å for Mn1-N8, and 2.3223(14) Å for Mn2-N8A.

The principal interaction of adjacent layers is the π - π stacking between the pyridine diimine head units of two adjacent molecules, this is observed between the overlapping sections as illustrated in Figure 2-12 below.

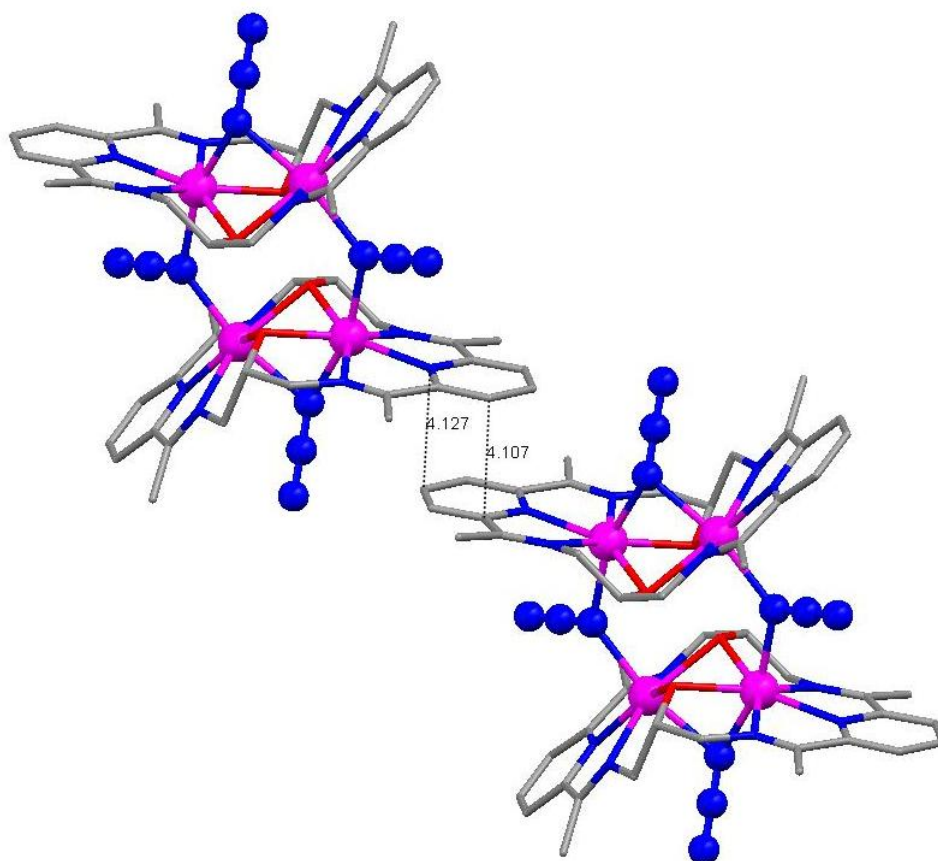


Figure 2-12 – π - π stacking of $[\text{Mn}_2(\text{HL1})(\text{N}_3)_2]_2^{2+}$

The centroid - centroid distance is 4.106 Å and the centroid of the ring is 3.439(1) Å from the mean plane of the second ring on the adjacent molecule under symmetry

operation $-x+2, -y+1, -z+4$. The π - π stacking continues between adjacent molecules of the complex and can be seen in the packing diagram as viewed down the a axis shown in Figure 2-13. The packing diagram in Figure 2-13 as viewed down the a axis illustrates how the molecules pack as sheets through π - π interactions on adjacent molecules.

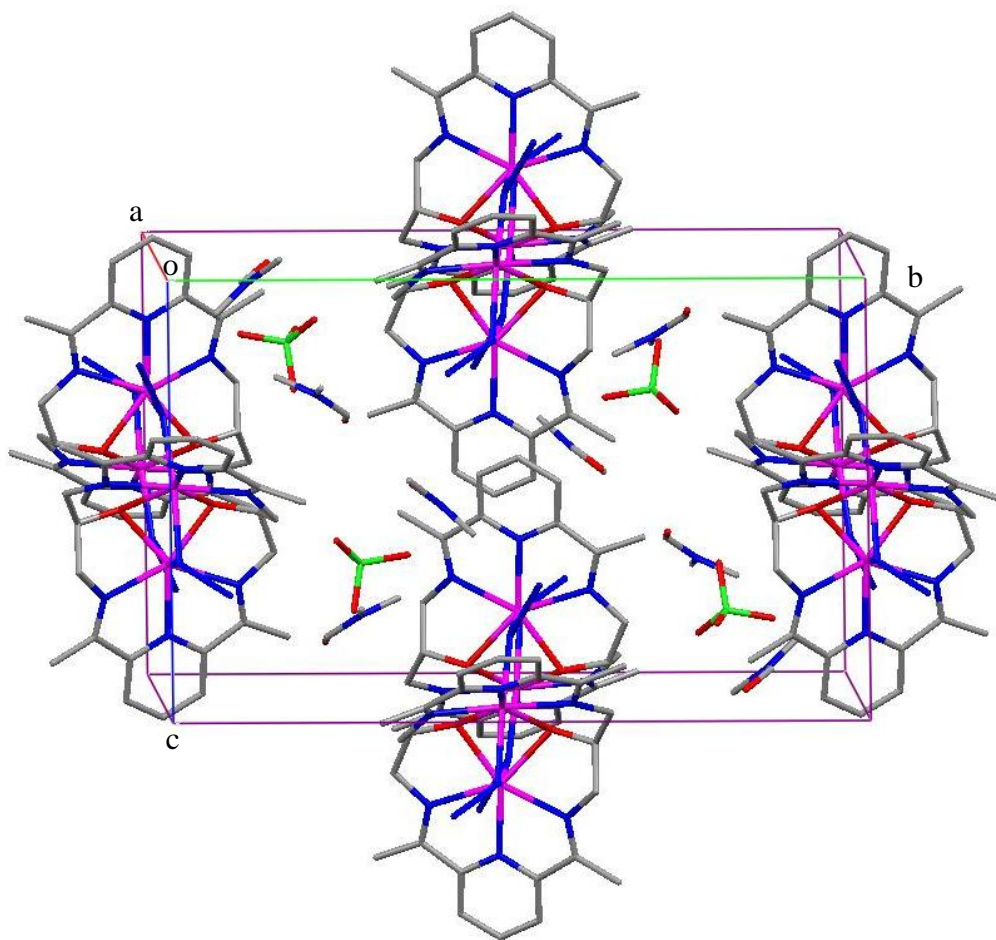


Figure 2-13 – Packing diagram for $[Mn_2(HL_2)(N_3)_2]_2(ClO_4)_2 \cdot 2DMF$ as viewed down the a axis

2.2.5 $[\text{Mn}_5(\text{L1})_2(\text{OAc})_2(\text{DMF})_2](\text{ClO}_4)_4 \cdot 4\text{DMF}$

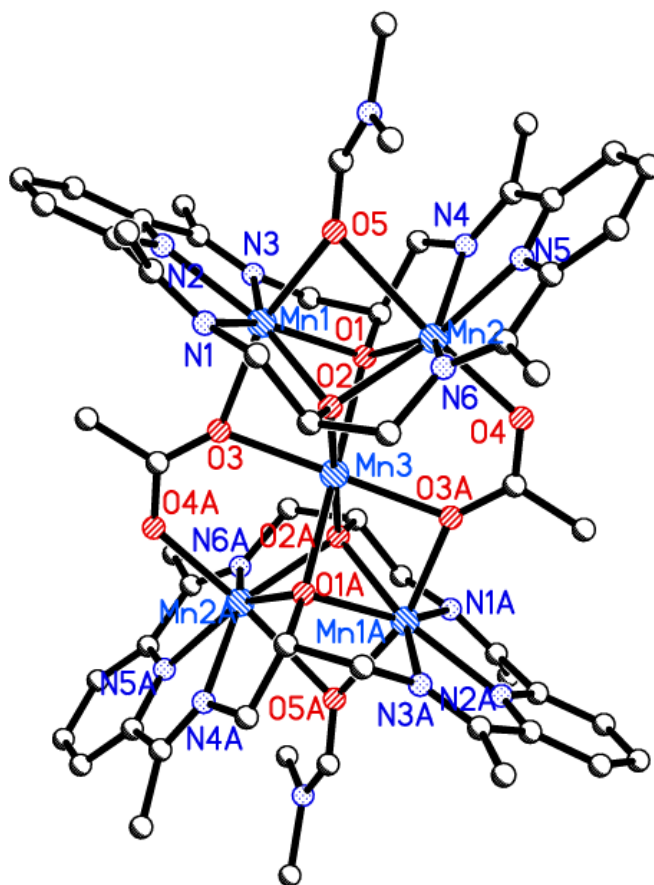


Figure 2-14 – Structure of $[\text{Mn}_5(\text{L1})_2(\text{OAc})_2(\text{DMF})_2]^{2+}$ with perchlorate anions, hydrogens and DMF solvate molecules omitted for clarity

Orange crystals of the complex $[\text{Mn}_5(\text{L1})_2(\text{OAc})_2(\text{DMF})_2](\text{ClO}_4)_4 \cdot 4\text{DMF}$ were obtained by slow diffusion of ether into a DMF solution of the complex, and the structure of $[\text{Mn}_5(\text{L1})_2(\text{OAc})_2(\text{DMF})_2]^{2+}$ is illustrated in Figure 2-14, this complex crystallised in the triclinic space group $P\bar{1}$ with $R1 = 0.0679$, details of the crystal structure and refinement can be found in Table 25 in appendix 1.

A similar structure $[\text{Mn}_5(\text{L1})(\text{OAc})_2(\text{ClO}_4)_2](\text{ClO}_4)_2 \cdot 2\text{H}_2\text{O}$, has previously been published by McKee and co-workers,⁹⁴ but is a different solvate to the one described here. The published structure crystallised in the monoclinic space group $P2_1/c$ with $R1 = 0.0816$.

The pentanuclear cation $[\text{Mn}_5(\text{L1})_2(\text{OAc})_2(\text{DMF})_2]^{2+}$ is centrosymmetric with two binuclear manganese macrocyclic units bridged by a central 6-coordinate manganese ion and two acetate groups. Selected bond lengths and angles for $[\text{Mn}_5(\text{L1})_2(\text{OAc})_2(\text{DMF})_2](\text{ClO}_4)_4 \cdot 4\text{DMF}$ are given in Table 6 below.

Table 6 - Selected bond lengths (Å) and bond angles (°) for $[\text{Mn}_5(\text{L1})_2(\text{OAc})_2(\text{DMF})_2](\text{ClO}_4)_4 \cdot 4\text{DMF}$

Mn(1)–N(2)	2.199(7)	Mn(1)–O(1)	2.205(5)
Mn(1)–O(3)	2.213(5)	Mn(1)–O(2)	2.222(5)
Mn(1)–N(3)	2.255(6)	Mn(1)–N(1)	2.254(6)
Mn(1)–O(5)	2.286(5)	Mn(1)–Mn(3)	3.0163(13)
O(1)–Mn(2)	2.199(5)	O(1)–Mn(3)	2.214(5)
N(4)–Mn(2)	2.257(6)	N(5)–Mn(2)	2.220(6)
N(6)–Mn(2)	2.260(6)	Mn(2)–O(4)	2.130(6)
Mn(2)–O(2)	2.190(5)	Mn(2)–Mn(3)	3.2245(12)
O(2)–Mn(3)	2.132(5)	O(3)–Mn(3)	2.207(5)

N(2)–Mn(1)–O(1)	144.4(2)	N(2)–Mn(1)–O(3)	104.4(2)
O(1)–Mn(1)–O(3)	83.15(19)	N(2)–Mn(1)–O(2)	146.2(2)
O(1)–Mn(1)–O(2)	69.06(18)	O(3)–Mn(1)–O(2)	79.45(18)
N(2)–Mn(1)–N(3)	71.0(3)	O(1)–Mn(1)–N(3)	74.4(2)
O(3)–Mn(1)–N(3)	89.3(2)	O(2)–Mn(1)–N(3)	142.7(2)
N(2)–Mn(1)–N(1)	72.4(3)	O(1)–Mn(1)–N(1)	141.5(2)
O(3)–Mn(1)–N(1)	100.1(2)	O(2)–Mn(1)–N(1)	73.9(2)
N(3)–Mn(1)–N(1)	143.4(3)	N(2)–Mn(1)–O(5)	91.5(2)
O(1)–Mn(1)–O(5)	87.98(19)	O(3)–Mn(1)–O(5)	162.6(2)
O(2)–Mn(1)–O(5)	83.37(19)	N(3)–Mn(1)–O(5)	102.7(2)
N(1)–Mn(1)–O(5)	77.8(2)		

During synthesis of the complex $[\text{Mn}_5(\text{L1})_2(\text{OAc})_2(\text{DMF})_2](\text{ClO}_4)_4 \cdot 4\text{DMF}$, the transmetallation reaction is carried out with a ligand to manganese ratio of 1:2.5 respectively which enables the macrocycle to form as a pentanuclear complex rather

than a tetranuclear complex, this would not be expected to form as a pentanuclear complex with MnCl_2 as the manganese salt due to the nature of the bonding involved. Acetate salts in methanol are sensitive to how the solution is treated and in turn affects how the transmetallation product forms.⁹⁴

Each oxygen atom of a carboxylate ion has two electron pairs, the one directed away from the R group is called the syn pair and the other is referred to as anti. Carboxylate ions can bind using either syn-syn or syn-anti binding modes, as illustrated in Figure 2-15 below⁹⁵⁻⁹⁷

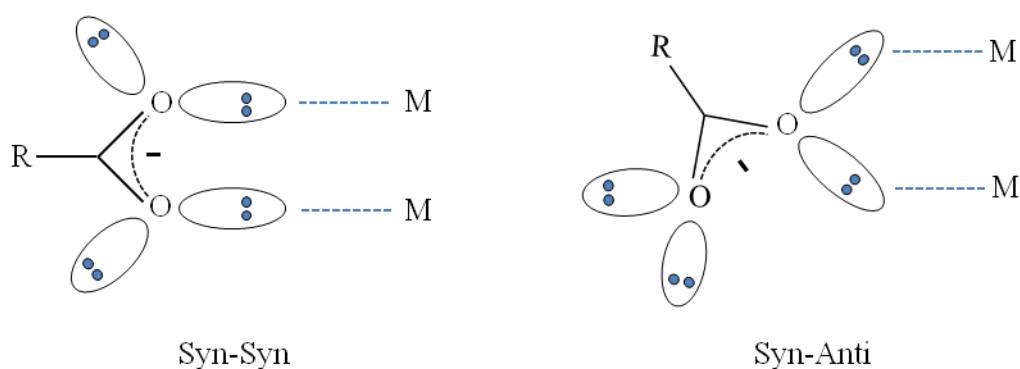


Figure 2-15 – *Different binding modes for carboxylate ligands*

The binding mode of the acetate ligands in the pentanuclear complex described here is classified as syn-(syn, anti), this is because there is both three atom and single atom bridging modes displayed. Firstly, Mn2 and Mn3 are linked by a three atom bridge but Mn3 and Mn1 are bridged by a single oxygen atom from the acetate ligand

The cation consists of two dinuclear macrocyclic units that are bridged by a six coordinate octahedral manganese atom and two supporting acetate groups. The diimine section of the macrocycle contains a slightly larger angle of $143.4(3)^\circ$ (for N3–Mn1–N1) than that observed for $[\text{Mn}_2(\text{HL1})(\text{Cl})_2]_2^{2+}$ and $[\text{Mn}_2(\text{HL1})(\text{N}_3)_2]_2^{2+}$, which is due to the two oxygen donors within the macrocycle binding to the central manganese ion. The central manganese is bonded to the two alkoxide oxygen donors from each macrocyclic unit and two oxygen donors from the bridging acetate

ligands. Bridging of the two manganese ions within the macrocyclic unit occurs via the oxygen of a DMF molecule used as a solvent for the recrystallisation. Acetate axial ligands bridge the two macrocyclic units with one oxygen bridging the central manganese ion and one manganese ion from one macrocyclic unit, the other oxygen binds to a manganese ion in the corresponding macrocyclic unit.

The principal interaction between adjacent molecules is π - π stacking between the pyridinediimine head units of two adjacent cations. The π - π stacking occurs due to the nature of the packing of molecules within a crystal lattice. This is observed between the overlapping adjacent sections as illustrated in Figure 2-16 below.

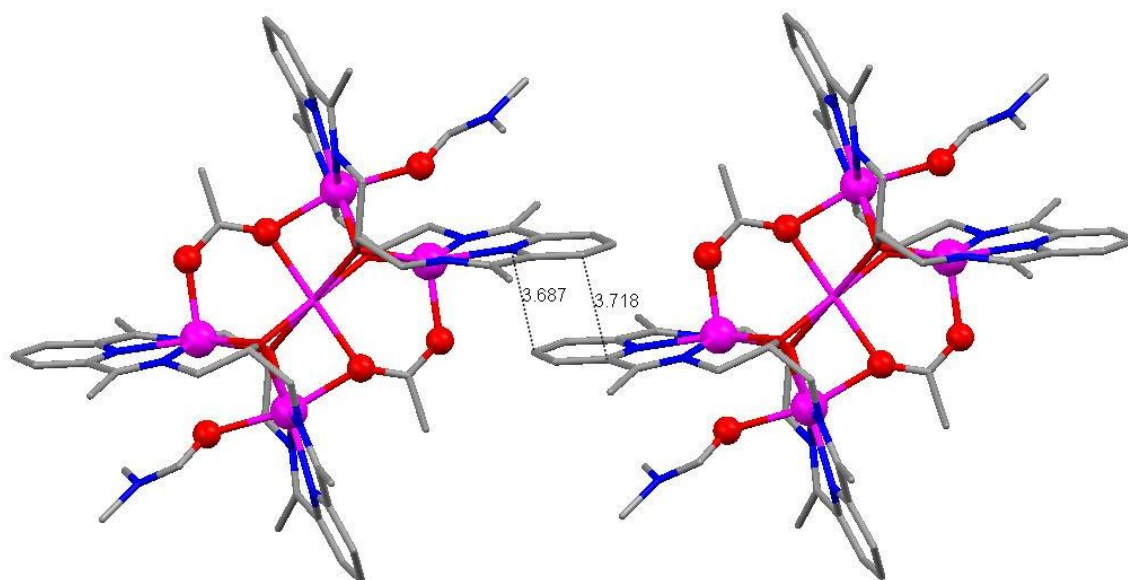


Figure 2-16 – π - π Stacking in $[Mn_5(LI)(OAc)_2(DMF)_2]^{2+}$

The centroid - centroid distance of the two rings is 3.704 Å and the centroid of the ring is 3.247(1) Å from the mean plane of the second ring on the adjacent molecule under symmetry operation $-x-1, -y+1, -z-1$. The π - π stacking continues between adjacent molecules of the complex and the π - π stacking can be seen in the packing diagram as viewed down the a axis shown in Figure 2-17.

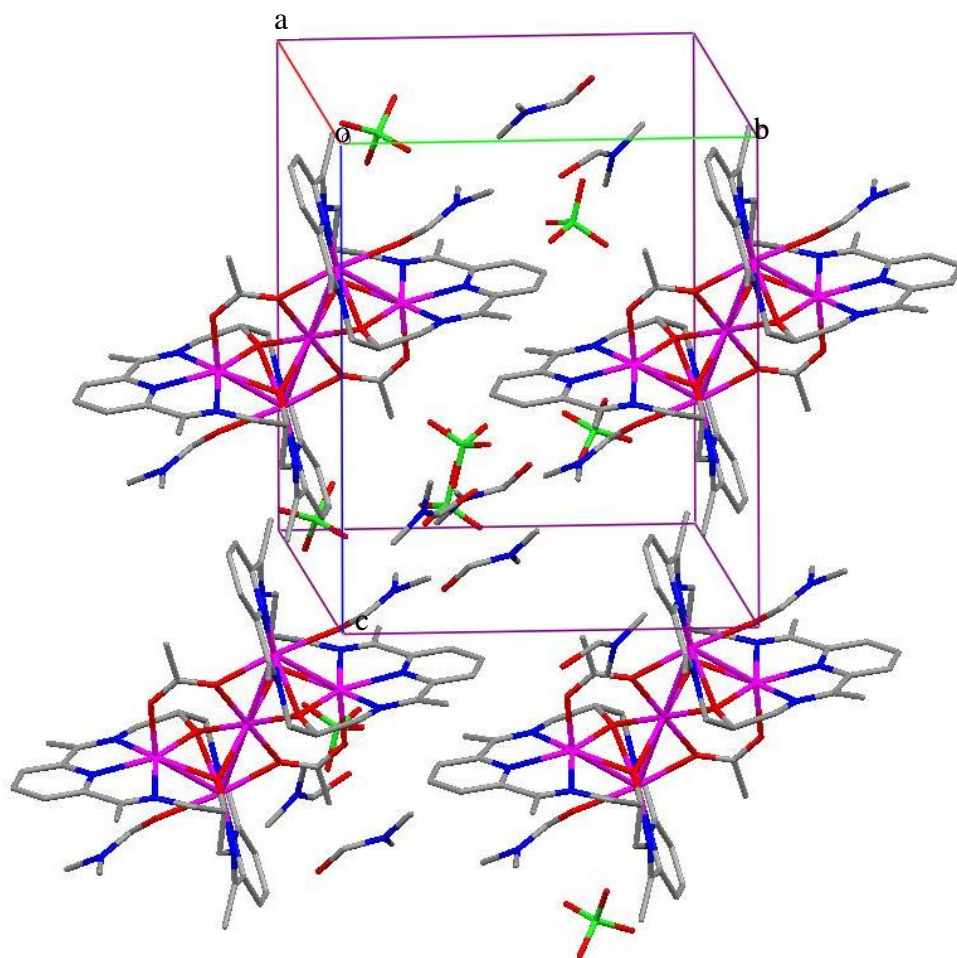


Figure 2-17 - Packing diagram for $[Mn_5(L1)(OAc)_2(DMF)_2](ClO_4)_4 \cdot 4DMF$ as viewed down the *a* axis

The packing diagram for $[Mn_5(L1)(OAc)_2(DMF)_2](ClO_4)_4 \cdot 4DMF$ as viewed down the *a* axis and shown in Figure 2-17 illustrates how the molecules pack through π - π interactions on adjacent molecules. This diagram has been extended downwards to illustrate the additional π - π stacking interactions that occur between the pyridyl head units of adjacent molecules.

2.2.6 $[\text{Mn}_2(\text{RedHL1})(\text{Cl})_2]_2[\text{MnCl}_4]\cdot 4\text{DMF}\cdot \text{EtOH}$

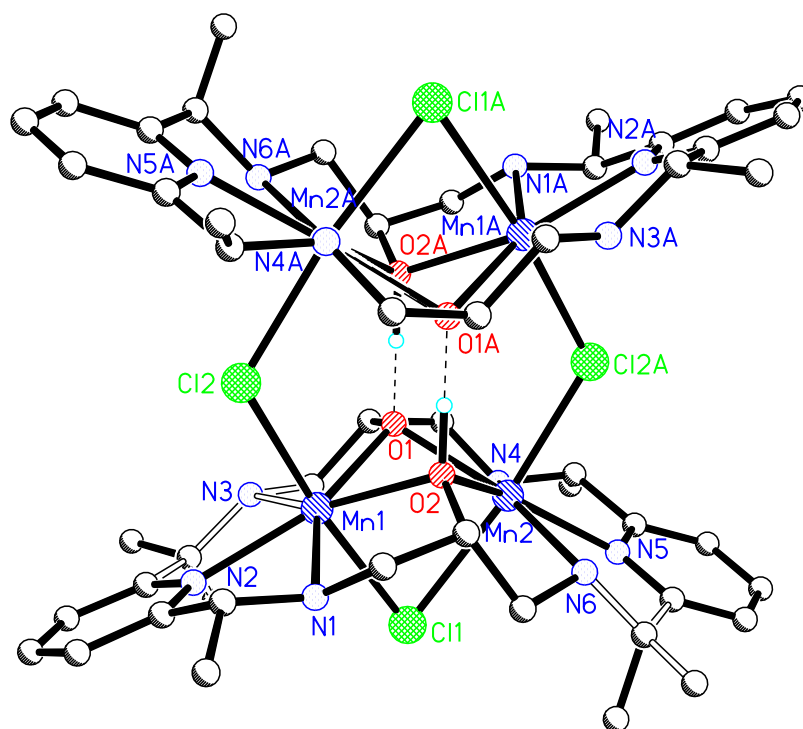


Figure 2-18 – Structure of $[\text{Mn}_2(\text{RedHL1})(\text{Cl})_2]_2^{2+}$ with the $[\text{MnCl}_4]^{2-}$ anion, hydrogens and solvent molecules omitted for clarity. Dashed lines represent hydrogen bonding

The complex $[\text{Mn}_2(\text{RedHL1})(\text{Cl})_2]_2\text{MnCl}_4\cdot 4\text{DMF}\cdot \text{EtOH}$ crystallised in the triclinic space group $P\bar{1}$ with $R = 0.0659$. The crystal structure of the $[\text{Mn}_2(\text{RedHL1})(\text{Cl})_2]_2^{2+}$ cation is illustrated in Figure 2-18. Data were collected using synchrotron radiation at Daresbury Laboratory SRS Station 9.8.⁹⁸ Details of the crystal structure and refinement can be found in Appendix 1.

The $[\text{Mn}_2(\text{RedHL1})(\text{Cl})_2]_2^{2+}$ cation was formed by reaction of the reduced ligand (RedHL1) with MnCl_2 in a methanol solvent under reflux. Each macrocycle binds two Mn(II) ions and the cation is dimeric with the two macrocyclic units linked by bridging chloride ions thus creating a tetramanganese system. During the synthesis of the molecule, there is a mono deprotonation of the macrocycles with the hydrogen freely refined on O2 and symmetry generated on O2A. The hydrogen bonding as

illustrated in Figure 2-18 appears different to that in $[\text{Mn}_2(\text{HL1})(\text{Cl})_2]_2^{2+}$ as illustrated Figure 2-8, the hydrogens presented here are positioned differently due to centrosymmetry within the molecule, here the second macrocyclic unit is symmetry generated. Selected bond lengths and angles for $[\text{Mn}_2(\text{RedHL1})(\text{Cl})_2]_2[\text{MnCl}_4].4\text{DMF.MeOH}$ are illustrated in Table 7 below:

Table 7 - Selected bond lengths (Å) and bond angles (°) for $[\text{Mn}_2(\text{RedHL1})(\text{Cl})_2]_2[\text{MnCl}_4].4\text{DMF.MeOH}$

Mn(1)–N(2)	2.259(5)	Mn(2)–N(5)	2.264(5)
Mn(1)–O(2)	2.290(3)	Mn(2)–O(2)	2.306(3)
Mn(1)–N(1)	2.336(5)	Mn(2)–Cl(1)	2.6553(16)
Mn(1)–Cl(1)	2.6419(17)	Mn(2)–N(4)	2.327(5)
Mn(1)–O(1)	2.260(4)	Mn(2)–N(6)	2.308(5)
Mn(1)–N(3)	2.327(5)	Mn(2)–Cl(2A)	2.5293(15)
Mn(1)–Cl(2)	2.5410(16)	N(1)–C(2)	1.461(7)
Mn(1)–Mn(2)	3.1900(11)	C(8)–N(3)	1.468(9)

N(2)–Mn(1)–O(1)	144.88(17)	N(4)–Mn(2)–Cl(1)	87.90(13)
O(1)–Mn(1)–O(2)	71.99(12)	Cl(1)–Mn(1)–Mn(2)	53.16(4)
O(1)–Mn(1)–N(3)	72.59(16)	O(1)–Mn(2)–N(6)	143.59(15)
N(2)–Mn(1)–N(1)	69.45(18)	O(1)–Mn(2)–O(2)	72.35(12)
O(2)–Mn(1)–N(1)	73.97(13)	N(6)–Mn(2)–O(2)	71.64(14)
N(2)–Mn(1)–Cl(2)	87.96(14)	N(5)–Mn(2)–N(4)	69.9(2)
O(2)–Mn(1)–Cl(2)	88.88(10)	O(2)–Mn(2)–N(4)	146.69(17)
N(1)–Mn(1)–Cl(2)	92.10(12)	N(5)–Mn(2)–Cl(2A)	89.00(13)
O(1)–Mn(1)–Cl(1)	83.16(10)	O(2)–Mn(2)–Cl(2A)	90.65(9)
N(3)–Mn(1)–Cl(1)	87.49(15)	O(1)–Mn(2)–Cl(1)	83.52(10)
Cl(2)–Mn(1)–Cl(1)	173.67(5)	N(6)–Mn(2)–Cl(1)	87.78(12)
N(2)–Mn(1)–O(2)	143.13(17)	O(1)–Mn(2)–N(5)	144.40(18)
N(2)–Mn(1)–N(3)	72.4(2)	N(5)–Mn(2)–N(6)	71.79(19)
O(2)–Mn(1)–N(3)	144.40(17)	N(5)–Mn(2)–O(2)	143.25(18)
O(1)–Mn(1)–N(1)	145.33(14)	O(1)–Mn(2)–N(4)	74.61(16)
N(3)–Mn(1)–N(1)	140.40(18)	N(6)–Mn(2)–N(4)	140.44(18)
O(1)–Mn(1)–Cl(2)	93.62(11)	O(1)–Mn(2)–Cl(2A)	90.58(10)
N(3)–Mn(1)–Cl(2)	96.77(15)	N(6)–Mn(2)–Cl(2A)	95.01(13)
N(2)–Mn(1)–Cl(1)	97.82(14)	N(4)–Mn(2)–Cl(2A)	93.83(13)
O(2)–Mn(1)–Cl(1)	84.94(10)	N(5)–Mn(2)–Cl(1)	97.78(13)
N(1)–Mn(1)–Cl(1)	87.53(13)	O(2)–Mn(2)–Cl(1)	84.33(9)
Cl(2)–Mn(1)–Mn(2)	121.01(4)	Cl(2A)–Mn(2)–Cl(1)	173.19(6)
Mn(1)–Cl(1)–Mn(2)	74.06(4)	Mn(2A)–Cl(2)–Mn(1)	118.43(5)

Symmetry operations for equivalent atoms A $-x+1, -y+1$

The pentagonal plane of the macrocycle contains three nitrogen atoms from the head unit with a bite angle of $140.40(18)^\circ$ (for N3–Mn1–N1) and $140.44(18)$ (for N6–Mn2–N4). The bridging angles between the manganese ions in one macrocyclic unit, are considerably smaller $74.06(4)^\circ$ (for Mn1–Cl1–Mn2) than the equivalent bridge angles for the chloride ions which bridge the two macrocyclic units $118.43(5)^\circ$ (for Mn2A–Cl2–Mn1). These angles are slightly larger than those observed for the complex $[\text{Mn}_2(\text{HL1})(\text{Cl})_2]_2(\text{ClO}_4)_2$. Bond distances observed for the manganese ions that are bridged within the macrocyclic unit are $2.6419(17)$ Å for Mn1–Cl1, and

2.6553(16) Å for Mn2–Cl11. The bond distances observed for the bridges that link the macrocyclic units are 2.5410(16) Å for Mn1–Cl12, and 2.5293(15) Å for Mn2–Cl12A.

Positional disorder exists about two of the methyl groups of the head unit where reduction of the imine bond has taken place. These were modelled with a 70:30 occupancy of the two positions.

The principal interaction between adjacent molecules is the π - π stacking that is present between the pyridinediimine head units of two adjacent cations, this is observed between the overlapping sections as illustrated in Figure 2-19 below. The centroid - centroid distance is 3.597 Å and the centroid of the ring is 3.396(1) Å from the mean plane of the second ring on the adjacent molecule under symmetry operation $-x, -y+1, -z$.

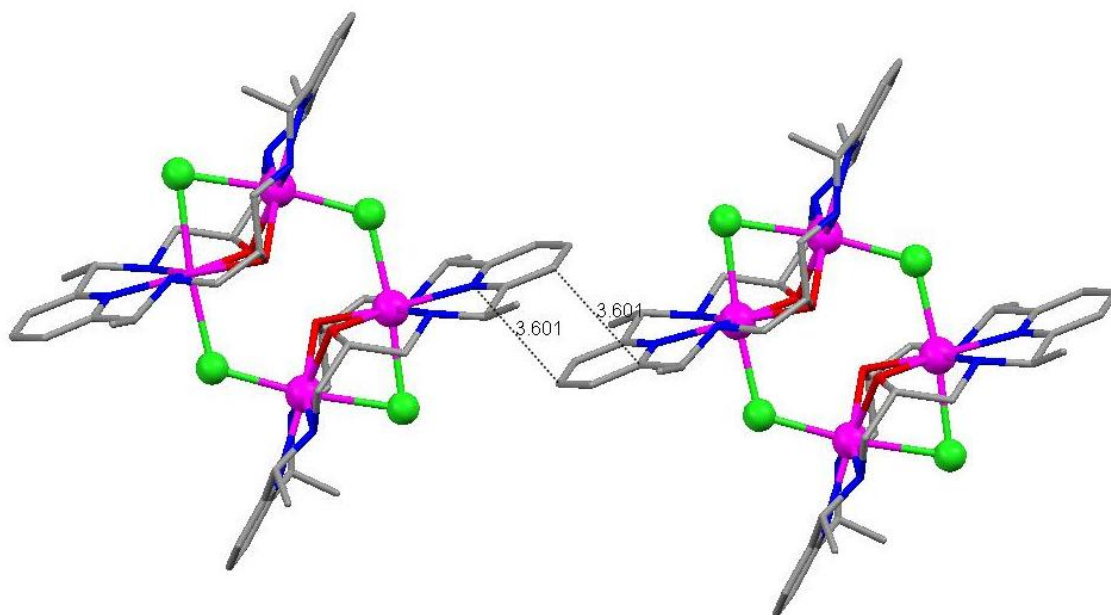


Figure 2-19 – π - π stacking for $[Mn_2(\text{RedHL1})(Cl)_2]_2^{2+}$

The packing diagram for $[Mn_2(\text{RedHL1})(Cl)_2]_2[MnCl_4] \cdot 4DMF \cdot MeOH$ as viewed down the b axis shown below in Figure 2-20.

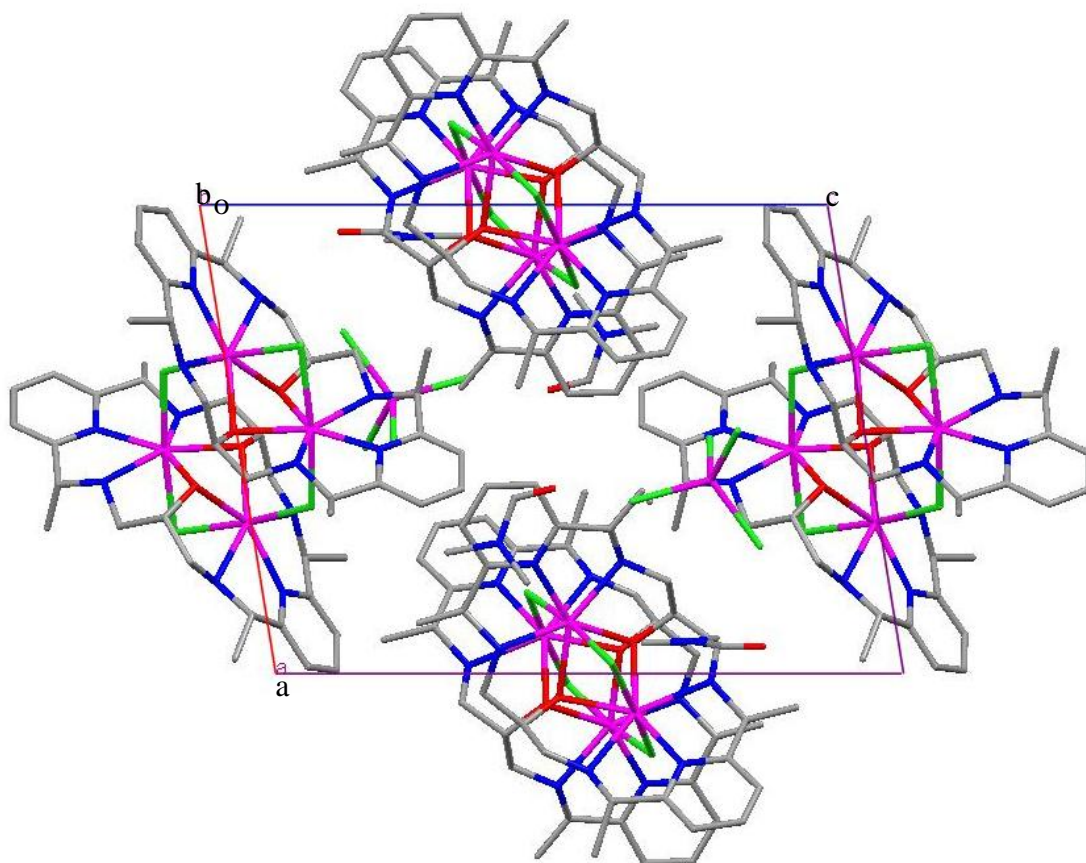


Figure 2-20 – Packing diagram for $[Mn_2(RedHL1)(Cl)_2]_2[MnCl_4].4DMF.MeOH$

The packing diagram as viewed down the b axis is shown in Figure 2-20, this diagram illustrates how the complex $[Mn_2(RedHL1)(Cl)_2]_2[MnCl_4].4DMF.MeOH$ packs with π - π stacking.

The complex $[Mn_2(RedHL1)(N_3)_2]_2(ClO_4)_2$ was also prepared with corresponding data obtained in both elemental analysis and FAB mass spectroscopy. IR analysis showed no $\nu_{(C=N)}$ stretch and a strong $\nu_{(N_3)}$ at 2050 cm^{-1} , however no crystals were analysed under single crystal X-ray diffraction. Despite varying conditions for crystal growth, the crystals of this complexes did not form.

2.2.7 Complexes of H₄L2

The [4+4] macrocycle H₄L2 shown in Figure 2-21 was prepared via Schiff base reaction of 2,6-diacetylpyridine with 1,3-diamino-2-hydroxypropane using manganese(II) perchlorate as a direct template, this was carried out by refluxing overnight in a methanolic solvent. This method has previously been published and the structure reported by McKee *et al.*^{99, 100} During the synthesis of the complexes of H₄L2, an orange solid formed in solution. The solid product was collected via filtration from the cooled reaction vessel and good analysis was obtained for the complexes of H₄L2.

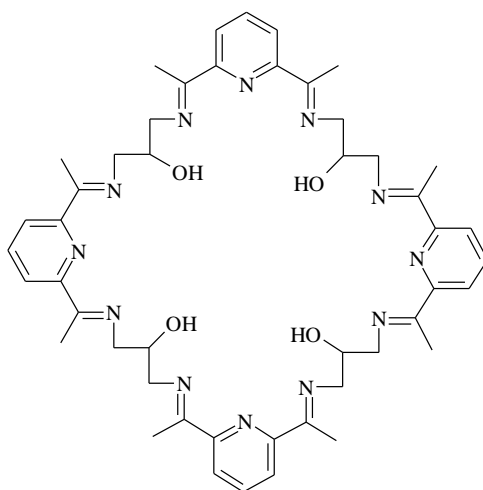
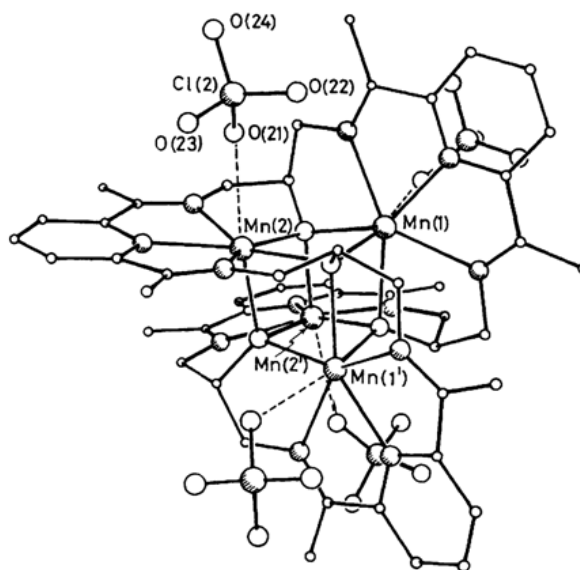


Figure 2-21 – H₄L2 Ligand

The crystal structure as published by McKee *et al.*⁹⁹ is illustrated below in Figure 2-22.



Taken from reference⁹⁹

Figure 2-22–Structure of $[Mn_4L_2](ClO_4)_4$

The published structure as shown in Figure 2-22 crystallised in the monoclinic space group $C2/c$ with $R1 = 0.043$. The $[Mn_4L_2]^{4+}$ cation contains a crystallographic 2-fold axis which passes through the cubane core of the molecule. All four alcohol groups were found to be deprotonated and each one bridges three manganese centres forming a cubane structure. Each manganese centre is seven coordinate with pentagonal bipyramidal geometry. The perchlorate anions are likely to be semi coordinated due to the long distances observed.

McKee *et al.*⁹⁹ initially showed a synthesis for the [4+4] complex by preparation of a barium precursor, followed by a transmetallation with manganese perchlorate. A possible route was proposed for the formation of the [4+4] complex as shown in Figure 2-23.

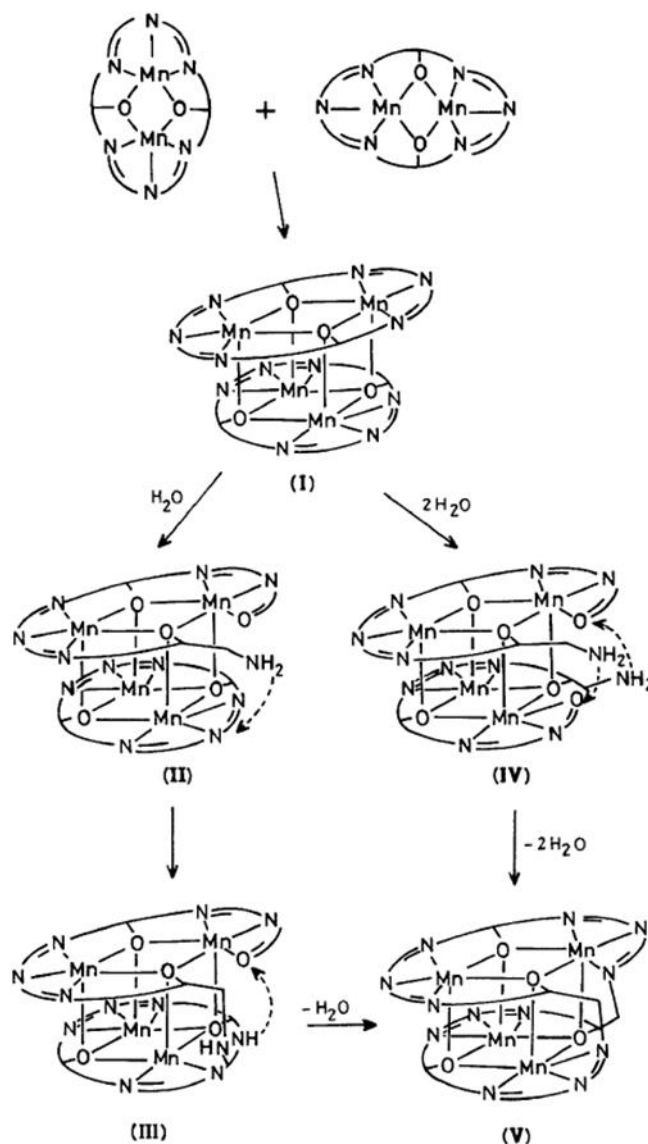


Figure 2-23 – Possible route for the formation of a [4+4] complex of L2

The reason that a [4+4] complex is able to form in this instance, is due to the lack of strongly bound axial ligands, this allows the formation of four Mn-alkoxide bonds during the transmetallation reaction. These four bonds then hold the ligands in an orientation which favours the [4+4] macrocycle.

In the scheme shown in Figure 2-23, Mn-alkoxide bonds can be formed between two of the binuclear macrocyclic units which are in a cofacial orientation (I) resulting in a cubane core. Transamination reactions occur via hydrolysis of the imine bond which results in the formation of (II) after which, the resulting terminal amine is free to rotate and can add at an imine which is on the second macrocycle *via* nucleophilic

attack at the carbon atom (III). One C-N bond then breaks to either reform (II) or leaving a new intermolecular imine link and releasing another free amine which is involved in a Schiff base reaction with the free carbonyl to form (V).⁹⁹

2.3 Macrocyclic ring contractions

The [2+2] macrocycle L3 shown in Figure 2-24 can be prepared via Schiff base template condensation as previously seen for ligand L1 but with the use of DFP as the head unit in place of DAP. The DFP head unit undergoes a condensation reaction with 1,3-diamino-2-hydroxypropane, utilising a Ba²⁺ ion^{1,92}. The barium macrocycle acts as a precursor for a transmetallation reaction in order to synthesise various manganese macrocycles with differing axial ligands.

For the ring contracted species, there is a nucleophilic attack at one of the imine bonds of H₂L3 from the OH group of the alcohol solvent used.

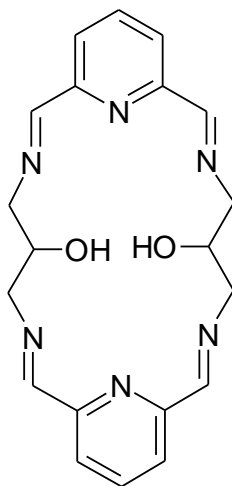


Figure 2-24– *Ligand H₂L3*

Ring contraction of the H₂L3 ligands forms the H₂L4 ligand as illustrated in Figure 2-25:

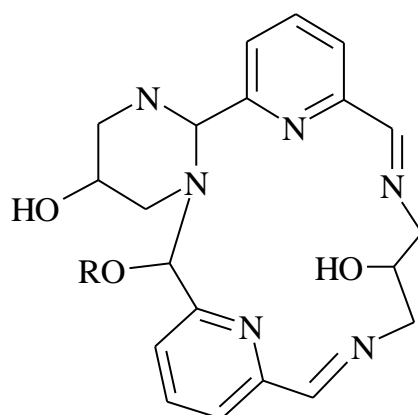


Figure 2-25 – Ring contracted ligand *H₂L4*

Each macrocycle was analysed using IR, elemental analysis and mass spectrometry and where possible, X-ray analysis was performed. The IR data were initially used to confirm the absence of an amine or carbonyl stretch associated with the reactant materials and the presence of an imine bond at $1637 - 1654 \text{ cm}^{-1}$. A band at $1586 - 1592 \text{ cm}^{-1}$ is associated with the pyridyl ring of the two head units.

2.3.1 [Mn(H₂L4)(NCS)₂].MeOH.DMF

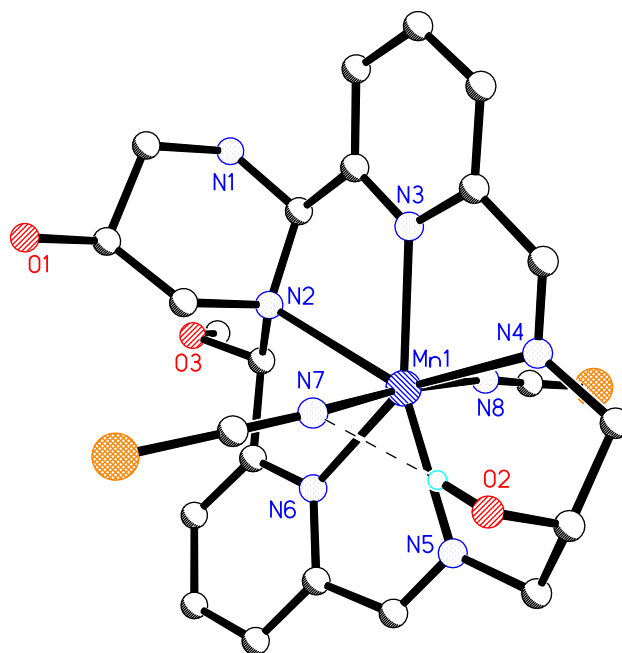


Figure 2-26 –Structure of [Mn(H₂L4)(NCS)₂].MeOH.DMF with solvate molecule and hydrogens omitted for clarity. Dashed line represents hydrogen bonding

Large yellow crystals of the complex shown in Figure 2-26 were obtained from a solution prepared by Soraya Sanchez-Ballester as part of an Erasmus project. Data were collected using synchrotron radiation at Daresbury Laboratory SRS Station 9.8.⁹⁸ [Mn(H₂L4)(NCS)₂].MeOH.DMF crystallised in the triclinic space group $P\bar{1}$ with $R1 = 0.0564$. The details of the crystal structure and refinement can be found in Table 28 of appendix 1.

The complex [Mn(H₂L4)(NCS)₂].MeOH.DMF was prepared *via* transmetallation of the precursor [Ba(H₂L3)(ClO₄)₂](ClO₄)₂. During this reaction, the macrocycle has undergone a ring contraction via nucleophilic attack from a solvent methanol molecule at one of the imine bonds, forming a six-membered ring that sits in a chair conformation. This process reduces the size of the cavity in the macrocycle and the size of the macrocycle is reduced from a 20 membered macrocycle to a 16 membered macrocycle, thus the ligand is a modified form that is derived from the complex

[Ba(H₂L3)(ClO₄)₂](ClO₄)₂. The mechanism for the ring contraction is given in Figure 2-27 below:

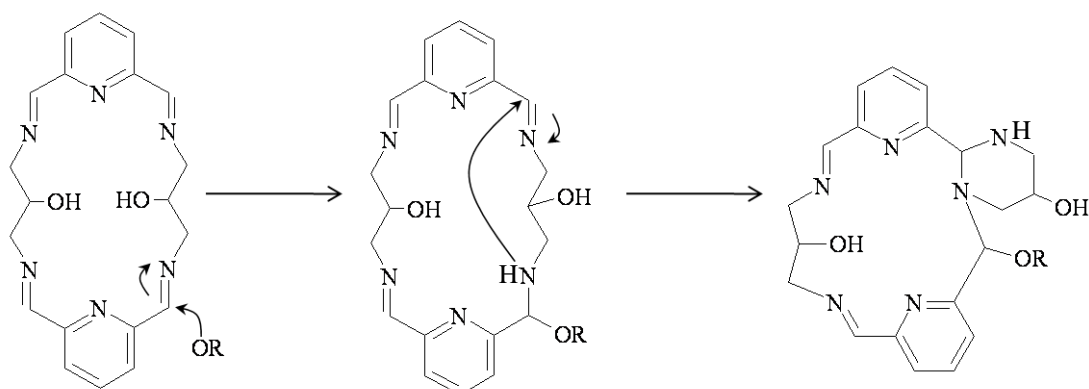


Figure 2-27 – Ring contraction mechanism

The molecule contains one seven coordinate manganese ion that is bound to five nitrogen donors from the macrocycle forming a pentagonal bipyramidal geometry, with two nitrogen bound thiocyanate axial ligands. The selected bond lengths and angles are given in Table 8 below:

Table 8 - Selected bond lengths [Å] and angles [°] for [Mn(H₂L4)(NCS)₂].MeOH.DMF

Mn(1)–N(8)	2.178(3)	Mn(1)–N(7)	2.237(3)
Mn(1)–N(6)	2.263(3)	Mn(1)–N(3)	2.274(3)
Mn(1)–N(4)	2.343(3)	Mn(1)–N(5)	2.425(3)
Mn(1)–N(8)	2.178(3)	Mn(1)–N(7)	2.237(3)

N(8)–Mn(1)–N(7)	174.80(12)	N(8)–Mn(1)–N(6)	86.89(11)
N(7)–Mn(1)–N(6)	90.54(11)	N(8)–Mn(1)–N(3)	92.16(11)
N(7)–Mn(1)–N(3)	92.81(11)	N(6)–Mn(1)–N(3)	136.58(11)
N(8)–Mn(1)–N(4)	94.16(11)	N(7)–Mn(1)–N(4)	85.93(11)
N(6)–Mn(1)–N(4)	151.37(11)	N(3)–Mn(1)–N(4)	72.02(10)
N(8)–Mn(1)–N(5)	94.34(12)	N(7)–Mn(1)–N(5)	80.53(11)
N(6)–Mn(1)–N(5)	70.35(11)	N(3)–Mn(1)–N(5)	152.68(10)
N(4)–Mn(1)–N(5)	81.05(11)	N(8)–Mn(1)–N(6)	86.89(11)
N(8)–Mn(1)–N(7)	174.80(12)		

The angle $72.02(10)^\circ$ for N3–Mn1–N4, is slightly larger than that observed for the manganese bound pyridine diimine sections for non contracted species of H₂L1, and is closer to the ideal angle of 72° for a pentagonal bipyramidal geometry. The bond length $2.570(6) \text{ \AA}$ for Mn1–N2, which is the nitrogen that has formed part of the six membered ring but remains bound to the manganese centre, is longer than all other Mn-donor bond lengths within the molecule.

There is some hydrogen bonding present within the molecule observed between the alcohol group from O2 and N7 of the nitrogen bound axial thiocyanate molecule, this hydrogen bond is illustrated in Figure 2-26.

The principal interaction of adjacent layers is the π - π stacking that is present between the pyridine diimine units of two adjacent molecules under symmetry operation $-x+3, -y+2, -z$. The π - π stacking is illustrated below in Figure 2-28.

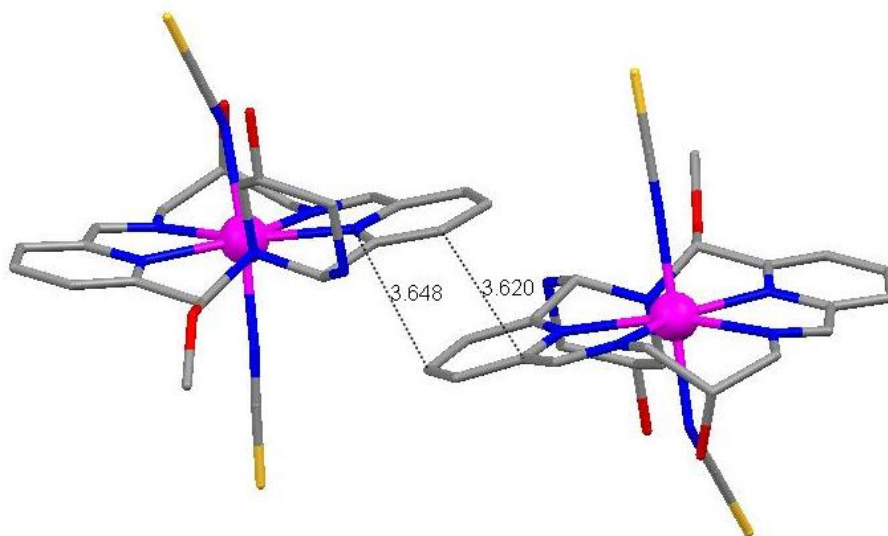


Figure 2-28 - π - π stacking for $[Mn(H_2LA)(NCS)_2].MeOH.DMF$

The centroid – centroid distance for the overlapping sections of the π - π stacking between the pyridyl head units is 3.585 Å.

2.4 Dinuclear complexes

2.4.1 $[\text{Mn}_2(\text{L6})(\text{NCS})_4] \cdot 2\text{DMF}$

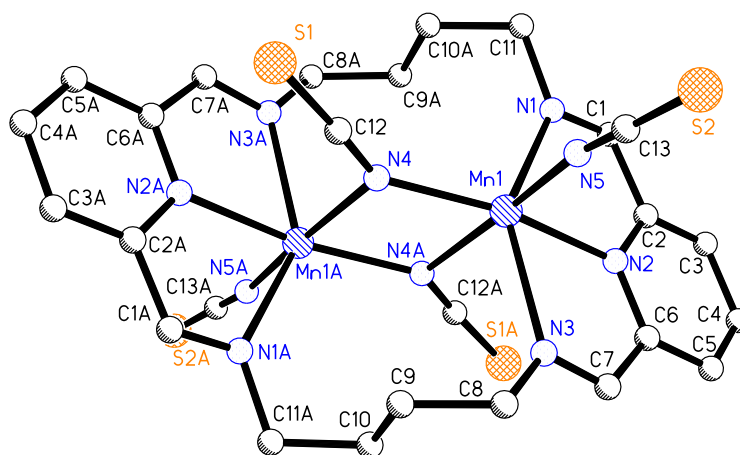


Figure 2-29 –Structure of $[\text{Mn}_2(\text{L6})(\text{NCS})_4]$ with solvent molecules and hydrogens omitted for clarity

The complex $[\text{Mn}_2(\text{L6})(\text{NCS})_4]$ was prepared via transmetallation of the barium precursor $[\text{Ba}(\text{L6})(\text{ClO}_4)_2]$ with manganese perchlorate in a 1:2 ratio followed quickly with the addition of excess sodium thiocyanate. The solution was stirred in methanol at room temperature overnight, during which time, a colour change was observed from clear to orange, with some orange solid present. Large orange crystals of $[\text{Mn}_2(\text{L6})(\text{NCS})_4] \cdot 2\text{DMF}$ were obtained via slow diffusion of ether into a DMF solution of redissolved clean product. The details of the crystal structure and refinement can be found in Table 30 in appendix 1. A similar structure with the formula $[\text{Mn}_2(\text{L6})(\text{NCS})_3(\text{CH}_3\text{O})]$ has previously been reported for this ligand system by McKee and coworkers¹⁰¹ and is available on the crystallographic structural database (CSD). The published structure was found to crystallise in the monoclinic spacegroup $P2_1/a$ with $R1 = 0.0452$. The published structure differs where one of the bridging thiocyanate ligands has been replaced by a μ -methoxy ligand.

The structure as illustrated in Figure 2-29 crystallised in the triclinic space group $P\bar{1}$ with $R1 = 0.0320$.

The $[\text{Mn}_2(\text{L6})(\text{NCS})_4]$ complex is centrosymmetric, and contains two equivalent manganese ions that are six coordinate, they are bound to three nitrogen atoms from the pyridinediimine head units of the macrocycle, a nitrogen atom from the terminal axial thiocyanate ligands and two from the bridging nitrogen bound thiocyanate ligands. The selected bond lengths and angles for $[\text{Mn}_2(\text{L6})(\text{NCS})_4] \cdot 2\text{DMF}$ are given in Table 9 below:

Table 9 - Selected bond lengths [\AA] and angles [$^\circ$] for $[\text{Mn}_2(\text{L6})(\text{NCS})_4] \cdot 2\text{DMF}$

Mn(1)–N(4)	2.091(7)	Mn(1)–N(5)	2.125(9)
Mn(1)–N(2)	2.204(10)	Mn(1)–N(1)	2.347(9)
Mn(1)–N(3)	2.371(9)		

N(4)–Mn(1)–N(5)	99.6(3)	N(4)–Mn(1)–N(2)	161.9(3)
N(5)–Mn(1)–N(2)	98.5(3)	N(4)–Mn(1)–N(1)	108.3(4)
N(5)–Mn(1)–N(1)	94.7(3)	N(2)–Mn(1)–N(1)	70.5(7)
N(4)–Mn(1)–N(3)	109.3(4)	N(5)–Mn(1)–N(3)	87.4(3)
N(2)–Mn(1)–N(3)	71.0(7)	N(1)–Mn(1)–N(3)	141.4(5)
Mn(1)–N(4)–Mn(1A)	105.7(3)		

Symmetry operations for equivalent atoms A $-x+1, -y, -z+1$

The macrocyclic ligand is stepped to allow bridging of the manganese centres and the manganese separation of 3.540 \AA (for Mn1-Mn1A) is slightly longer than that of the published structure $[\text{Mn}-\text{Mn}', 3.418 \text{\AA}]$. The angle of the thiocyanate bridge was found to be $105.7(3)^\circ$ (for Mn1–N4–Mn1A). The pyridinediimine head unit sits with a bite angle of $141.4(5)^\circ$ (for N1–Mn1–N3) which is just slightly larger than the equivalent unit for the reported structure of $140.5(2)^\circ$. There remains two uncoordinated DMF solvent molecules for the structure reported here.

The principal interaction between molecules of $[\text{Mn}_2(\text{L6})(\text{NCS})_4]$ is the π - π stacking that is present between the pyridine diimine units of two adjacent molecules as illustrated in Figure 2-30 below.

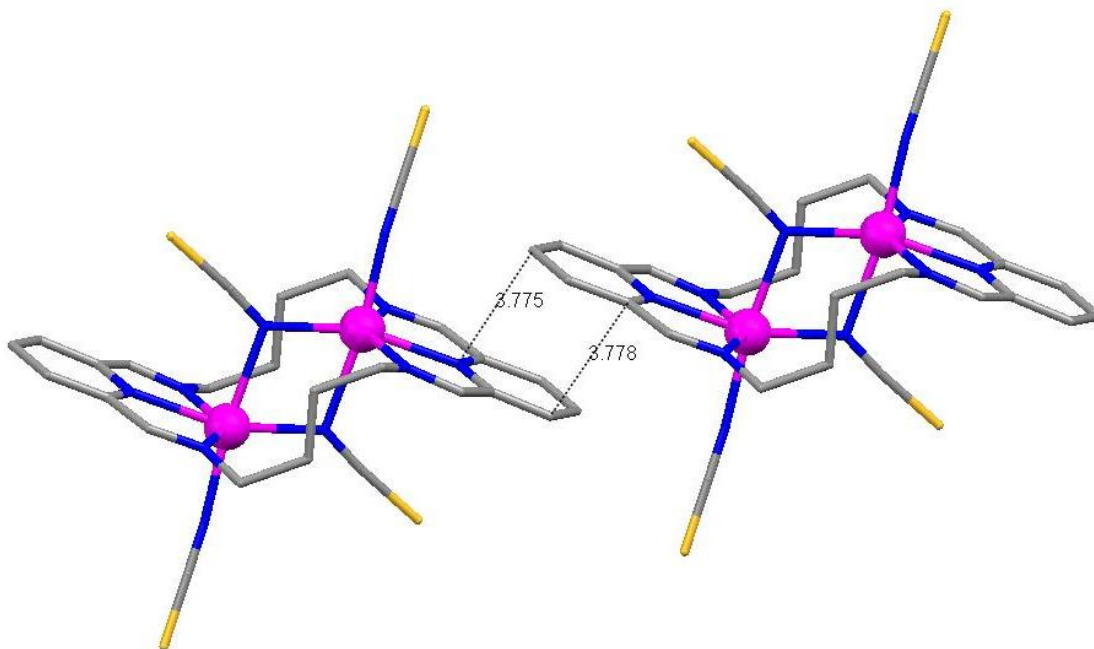


Figure 2-30 – π - π stacking for $[\text{Mn}_2(\text{L6})(\text{NCS})_4]$

The centroid - centroid distance is 3.771 Å and the centroid of the ring is 3.371(1) Å from the mean plane of the second ring under symmetry operation $-x + 1, -y + 1, -z + 1$.

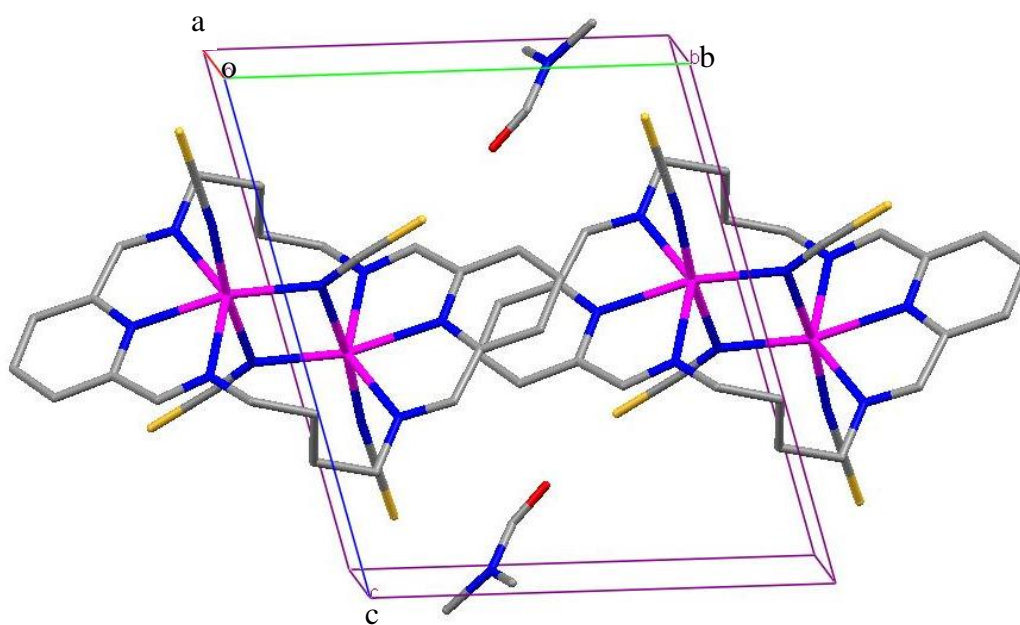


Figure 2-31 – Packing diagram for $[\text{Mn}_2(\text{L6})(\text{NCS})_4]$ as viewed down the a axis

The diagram in Figure 2-31 shows how molecules of the complex $[\text{Mn}_2(\text{L6})(\text{NCS})_4] \cdot 2\text{DMF}$ are packed as viewed down the a axis, with the main π - π stacking interaction between molecules of $[\text{Mn}_2(\text{L6})(\text{NCS})_4]$.

2.4.2 [Pb₂(L8)(NCS)₄]

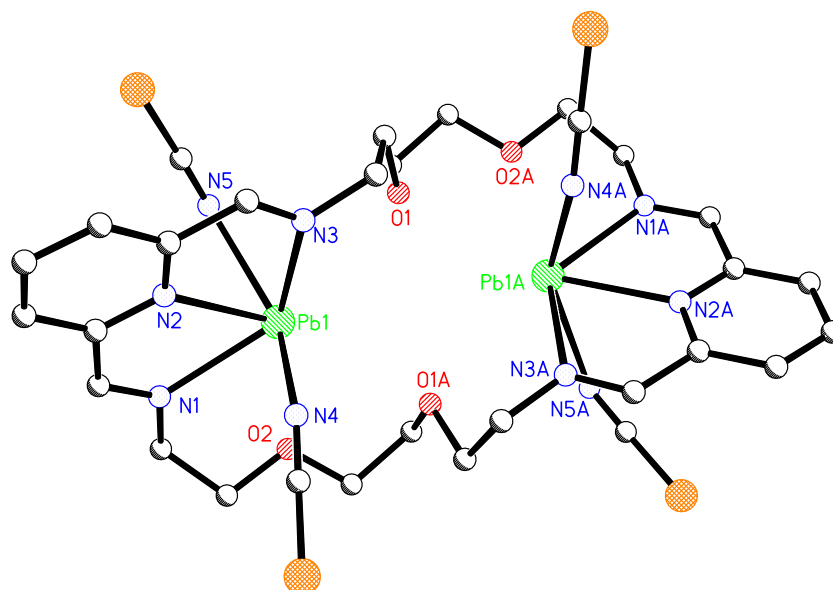


Figure 2-32 –Structure of [Pb₂(L8)(NCS)₄] with hydrogens omitted for clarity

Large yellow crystals of the complex shown in Figure 2-32 were obtained from a solution prepared by Rebecca Dennet in preparation for a transmetalation reaction with manganese as part of a BSc honours project. [Pb₂(L8)(NCS)₄] crystallised in the orthorhombic space group *pbcn* with R1 = 0.0276. The details of the crystal structure and refinement can be found in Table 31 in Appendix 1.

A similar structure which differs where the head units were formed from diacetyl pyridine have previously been published by Drew *et al.*¹⁹ which crystallised in the orthorhombic space group *pnca* with R1 = 0.087. The published structure contains a 30 membered macrocycle with a 2 fold axis that is non planar. The Pb ion was found to bond to three nitrogen atoms [2.54(3), 2.56(3), 2.47(2) Å] and two oxygen atoms [2.96(3), 2.88(3) Å] from the macrocycle.

The structure obtained here as shown in Figure 2-32 also contains a thirty membered macrocycle that is non planar and consists of two pyridine diimine head units with a total of six nitrogen donor atoms and four oxygen donor molecules along the length

of the macrocycle. Selected bond lengths and angles for the structure described are shown in Table 10 below:

Table 10 - Selected bond lengths [Å] and angles [°] for [Pb₂(L8)(NCS)₄]

N(1)–Pb(1)	2.562(3)	N(2)–Pb(1)	2.536(3)
N(3)–Pb(1)	2.622(3)	Pb(1)–N(4)	2.497(3)
Pb(1)–N(5)	2.708(3)		

N(4)–Pb(1)–N(2)	74.76(10)	N(4)–Pb(1)–N(1)	83.74(11)
N(2)–Pb(1)–N(1)	63.84(9)	N(4)–Pb(1)–N(3)	80.86(11)
N(2)–Pb(1)–N(3)	63.37(9)	N(1)–Pb(1)–N(3)	127.16(9)
N(4)–Pb(1)–N(5)	148.49(10)	N(2)–Pb(1)–N(5)	74.31(9)
N(1)–Pb(1)–N(5)	88.06(9)	N(3)–Pb(1)–N(5)	80.09(9)

The Pb(II) ion was found to bond to the three nitrogen atoms of the pyridine diimine section with 2.562(3) Å (for N1–Pb1), 2.536(3) Å (for N2–Pb1) and 2.622(3) Å (for N3–Pb1) which are similar equivalent bond lengths for the published structure.

There are two Pb metal ions coordinated to the macrocycle with each ion bound to the nitrogens of the pyridine diimine head unit providing an angle of 127.16(9) ° (for N1–Pb1–N3). Each metal ion is bound to a thiocyanate molecule both above and below the plane of the macrocycle with an angle of 148.49(10)°. The structure published by Drew *et al*, show that the Pb molecules are sulphur bound to the thiocyanate molecules [2.91(2) and 3.00(2) Å and with Pb-S-C angles of 102° and 104°]. The structure described here shows that the Pb atoms are nitrogen bound to the axial thiocyanate ligands with bond lengths of 2.497(3) Å (for Pb1–N4) and 2.708(3) Å (for Pb1–N5) with Pb-N-C angles of 149.78° and 122.64°.

2.5 [1+1] Mononuclear complexes

Low molecular weight seven coordinate manganese complexes are of interest for their potential use as working antioxidants, here, a range of [1+1] mononuclear complexes were synthesised in good yield using a Schiff base condensation reaction with manganese as a direct template. These were carried out utilising either a 2,6-diacetylpyridine or 2,6-diformyl pyridine head unit and variations in axial ligand. Infrared analysis was initially used to confirm the presence of an imine bond presenting a sharp peak at 1637 to 1648 cm^{-1} , and a disappearance of a carbonyl stretch at $\sim 1700 \text{ cm}^{-1}$, NCS peaks were observed between 2019 to 2057 cm^{-1} and perchlorate peaks were observed at ~ 1088 and 625 cm^{-1} . FAB mass spectroscopy analysis confirmed that the [1+1] reaction had taken place and elemental analysis were carried out for each of the mononuclear complexes. A borohydride reduction reaction was carried out directly on the manganese complexes with very low yield and only one complex $[\text{Mn}(\text{RedL10})(\text{H}_2\text{O})_2](\text{ClO}_4)_2$ provided crystals that were suitable for X-ray analysis.

2.5.1 $[\text{Mn}(\text{L9})(\text{OH}_2)_2](\text{ClO}_4)_2$

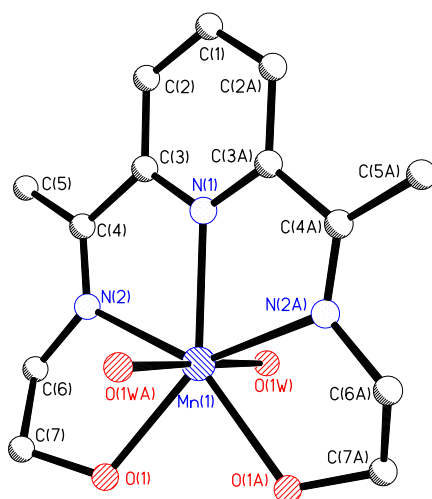


Figure 2-33 – Structure of $[\text{Mn}(\text{L9})(\text{OH}_2)_2]^{2+}$ with perchlorate anions and hydrogens omitted for clarity

Large orange crystals of $[\text{Mn}(\text{L9})(\text{OH}_2)_2](\text{ClO}_4)_2$ crystallised in the monoclinic spacegroup $C2/c$ with $R1 = 0.0343$. The details of the crystal structure and refinement can be found in Table 32 in Appendix 1.

The crystal structure has previously been published by McKee and co workers.¹⁰² The published structure was also found to crystallise in the monoclinic spacegroup $C2/c$ with $R = 0.064$

There is a crystallographic two fold axis passing through Mn1-N1 and C1. The crystal structure of $[\text{Mn}(\text{L9})(\text{OH}_2)_2]^{2+}$ as illustrated in Figure 2-33 contains a single seven-coordinate manganese ion that is coordinated to the N_3O_2 donor set of the ligand which forms a pentagonal plane, two exogenous water molecules are bound to the manganese in the axial positions in preference to the perchlorate anions which remain uncoordinated.

Selected bond lengths and angles for $[\text{Mn}(\text{L9})(\text{OH}_2)_2](\text{ClO}_4)_2$ are given in Table 11 below:

Table 11 - Selected bond lengths [\AA] and angles [$^\circ$] for $[\text{Mn}(\text{L9})(\text{OH}_2)_2](\text{ClO}_4)_2$

Mn(1)–O(1WA)	2.2195(12)	Mn(1)–N(1)	2.2613(17)
Mn(1)–O(1)	2.2496(12)	Mn(1)–N(2)	2.2861(12)

O(1WA)–Mn(1)–O(1W)	179.06(7)	O(1WA)–Mn(1)–O(1)	82.74(5)
O(1W)–Mn(1)–O(1)	96.53(5)	O(1)–Mn(1)–O(1A)	78.12(6)
O(1W)–Mn(1)–N(1)	90.47(4)	O(1)–Mn(1)–N(1)	140.94(3)
O(1WA)–Mn(1)–N(2)	95.64(5)	O(1W)–Mn(1)–N(2)	84.69(5)
O(1)–Mn(1)–N(2)	72.75(5)	O(1A)–Mn(1)–N(2)	146.61(5)
N(1)–Mn(1)–N(2)	69.72(3)	N(2)–Mn(1)–N(2A)	139.43(7)

Symmetry operations for equivalent atoms A $-x, y, -z+1/2$

The manganese ion has approximate pentagonal bipyramidal geometry where the donors of the pentagonal plane are the three nitrogens from the pyridine diimine head unit of the molecule which provides an angle of $139.43(7)^\circ$ (for N2-Mn1-N2A)

resulting in a slight distortion from a regular pentagonal plane of 138° , and two oxygen atoms from the ligand. The axial ligands provide an angle of $179.06(7)^\circ$ (for O1WA–Mn1–O1W) which is slightly bent away from the ideal linear angle of 180° .

The packing diagram for $[\text{Mn}(\text{L9})(\text{OH}_2)_2](\text{ClO}_4)_2$ as viewed down the b axis is shown in Figure 2-34.

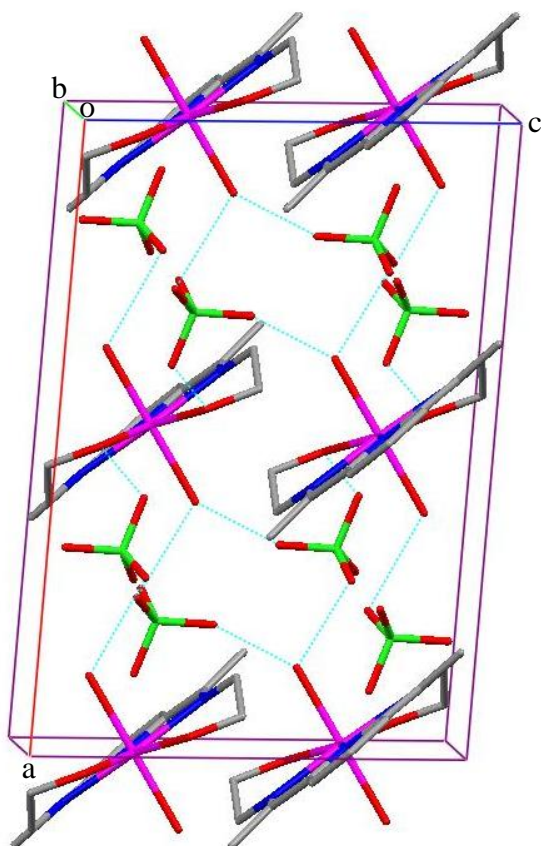


Figure 2-34 – Packing diagram for $[\text{Mn}(\text{L9})(\text{OH}_2)_2](\text{ClO}_4)_2$ as viewed down the b axis

Figure 2-34 shows that the crystals pack as hydrogen bonded sheets, with hydrogen bonds observed between the axial bound water molecules and the unbound perchlorate anions with distances of 2.799 \AA and 2.895 \AA .

2.5.2 [Mn(L9)(Cl)₂]

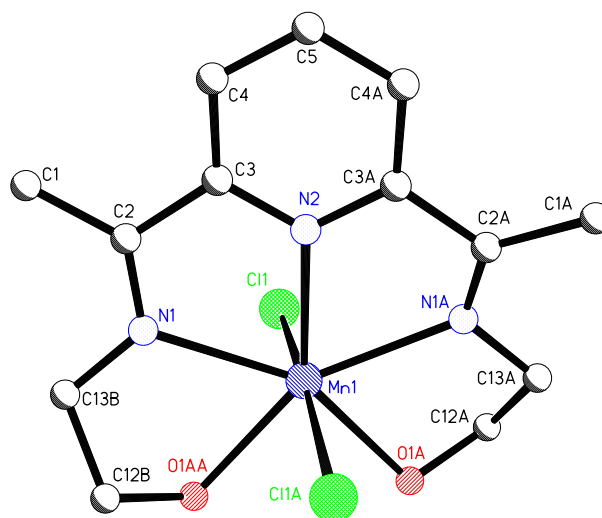


Figure 2-35 –Structure of [Mn(L9)(Cl)₂] with hydrogens omitted for clarity

Large orange crystals of the complex [Mn(L9)(Cl)₂] crystallised in the monoclinic space group *I2/a* with $R_1 = 0.0273$. The details of the crystal structure and refinement can be found in Table 33 in Appendix 1

The crystal structure has previously been published by McKee and co workers.¹⁸ The published structure which was a different solvate to the one described here crystallised in the triclinic space group $P\bar{1}$ with $R_1 = 0.0363$.

There is a crystallographic two fold axis passing through Mn1-N2 and C5. The crystal structure as shown in Figure 2-35 crystallised in the same manner as the complex [Mn(L9)(OH₂)₂](ClO₄)₂ previously described with two exogenous chloride ions bound to the manganese in the axial position in place of water molecules. There are no uncoordinated perchlorate ions for this structure due to the negative charge that is present on the chloride axial ligands.

Selected bond lengths and angles for [Mn(L9)(Cl)₂] are shown in Table 12.

Table 12 - Selected bond lengths [\AA] and angles [$^\circ$] for $[\text{Mn}(\text{L9})(\text{Cl})_2]$

Mn(1)–N(2)	2.2983(15)	Mn(1)–N(1)	2.3445(11)
Mn(1)–O(1A)	2.3736(9)	Mn(1)–Cl(1)	2.4901(3)

N(2)–Mn(1)–N(1)	68.09(3)	N(2)–Mn(1)–O(1A)	138.99(2)
N(1)–Mn(1)–O(1A)	152.84(4)	N(2)–Mn(1)–Cl(1)	95.119(10)
N(1)–Mn(1)–Cl(1)	88.69(3)	O(1A)–Mn(1)–Cl(1)	86.62(2)
Cl(1)–Mn(1)–Cl(1A)	169.762(19)	N(1)–Mn(1)–N(1A)	136.17(6)

Symmetry operations for equivalent atoms A $-x+1, y, -z+3/2$

The nitrogen atoms from the pyridine diimine head unit of the molecule provide an angle of $136.17(6)^\circ$ (for N1–Mn1–N1A) which is slightly smaller than that of the equivalent angle for the water bound complex $[\text{Mn}(\text{L9})(\text{OH}_2)_2](\text{ClO}_4)_2$ described above, the angle results in a slight distortion from a regular pentagonal plane of 138° , the manganese is also bound to the two oxygen atoms of the pentagonal plane from the ligand. The axial ligands provide an angle of $169.762(19)^\circ$ (for Cl1–Mn1–Cl1A) which is slightly bent away from the ideal linear 180° angle and this is more pronounced than that observed for the water bound complex $[\text{Mn}(\text{L9})(\text{OH}_2)_2](\text{ClO}_4)_2$ described above due to the larger radius of the chloride ligand.

Hydrogen bonding of adjacent molecules is present and is illustrated in Figure 2-36.

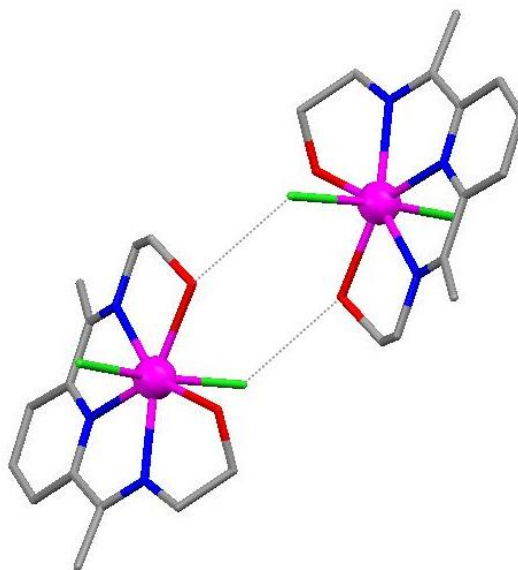


Figure 2-36 – *Hydrogen bonding in [Mn(L9)(Cl)₂].*

The hydrogen bonds exist between O1A within the pentagonal plane of the ligand and the axial ligand Cl1 with a distance of 3.158 Å.

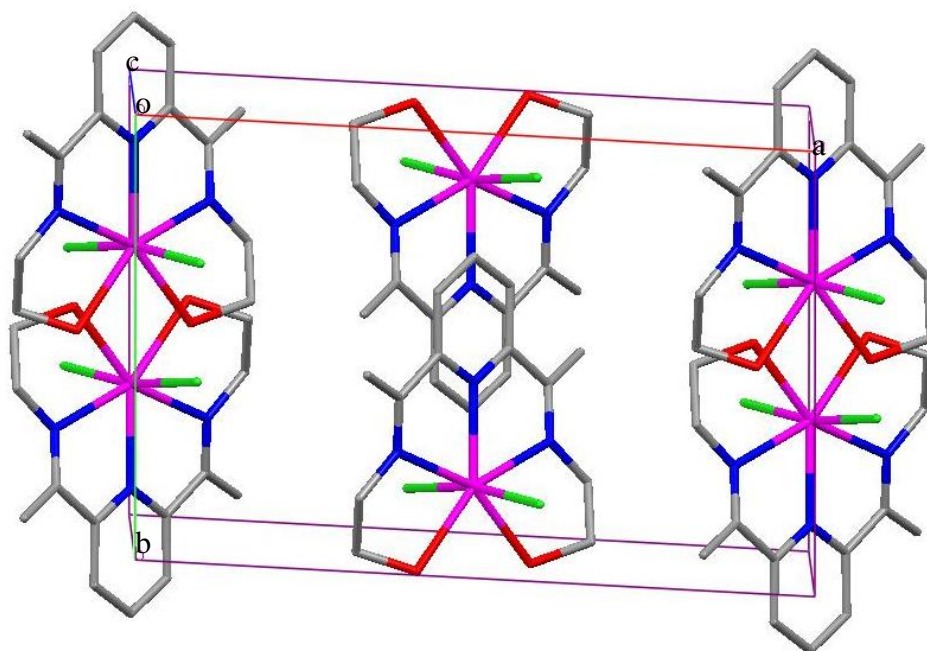


Figure 2-37 – *Packing diagram for [Mn(L9)(Cl)₂] as viewed down the c axis*

The packing diagram for $[\text{Mn}(\text{L9})(\text{Cl})_2]$ illustrated in Figure 2-37 also shows that there is some π - π stacking interactions between the pyridine unit of one molecule with an imine from a second molecule with a distance of 4.145 Å.

2.5.3 $[\text{Mn}(\text{L10})(\text{OH}_2)_2](\text{ClO}_4)_2$

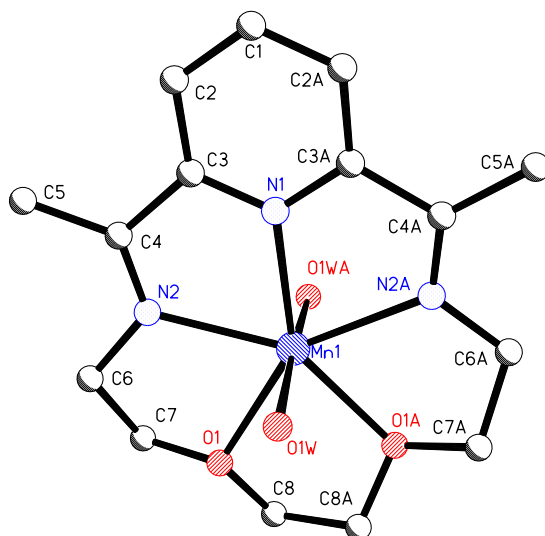


Figure 2-38 –Structure for $[\text{Mn}(\text{L10})(\text{OH}_2)_2]^{2+}$ with perchlorate anions and hydrogens omitted for clarity

Large orange crystals of the complex $[\text{Mn}(\text{L10})(\text{OH}_2)_2](\text{ClO}_4)_2$ were found to crystallise in the monoclinic spacegroup $C2/c$ with $R1 = 0.0320$. The details of the crystal structure and refinement can be found in Table 34 in Appendix 1

The crystal structure of the $[1+1] [\text{Mn}(\text{L10})(\text{OH}_2)_2]^{2+}$ cation as illustrated in Figure 2-38 contains a single seven-coordinate manganese ion that is coordinated to the N_3O_2 donor set of the ligand that forms a pentagonal plane, two exogenous water molecules are bound to the manganese in the axial position in preference to the perchlorate anions which remain uncoordinated to the manganese.

The molecule has a crystallographic 2-fold axis which runs through (Mn1-N1-C1) and the manganese ion has approximate pentagonal bipyramidal geometry where the donors of the pentagonal plane are the three nitrogen atoms from the pyridinediimine

head unit of the molecule. Selected bond lengths and angles for $[\text{Mn}(\text{L10})(\text{OH}_2)_2](\text{ClO}_4)_2$ are given in Table 13:

Table 13 - Selected bond lengths [\AA] and angles [$^\circ$] for $[\text{Mn}(\text{L10})(\text{OH}_2)_2](\text{ClO}_4)_2$

Mn(1)–O(1W)	2.1924(15)	Mn(1)–N(1)	2.211(2)
Mn(1)–N(2)	2.2518(17)	Mn(1)–O(1)	2.2610(15)
C(4)–N(2)	1.272(3)		

O(1W)–Mn(1)–N(1)	93.41(4)	O(1W)–Mn(1)–N(2)	91.92(6)
N(1)–Mn(1)–N(2)	71.03(4)	O(1W)–Mn(1)–O(1)	83.70(6)
N(1)–Mn(1)–O(1)	143.19(4)	N(2)–Mn(1)–O(1)	72.40(6)
O(1WA)–Mn(1)–O(1W)	173.19(9)	N(2A)–Mn(1)–N(2)	142.07(9)

Symmetry operations for equivalent atoms A $-x, y, -z + 1/2$

The pyridine diimine head unit provides an angle of $142.07(9)^\circ$ (for N2A–Mn1–N2) which is slightly larger than that of the equivalent angle for the water bound complex $[\text{Mn}(\text{L9})(\text{OH}_2)_2](\text{ClO}_4)_2$ described above, the angle results in a slight distortion from a regular pentagonal plane of 138° , the manganese is also bound to the two oxygen atoms of the pentagonal plane from the ligand. The axial ligands with an angle of $173.19(9)^\circ$ (for O1WA–Mn1–O1W) are slightly bent away from the ideal linear 180° angle and this is more pronounced than that observed for the water bound complex $[\text{Mn}(\text{L9})(\text{OH}_2)_2](\text{ClO}_4)_2$ described above.

The principal interactions between molecules are the hydrogen bonds which exist between the axial water molecules and the uncoordinated perchlorate anions. The packing diagram for $[\text{Mn}(\text{L10})(\text{OH}_2)_2](\text{ClO}_4)_2$ as viewed down the b axis is shown below in Figure 2-39.

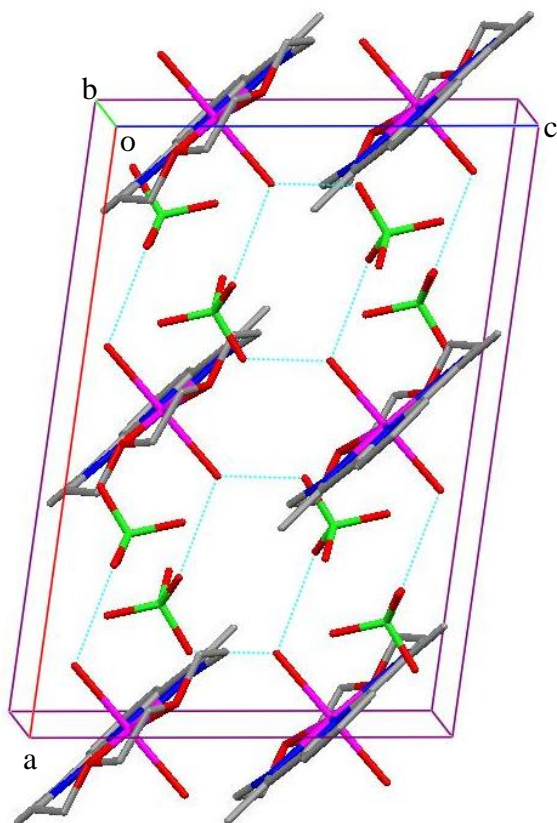


Figure 2-39 – Packing diagram for $[Mn(L10)(OH_2)_2](ClO_4)_2$ as viewed down the *b* axis

Figure 2-39 shows that the crystals pack as hydrogen bonded sheets in a similar fashion to that of the complex $[Mn(L9)(OH_2)_2](ClO_4)_2$, described previously with distances of 2.794 Å and 2.806 Å for the observed hydrogen bonds.

2.5.4 [Mn(RedL10)(OH₂)₂](Cl)₂

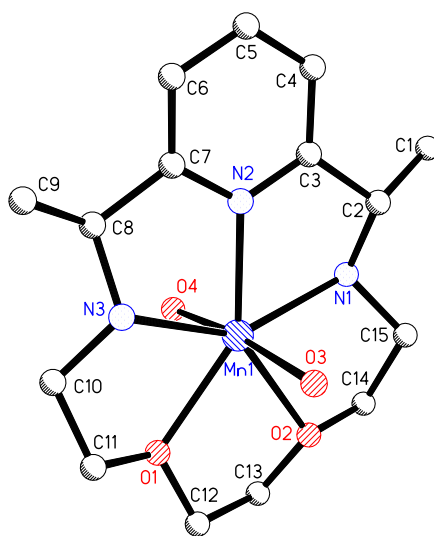


Figure 2-40 – Structure of $[\text{Mn}(\text{RedL10})(\text{OH}_2)_2]^{2+}$ with chloride anions omitted for clarity

The crystal structure of the $[\text{Mn}(\text{RedL10})(\text{OH}_2)_2]^{2+}$ cation is illustrated in Figure 2-40. $[\text{Mn}(\text{RedL10})(\text{OH}_2)_2](\text{Cl})_2$ crystallised in the monoclinic spacegroup $P2_1/c$ with $R1 = 0.0599$. The details of the crystal structure and refinement can be found in Table 35 in Appendix 1.

$[\text{Mn}(\text{RedL10})(\text{OH}_2)_2](\text{Cl})_2$ crystallises in the same manner as the previously described imine analogue $[\text{Mn}(\text{L10})(\text{OH}_2)_2](\text{ClO}_4)_2$. The bond distance for the imine bond in the original complex $[\text{Mn}(\text{L10})(\text{OH}_2)_2](\text{ClO}_4)_2$ was found to be 1.272(3) Å. The increased bond length for the reduced analogue $[\text{Mn}(\text{RedL10})(\text{OH}_2)_2]2\text{Cl}$ for the equivalent bond is 1.442(11) Å (for N1–C2) and 1.461(11) Å (for C8–N3), this increased bond length is a good indication that the reduction reaction has been successful.

The selected bond lengths and angles for $[\text{Mn}(\text{RedL10})(\text{OH}_2)_2](\text{Cl})_2$ are given in Table 14.

Table 14 - Selected bond lengths [\AA] and angles [$^\circ$] for $[\text{Mn}(\text{RedL10})(\text{OH}_2)_2](\text{Cl})_2$

Mn(1)–O(3)	2.180(8)	Mn(1)–N(3)	2.286(6)
Mn(1)–N(2)	2.208(7)	Mn(1)–N(1)	2.290(7)
Mn(1)–O(1)	2.288(6)	N(1)–C(2)	1.442(11)
Mn(1)–O(2)	2.308(5)	C(8)–N(3)	1.461(11)
Mn(1)–O(4)	2.187(6)		

O(3)–Mn(1)–O(4)	172.2(3)	O(3)–Mn(1)–N(2)	92.6(3)
O(4)–Mn(1)–N(2)	95.0(2)	O(3)–Mn(1)–N(3)	86.9(3)
O(4)–Mn(1)–N(3)	96.6(2)	N(2)–Mn(1)–N(3)	72.4(2)
O(3)–Mn(1)–O(1)	94.7(3)	O(4)–Mn(1)–O(1)	79.7(2)
N(2)–Mn(1)–O(1)	144.5(2)	N(3)–Mn(1)–O(1)	73.4(2)
O(3)–Mn(1)–N(1)	94.0(3)	O(4)–Mn(1)–N(1)	87.1(2)
N(2)–Mn(1)–N(1)	72.9(2)	N(3)–Mn(1)–N(1)	145.3(2)
O(1)–Mn(1)–N(1)	140.8(2)	O(3)–Mn(1)–O(2)	82.6(2)
O(4)–Mn(1)–O(2)	90.4(2)	N(2)–Mn(1)–O(2)	145.2(2)
N(3)–Mn(1)–O(2)	141.1(2)	O(1)–Mn(1)–O(2)	70.3(2)
N(1)–Mn(1)–O(2)	73.1(2)		

The manganese ion has approximate pentagonal bipyramidal geometry where the donors of the pentagonal plane are the three nitrogen atoms from the pyridine diimine head unit of the molecule providing an angle of $72.9(2)^\circ$ (for N2–Mn1–N1) which is slightly larger than that of the equivalent angle for the water bound complex $[\text{Mn}(\text{L10})(\text{OH}_2)_2](\text{ClO}_4)_2$ before reduction as described above, the angle is slightly distorted from a regular pentagonal plane of 72° . The Mn-N bond lengths where the reduction has taken place are longer with $2.290(7) \text{ \AA}$ for Mn1–N1 and $2.286(6) \text{ \AA}$ for Mn1–N3 when compared to the complex $[\text{Mn}(\text{L10})(\text{OH}_2)_2](\text{ClO}_4)_2$ described above. The manganese is also bound to the two oxygen atoms of the pentagonal plane from the ligand. The axial ligands are slightly bent with an angle of $172.2(3)^\circ$ (O3–Mn1–O4) from the ideal linear angle of 180° .

Hydrogen bonding exists between the axial water bound molecules and the unbound chloride anions, as illustrated in Figure 2-41.

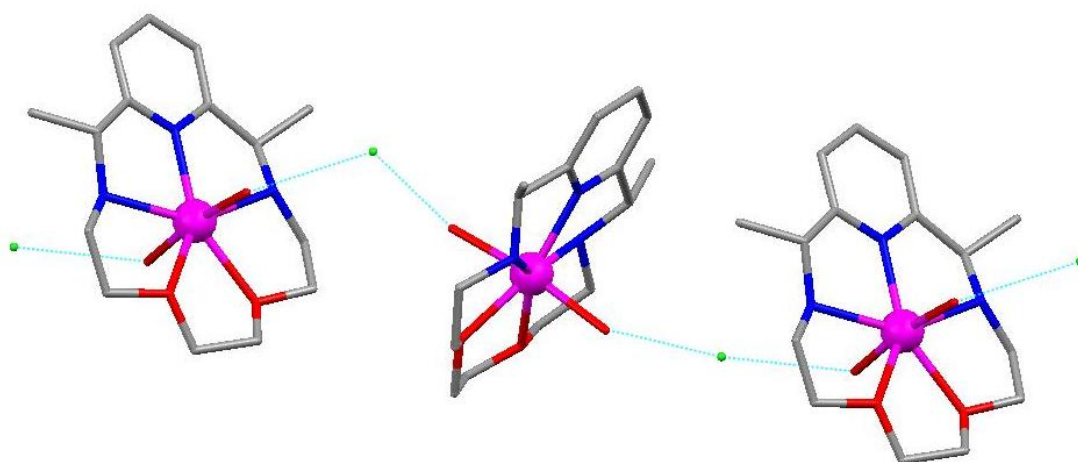


Figure 2-41 – Hydrogen bonding for $[Mn(RedL10)(OH_2)_2](Cl)_2$

There is π - π stacking present between the pyridine diimine units of two adjacent molecules as shown in Figure 2-42 below.

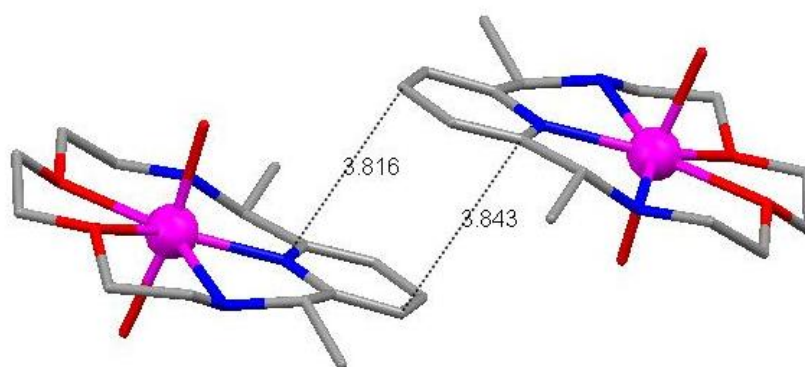


Figure 2-42 - π - π stacking for $[Mn(RedL10)(OH_2)_2](Cl)_2$

The centroid - centroid distance is 3.819 Å and the centroid of the ring is 3.658 Å from the mean plane of the second ring under symmetry operation $-x, -y-1, -z-1$.

2.5.5 [Mn(L10)(NCS)₂].DMF

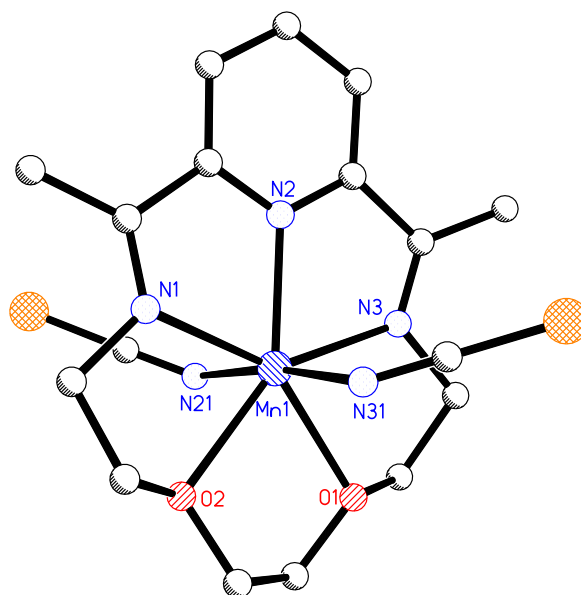


Figure 2-43 –Structure for [Mn(L10)(NCS)₂].DMF with solvate molecule and hydrogens omitted for clarity

Irregular shaped orange crystals of the complex [Mn(L11)(NCS)₂].DMF as illustrated in Figure 2-43 crystallised in the triclinic space group $P\bar{1}$ with $R1 = 0.0509$ (Figure 2-43). The details of the crystal structure and refinement can be found in Table 36 in Appendix 1. The crystal structure has previously been published by Drew and co-workers² without the presence of a DMF solvate molecule. The published structure also crystallised in the triclinic space group $P\bar{1}$ with $R1 = 0.075$. The crystal structure as illustrated in Figure 2-43 crystallises in the same manner as the water bound complex [Mn(L10)(H₂O)](ClO₄)₂ with two exogenous thiocyanate ions which are nitrogen bound to the manganese in the axial positions. Due to the negative charge on the axial ligands, there are no uncoordinated anions present.

Selected bond lengths and angles for [Mn(L10)(NCS)₂].DMF are given in Table 15.

Table 15 - Selected bond lengths [\AA] and angles [$^\circ$] for $[\text{Mn}(\text{L10})(\text{NCS})_2]\cdot\text{DMF}$

Mn(1)–N(2)	2.212(3)	Mn(1)–N(31)	2.229(4)
Mn(1)–N(21)	2.240(4)	Mn(1)–N(3)	2.246(3)
Mn(1)–N(1)	2.246(4)	Mn(1)–O(1)	2.279(3)
Mn(1)–O(2)	2.295(3)		

N(2)–Mn(1)–N(31)	94.13(12)	N(2)–Mn(1)–N(21)	93.70(11)
N(31)–Mn(1)–N(21)	172.11(11)	N(2)–Mn(1)–N(3)	70.57(12)
N(31)–Mn(1)–N(3)	90.37(13)	N(21)–Mn(1)–N(3)	93.14(13)
N(2)–Mn(1)–N(1)	70.84(11)	N(31)–Mn(1)–N(1)	91.75(14)
N(21)–Mn(1)–N(1)	89.90(14)	N(3)–Mn(1)–N(1)	141.41(11)
N(2)–Mn(1)–O(1)	143.54(10)	N(31)–Mn(1)–O(1)	83.06(12)
N(21)–Mn(1)–O(1)	91.21(12)	N(3)–Mn(1)–O(1)	73.10(12)
N(1)–Mn(1)–O(1)	145.34(10)	N(2)–Mn(1)–O(2)	143.29(11)
N(31)–Mn(1)–O(2)	90.64(11)	N(21)–Mn(1)–O(2)	82.50(11)
N(3)–Mn(1)–O(2)	145.87(10)	N(1)–Mn(1)–O(2)	72.64(10)
O(1)–Mn(1)–O(2)	73.18(11)		

The manganese ion has approximate pentagonal bipyramidal geometry where the donors of the pentagonal plane are the three nitrogen atoms from the pyridine diimine head unit of the molecule providing an angle of $70.84(11)^\circ$ for N2–Mn1–N1 which is slightly smaller than that of the equivalent angle for the water bound complex $[\text{Mn}(\text{L10})(\text{OH}_2)_2](\text{ClO}_4)_2$ as described above, the angle is slightly distorted from a regular pentagonal plane of 72° , the manganese ion is also bound to the two oxygen donors of the pentagonal plane from the ligand. The axial ligands with an angle of $172.11(11)^\circ$ (for N31–Mn1–N21) are slightly bent away from the ideal linear angle of 180° . The molecule crystallises with one uncoordinated molecule of DMF which was used as a solvent during the recrystallisation process.

Some π - π stacking is present between the pyridine diimine units of two adjacent macrocycles as shown in Figure 2-44.

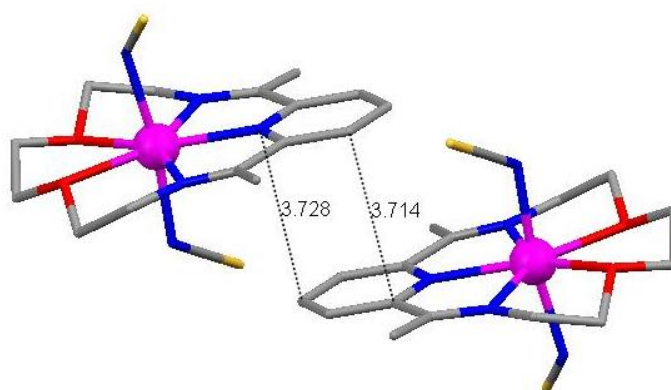


Figure 2-44 – π - π stacking for $[Mn(L10)(NCS)_2]$

The centroid - centroid distance is 3.724 Å and the centroid of the ring is 3.360(1) Å from the mean plane of the second ring under symmetry operation 1-x, 1-y, -z.

2.5.6 $[Mn(L11)(Cl)_2]$

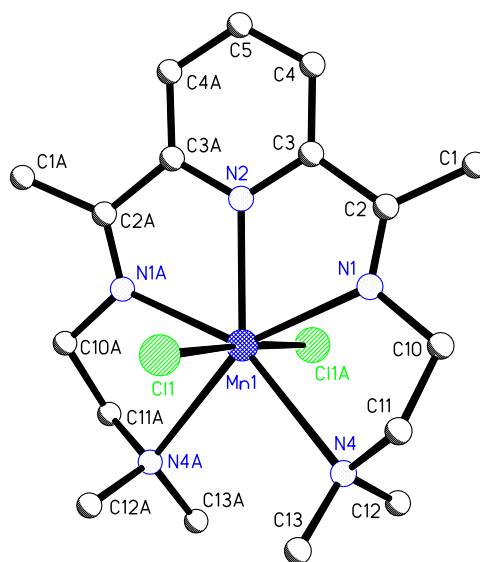


Figure 2-45 – Structure for $[Mn(L11)(Cl)_2]$

Yellow crystals of the complex $[Mn(L11)(Cl)_2]$ were found to crystallise in the monoclinic space group $C2/c$ with $R = 0.0363$ (Figure 2-45). The details of the crystal structure and refinement can be found in Table 37 in Appendix 1

The structure as shown in Figure 2-45 contains a single seven-coordinate manganese ion that is coordinated to all five nitrogen donors of the ligand which form a pentagonal plane, two exogenous chloride ligands are bound to the manganese in the axial position.

The molecule contains a crystallographic 2-fold axis which runs through Mn1-N2 and C5. The manganese atom has approximate pentagonal bipyramidal geometry. The selected bond lengths and angles for the complex [Mn(L11)(Cl)₂] are given in Table 16 below:

Table 16 - Selected bond lengths [Å] and angles [°] for [Mn(L11)(Cl)₂]

Mn(1)–N(2)	2.329(2)	Mn(1)–N(1)	2.3722(15)
Mn(1)–Cl(1)	2.4645(4)	Mn(1)–N(4)	2.6707(16)

N(2)–Mn(1)–N(1)	67.40(4)	N(2)–Mn(1)–Cl(1)	91.656(14)
N(1)–Mn(1)–Cl(1)	93.65(4)	N(2)–Mn(1)–N(4)	136.65(4)
N(1)–Mn(1)–N(4)	69.55(5)	N(1A)–Mn(1)–N(1)	134.79(8)
Cl(1A)–Mn(1)–Cl(1)	176.69(3)		

Symmetry operations for equivalent atoms A $-x, y, -z+1/2$

The donors of the pentagonal plane are the three nitrogen atoms from the pyridine diimine head unit of the molecule providing an angle of 134.79(8) (N1A–Mn1–N1) which is slightly smaller than the equivalent angles in complexes of L9 and L10 as described above, the angle is slightly distorted from a regular pentagonal plane of 108°, the manganese ion is also bound to a further two nitrogen donors of the pentagonal plane from the ligand and these are shown to have longer bond lengths than that observed for the other nitrogen donors of the pentagonal plane, with 2.6707(16) Å observed for Mn1–N4. The axial ligands provide an angle of 176.69(3)° (for Cl1–Mn1–Cl1A) which is slightly bent away from the ideal linear angle of 180° but is less pronounced than for the chloride bound complex of L9 [Mn(L9)(Cl)₂] previously described.

There is some π - π stacking that is present between the pyridine diimine units of two macrocycles as shown in Figure 2-46 below.

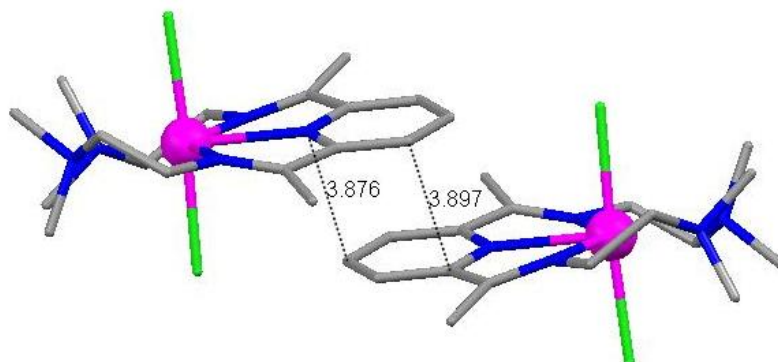


Figure 2-46 – π - π stacking for $[Mn(L11)(Cl)_2]$

The centroid - centroid distance is 3.877 Å and the centroid of the ring is 3.340(1) Å from the mean plane of the second ring under symmetry operation $-x, -y, -z$.

2.5.7 [Mn(L12)(OH₂)(Cl)]ClO₄

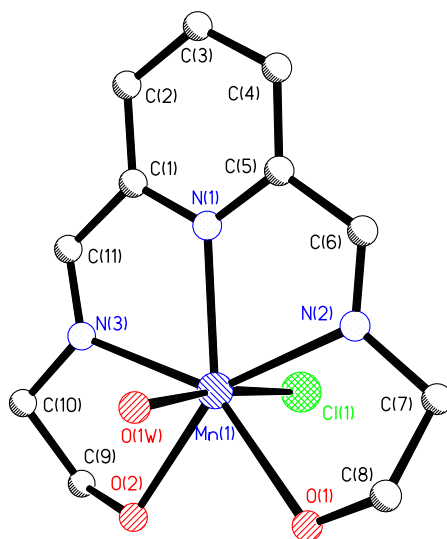


Figure 2-47 –Structure for [Mn(L12)(OH₂)(Cl)]⁺ with perchlorate anion omitted for clarity

Orange crystals of the complex [Mn(L12)(OH₂)(Cl)](ClO₄) were obtained from a solution prepared by Soraya Sanchez-Ballester as part of an Erasmus project. [Mn(L12)(OH₂)(Cl)](ClO₄) crystallised in the triclinic space group $P\bar{1}$ with $R_1 = 0.0480$. The details of the crystal structure and refinement can be found in Table 38 in Appendix 1

The crystal structure of the [Mn(L12)(OH₂)(Cl)]⁺ cation is illustrated in Figure 2-45, it contains a single seven coordinate manganese ion that is coordinated to the N₃O₂ donor set of the ligand which forms a pentagonal plane, one exogenous chloride, and one water ligand are bound to the manganese in the axial position in favour of the perchlorate anion which remains uncoordinated to the molecule.

Selected bond lengths and angles for [Mn(L12)(OH₂)(Cl)](ClO₄) are given in Table 17.

Table 17 - Selected bond lengths [\AA] and angles [$^\circ$] for $[\text{Mn}(\text{L12})(\text{OH}_2)(\text{Cl})](\text{ClO}_4)$

Mn(1)–O(1W)	2.202(5)	Mn(1)–N(1)	2.273(6)
Mn(1)–N(2)	2.280(6)	Mn(1)–N(3)	2.292(6)
Mn(1)–O(2)	2.297(5)	Mn(1)–O(1)	2.349(5)
Mn(1)–Cl(1)	2.507(3)		

O(1W)–Mn(1)–N(1)	91.47(19)	O(1W)–Mn(1)–N(2)	91.2(2)
N(1)–Mn(1)–N(2)	69.0(2)	O(1W)–Mn(1)–N(3)	91.1(2)
N(1)–Mn(1)–N(3)	69.1(2)	N(2)–Mn(1)–N(3)	138.1(2)
O(1W)–Mn(1)–O(2)	90.81(19)	N(1)–Mn(1)–O(2)	140.7(2)
N(2)–Mn(1)–O(2)	150.1(2)	N(3)–Mn(1)–O(2)	71.6(2)
O(1W)–Mn(1)–O(1)	79.23(18)	N(1)–Mn(1)–O(1)	139.1(2)
N(2)–Mn(1)–O(1)	71.4(2)	N(3)–Mn(1)–O(1)	149.6(2)
O(2)–Mn(1)–O(1)	79.69(18)	O(1W)–Mn(1)–Cl(1)	173.07(15)
N(1)–Mn(1)–Cl(1)	94.62(15)	N(2)–Mn(1)–Cl(1)	87.86(16)
N(3)–Mn(1)–Cl(1)	94.19(17)	O(2)–Mn(1)–Cl(1)	86.57(14)
O(1)–Mn(1)–Cl(1)	93.98(13)		

As with the mononuclear complexes which contain the diacetylpyridine head unit previously described, the manganese ion for mononuclear complexes containing the diformyl pyridine head unit have approximate pentagonal bipyramidal geometry where the donors of the pentagonal plane are the three nitrogen atoms from the pyridine diimine head unit of the molecule providing an angle of $138.1(2)^\circ$ (for N2–Mn1–N3), the manganese ion is also bound to the two oxygen donors of the pentagonal plane from the ligand. The axial ligands with an angle of $173.07(15)^\circ$ (for O1W–Mn1–Cl1) are slightly bent away from the ideal linear angle of 180° .

Hydrogen bonding exists between the O1 molecule which forms part of the ligand structure and the Cl1 axial ligand on adjacent molecules with a distance of 2.144 \AA and this can be seen in Figure 2-48 below.

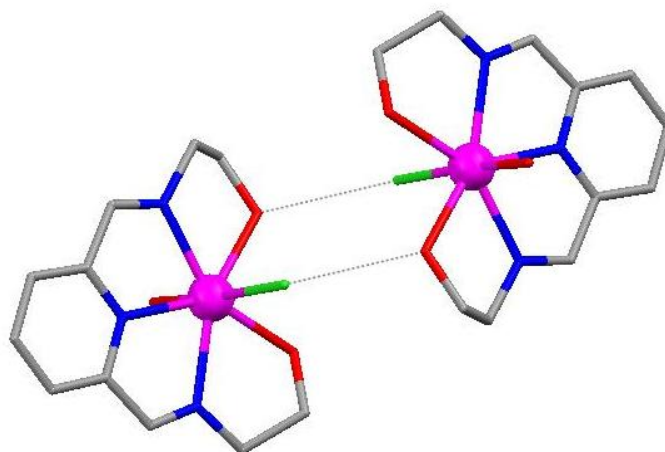


Figure 2-48 – *Hydrogen bonding on adjacent molecules of $[Mn(L12)(OH_2)(Cl)](ClO_4)$*

In addition to the hydrogen bonding that is observed, there are some π - π stacking interactions that exist between the pyridine diimine units on adjacent molecules, this can be seen below in Figure 2-49.

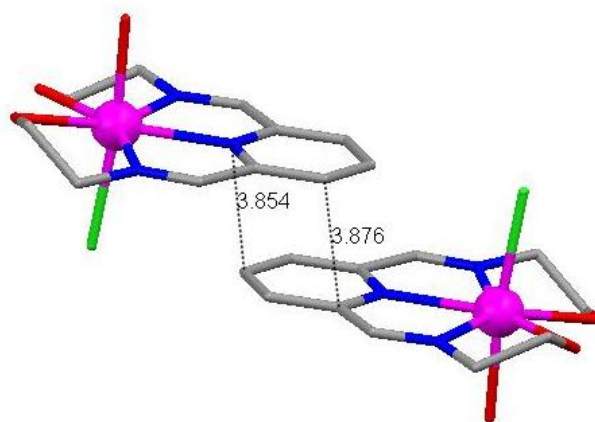


Figure 2-49 - *π - π stacking for $[Mn(L12)(OH_2)(Cl)](ClO_4)$*

The centroid - centroid distance is 3.849 Å and the centroid of the ring is 3.293(1) Å from the mean plane of the second ring under symmetry operation $-x+1, -y+2, -z+1$.

2.5.8 [Mn(L12)(OH₂)₂](ClO₄)₂

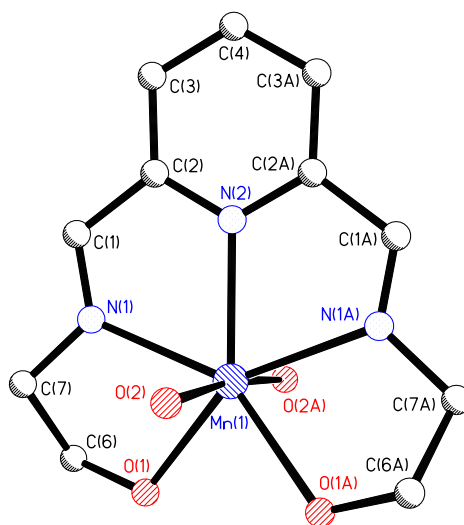


Figure 2-50 –Structure of $[\text{Mn}(\text{L12})(\text{OH}_2)_2]^{2+}$ with perchlorate anions omitted for clarity

The crystal structure of the $[\text{Mn}(\text{L12})(\text{OH}_2)_2]^{2+}$ cation is illustrated in Figure 2-50. Orange crystals of the complex $[\text{Mn}(\text{L12})(\text{OH}_2)_2](\text{ClO}_4)_2$ were obtained from a solution prepared by Soraya Sanchez-Ballester as part of an Erasmus project. The complex crystallised in the monoclinic space group $C2/c$ with $R1 = 0.0407$. The details of the crystal structure and refinement can be found in Table 39 in Appendix 1.

The crystal structure shown in Figure 2-50 contains a single seven coordinate manganese ion that is coordinated to the N_3O_2 donor set of the ligand which forms a pentagonal plane, two exogenous water ligands are bound to the manganese in the axial position in favour of the two uncoordinated perchlorate anions.

The molecule contains a crystallographic 2-fold axis that passes through Mn1-N2 and C4. Selected bond lengths and angles for $[\text{Mn}(\text{L12})(\text{OH}_2)_2](\text{ClO}_4)_2$ are given Table 18 below:

Table 18 - Selected bond lengths [\AA] and angles [$^\circ$] for $[\text{Mn}(\text{L12})(\text{OH}_2)_2](\text{ClO}_4)_2$

Mn(1)–O(2)	2.1913(15)	Mn(1)–O(1)	2.2836(14)
Mn(1)–N(1)	2.2921(16)	Mn(1)–N(2)	2.296(2)

O(2)–Mn(1)–O(1)	95.45(6)	O(2)–Mn(1)–N(1)	87.10(6)
O(1)–Mn(1)–N(1)	71.81(6)	O(2)–Mn(1)–N(2)	93.38(4)
O(1)–Mn(1)–N(2)	138.94(4)	N(1)–Mn(1)–N(2)	68.69(5)
O(2A)–Mn(1)–O(2)	173.25(9)	N(1)–Mn(1)–N(1A)	137.39(9)

Symmetry operations for equivalent atoms A $-x, y, -z+3/2$

The manganese ion has approximate pentagonal bipyramidal geometry as described for previous mononuclear complexes, where the donors of the pentagonal plane are the three nitrogen atoms from the pyridine diimine head unit of the molecule providing an angle of $137.39(9)^\circ$ (for N1–Mn1–N1A) which is slightly distorted from a regular pentagonal plane of 138° and also slightly smaller than that previously described for the complex $[\text{Mn}(\text{L9})(\text{OH}_2)_2](\text{ClO}_4)_2$ which contains a dimethyl head unit. The manganese ion is also bound to the two oxygen donors of the pentagonal plane from the ligand. The axial ligands are slightly bent with an angle of $173.25(9)^\circ$ (O2–Mn1–O2A) away from the ideal linear angle of 180° .

The packing diagram for the complex $[\text{Mn}(\text{L12})(\text{OH}_2)_2](\text{ClO}_4)_2$ as viewed down the *b* axis is illustrated below in Figure 2-51.

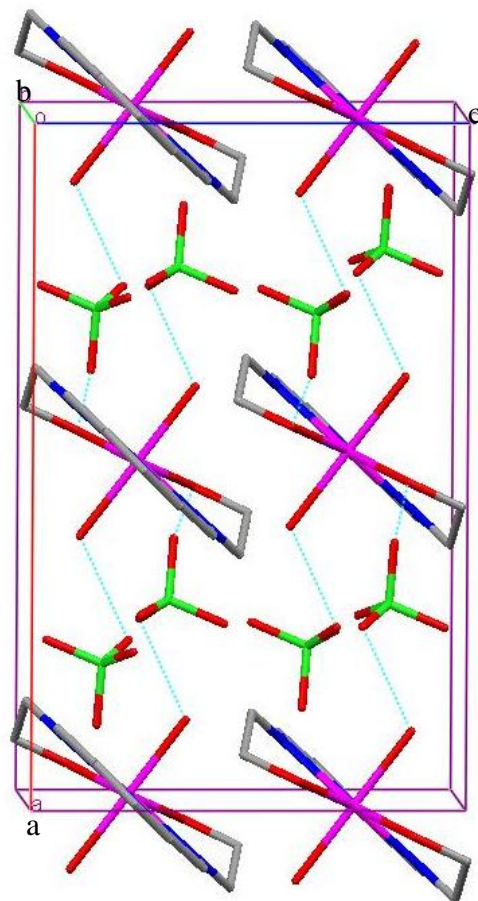


Figure 2-51 – Packing diagram for $[Mn(L12)(OH_2)_2](ClO_4)_2$ as viewed down the b axis

The packing diagram for $[Mn(L12)(OH_2)_2](ClO_4)_2$ as shown in Figure 2-51 illustrates how the molecules pack with hydrogen bonds which exist between the axial bound water molecules and the uncoordinated perchlorate anions with a distance of 2.785 Å and further hydrogen bonding which exists from the perchlorate anion to an oxygen atom (O1) from the ligand of an adjacent molecule with a distance of 2.808 Å.

2.5.9 [Mn(L13)(OH₂)₂](ClO₄)₂

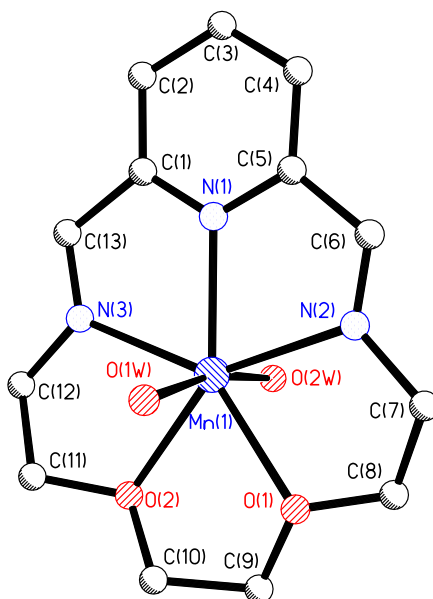


Figure 2-52 - Structure of $[\text{Mn}(\text{L13})(\text{OH}_2)_2]^{2+}$ with perchlorate anions and hydrogens omitted for clarity

Orange crystals of the complex $[\text{Mn}(\text{L13})(\text{OH}_2)_2](\text{ClO}_4)_2$ as illustrated in Figure 2-52 were obtained from a solution prepared by Soraya Sanchez-Ballester as part of an Erasmus project. The complex crystallised in the monoclinic space group $P2_1/c$ with $R1 = 0.0677$. The details of the crystal structure and refinement can be found in Table 40 in Appendix 1.

The structure of the $[\text{Mn}(\text{L13})(\text{OH}_2)_2]^{2+}$ cation as shown in Figure 2-52 forms in the same manner as described previously for mononuclear complexes and contains two exogenous water ligands that are bound to the manganese in the axial position in favour of the uncoordinated perchlorate anions.

The molecule contains a crystallographic 2-fold axis that passes through Mn1-N1 and C3. Selected bond lengths and angles for $[\text{Mn}(\text{L13})(\text{OH}_2)_2](\text{ClO}_4)_2$ are given in Table 19:

Table 19 - Selected bond lengths [\AA] and angles [$^\circ$] for $[\text{Mn}(\text{L13})(\text{OH}_2)_2](\text{ClO}_4)_2$

Mn(1)–N(1)	2.233(7)	Mn(1)–O(1W)	2.216(8)
Mn(1)–O(2W)	2.239(8)	Mn(1)–O(1)	2.248(7)
Mn(1)–O(2)	2.271(7)	Mn(1)–N(2)	2.250(8)
Mn(1)–N(3)	2.267(9)		

N(1)–Mn(1)–O(1W)	96.7(3)	N(1)–Mn(1)–O(2W)	93.4(3)
O(1W)–Mn(1)–O(2W)	169.9(3)	N(1)–Mn(1)–O(1)	144.1(3)
O(1W)–Mn(1)–O(1)	82.4(3)	O(2W)–Mn(1)–O(1)	88.9(3)
N(1)–Mn(1)–O(2)	142.1(3)	O(1W)–Mn(1)–O(2)	89.5(3)
O(2W)–Mn(1)–O(2)	83.1(3)	O(1)–Mn(1)–O(2)	73.7(3)
N(1)–Mn(1)–N(2)	71.1(3)	O(1W)–Mn(1)–N(2)	92.0(3)
O(2W)–Mn(1)–N(2)	90.3(4)	O(1)–Mn(1)–N(2)	73.0(3)
O(2)–Mn(1)–N(2)	146.2(3)	N(1)–Mn(1)–N(3)	70.2(3)
O(1W)–Mn(1)–N(3)	93.3(3)	O(2W)–Mn(1)–N(3)	91.0(3)
O(1)–Mn(1)–N(3)	145.6(3)	O(2)–Mn(1)–N(3)	72.2(3)
N(2)–Mn(1)–N(3)	141.4(3)		

The manganese ion has approximate pentagonal bipyramidal geometry where the donors of the pentagonal plane are the three nitrogen atoms from the pyridine diimine head unit of the molecule, providing an angle of $71.1(3)^\circ$ (for N1–Mn1–N2) which is slightly distorted from a regular pentagonal plane of 72° , and is similar to the equivalent angle for the complex $[\text{Mn}(\text{L10})(\text{OH}_2)_2](\text{ClO}_4)_2$ previously described which contains the dimethyl head unit. The angle for the pyridine diimine unit is slightly larger for this complex than was described for the complex $[\text{Mn}(\text{L12})(\text{OH}_2)_2](\text{ClO}_4)_2$. The manganese ion is also bound to the two oxygen donors of the pentagonal plane from the ligand. The axial ligands are slightly bent with an angle of $169.9(3)^\circ$ (for O1W–Mn1–O2W) away from the ideal linear angle of 180° , this is more pronounced than that previously described for both $[\text{Mn}(\text{L10})(\text{OH}_2)_2](\text{ClO}_4)_2$ and $[\text{Mn}(\text{L12})(\text{OH}_2)_2](\text{ClO}_4)_2$.

The packing diagram for $[\text{Mn}(\text{L13})(\text{OH}_2)_2](\text{ClO}_4)_2$ as viewed down the *a* axis is shown below in Figure 2-53.

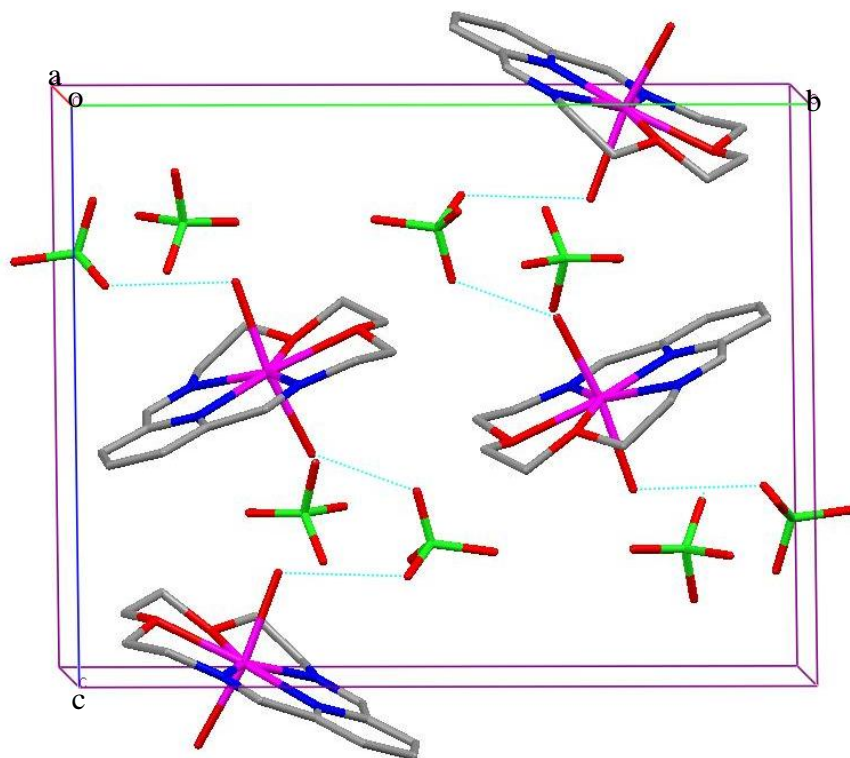


Figure 2-53 – Packing diagram for $[\text{Mn}(\text{L13})(\text{OH}_2)_2](\text{ClO}_4)_2$ as viewed down the *a* axis

The packing diagram for $[\text{Mn}(\text{L13})(\text{OH}_2)_2](\text{ClO}_4)_2$ as shown in Figure 2-53, illustrates how the molecules pack *via* hydrogen bonding which exists between the uncoordinated perchlorate anions and the axial bound water ligands on adjacent molecules with distances of 2.996 Å and 3.028 Å respectively.

2.5.10[Mn(L15)(Cl)₂].MeOH

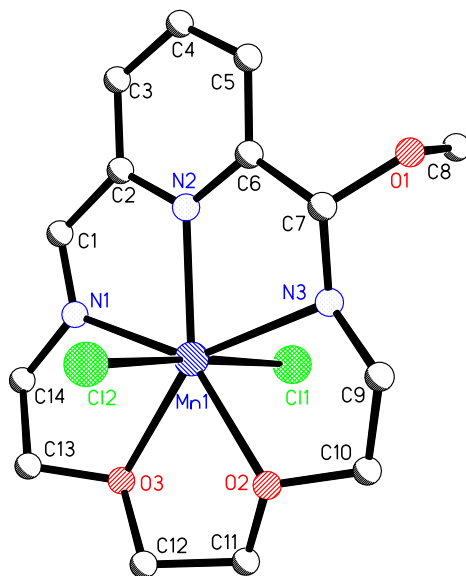


Figure 2-54 –Structure for [Mn(L15)(Cl)₂].MeOH

Orange crystals of the complex [Mn(L15)(Cl)₂].MeOH were crystallised in the triclinic space group $P\bar{1}$ with $R1 = 0.0394$ (see Figure 2-54). The details of the crystal structure and refinement can be found in Table 42 in appendix 1

The complex [Mn(L15)(Cl)₂].MeOH was prepared as for complex [Mn(L13)(Cl)₂], however, during the reaction, one of the imine bonds in this complex has undergone nucleophilic attack from a solvent methanol molecule which has become part of the ligand structure. During this reaction, the original imine bond length, taken from the water bound complex [Mn(L13)(OH₂)(ClO₄)₂], was found to be 1.272(3) Å, however, the equivalent bond where the nucleophilic attack has taken place, has led to an increase in bond length to 1.438(3) Å (for C7–N3) which indicates that a single bond is present for the complex [Mn(L15)(Cl)₂].MeOH.

The crystal structure as shown in Figure 2-54 contains a single seven coordinate manganese ion that is coordinated to the N₃O₂ donor set of the ligand which forms a pentagonal plane, two exogenous chloride ligands are bound to the manganese in the axial position.

Selected bond lengths and angles are given below in Table 20 below:

Table 20 - Selected bond lengths [\AA] and angles [$^\circ$] for $[\text{Mn}(\text{L15})(\text{Cl})_2]\cdot\text{MeOH}$

Mn(1)–N(2)	2.232(2)	Mn(1)–N(1)	2.249(2)
Mn(1)–O(2)	2.2528(18)	Mn(1)–O(3)	2.3037(19)
Mn(1)–N(3)	2.331(2)	Mn(1)–Cl(2)	2.5311(8)
Mn(1)–Cl(1)	2.5697(8)	C(7)–N(3)	1.438(3)

N(2)–Mn(1)–N(1)	71.73(9)	N(2)–Mn(1)–O(2)	143.32(8)
N(1)–Mn(1)–O(2)	144.54(8)	N(2)–Mn(1)–O(3)	142.76(8)
N(1)–Mn(1)–O(3)	71.04(8)	O(2)–Mn(1)–O(3)	73.83(7)
N(2)–Mn(1)–N(3)	70.81(8)	N(1)–Mn(1)–N(3)	141.66(8)
O(2)–Mn(1)–N(3)	73.70(7)	O(3)–Mn(1)–N(3)	145.54(7)
N(2)–Mn(1)–Cl(2)	88.84(6)	N(1)–Mn(1)–Cl(2)	90.34(6)
O(2)–Mn(1)–Cl(2)	86.37(5)	O(3)–Mn(1)–Cl(2)	92.41(5)
N(3)–Mn(1)–Cl(2)	96.77(6)	N(2)–Mn(1)–Cl(1)	94.86(6)
N(1)–Mn(1)–Cl(1)	94.70(6)	O(2)–Mn(1)–Cl(1)	88.23(5)
O(3)–Mn(1)–Cl(1)	87.12(5)	N(3)–Mn(1)–Cl(1)	80.65(6)
Cl(2)–Mn(1)–Cl(1)	174.49(3)		

The manganese ion sits in a pentagonal bipyramidal geometry where the donors of the pentagonal plane are the three nitrogen atoms from the pyridine diimine head unit of the molecule providing an angle of $71.73(9)^\circ$ (for N2–Mn1–N1) which is slightly distorted from a regular pentagonal plane of 72° , this angle is very similar to that reported for the equivalent angle in the complex $[\text{Mn}(\text{L13})(\text{OH}_2)_2](\text{ClO}_4)_2$, the manganese ion is also bound to the two oxygen donors of the pentagonal plane from the ligand. The axial ligands are slightly bent away with an angle of $174.49(3)^\circ$ (for Cl2–Mn1–Cl1) from the ideal linear angle of 180° .

There is some π - π stacking that is present between the pyridinediimine units of two adjacent macrocycles as shown in Figure 2-55 below.

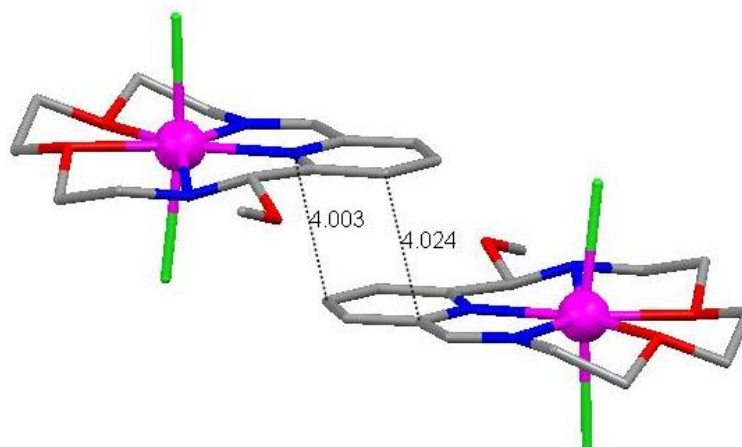


Figure 2-55 – π - π stacking for $[Mn(L15)(Cl)_2].MeOH$

The centroid - centroid distance is 4.003 Å and the centroid of the ring is 3.629(1) Å from the mean plane of the second ring under symmetry operation $-x+1, -y, -z$.

2.6 Tripodal ligands

Tripodal amines are important in the design of Schiff base complexes and by altering the arm lengths of the ligands, slight changes in geometry can be imposed onto a metal centre and increased flexibility may occur which may bring about changes in the biological activity of the molecule. Tripodal ligands were prepared and used in a Schiff base condensation reaction with salicylaldehyde.

Tren is a commonly used commercially available symmetrical tripodal amine and was used without further purification in the synthesis of a Schiff base manganese tripodal complex with salicylaldehyde.

The synthesis of asymmetric tripodal amines were attempted using the methods outlined by Blackman *et al.*³⁰ by varying the arm lengths of the tripod. The syntheses of the products have been carried out with varying molar ratios of $MnCl_2 \cdot 4H_2O$ to ligand. Initially attempts were made to prepare mononuclear complexes with a 1:1 stoichiometry of $MnCl_2 \cdot 4H_2O$ to ligand, this was then extended to form the μ -oxo tetranuclear complexes with a cubane core by using excess $MnCl_2 \cdot 4H_2O$.^{30, 36, 37}

Each complex was analysed using IR, elemental analysis and mass spectrometry. Suitable crystals did not form for X-ray crystallography to be performed. This may be due to lack of symmetry in the molecules. Complete condensation of all the primary amine groups was confirmed by the lack of a $\nu_{(\text{N-H})}$ stretching band in the region $3150 - 3450 \text{ cm}^{-1}$ and the presence of a $\nu_{(\text{C=N})}$ stretch.

In forming the asymmetric tripods as HCl salts, problems were first encountered in the neutralisation of the ligand to enable the tripod to undergo a Schiff base reaction with salicylaldehyde. Initial attempts included the use of a methanolic sodium hydroxide (NaOH) solution to alter the pH of the solution containing the tripod. However this method seemed unsuccessful and it seemed possible to easily add too much of the NaOH and it is possible that a sodium salt of the tripodal ligand can be formed. The use of sodium hydrogen carbonate was then used to neutralise the tripod, and this method again was unsuccessful. Finally, triethylamine was used and has led to the preparation of successful asymmetric tripodal amines.

During the Schiff base reaction of the tripod with salicylaldehyde, an imine bond is formed. Attempts to reduce the imine bonds were carried out with the use of borohydride. The product was analysed using IR initially, the imine stretch disappeared on formation of the reduced ligands. This confirmed the reaction was successful. The results of the reduction seem to be successful and the catalase activity of the products of the reduction can be compared to those of the complexes containing the imine bonds. However, crystals could not be formed for the tripodal ligands which may be due to lack of symmetry in the molecules.

The crystal structures of the complexes reported here show that the molecules have formed as seven coordinate Mn(II) complexes. The crystal structures have also clarified how the complexes have formed, whether as [2+2], [2+2] dimeric molecules, ring contractions or [1+1] mononuclear complexes. The appropriate bond lengths and angles have been indicated to show where differences arise around the metal centres and how the axial ligands have bonded. These parameters are important

for structure activity relationships as these may provide the key to understanding the nature of the antioxidant activities of the complexes tested.

3 Chapter Three – Biological testing

3.1 Electrochemistry

Electrochemical data were obtained using a 0.5 mmol solution of complex in acetonitrile, with 0.1 M tertiarybutylammonium perchlorate as the supporting electrolyte. A 5 mmol ferrocene standard solution was prepared with 0.1 M tertiarybutylammonium perchlorate as the supporting electrolyte. A single compartment cell was used containing a platinum working electrode, a platinum counter electrode and a Ag/Ag⁺ reference electrode. All cyclic voltammograms were recorded at room temperature, using a scan rate of 100 mV/s⁻¹.

The Ag/Ag⁺ reference electrode was placed into the solution as a solid silver wire and is referred to as a pseudo reference electrode, so called because although it provides a constant potential, the reference potential is unknown and varies with different conditions. The presence of the ferrocene (Fc) is important as an internal standard for determining the potential scale if any electrochemical peaks were to be quoted from the samples under analysis. Thus, it is common practice to measure the reversible redox potentials for the oxidation of Fc to Fc⁺ versus the reference electrode and subsequently correct potentials to the Fc/Fc⁺ scale, see Figure 3-1.¹⁰³

Results were recorded using an EG&G potentiostat/galvanostat model 263A and the programme Powersuite.

Initial testing of some of the seven coordinate manganese complexes was conducted in order to look for any redox activity of the compounds. The results from the electrochemistry are illustrated in Figure 3-2.

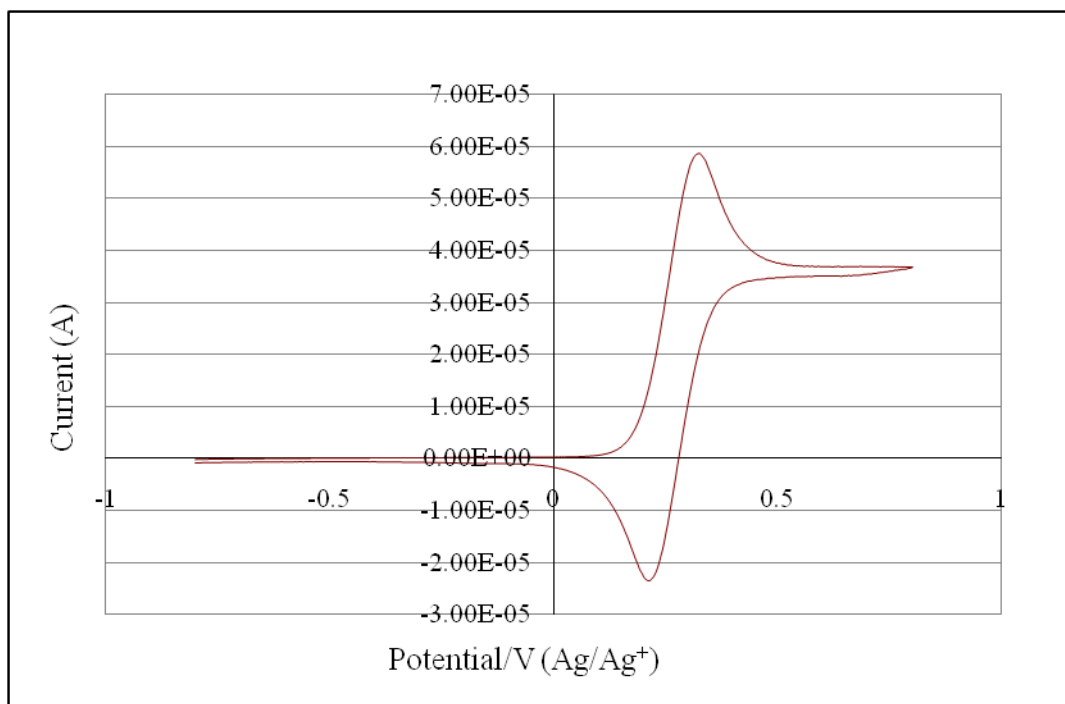
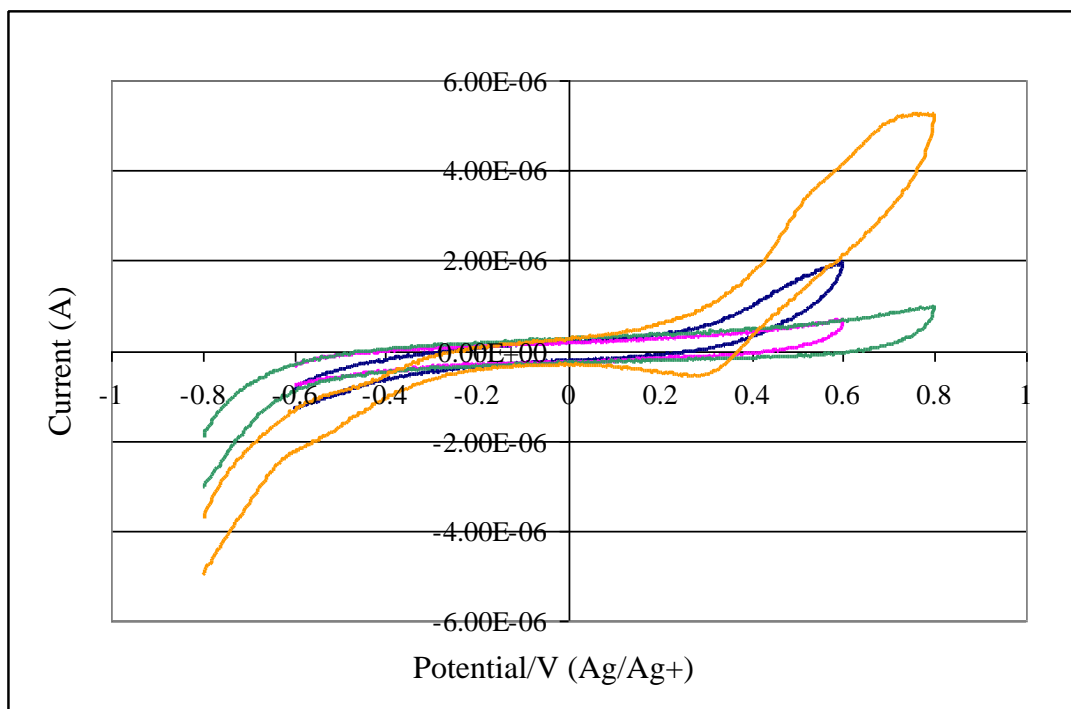


Figure 3-1 – *Cyclic voltammogram of ferrocene standard*

The cathodic peak (E_{pc}) for ferrocene occurred at a potential of 0.33 V and the anodic peak (E_{pa}) occurred at 0.20 V. The redox couple $E_{1/2}$ then occurred at $E_{1/2} = (E_{pc} + E_{pa})/2 = 0.27$ V. The fc/fc^+ couple occurs at 0.40 V versus the standard hydrogen electrode (SHE).¹⁰⁴



- $[\text{Mn}_2(\text{HL1})(\text{N}_3)_2]_2(\text{ClO}_4)_2$
- $[\text{Mn}_2(\text{HL1})(\text{OAc})_2]_2(\text{ClO}_4)_2$
- $[\text{Mn}_4(\text{L2})(\text{ClO}_4)_2]_2$
- $[\text{Mn}(\text{L10})(\text{H}_2\text{O})_2](\text{ClO}_4)_2$

Figure 3-2 – Cyclic voltammetry of seven-coordinate manganese complexes

Figure 3-2 shows that the complexes tested are electrochemically silent in the potential range $-0.8 - 0.8$ V and that the seven-coordinate Mn(II) complexes are resistant to oxidation, however, there is a slight increase in current which may suggest that some electrochemistry could be observed with a higher potential window. The complex $[\text{Mn}_2(\text{HL1})(\text{N}_3)_2]_2(\text{ClO}_4)_2$ presents a higher increase in current when compared to the other seven-coordinate complexes that were tested. The slight increase in current may be due to the axial azide ligand as this complex has the same ligand system as that of the acetate bound complex, $[\text{Mn}_2(\text{HL1})(\text{OAc})_2]_2(\text{ClO}_4)_2$.

Seven-coordinate Mn(II) complexes with pentagonal bipyramidal geometry have previously been shown to be electrochemically silent as published by McKee and co workers.⁹⁴ Seven-coordinate manganese complexes containing a pentagonal bipyramidal geometry generally do not show metal-based redox activity, and this has

previously been suggested by McKee and coworkers⁹⁴ to be due to a Franck Condon barrier, where electron motion is effectively instantaneous in relation to the nuclear motion and reorganisation of the reactant atoms and surrounding materials is achieved by thermal fluctuations, the vibrational energy associated with the structural reorganisation of the molecule is high for the initial geometry.^{105, 106}

3.2 Superoxide dismutase activity

Many of the complexes that were synthesised were subjected to indirect testing of their superoxide dismutase activity using the xanthine / xanthine oxidase indirect method as described below, firstly to see if there is any activity. The intention of this was to see what effects different axial ligands may have on the activity, determine if the number of manganese ions present has a substantial effect on the rates observed, and what effect the reduction of imine bonds has, altogether providing a catalogue of results to compare. The different rates may help identify the functional requirements for a superoxide dismutase mimic. To complement the results, it was hoped that a direct method of analysis could be achieved so that accurate results could be obtained for catalytic activity, however, although convincing results for the direct method have not yet been obtained, there is scope for the development of the method, and method development thus far is described below.

3.2.1 Indirect analysis

In collaboration with Prof. M. Devereux and Dr. A. Kellet at the Dublin Institute of Technology, the superoxide dismutase activities of the metal complexes were assessed using an indirect modified nitro-blue-tetrazolium (NBT) assay with xanthine–xanthine oxidase system as the source of $O_2^{\cdot-}$. In this method, the xanthine oxidase aerobically oxidises the xanthine to urate, producing $O_2^{\cdot-}$ in the process. Nitro blue tetrazolium (NBT) is used as an indicator, this scavenges the $O_2^{\cdot-}$ formed in the reaction, which causes reduction of the yellow NBT^{2+} to the blue formazan (MF^+) as illustrated below in Figure 3-3.

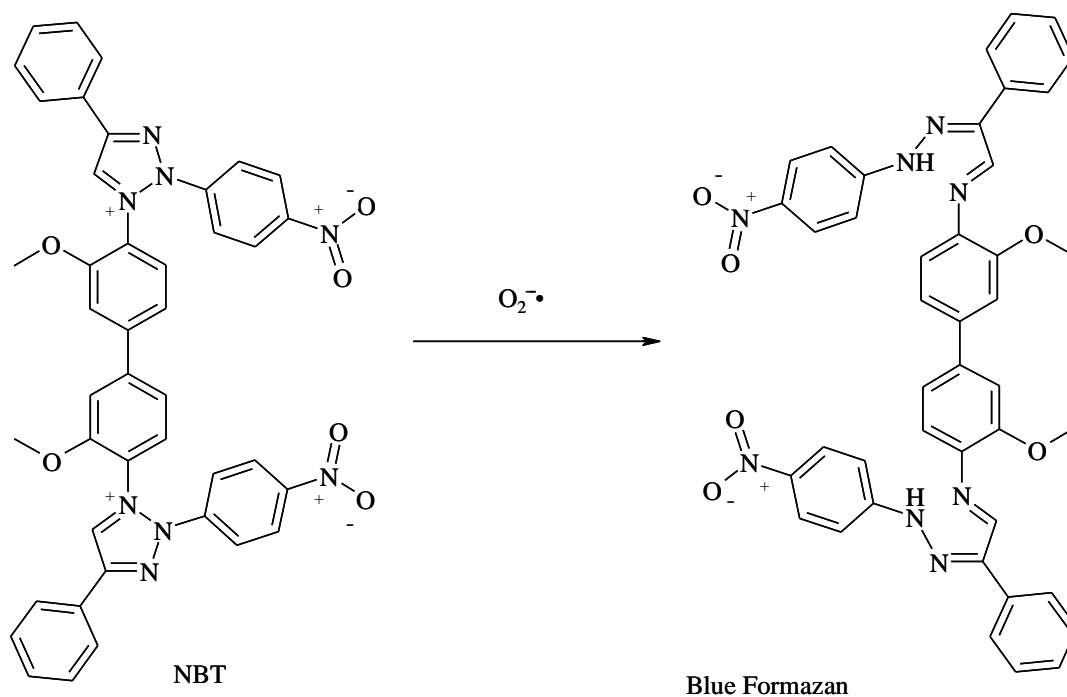


Figure 3-3 – Reaction of NBT to blue formazan

The quantitative reduction of NBT to blue formazan by the $\text{O}_2^{\bullet-}$ was followed spectrophotometrically at 550 nm and 25°C for 180 s (results from 60 – 180s were used). In the presence of a SOD mimic, the absorbance values of the blue formazan decrease with increasing concentration of complex, this is because the SOD mimic will compete with the NBT to scavenge the $\text{O}_2^{\bullet-}$, this then allows the SOD activity of the complex to be calculated.^{72, 73} The NBT assay is an indirect method of analysis because the extent of the reduction of the appearance of the blue formazan in the presence of a SOD mimic is taken as a measure of SOD activity. The use of an indirect method could present potential problems because side reactions that may occur can interfere with the measurements made and the mechanism of catalysis cannot be determined. However, the indirect method offers conditions that approximate better the *in vivo* conditions and the reaction is not measured on a millisecond timescale as with the direct method.

The indirect method assumes that there are no side reactions occurring and that only the catalytic superoxide dismutase reaction is taking place. A schematic representation of the xanthine/xanthine oxidase method is illustrated in Figure 3-4.

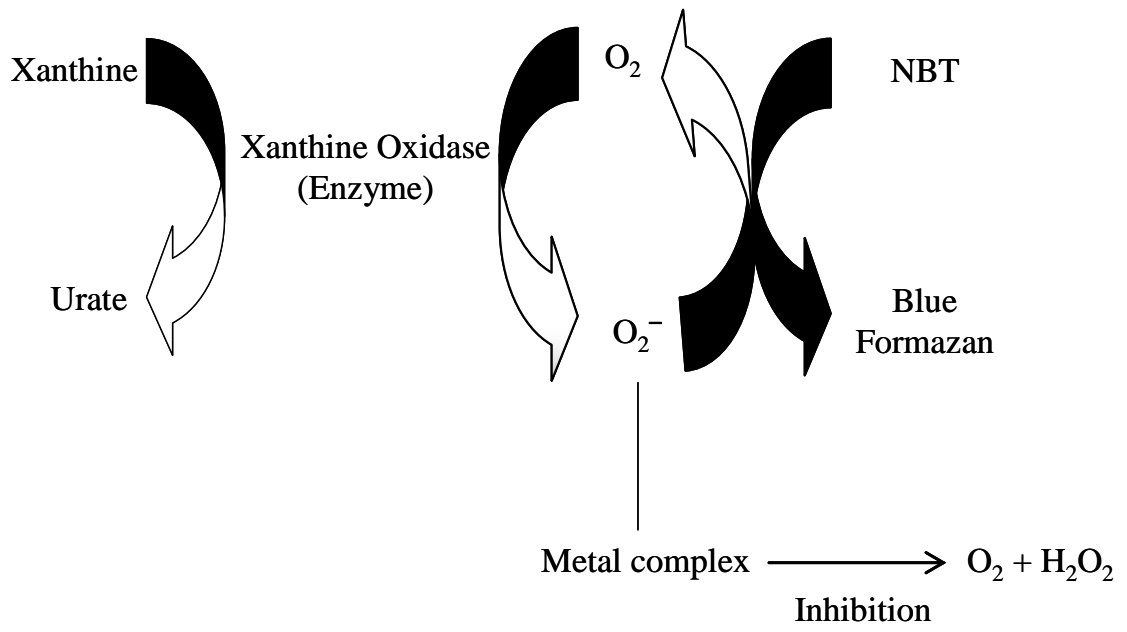


Figure 3-4 – Schematic representation of the NBT indirect assay method

3.2.2 Experimental

All reagents were obtained from Sigma–Aldrich Chemical Co. Ltd., and all glassware was washed in nitric acid and solutions protected from light using aluminium foil to prevent degradation of any chemicals.

Solution 1 was prepared by adding sodium xanthine (50 μM), and NBT (0.01617 g, 100 μM) to a volumetric flask (200 ml) and made to volume with phosphate buffer solution (50 mM, pH 7.8).

Solution 2 was prepared as a 1:10 dilution of xanthine oxidase in phosphate buffer solution (50 mM, pH 7.8), which was stored on ice throughout to prevent the enzyme from denaturing.

Solution 3 was prepared by dissolving the complex in dimethylsulfoxide (0.1 mmol, 50 ml). Dimethylsulfoxide was used because it does not affect the production of superoxide at volumes up to 30 μl .

The prepared solutions were then added to a 1 cm path length quartz cuvette in varying amounts as described in Table 21 using a micropipette.

Table 21 - Volumes of solutions used for the NBT assay

Total Volume (ml)	Solution 1 (X+NBT) (ml)	Phosphate buffer solution (μl)	Solution 2 (XO) (μl)	Solution 3 (Complex) (μl)
3.05	3.0	30	20	0
3.05	3.0	20	20	10
3.05	3.0	10	20	20
3.05	3.0	0	20	30

The results of the SOD testing for three different concentrations of $[\text{Mn}_2(\text{HL1})(\text{Cl})_2]_2(\text{ClO}_4)_2$ and also without any added complex are shown below in

Figure 3-5. The graph shows the absorbance values of blue formazan obtained at 550 nm versus time for each experiment and calculations were made using the results from 1 – 3 minutes.

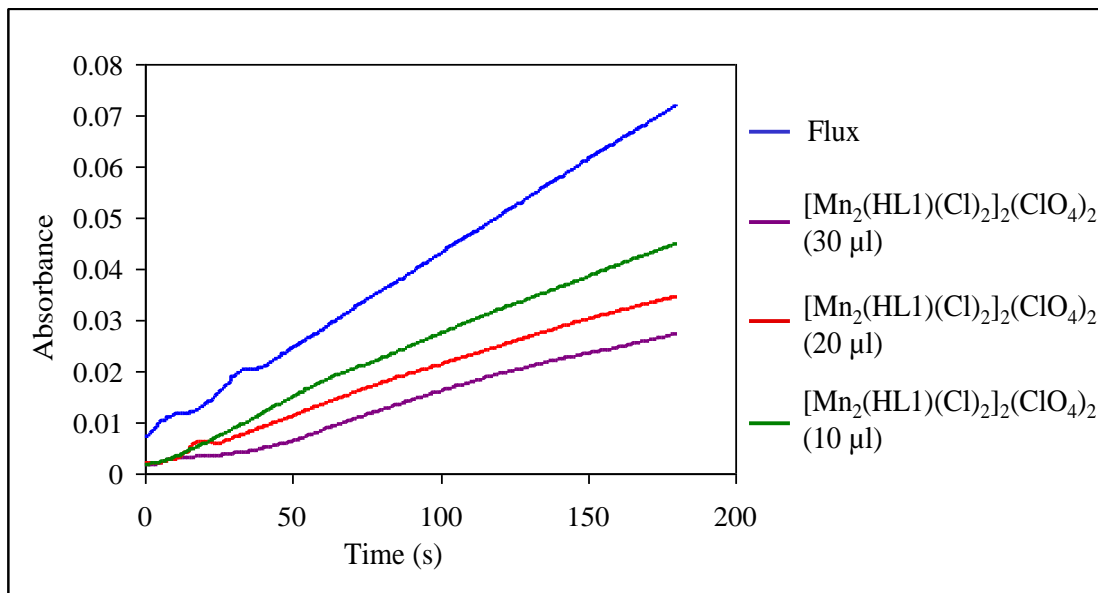


Figure 3-5 – Graph showing SOD activity of $[Mn_2(HL1)(Cl)_2]_2(ClO_4)_2$

For the reference sample, which contains no SOD mimic, the rate of change of absorbance is 0.025 per minute, and represents the rate of formation of $O_2^{\cdot-}$ without any complex added and this is referred to as the flux. The flux is used to calculate the % inhibition of NBT in the presence of a complex, when the inhibition of NBT is 100% then the rate of change of absorbance is equal to 0. When there is 0% inhibition, the rate of change of absorbance is equal to the slope of the flux. The calibration graph is illustrated in Figure 3-6, i.e:

% Inhibition	Change in absorbance per second
0	3.6165×10^{-4} (slope)
100	0

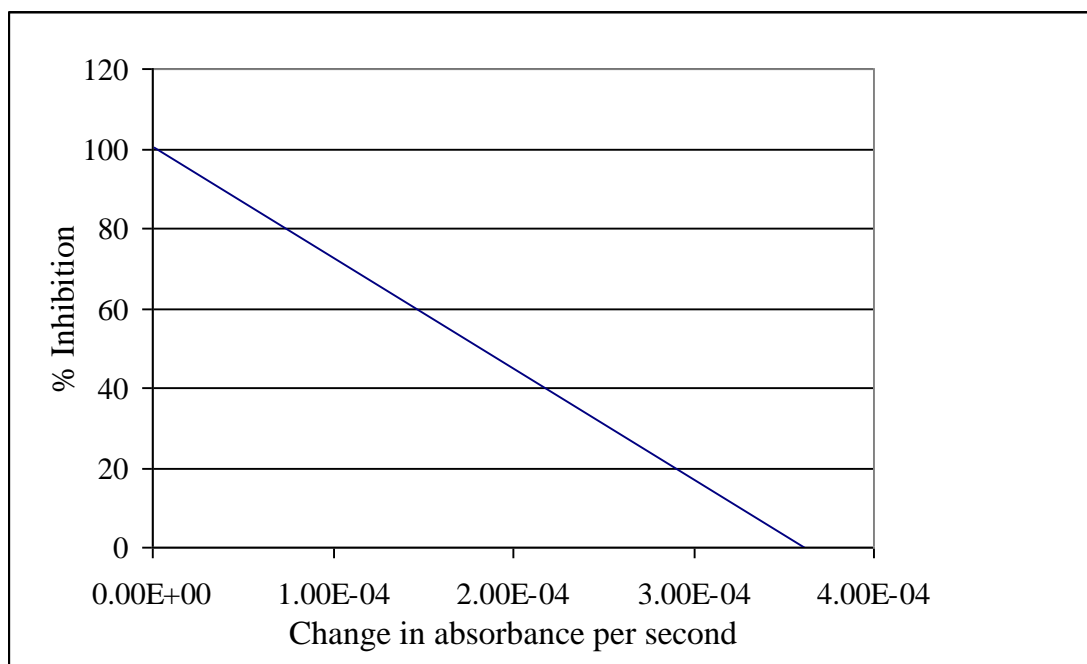


Figure 3-6 – Calibration graph for NBT assay

The % inhibition for each concentration is then calculated from the graph shown in Figure 3-6 using the equation $y = m x + c$, where $y =$ % inhibition and $x =$ rate for each concentration substituted and obtained from the graph in Figure 3-5. After calculating the concentration of the compound in each sample, a graph showing % inhibition versus concentration is produced as shown in Figure 3-7. The graph was used to calculate the half maximal inhibitory concentration referred to as the IC_{50} value, which is derived from linear regression analyses and given as the concentration (μM) equivalent to 1 unit of SOD activity. One unit of SOD activity is the concentration of the complex that causes 50% inhibition in the reduction of NBT, i.e from the equation obtained from the graph in Figure 3-7 where $y = 50$.

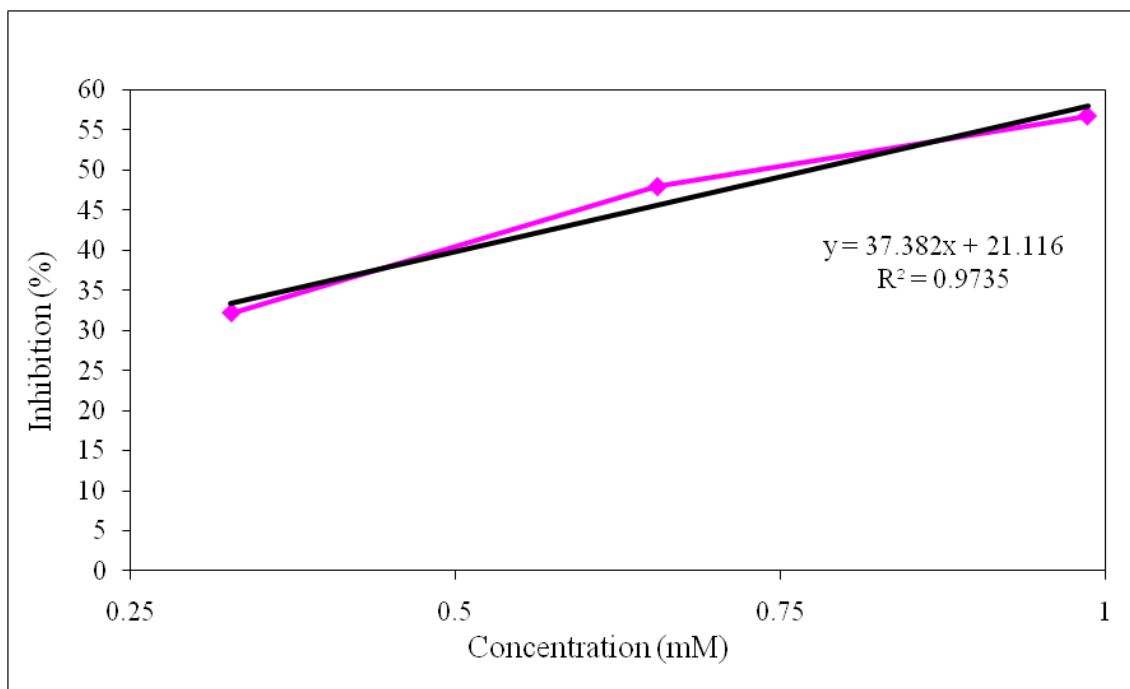


Figure 3-7 - Graph of inhibition (%) versus concentration for complex $[Mn_2(HL1)(Cl)_2]_2(ClO_4)_2$

The IC_{50} values, which are dependent upon the detector used, and the concentration of the detector [NBT], can be used to calculate the apparent kinetic rate K_{McCF} using the calculation proposed by McCord and Fridovich shown in Equation 3^{107, 108} where k_{NBT} (pH 7.8) = $5.94 \times 10^4 \text{ mol}^{-1} \text{ L s}^{-1}$:

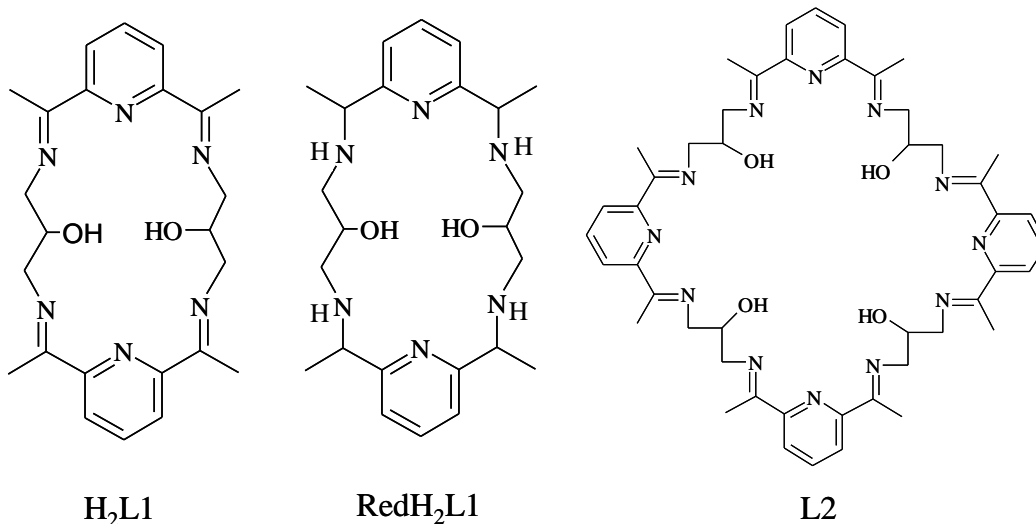
$$K_{McCF} = k_{NBT} \times [NBT] / IC_{50}$$

Equation 3 – Equation for the kinetic SOD rate of activity K_{McCF}

The calculated rates are more appropriate for a comparison of results with literature values, as IC_{50} values will be smaller where a lower [NBT] has been used and the calculated rate is independent of both the nature and concentration of detector used.

3.2.3 Results

Polynuclear complexes



Complex	IC ₅₀ (μM) (NBT assay)	<i>k</i> _{McCF} (M ⁻¹ s ⁻¹)
[Mn ₂ (HL1)(Cl) ₂] ₂ (ClO ₄) ₂	0.77	7.7 x 10 ⁶
[Mn ₂ (RedHL1)(Cl) ₂] ₂ MnCl ₄	0.82	7.2 x 10 ⁶
[Mn ₂ (HL1)(N ₃) ₂] ₂ (ClO ₄) ₂	1.53	3.7 x 10 ⁶
[Mn ₂ (RedHL1)(N ₃) ₂] ₂ (ClO ₄) ₂	0.99	6.0 x 10 ⁶
[Mn ₂ (HL1)(NCS) ₂] ₂ (ClO ₄) ₂	Inactive	0
[Mn ₂ (L1)(OAc) ₂] ₂ (ClO ₄) ₂	1.60	3.6 x 10 ⁶
[Mn ₅ (L1) ₂ (OAc) ₂ (ClO ₄) ₂](ClO ₄) ₂	1.07	5.7 x 10 ⁶
[Mn ₄ (L2)(ClO ₄) ₄]	1.30	4.6 x 10 ⁶
[Mn ₄ (L2)(ClO ₄) ₂ (NCS) ₂]	0.90	6.6 x 10 ⁶

For the complexes tested, [Mn₂(HL1)(Cl)₂]₂(ClO₄)₂ showed the greatest potential as a working SOD mimic displaying an IC₅₀ value of 0.77 μM which gives a calculated *k*_{McCF} value of 7.7x10⁶ M⁻¹s⁻¹. Although the complex [Mn₅(L1)₂(OAc)₂(ClO₄)₂](ClO₄)₂ also showed high activity and contains the same ligand structure as [Mn₂(HL1)(Cl)₂]₂(ClO₄)₂, the extra manganese centre did not

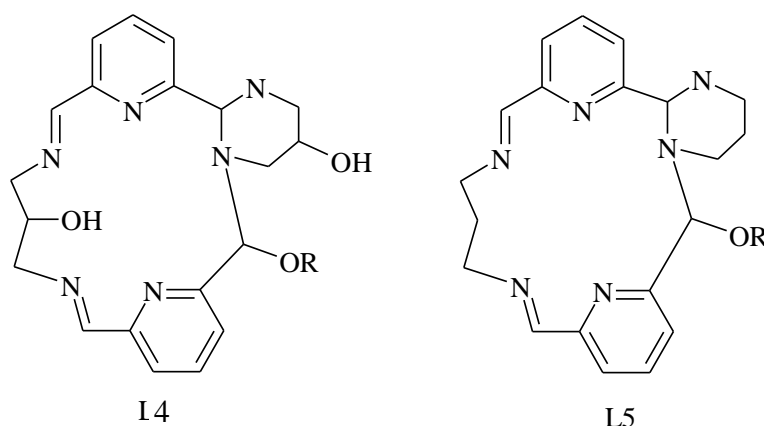
produce a higher rate as may be expected. This may be due to the bridging basic acetate ligands producing an inhibition of the SOD activity. This also indicates that the bridging chloride ligand is important for the observed rate of superoxide dismutase activity. A chloride ligand is expected to dissociate more readily from the manganese than an acetate ligand. Thus, the results may suggest that the ease of dissociation of the ligand is important and that the ligand may be substituted by the incoming superoxide molecule. This is supported by the result obtained for the polynuclear complex of L1 $[\text{Mn}_2(\text{HL1})(\text{NCS})_2]_2(\text{ClO}_4)_2$ containing the strongly bound thiocyanate axial ligand which did not display any SOD activity.

A reduction of the imine bonds, forming the complex $[\text{Mn}_2(\text{RedHL1})(\text{Cl})_2]_2[\text{MnCl}_4]$ which is similar in structure to $[\text{Mn}_2(\text{HL1})(\text{Cl})_2]_2(\text{ClO}_4)_2$ produced a slight reduction in the rate of superoxide dismutase activity with an IC_{50} value of $0.82 \mu\text{M}$ and a K_{McCF} value of $7.2 \times 10^6 \text{ M}^{-1}\text{s}^{-1}$. This may mean that the complex contains a more ideal geometry before the reduction has taken place for the SOD activity to occur at the manganese centre, however, there is a difference in the counter ion that is present in the two complexes, the reduced analogue contains a MnCl_4 ion which could possibly interfere with the SOD activity that has been observed. There is also a possibility that the differences that have been observed are due to errors that may be encountered in the method and that the reduction for this complex system does not alter the geometry of the manganese enough to increase the SOD activity significantly. However, the results that have been obtained for the complex $[\text{Mn}_2(\text{HL1})(\text{N}_3)_2]_2(\text{ClO}_4)_2$ and the reduced analogue $[\text{Mn}_2(\text{RedHL1})(\text{N}_3)_2]_2(\text{ClO}_4)_2$ which gave calculated K_{McCF} values of $3.7 \times 10^6 \text{ M}^{-1}\text{s}^{-1}$ and $6.0 \times 10^6 \text{ M}^{-1}\text{s}^{-1}$ respectively, suggest that a reduction for this complex does produce an increase in SOD activity which may be due to an increase in the flexibility of the ligand, allowing easier access to the manganese centres for the superoxide radical.

Complexes of L2 also showed good SOD activity with the complexes $[\text{Mn}_4(\text{L2})(\text{ClO}_4)_4]$ and $[\text{Mn}_4(\text{L2})(\text{ClO}_4)_2(\text{NCS})_2]$ showing calculated K_{McCF} values of $4.6 \times 10^6 \text{ M}^{-1}\text{s}^{-1}$ and $6.6 \times 10^6 \text{ M}^{-1}\text{s}^{-1}$ respectively, the difference that is observed shows that the presence of the thiocyanate bound axial ligands for this ligand system increases SOD activity. The [4+4] nature of L2 and the dimeric [2+2] nature of

complexes for L1, produce different structures for each types of complex and there may be less access to the manganese centres for complexes of L2, it is possible that the bulkier perchlorate ligands prevent access to the manganese centres for the superoxide molecule to react. It could be possible to test this with the presence of different axial ligands such as the chloride ligand which is less bulky and less strongly bound than the thiocyanate ligand which would be expected to produce a faster rate of SOD activity than that found for the thiocyanate bound complex.

Mononuclear complexes – Ring contracted species



Where R refers to either MeOH or EtOH

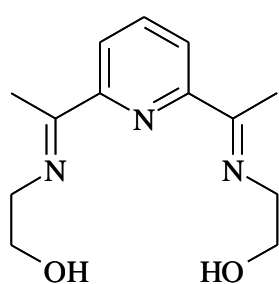
Complex	IC ₅₀ (μM) (NBT assay)	<i>k</i> _{M_{CCF}} (M ⁻¹ s ⁻¹)
[Mn(L4)(NCS) ₂].MeOH	2.70	2.2 x 10 ⁶
[Mn(L4)(NCS) ₂].EtOH	3.77	1.6 x 10 ⁶
[Mn(L4)(N ₃) ₂].MeOH	1.10	5.2 x 10 ⁶
[Mn(L5)(NCS) ₂].MeOH	Inactive	0

The ring contracted species [Mn(L4)(NCS)₂].MeOH and [Mn(L4)(N₃)₂].MeOH proved to possess high rates of catalytic activity even in the presence of a thiocyanate ligand which apparently rendered alternative ligand system complexes inactive. The complex [Mn(L4)(N₃)₂].MeOH showed the highest rate of activity with a calculated *K*_{M_{CCF}} of 5.2 x 10⁶ M⁻¹ s⁻¹ when compared to the thiocyanate bound complex [Mn(L4)(NCS)₂].MeOH which had a calculated *K*_{M_{CCF}} of 2.2 x 10⁶ M⁻¹ S⁻¹. Consequently, there is potential for even higher rates to be achieved with the

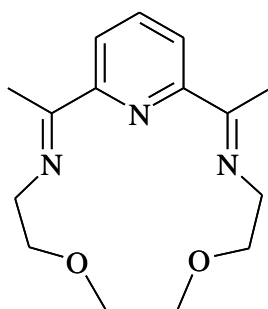
presence of alternative axial ligands such as the chloride or aqua ligands, these complexes when compared to those of the tetranuclear complexes of L1 have no bridging ligands and are not dimers. This may be important for the mechanism of SOD activity, possibly providing an easier access for the $O_2^{\cdot-}$ ion to the manganese centre. SOD activity was also found to decrease when the MeOH group was replaced with EtOH across the imine bond for complexes of L4, and this may lead to a slightly different geometry at the metal centre.

The complex $[Mn(L5)(NCS)_2].MeOH$ did not show any superoxide dismutase activity, and the difference between the complexes of L4 and L5 is the presence of the OH groups that are present in the ligand system of L4, despite the OH groups remaining uncoordinated to the manganese ion. The OH group is present in L4 in the six membered ring that is formed during the ring contraction process, the presence of the OH group may stabilise the position that the nitrogen is coordinated to the manganese centre by possibly introducing rigidity into the system, however, the L5 complex did contain a thiocyanate axial ligands which when present in the tetranuclear complex $[Mn_2(HL1)(NCS)_2]_2(ClO_4)_2$, was also inactive, so with the presence of an alternative axial ligand, there is the potential for SOD activity to be observed for this ligand system.

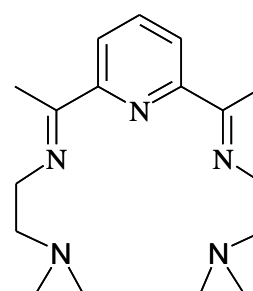
Mononuclear complexes



L9



L10



L11

Complex	IC ₅₀ (μM) (NBT assay)	<i>k</i> _{MCCF} (M ⁻¹ s ⁻¹)
[Mn(L9)(Cl) ₂]	2.44	2.4 x 10 ⁶
[Mn(L9)(OH) ₂](ClO ₄) ₂	2.08	2.9 x 10 ⁶
[Mn(L10)(Cl) ₂]	Inactive	0
[Mn(L11)(Cl) ₂]	2.91	2.0 x 10 ⁶
[Mn(L12)(Cl) ₂]	2.60	2.3 x 10 ⁶
[Mn(L15)(NCS) ₂].MeOH	2.09	2.8 x 10 ⁶

The mononuclear complexes [Mn(L9)(Cl)₂], [Mn(L10)(Cl)₂] and [Mn(L11)(Cl)₂] were the least active of the ligand systems tested, with [Mn(L10)(Cl)₂] inactive as a SOD mimic. The complex [Mn(L10)(Cl)₂] is a macrocyclic complex and contains a more rigid ligand structure than [Mn(L9)(Cl)₂] or [Mn(L11)(Cl)₂]. All three complexes contain two methyl groups on the pyridine diimine head unit of the complex. The complex [Mn(L9)(Cl)₂] contains two oxygen donor molecules in the ligand system as well as three nitrogen donors from the head unit all forming the pentagonal plane of the molecule, whereas [Mn(L11)(Cl)₂] contains five nitrogen donor atoms, rates for *K*_{MCCF} of 2.4 x 10⁶ and 2.0 x 10⁶ M⁻¹ s⁻¹ have been reported here respectively and although the rates are very similar, a slight increase in rate was obtained for complex [Mn(L9)(Cl)₂] indicating that the type of donor in the ligand system is also important.

The fact that there are differing rates for SOD activity with slight differences in geometry and ligand systems, indicates that the metal does not dissociate from the ligand for those complexes tested and that the geometry has some effect on the rates that have been achieved with the ease of dissociation for the axial ligand being an important factor for the design of a SOD mimic. The rates that have been reported fall within the ranges for SOD activity of other previously published structures.

Some values for SOD activity obtained from the literature are given in Table 22.

Table 22 – Values for SOD activity of known compounds

Compound	K_{cat} (M⁻¹ s⁻¹)	Method
Mn(ClO ₄) ₂ + EDTA ¹⁰⁹	3.4 x 10 ⁴	Indirect
Mn(ClO ₄) ₂ ¹⁰⁹	1.3 x 10 ⁶	Indirect
SODm1 ⁶⁷	3.6 x 10 ⁶	Pulse radiolysis
SODm2 ⁶⁷	2.35 x 10 ⁸	Pulse radiolysis
SODm3 ⁶⁷	Inactive	Pulse radiolysis
M40403 ¹¹⁰	1.6 x 10 ⁷	Stopped-flow
MnSOD ^{56, 111}	5.5 x 10 ⁸	Indirect
S,S-Dimethyl-M40403 ³⁹	1.6 x 10 ⁹	Stopped-flow
Cu/Zn SOD ^{54, 112}	2 x 10 ⁹	Pulse radiolysis

* For structure of SODm1, SODm2 and SODm3 see Figure 1-26

* For structure of M40403 see Figure 1-24

The results for SOD activity obtained from the literature show that there are complexes that have been prepared with catalytic rates of activity that exceed that of the natural MnSOD enzyme itself, and that changes in geometry of the manganese centre can provide a faster rate of reaction. The table also shows that Mn(ClO₄)₂ has a high rate of catalytic activity, and when EDTA⁴⁻ was added to the solution, the reaction was partly inhibited. The results that have been obtained for the complexes in this thesis, have shown higher rates than that of Mn(ClO₄)₂ which supports the idea that the ligand and its geometry on the manganese centre is providing some impact on the rate that is being achieved.

3.2.4 Direct analysis – Stopped-flow technique 1

Stop-flow analysis is a direct method for measuring the fast rate of superoxide dismutase activity. The superoxide radical is generated at initially high concentrations and then the decay of the superoxide absorbance is followed spectrophotometrically in the UV region, allowing a precise measurement of the rate to be made.⁷⁵ The stopped-flow technique is limited to complexes with a K_{cat} higher than $1.5 \times 10^5 \text{ M}^{-1}\text{s}^{-1}$ because superoxide self-dismutates with a second order rate constant of $1.5 \times 10^5 \text{ M}^{-1}\text{s}^{-1}$ at 21 °C. The direct method is less prone to false positives than the indirect methods;⁷² thus, attempts were made to develop a method of analysis using a stopped-flow technique to complement the results obtained for the indirect xanthine/xanthine oxidase method previously described.

A schematic representation of the stopped-flow equipment is shown below in Figure 3-8. Superoxide solution is placed into syringe A and complex solution is placed into syringe B; on pushing the driver, liquid from both syringes is pushed out into the mixer in a 1:1 ratio into the cell and optical measurements are recorded.

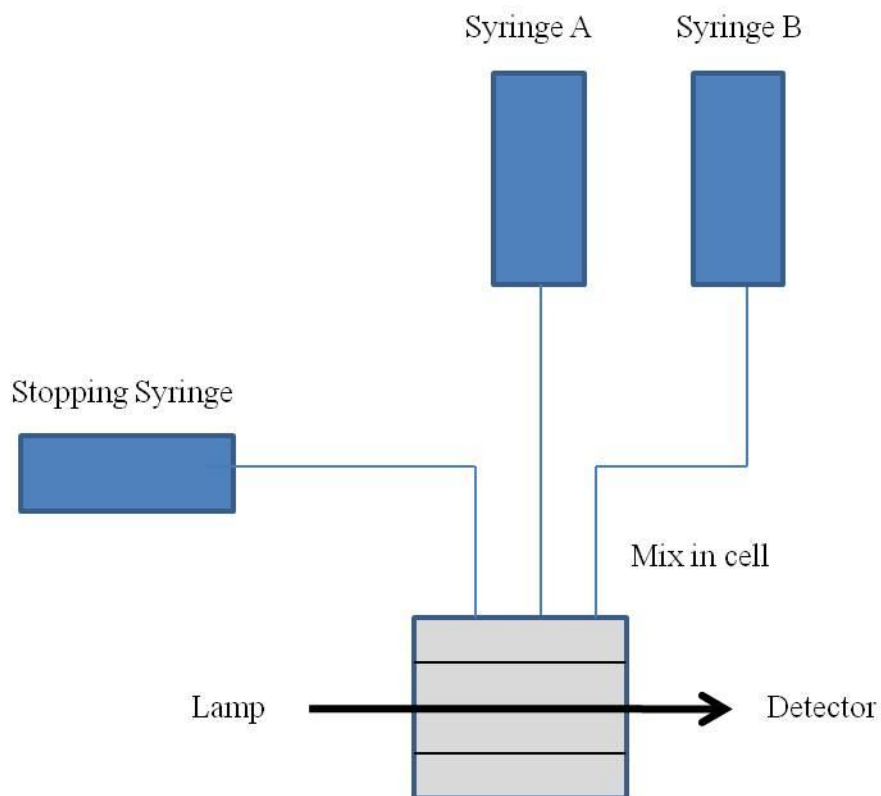


Figure 3-8 – *Schematic representation of stopped-flow equipment*

For the stopped-flow technique, the experimental set up consisted of an SFA-20 stopped-flow set up connected to a HP 8453 diode array detector.

Experimental

A solution of potassium superoxide was prepared under nitrogen, by adding potassium superoxide (0.201 g) and tertiary butylammonium perchlorate (1.703 g, 0.10 M to increase ionic strength) into a volumetric flask (50 ml) and made to volume with analytical grade dimethylsulfoxide (DMSO). The solution was then placed into an ultra sonic bath for 30 mins, or until the solution was yellow, indicating the presence of superoxide. The solution was then filtered to remove any excess solid potassium superoxide. This was stored in darkness by wrapping in aluminium foil to prevent decomposition through irradiation.

A solution of $[\text{Mn}_2(\text{RedHL}_2)(\text{Cl})_2]_2[\text{MnCl}_4]$ (0.0073 g, 1×10^{-4} M) was prepared by making to volume in analytical grade DMSO (50 ml) and varying concentrations in

the range 1×10^{-5} M to 1×10^{-7} M were prepared *via* serial dilution of the initial complex solution.

A solution of $[\text{Mn}(\text{L10})(\text{OH}_2)_2]_2(\text{ClO}_4)_2$ (0.0028g, 1×10^{-4} M) was prepared by making to volume in analytical grade DMSO (50 ml) and varying concentrations in the range 1×10^{-5} M to 1×10^{-7} M were prepared *via* serial dilution of the initial complex solution.

During analysis, superoxide solution was placed into syringe A. Complex solution was placed into syringe B (see Figure 3-8). The two solutions were then pushed into the cell where the solutions mix in a 1:1 ratio. This allows changes in absorbance to be measured at 270 nm upon mixing.

3.2.5 Results

Absorbance spectra were initially recorded and used to determine where λ_{max} appears for both the superoxide solution and the complex solution by placing the analyte of interest into syringe A and pure DMSO in to syringe B (see Figure 3-8) then injecting the solutions into the cell, this was carried out to see that there was no overlap of the peaks from the two solutions. Figure 3-9 below demonstrates the observed superoxide peak which was recorded at both the start of the analysis and at the end of the analysis to confirm that the superoxide solution was stable throughout.

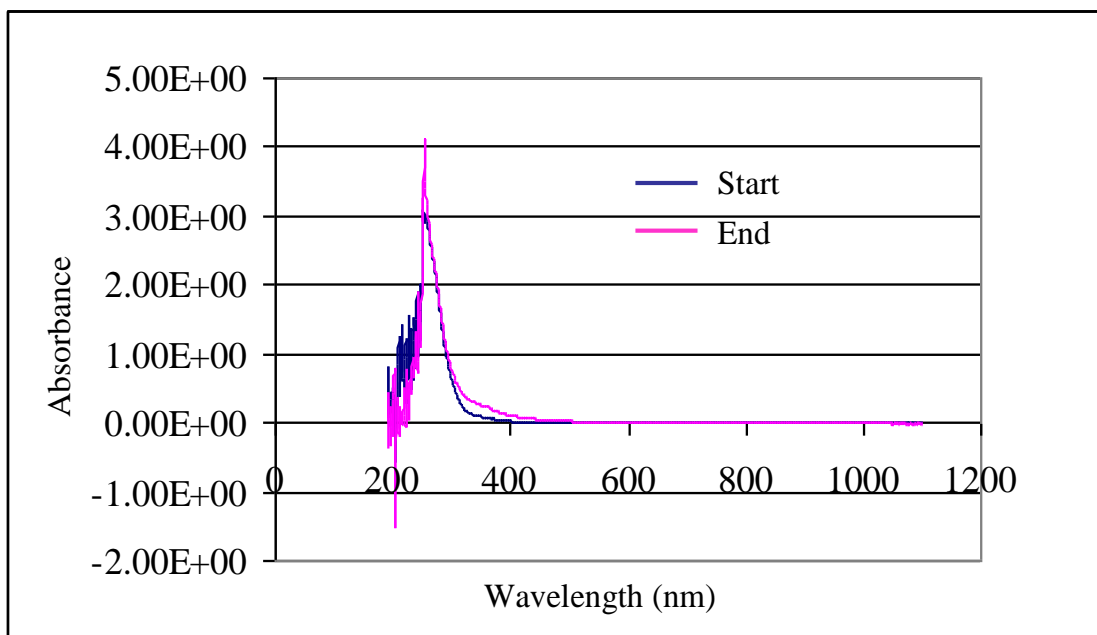


Figure 3-9 – Absorbance spectrum for a superoxide solution

The concentration of superoxide solution was calculated as $0.002 \text{ mol}^{-1} \text{ dm}^3$. Taken from the known extinction coefficient of $2686 \pm 29 \text{ M}^{-1} \text{ cm}^{-1}$ for superoxide in DMSO.^{113, 114}

The overlay of the absorbance peaks for the superoxide solution and the complex $[\text{Mn}_2(\text{RedHL}_2)(\text{Cl})_2]_2[\text{MnCl}_4]$ are shown in Figure 3-10.

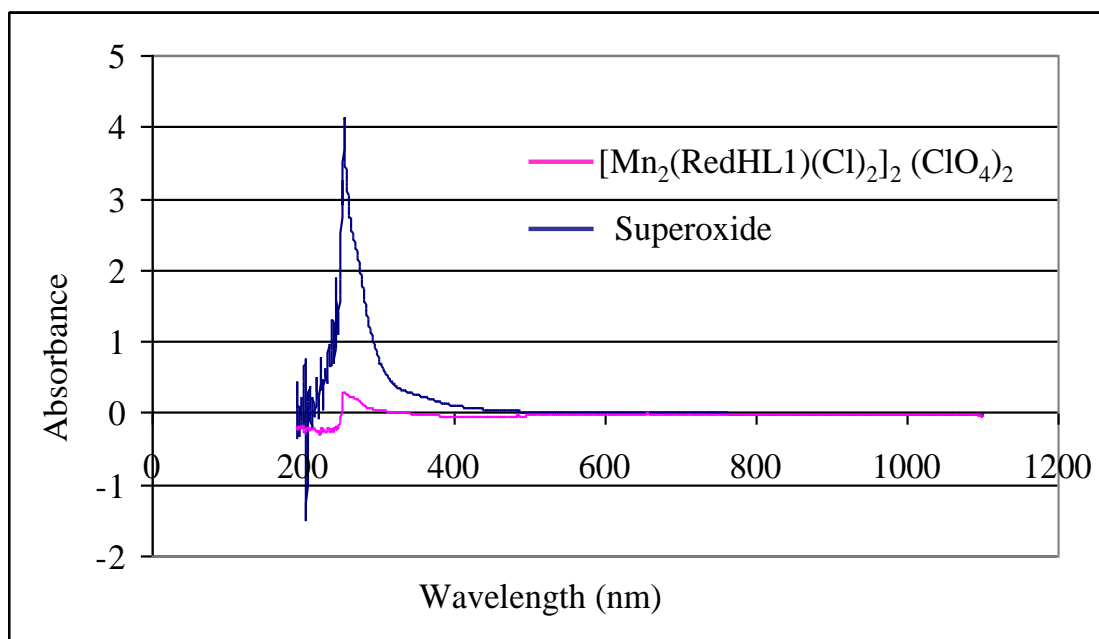


Figure 3-10 – Absorbance spectrum of $[\text{Mn}_2(\text{RedHL1})(\text{Cl})_2]_2(\text{ClO}_4)_2$ overlaid with superoxide

The absorbance spectrum shown in Figure 3-10 confirms that there is no overlap in absorbance at 270 nm between the complex $[\text{Mn}_2(\text{RedHL}_2)(\text{Cl})_2]_2[\text{MnCl}_4]$ solution and the superoxide solution. This confirms that the kinetic trace can be followed for superoxide at 270 nm without interference from the complex solution.

The kinetic trace for the stopped-flow analysis of superoxide mixed with the complex $[\text{Mn}_2(\text{RedHL}_2)(\text{Cl})_2]_2[\text{MnCl}_4]$ at a concentration of 1×10^{-7} M as followed at 270 nm is shown below in Figure 3-11.

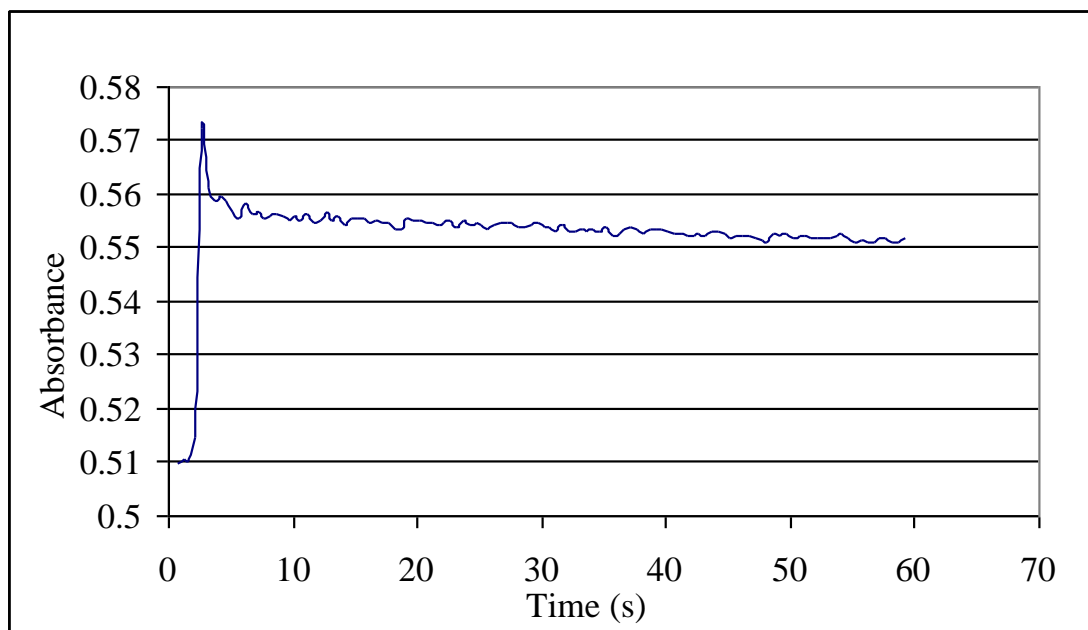


Figure 3-11 – Kinetic trace for stopped-flow analysis of superoxide and $1 \times 10^{-7} M$ $[Mn_2(RedHL_2)(Cl)_2]_2[MnCl_4]$

The kinetic trace illustrated in Figure 3-11 shows that the reaction is complete on mixing of the solutions. There is an increase in absorbance as the solutions enter the cell, however, only the tail end of the reaction can be seen for this example. The absorbance reading becomes stable at ~ 0.554 which may be due to the complex in the solution. This shows that the complex has not been broken down during the reaction. The kinetic trace shown is for the lowest concentration of complex that was prepared, previous analyses were carried out at concentrations of $1 \times 10^{-4} M$ and the kinetic trace was similar in appearance to that shown in Figure 3-11. Lower concentrations were analysed, with the intention of slowing the reaction to a level that could be measured with the technique described.

The same analysis were carried out with the mononuclear complex $[Mn(L10)(H_2O)_2](ClO_4)_2$ which has been shown to have a lower catalytic activity than the complex $[Mn_2(RedHL_2)(Cl)_2]_2[MnCl_4]$ as shown using the indirect NBT assay previously described. The absorbance spectrum of $[Mn(L10)(H_2O)_2](ClO_4)_2$ overlaid with superoxide is shown below in Figure 3-12.

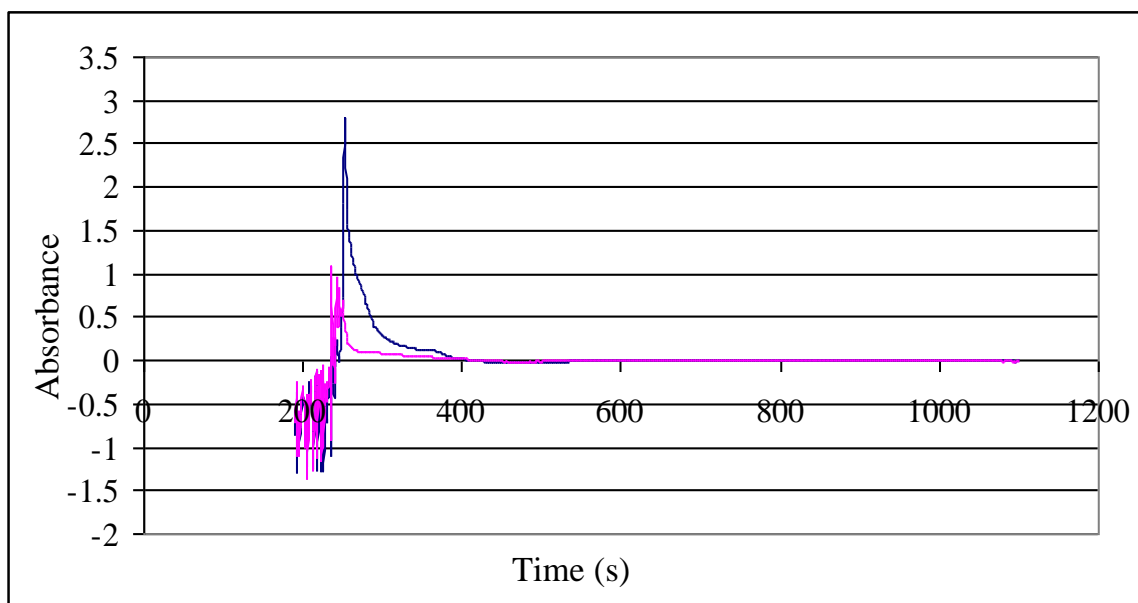


Figure 3-12 – Overlay of superoxide with $[Mn(L10)(H_2O)_2](ClO_4)_2$

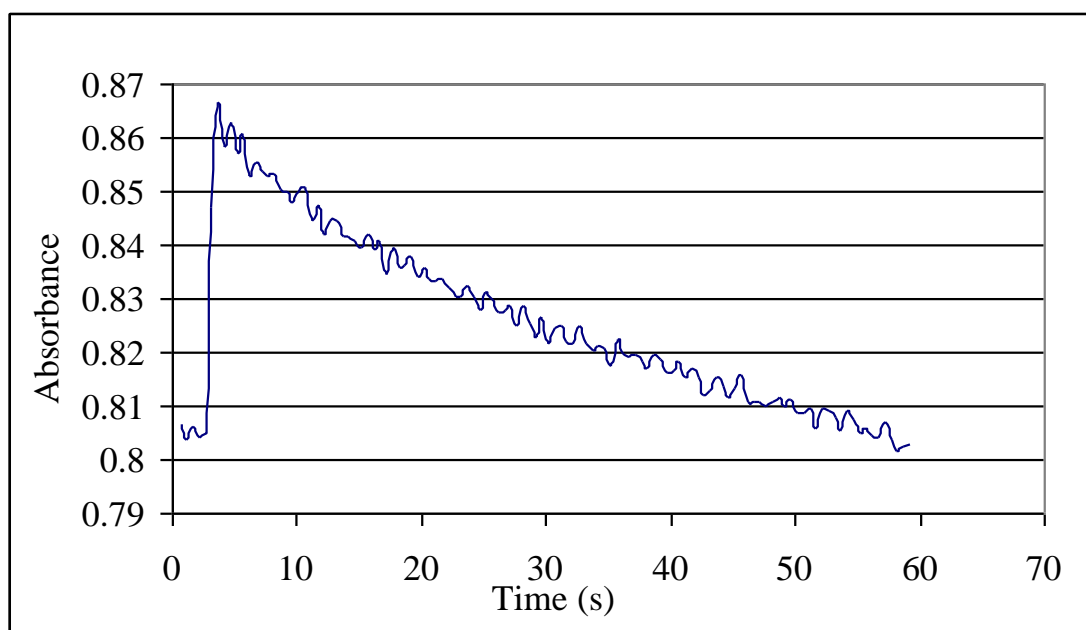


Figure 3-13 – Kinetic trace for stopped-flow analysis of superoxide and $1 \times 10^{-7} M$ $[Mn(L10)(H_2O)_2](ClO_4)_2$

The kinetic trace as shown in Figure 3-13, also shows the initial increase in absorbance as the solutions enter the cell. The absorbance then falls slowly from 0.867 down to 0.805. This may be due to changes occurring to the complex whilst in solution.

Despite many attempts using the diode array detector, this technique was unsuccessful for monitoring the reactions for superoxide due to its detection limit of 0.5 s. However absorbance values could be used to monitor where λ_{\max} appears for any complex under analysis and ensure no overlap occurs between the complex and the superoxide peak.

3.2.6 Direct analysis – Stopped-flow technique 2

In attempts to allow measurement of faster rates by the stopped-flow technique, the stopped-flow equipment was coupled with a fluorimeter which was used as the light source and an oscilloscope to allow a faster measurement to be made (see fig Figure 3-14 below). For this experiment, the amount of light passing through the cell was recorded at 270 nm, so when superoxide which absorbs light at 270 nm entered the cell, the amount of light hitting the detector was reduced, hence a drop in voltage was recorded on the oscilloscope. The voltage was then expected to rise back to the base level reading as the superoxide is broken down.

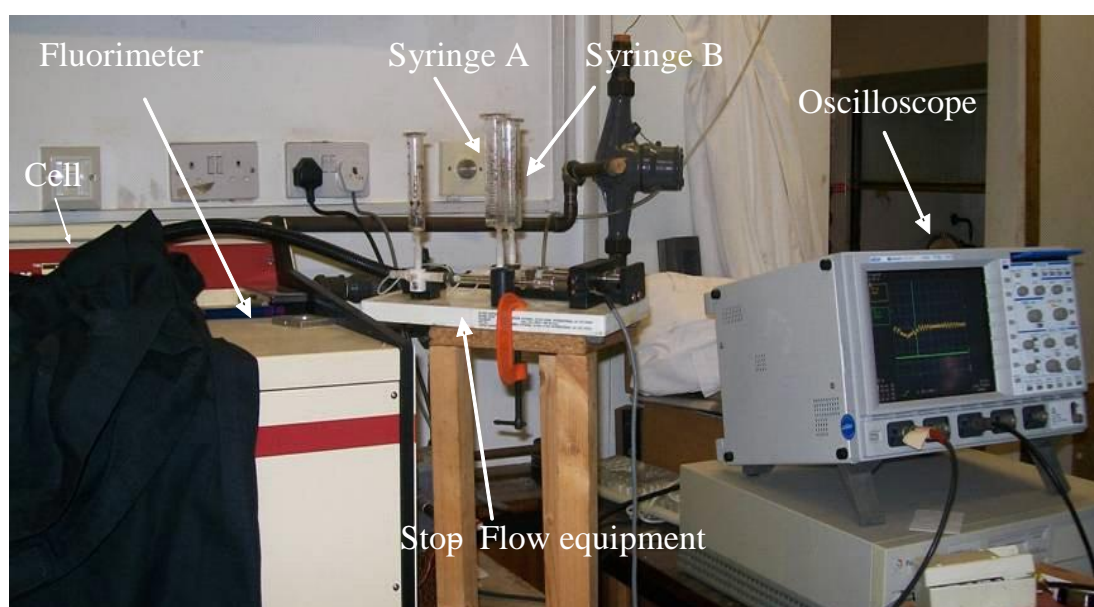


Figure 3-14 – *Stop-flow set up*

(see Figure 3-8 for schematic representation of the stopped-flow equipment)

Experimental

A solution of superoxide was prepared as previously described for the stopped-flow technique 1. A solution of $[\text{Mn}_2(\text{RedHL}_2)(\text{Cl})_2]_2\text{MnCl}_4$ (0.0073g, $1 \times 10^{-4}\text{M}$) was prepared by making to volume in DMSO (50 ml) and varying concentrations in the range $1 \times 10^{-5}\text{ M}$ to $1 \times 10^{-7}\text{ M}$ were prepared *via* serial dilution of the complex solution. A solution of $[\text{Mn}(\text{L10})(\text{OH}_2)_2]_2(\text{ClO}_4)_2$ (0.0028g, $1 \times 10^{-4}\text{M}$) was prepared by making to volume in DMSO (50 ml) and varying concentrations in the range $1 \times 10^{-5}\text{ M}$ to $1 \times 10^{-7}\text{ M}$ were prepared *via* serial dilution of the complex solution. Complex solutions were prepared with a controlled amount of water, 0.06 % once mixed in the cuvette.⁵⁶ During analysis: superoxide solution was placed into syringe A and complex solution was placed into syringe B (see Figure 3-8), the two solutions were then pushed into the cell where the solutions mix in a 1:1 ratio. Results were recorded on a Lecroy waverunner LT364 500MHz oscilloscope as voltage versus time at 270 nm and the results exported into excel for manipulation.

3.2.7 Results

Initial experiments involved the detection of superoxide at 270 nm during mixing with $[\text{Mn}_2(\text{RedHL}_2)(\text{Cl})_2]_2[\text{MnCl}_4]$ and to see if any changes occur with varying concentrations of complex. This complex was chosen due to its activity observed using the modified NBT assay described earlier. As seen previously in Figure 3-10 no interference in the absorbance peaks were observed for this complex with superoxide at 270 nm as shown in Figure 3-15, so any change in voltage is due to the presence of superoxide in the solution.

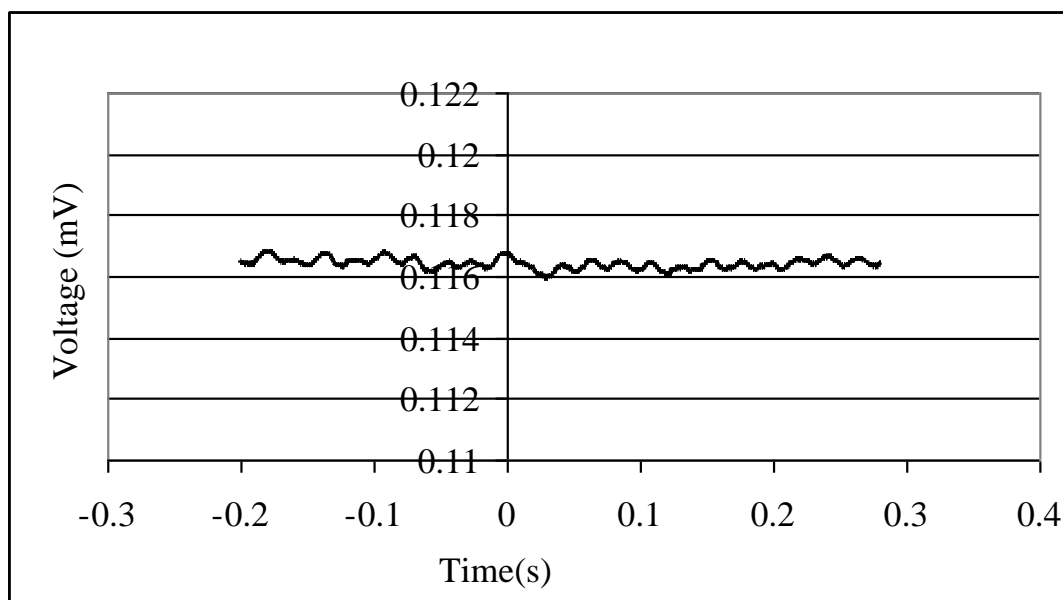


Figure 3-15 – Pure DMSO

Figure 3-15 shows that there is no change in voltage observed when a sample of pure DMSO is analysed at a wavelength of 270 nm

The following output readings of voltage versus time were obtained for superoxide when combined in the stopped-flow with different concentrations of the complex $[\text{Mn}_2(\text{RedHL}_2)(\text{Cl})_2]_2[\text{MnCl}_4]$, these were recorded to see any differences that may be observed in the peak and whether the reaction could be slowed enough for a catalytic rate to be measured.

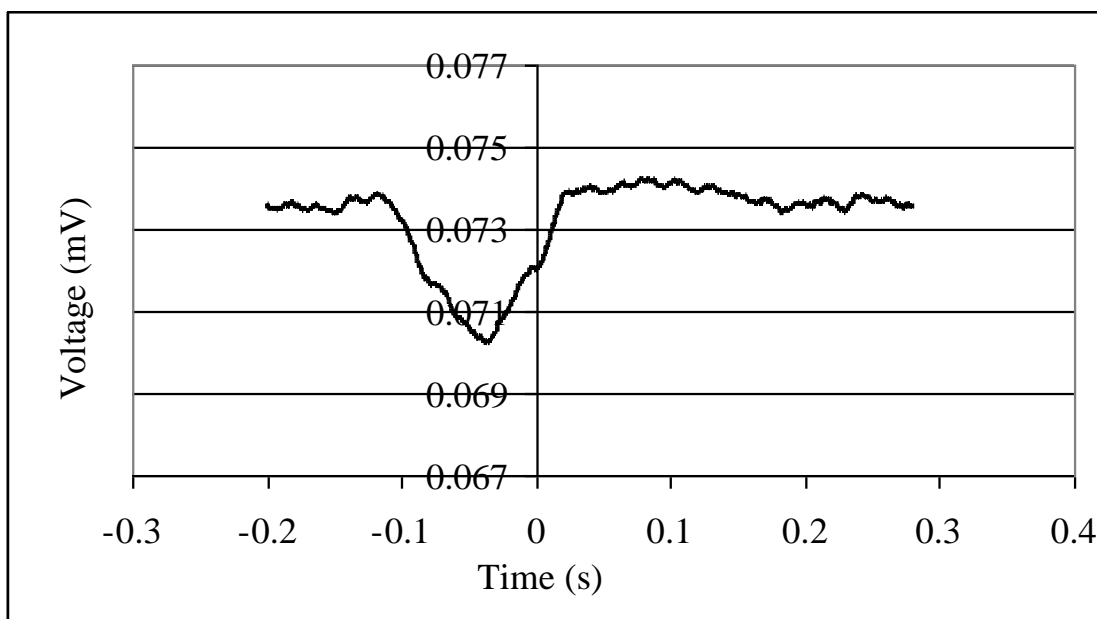


Figure 3-16 - Reaction of superoxide solution with $1 \times 10^{-4} M$
 $[Mn_2(RedHL2)(Cl)_2]_2[MnCl_4]$

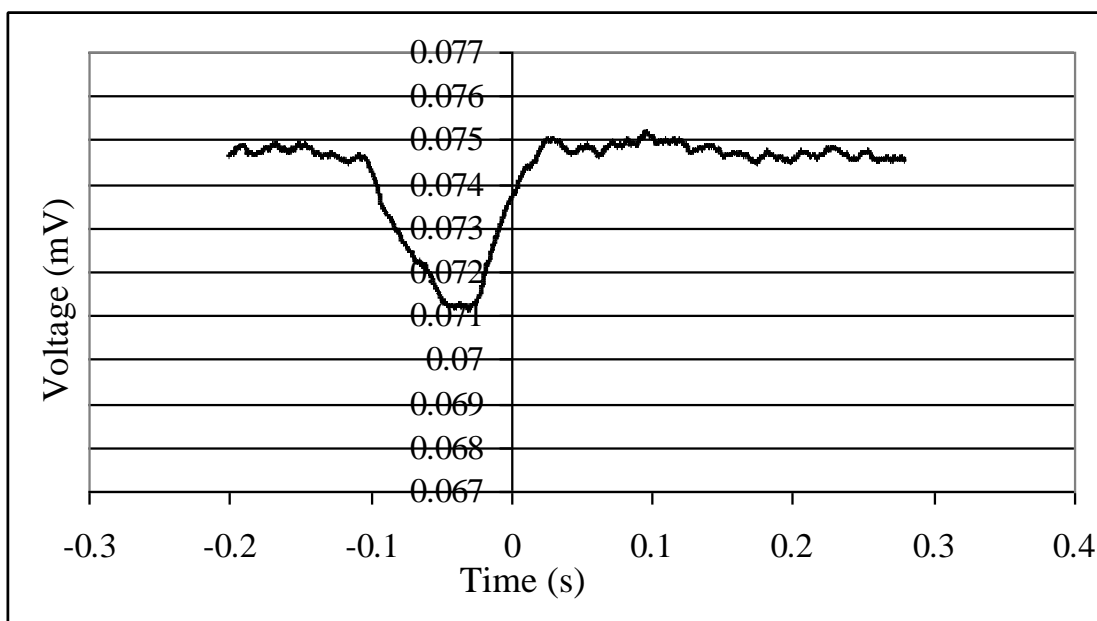


Figure 3-17 - Reaction of superoxide solution with $1 \times 10^{-5} M$
 $[Mn_2(RedHL2)(Cl)_2]_2[MnCl_4]$

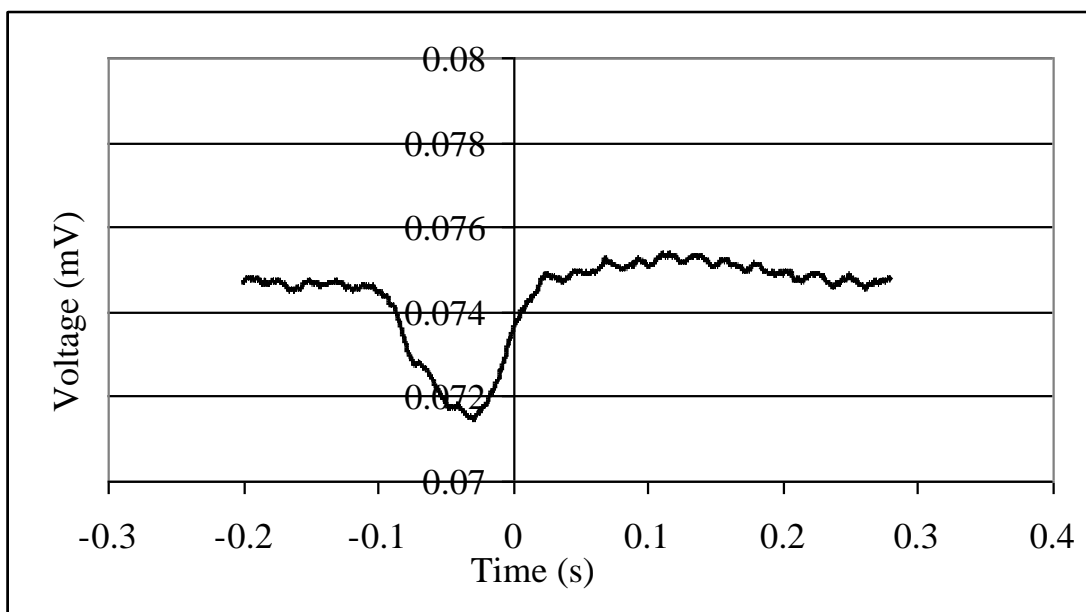


Figure 3-18 - Reaction of superoxide solution with $1 \times 10^{-6} M$
 $[Mn_2(RedHL_2)(Cl)_2]_2[MnCl_4]$

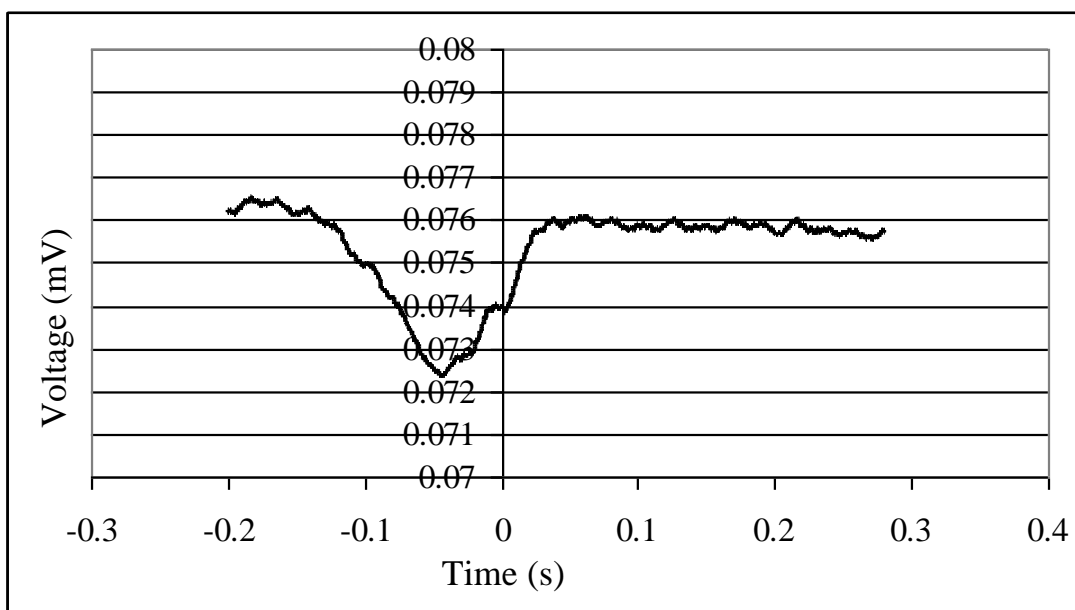


Figure 3-19 - Reaction of superoxide solution with $1 \times 10^{-7} M$
 $[Mn_2(RedHL_2)(Cl)_2]_2[MnCl_4]$

The results that were obtained for the different concentrations of complex $[Mn_2(RedHL_2)(Cl)_2]_2MnCl_4$ could not be used for the measurement of a catalytic rate as there was not a significant difference in the voltage rise back to the base line level

which represents the decay of superoxide, this is likely to be due to the reaction being complete on a scale that is too fast for the stopped-flow set up which has a mixing time of 30 ms.

The previous experiment was then repeated using the mononuclear complex $[\text{Mn}(\text{L10})(\text{H}_2\text{O})_2](\text{ClO}_4)_2$. This complex was chosen due to its much lower activity as observed using the modified NBT assay technique, this was with the intention of slowing the reaction down which would help to enable more measureable peaks.

The overlay of the absorption spectrum for superoxide with the complex $[\text{Mn}(\text{L10})(\text{H}_2\text{O})_2](\text{ClO}_4)_2$ was previously illustrated in Figure 3-12 and was shown not to interfere with the superoxide at a wavelength of 270 nm.

The following output readings of voltage versus time were obtained for superoxide when combined in the stopped-flow with different concentrations of the complex $[\text{Mn}(\text{L10})(\text{H}_2\text{O})_2](\text{ClO}_4)_2$.

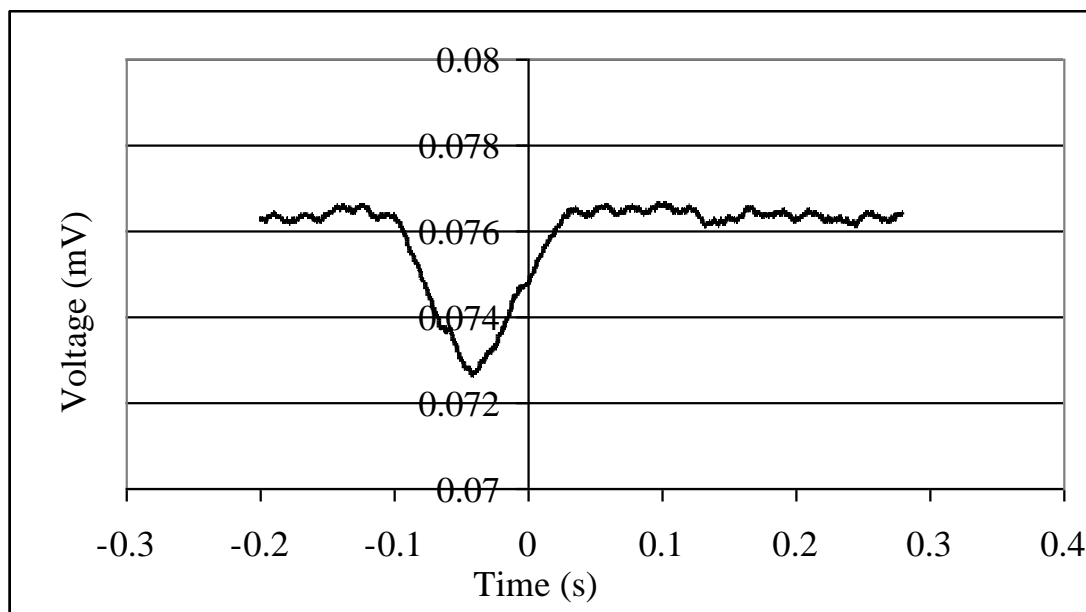


Figure 3-20 – Reaction of superoxide solution with $1 \times 10^{-4} \text{ M}$
 $[\text{Mn}(\text{L10})(\text{H}_2\text{O})_2](\text{ClO}_4)_2$

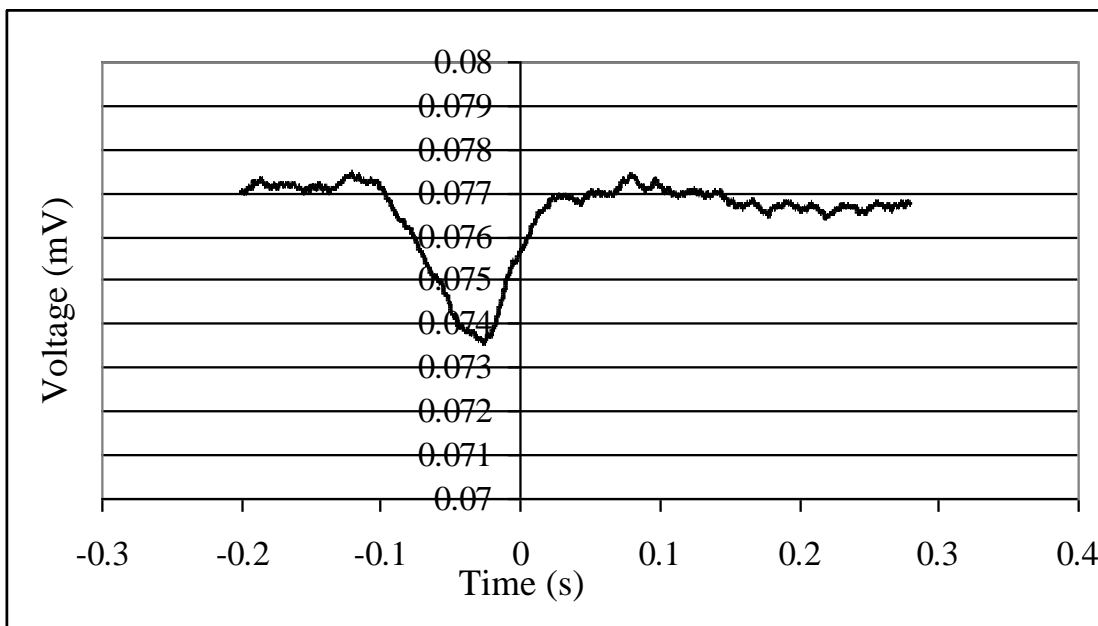


Figure 3-21 – Reaction of superoxide solution with $1 \times 10^{-5} M$
 $[Mn(L10)(H_2O)_2](ClO_4)_2$

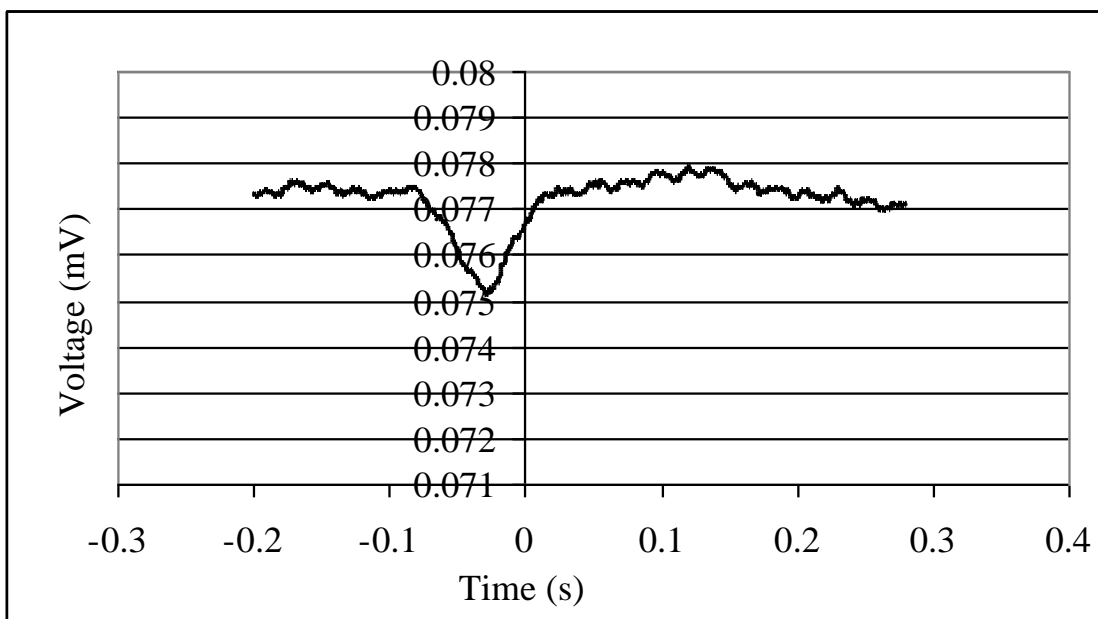


Figure 3-22 – Reaction of superoxide solution with $1 \times 10^{-6} M$
 $[Mn(L10)(H_2O)_2](ClO_4)_2$

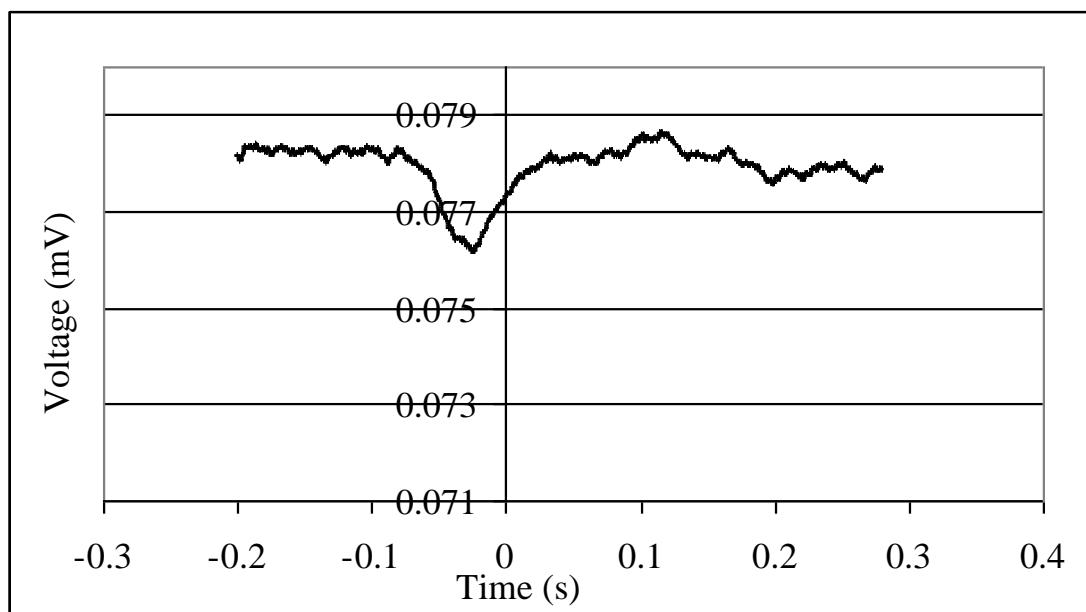


Figure 3-23 - Reaction of superoxide solution with $1 \times 10^{-7} M$
 $[Mn(L10)(H_2O)_2](ClO_4)_2$

Optimisation of this technique may be obtained with altering the amount of superoxide in the sample as well as that of the complex which may provide a more accurate result for this type of method. There is a possibility that the optimisation may be different with each complex as those with a faster catalytic activity may require a lower concentration of complex and a higher concentration of superoxide to enable a measurement to be made.

For all of the measurements that were made using the stopped-flow technique 2, it seems apparent that the voltage drop that is observed on mixing may be due to the turbidity of the DMSO mixing with water and this could be overcome with further testing with the technique which may involve varying the amount of water present and altering the ratio in which the two syringes mix. It is possible that the reaction is occurring on a millisecond mixing scale as the voltage drop is present before 0 seconds. To enable the reaction to be monitored and produce accurate kinetic rates, the reaction must be brought to a scale that allows measurement after the solutions have fully mixed, this could possibly be achieved with further probing of lower concentrations, lower temperatures and where possible, the addition of a microcuvette to minimise the dead time of stopped-flow technique.

3.3 Catalase Activity

The equipment for measuring catalase activity was set up for oxygen collection using two upturned 1000 cm³ measuring cylinders containing water. A water bath was maintained with a constant temperature of 25 °C as illustrated in Figure 3-24.



Figure 3-24 – *Equipment used for measuring catalase activity*

Volumetric determination of oxygen evolved was carried out by allowing the temperature of the water in the tank to equilibrate to 25 °C for a minimum of thirty minutes. Once complete, a sample of complex (1mg) was placed into methanol (1 ml) inside a three-necked round bottom flask. The solution was stirred and the flask sealed. Hydrogen peroxide (7.25 mol l^{-1} , 2 ml) was then injected through a rubber septum into the round bottom flask and the oxygen evolution was monitored every 10 seconds for 10 minutes. Each sample was tested with and without the addition of base (triethylamine). In the cases where triethylamine was used, 0.010g was added to the flask before the addition of hydrogen peroxide. The addition of base during catalase testing has previously been shown to increase catalytic activity.^{83, 84}

The hydrogen peroxide used was standardised by titration with KMnO_4 , followed with standardisation of the KMnO_4 with $(\text{NH}_4)_2\text{Fe}(\text{II})(\text{SO}_4)_2 \cdot 6\text{H}_2\text{O}$. The hydrogen peroxide was found to have a concentration of $7.25 \pm 0.08 \text{ mol l}^{-1}$. When 100 % of the hydrogen peroxide (2 ml) is broken down a volume of 162 ml of oxygen would be expected to be produced when the reaction is complete. However the amount that was collected was often 60 – 100 ml higher than that calculated, this may be due to the exothermic nature of the reaction as this would cause the volume of gas to expand.

3.3.1 Results

Initial tests were carried out on the known catalase mimic; $\text{cis-}[\text{Mn}(\text{phen})_2\text{Cl}_2]$ to check the equipment before use with the prepared samples. The results for catalase activity of $\text{cis-}[\text{Mn}(\text{phen})_2\text{Cl}_2]$ have previously been reported by McCann *et al*⁸⁰ which showed that approximately 5382 molecules of hydrogen peroxide were broken down for each manganese atom in the complex during the first minute, known as the turnover number (see Equation 4). On repeating this experiment with the set up described here, approximately 5314 molecules of hydrogen peroxide were broken down for each manganese atom in the complex during the first minute. There is expected to be some error in the readings obtained for the set up described. McCann *et al*⁸⁰ also showed that a simple manganese salt (MnCl_2) was considerably less active than the complex $\text{cis-}[\text{Mn}(\text{phen})_2\text{Cl}_2]$ with 918 molecules of hydrogen peroxide broken down for each manganese ion during the first minute.

Calculation for turnover number:



It is assumed that 1 mole of O_2 occupies 22400 ml, and 1 ml then contains $(1/22400) = 45 \times 10^{-6}$ moles of oxygen. Thus 90×10^{-6} moles of hydrogen peroxide are broken down for every 1 ml of oxygen that is produced. This equates to $(90 \times 10^{-6} \times (N_A)) =$

5.4198×10^{19} molecules of hydrogen peroxide broken down for every 1 ml of oxygen that is produced.

The number of molecules of complex that are present in the sample =
(Mass(g)/Rmm) $\times N_A$

* N_A = Avagadro's Constant = $6.022 \times 10^{23} \text{ mol}^{-1}$

For the overall calculation of turnover number, the following calculation was then used:

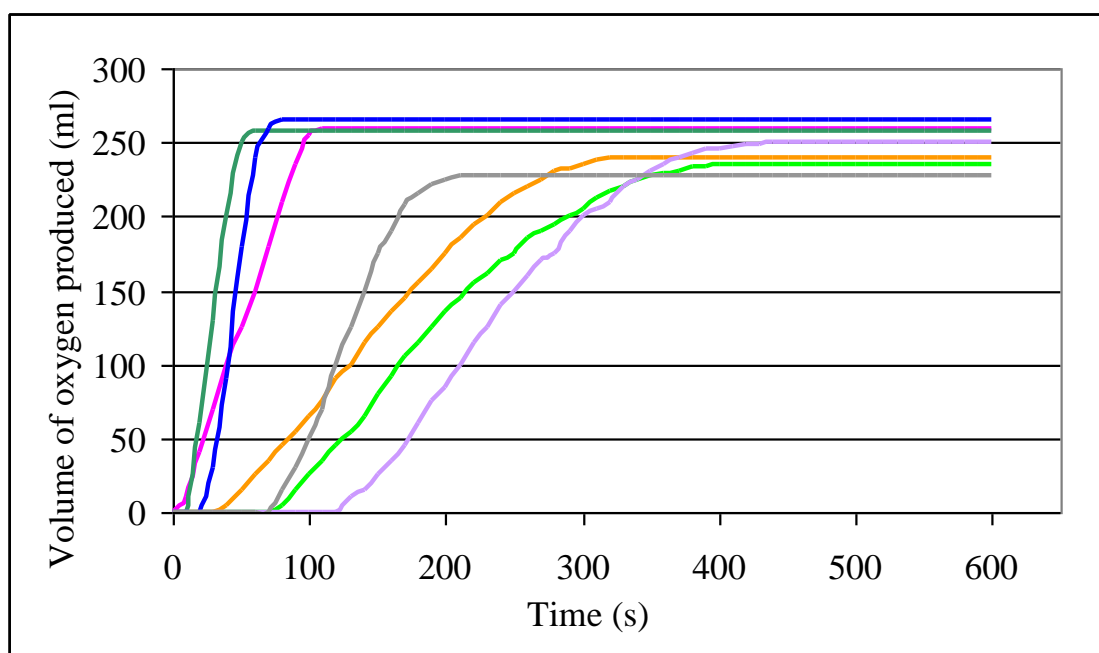
$$(5.4198 \times 10^{19} \times \text{Rate (ml/s}^{-1}\text{)}) / \text{Number of molecules of complex present}$$

Equation 4 – *Calculation for turnover number*

A test was first carried out without any complex present, both with and without base which showed that there were no measureable amounts of oxygen released. Each complex was then tested for catalase activity without the presence of triethylamine and no activity was observed for any complex except for those complexes containing the acetate bridging ligand. A carboxylate group in the active site of the naturally occurring enzyme is known to be one of the most important structural features of the catalase.^{78, 81, 115}

Polynuclear complexes of H₂L1

Polynuclear complexes of H₂L1 including their reduced analogues have been compared to see what effect the different axial ligands and the ligand structure have on the activity of the complexes. The results of the catalase testing for complexes of H₂L1 and RedH₂L1 with base added, are illustrated in Figure 3-25 and complexes of H₄L2 are illustrated in Figure 3-27 below.



- [Mn₂(HL1)(Cl)₂]₂(ClO₄)₂
- [Mn₂(RedHL1)(Cl)₂]₂(MnCl₄)
- [Mn₂(HL1)(N₃)₂]₂(ClO₄)₂
- [Mn₂(RedHL1)(N₃)₂]₂(ClO₄)₂
- [Mn₅(HL1)₂(OAc)₂(ClO₄)₂](ClO₄)₂
- [Mn₂(HL1)(OAc)₂]₂(ClO₄)₂
- [Mn₂(HL1)(NCS)₂]₂NCS

Figure 3-25 – Catalase activity of polynuclear complexes of H₂L1 and RedH₂L1

The graph displayed in Figure 3-25 shows the catalase activity for complexes of L1 with base and demonstrates clear differences in the curves obtained for catalase activity. The results have been used to calculate the number of molecules of H₂O₂ broken down by one molecule of complex known as the turnover number, both after

1 minute and during the fastest rate of reaction. The rate of the reaction during the fastest part of the reaction has been taken from the slope of the graph during the catalase activity.

Complex	Fastest rate (ml/s⁻¹)	Turnover Number*^a	Turnover after 60 seconds
[Mn ₂ (HL1)(Cl) ₂] ₂ (ClO ₄) ₂	1.1	130	7807
[Mn ₂ (RedHL1)(Cl) ₂] ₂ [MnCl ₄]	2.7	328	21302
[Mn ₂ (HL1)(N ₃) ₂] ₂ (ClO ₄) ₂	1.1	49	7830
[Mn ₂ (RedHL1)(N ₃) ₂] ₂ (ClO ₄) ₂	6.1	867	52006
[Mn ₅ (HL1) ₂ (OAc) ₂ (ClO ₄) ₂](ClO ₄) ₂	7.2	975	58524
[Mn ₂ (HL1)(OAc) ₂] ₂ (ClO ₄) ₂	1.2	141	0
[Mn ₂ (HL1)(NCS) ₂] ₂	2	197	0

*Turnover number = Maximum number of molecules of hydrogen peroxide converted to oxygen per molecule of complex¹¹⁶

^a = Per second during the fastest part of the reaction

The turnover after 60 second was calculated to highlight those complexes which showed an induction period.

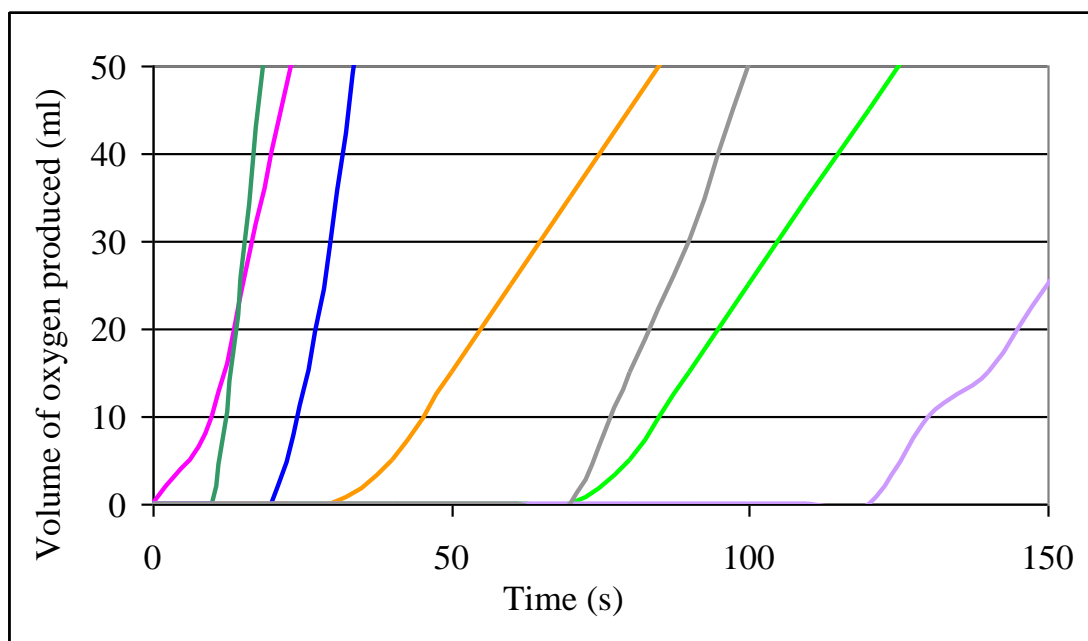
The results that are obtained for catalase activity are subject to errors, thus the turnover number that is calculated is an approximate figure in which the error is difficult to estimate due to the set up of the equipment, changes in temperature that may occur and the volumes and weights that are used, however, several of the tests were repeated and those results were reproducible.

Initial observations indicate that the pentanuclear μ -OAc complex [Mn₅(HL1)₂(OAc)₂(ClO₄)₂](ClO₄)₂ is the most efficient catalase mimic of those tested in this set of results with the fastest rate observed at 7.2 ml/s⁻¹ and approximately 1000 molecules of hydrogen peroxide broken down per second for each molecule of complex during the fastest rate of activity and approximately 59000 molecules broken down after one minute. Although the complex [Mn₅(HL1)₂(OAc)₂(ClO₄)₂](ClO₄)₂ shows the fastest rate, the reduced μ -N₃ complex

$[\text{Mn}_2(\text{RedHL1})(\text{N}_3)_2]_2(\text{ClO}_4)_2$ has the highest initial rate of activity with approximately 52000 molecules of hydrogen peroxide broken down after the first minute of activity when compared to approximately 33000 molecules broken down by $[\text{Mn}_5(\text{HL1})_2(\text{OAc})_2(\text{ClO}_4)_2](\text{ClO}_4)_2$ after one minute. The $\mu\text{-N}_3$ complex displayed a shorter initial delay in undergoing catalytic activity but did not reach the rates observed by the pentanuclear $\mu\text{-OAc}$ complex.

When the results for catalase activity are compared for differences between the imine and the reduced amine analogues, it can be seen that there is a significant increase in catalase activity for the reduced analogue of each of the complex type tested. The complex containing the azide ligand shows the fastest catalase activity when compared with both the chloro and the isothiocyanate analogue. This is true for both the imine and amine form of the complexes as a direct comparison. Catalase activity is slow to begin in the presence of an isothiocyanate axial ligand which suggests that the isothiocyanate ligand hinders catalase activity and there is a possibility that the delay is due to a ligand exchange that occurs at the manganese centre in the presence of H_2O_2 , and when compared to the azide and the chloro complex, the isothiocyanate ligand is more tightly bound to the manganese centre, requiring more energy to remove the ligand.

A close up diagram of the graph shown in Figure 3-25 has been produced to show a clearer picture of the delay that is observed for the complexes before catalase activity begins and is shown below in Figure 3-26.



- [Mn₂(HL1)(Cl)₂]₂(ClO₄)₂
- [Mn₂(RedHL1)(Cl)₂]₂(MnCl₄)
- [Mn₂(HL1)(N₃)₂]₂(ClO₄)₂
- [Mn₂(RedHL1)(N₃)₂]₂(ClO₄)₂
- [Mn₅(HL1)₂(OAc)₂(ClO₄)₂](ClO₄)₂
- [Mn₂(HL1)(OAc)₂]₂(ClO₄)₂
- [Mn₂(HL1)(NCS)₂]₂NCS

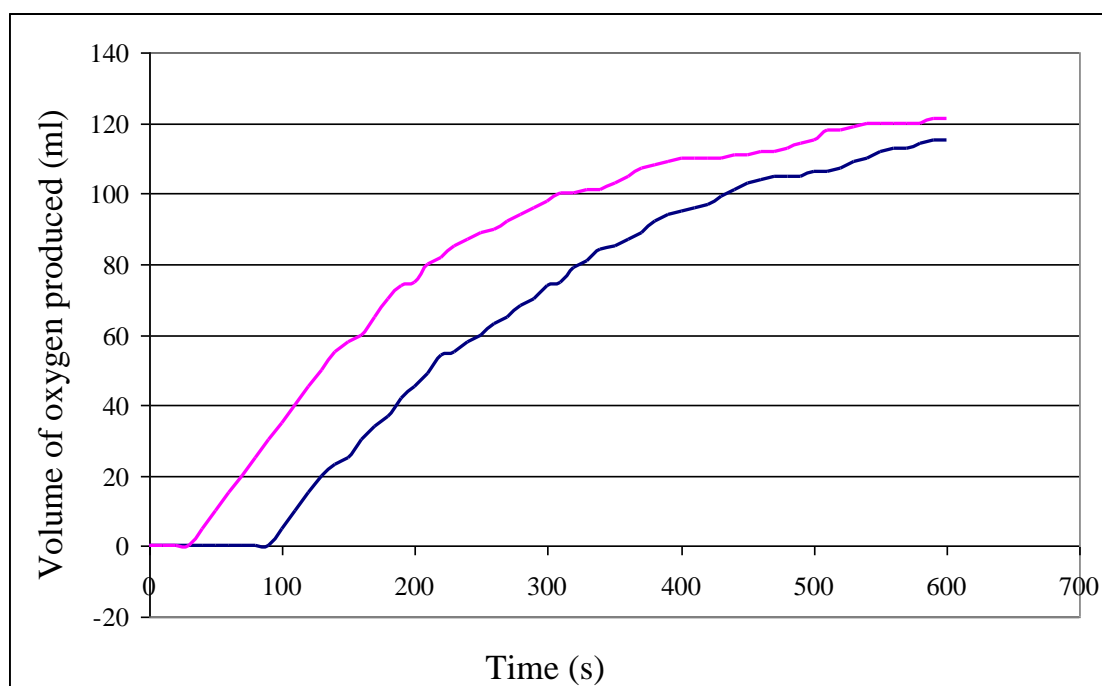
Figure 3-26 – Induction periods for catalase activity of *L1* complexes

The diagram in Figure 3-26, clearly shows that there is some delay for each complex tested except that of [Mn₂(RedHL1)(Cl)₂]₂(MnCl₄). The immediate reaction that is observed for this complex may partly be due to the extra manganese that is present in the counter ion, which is not present in the imine analogue [Mn₂(HL1)(Cl)₂]₂(ClO₄)₂ or in the reduced azide bound complex [Mn₂(RedHL1)(N₃)₂]₂(ClO₄)₂.

The delay that is observed for most complexes may be due to some rearrangement that is taking place within the ligand before catalase activity can be observed. In the natural catalase enzyme, it is thought that the H₂O₂ replaces the terminal H₂O ligand from one of the Mn(III) centres and protonates the μ-oxo bridge. The reduction of the manganese dimer then results in the formation and release of O₂ (see Figure 1-30). The difference in the delay for each complex may be due to a removal of the axial ligands or at least one axial ligand before the reaction can take place, which

may be why there is a difference in the amount of delay that is observed depending on how strongly bound the axial ligand is to the manganese centre. Dismukes *et al* have previously suggested that the number of strong donors at the metal centre are important to activate substrates.⁸⁸ The complex which showed the longest delay was $[\text{Mn}_2(\text{HL1})(\text{OAc})_2]_2(\text{ClO}_4)_2$. The differences may also indicate the stability of the complexes and maybe that the complex $[\text{Mn}_2(\text{HL1})(\text{OAc})_2]_2(\text{ClO}_4)_2$ is resistant to rearrangement. The results also suggest that the ligand may still be bound to the manganese ion and that it is not free manganese that is causing the reaction because there are clear differences observed in the rate that catalase activity occurs once the reaction begins for different complexes, and the turnover number is also much higher than that reported earlier by McCann *et al*⁸⁰ for the simple manganese salt MnCl_2 .

Polynuclear complexes of L2



- $[\text{Mn}_4(\text{L2})(\text{ClO}_4)_4]$
- $[\text{Mn}_4(\text{L2})(\text{NCS})_2](\text{ClO}_4)_2$

Figure 3-27 - Catalase activity for polynuclear complexes of H_4L2

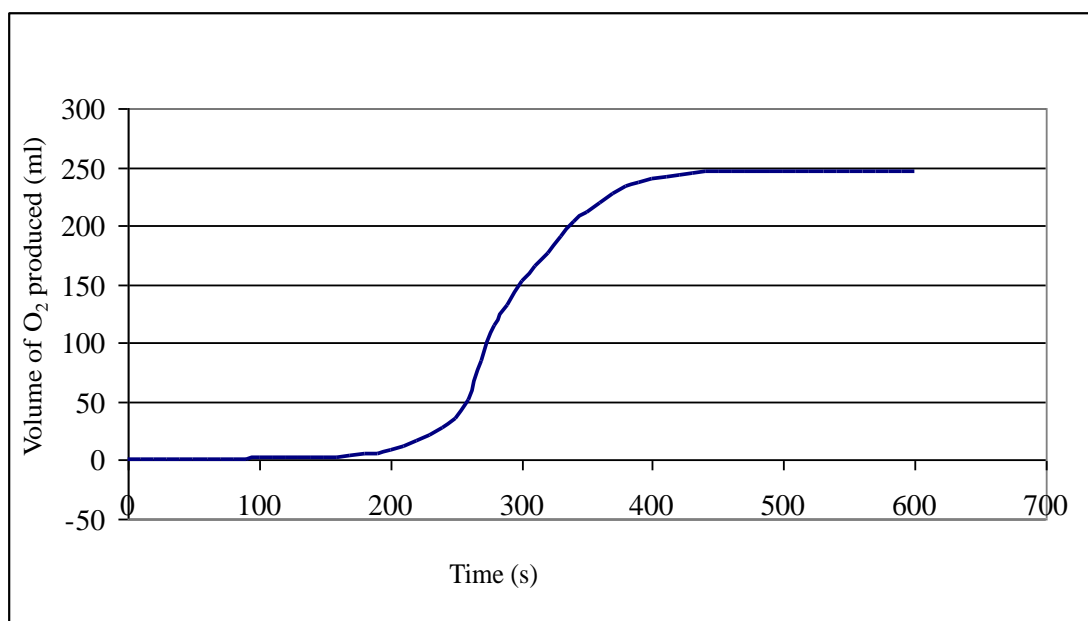
Complex	Fastest rate (ml/s⁻¹)	Turnover Number*^a	Turnover after 60 seconds
[Mn ₄ (HL2)(NCS) ₂](ClO ₄) ₂	0.4	46	2757
[Mn ₄ (HL2)(ClO ₄) ₄]	0.4	41	0

*Turnover number = Maximum number of molecules of hydrogen peroxide converted to oxygen per molecule of complex¹¹⁶

^a = Per second during the fastest part of the reaction

The graph shown in Figure 3-27 shows that the [4+4] ring expanded complexes of H₄L2 are much less active than the complexes of H₂L1 and although both complexes of H₄L2 show the same shaped curve and rate for catalase activity, the perchlorate bound complex [Mn₄(HL2)(ClO₄)₄] shows a longer initial delay before catalase activity is observed. For the complexes of H₄L2, it appears that the presence of the isothiocyanate ligand improves catalase activity in this ligand system whereas the presence of the isothiocyanate ligand decreased catalase activity for complexes of H₂L1, this may be due to the structure of the ligands. The ligand system of H₄L2 forms as a [4+4] structure with a cubane core involving the manganese centres, whereas H₂L1 forms as a dimeric molecule that is bridged by the axial ligands. The dimeric molecule is more likely to come apart than the ligand of H₄L2 which may provide more access for the hydrogen peroxide molecules to react with the manganese centres and for catalase activity to be observed. For the hydrogen peroxide molecules to react with the manganese centres of H₄L2, there may have to be some rearrangement of the ligand system as a whole, or that there is limited access to the manganese centres for the axial ligands to be displaced by the hydrogen peroxide molecules. It may be possible, that the hydrogen peroxide molecule needs to get into close proximity to the manganese centre before catalase activity can begin and with the structure of H₄L2, the perchlorate ligand which is more bulky than the isothiocyanate ligand may be preventing the hydrogen peroxide molecule having access to the only site possible to react with the manganese where there could be a transition state in which the manganese is bound to both the axial ligand and the hydrogen peroxide molecule before catalase activity begins.

The result for catalase activity of the pentanuclear complex $[\text{Mn}_5(\text{HL1})_2(\text{OAc})_2(\text{ClO}_4)_2](\text{ClO}_4)_2$ without the addition of the base triethylamine is shown below in Figure 3-28. The profile for this complex with the addition of triethylamine is shown in Figure 3-25.



— $[\text{Mn}_5(\text{HL1})_2(\text{OAc})_2(\text{ClO}_4)_2](\text{ClO}_4)_2$

Figure 3-28 – Catalase activity for $[\text{Mn}_5(\text{HL1})_2(\text{OAc})_2(\text{ClO}_4)_2](\text{ClO}_4)_2$ without the addition of base

Complex	Fastest rate (ml/s ⁻¹)	Turnover Number* ^a	Turnover after 60 seconds
$[\text{Mn}_5(\text{HL1})_2(\text{OAc})_2(\text{ClO}_4)_2](\text{ClO}_4)_2$ (without addition of triethylamine)	1.7	32	0

*Turnover number = Maximum number of molecules of hydrogen peroxide converted to oxygen per molecule of complex¹¹⁶

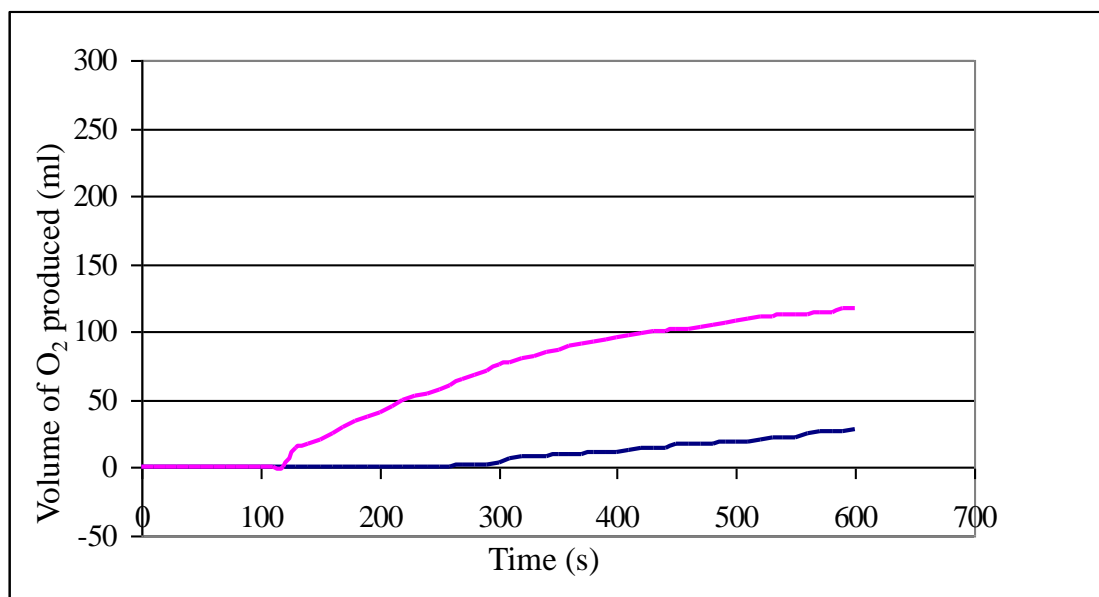
^a = Per second during the fastest part of the reaction

Catalase activity for the complex $[\text{Mn}_5(\text{HL1})_2(\text{OAc})_2(\text{ClO}_4)_2](\text{ClO}_4)_2$ without the addition of triethylamine was found to show a long induction period, but once catalase activity occurs, it continues at a rate of 1.7 ml/s⁻¹ with approximately 30

molecules of hydrogen peroxide broken down for each molecule of complex per second. The fact no other complexes of L1 show any catalase activity without the presence of base, indicates that the acetate group is important for this type of complex. Bridging carboxylate ligands are suggested to prevent the formation of $\text{Mn}^{\text{(II)}}\text{Mn}^{\text{(III)}}$ or $\text{Mn}^{\text{(III)}}\text{Mn}^{\text{(IV)}}$ oxidation states which are kinetically inactive.¹¹⁷ The bridging central manganese in the complex $[\text{Mn}_5(\text{HL1})_2(\text{OAc})_2(\text{ClO}_4)_2](\text{ClO}_4)_2$ is in an octahedral environment which no other complex tested possesses, this too may be an important feature of the complex. Some activity was observed for the tetranuclear complex, although this was not initiated until after ten minutes had passed, so the extra manganese centre is also a key factor for this ligand system. The sigmoidal shape of the curve that is obtained for the catalase activity of the complex $[\text{Mn}_5(\text{HL1})_2(\text{OAc})_2(\text{ClO}_4)_2](\text{ClO}_4)_2$ without the addition of base is also of importance as it gives the representation of a cooperative binding curve that is observed for the oxygen binding of haemoglobin. Cooperative binding occurs due to substrate activation of the catalyst, this is where the affinity of a ligand for a molecule with several binding sites increases once one substrate ligand becomes bound to the molecule, so here, it may be that there is a long induction period, but once the hydrogen peroxide becomes bound to the complex, the affinity for the hydrogen peroxide to bind to the manganese centres increases depending on the amount of hydrogen peroxide that has become bound. Sigmoidal curves are characteristic of transitions between two different states, which involves the making or disruption of numerous weak interactions which are non covalent bonds.¹¹⁸⁻¹²⁰

Ring contracted species

Catalase activity for the ring contracted complexes of L4 and L5 were tested and compared as shown below in Figure 3-29.



— [Mn(L5)(NCS)₂].MeOH

— [Mn(L4)(NCS)₂].EtOH

Figure 3-29 – Catalase activity for ring contracted species

Complex	Fastest rate (ml/s ⁻¹)	Turnover Number* ^a	Turnover after 60 seconds
[Mn(L4)(Cl) ₂].MeOH	0	0	0
[Mn(L4)(NCS) ₂].MeOH	0	0	0
[Mn(L4)(NCS) ₂].EtOH	0.001	0	0
[Mn(L5)(NCS) ₂].MeOH	0.35	14	0

*Turnover number = Maximum number of molecules of hydrogen peroxide converted to oxygen per molecule of complex¹¹⁶

^a = Per second during the fastest part of the reaction

The results show that the ring contracted species have very limited catalase activity. Of the complexes tested, only [Mn(L4)(NCS)₂].EtOH and [Mn(L5)(NCS)₂].MeOH showed any activity, and [Mn(L4)(NCS)₂].EtOH did not show any signs of activity until after 4 minute, and once oxygen was being produced, the reaction continued at a rate of 0.001 ml/s⁻¹. The complex [Mn(L5)(NCS)₂].MeOH was shown to be slightly faster producing oxygen at a rate of 0.35 ml/s⁻¹, and breaking down 14 molecules of

hydrogen peroxide per molecule of complex per second during the fastest rate. The differences observed suggest that the overall ligand structure has some effect on the rate of activity because, in this case, when comparing the complexes $[\text{Mn}(\text{L4})(\text{NCS})_2]\cdot\text{MeOH}$ and $[\text{Mn}(\text{L5})(\text{NCS})_2]\cdot\text{MeOH}$, the complexes are very similar and the axial ligands are the same, however, the complex $[\text{Mn}(\text{L4})(\text{NCS})_2]\cdot\text{MeOH}$ has the addition of an OH group within the ligand structure which results in a slower rate of catalase activity. The extra OH group in the L3 ligand system are not bound to the manganese ion directly but it is hydrogen bonded to the axial NCS ligand, which may be preventing the thiocyanate ligand from being removed to enable the hydrogen peroxide to bind to the manganese centre. The L5 complex ligand system may provide more access to the manganese for the hydrogen peroxide molecule which is consequently broken down. The overall lack of activity observed for the ring contracted species may also be due to the formation of the ring within the ligand system, which may prevent a rearrangement of the molecule occurring to allow access of the hydrogen peroxide molecule to the manganese centre thus enabling catalase activity.

The results also suggest that the complexes do not degrade and that the manganese does not become displaced from the ligand system, this is because there is either no activity observed, which if the manganese was displaced, there would be expected to at least some activity, or for the two complexes which showed slight activity, there are differences in the observed rate which supports the idea that the manganese bound to the different ligands leads to the differences in the rate of catalase activity.

Dinuclear complex L6

Naturally occurring manganese catalase has been shown to possess a dinuclear manganese centre.^{77, 78} The results for catalase activity of the dinuclear complex prepared using ligand L6 is shown in Figure 3-30.

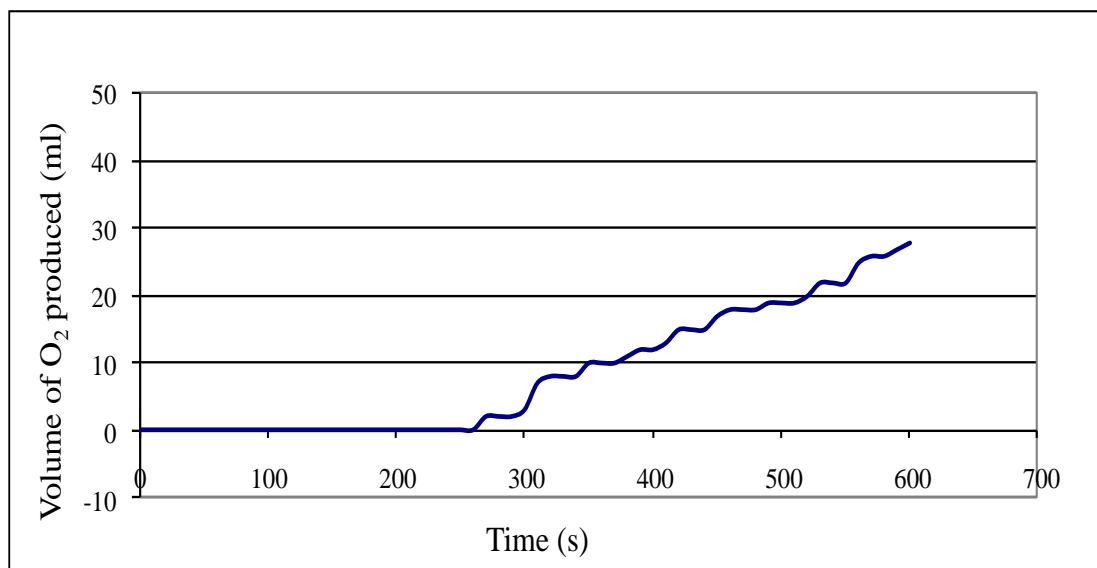


Figure 3-30 – Catalase activity for dinuclear complex $[Mn_2(L6)(NCS)_4]$

Complex	Fastest rate (ml/s ⁻¹)	Turnover Number* ^a	Turnover after 60 seconds
$[Mn_2(L6)(NCS)_4]$	0.1	7	0

*Turnover number = Maximum number of molecules of hydrogen peroxide converted to oxygen per molecule of complex¹¹⁶

^a = Per second during the fastest part of the reaction

The result obtained for complex L6 show that overall, the complex has very little catalase activity when compared to the polynuclear complexes of L1 and L2. The complex tested contains nitrogen bound thiocyanate axial ligands which were shown to reduce catalase activity for complexes of L1 and L2 and each manganese centre in the complex $[Mn_2(L6)(NCS)_4]$ is bridged by two thiocyanate axial ligands and bound to a further thiocyanate ligand each. The bridging thiocyanate ligands would be difficult to remove and the initiation of catalase activity may be initiated at the non bridging thiocyanate axial ligands, so it is possible that with alternative axial ligands in place of the thiocyanate ligands such as the $-\mu Cl$ bridge, the activity could be improved for complexes with the ligand system L6, however, attempts to synthesis such complexes were unsuccessful.

[1+1] Mononuclear complexes

For clarity, the catalase activity for the mononuclear complexes with a diacetylpyridine head unit which contains a methyl group which is attached to the imine bonds are shown first in Figure 3-31. The results for catalase activity for the mononuclear complexes with a diformylpyridine head unit, where there are no methyl groups present across the imine bonds are shown in Figure 3-32.

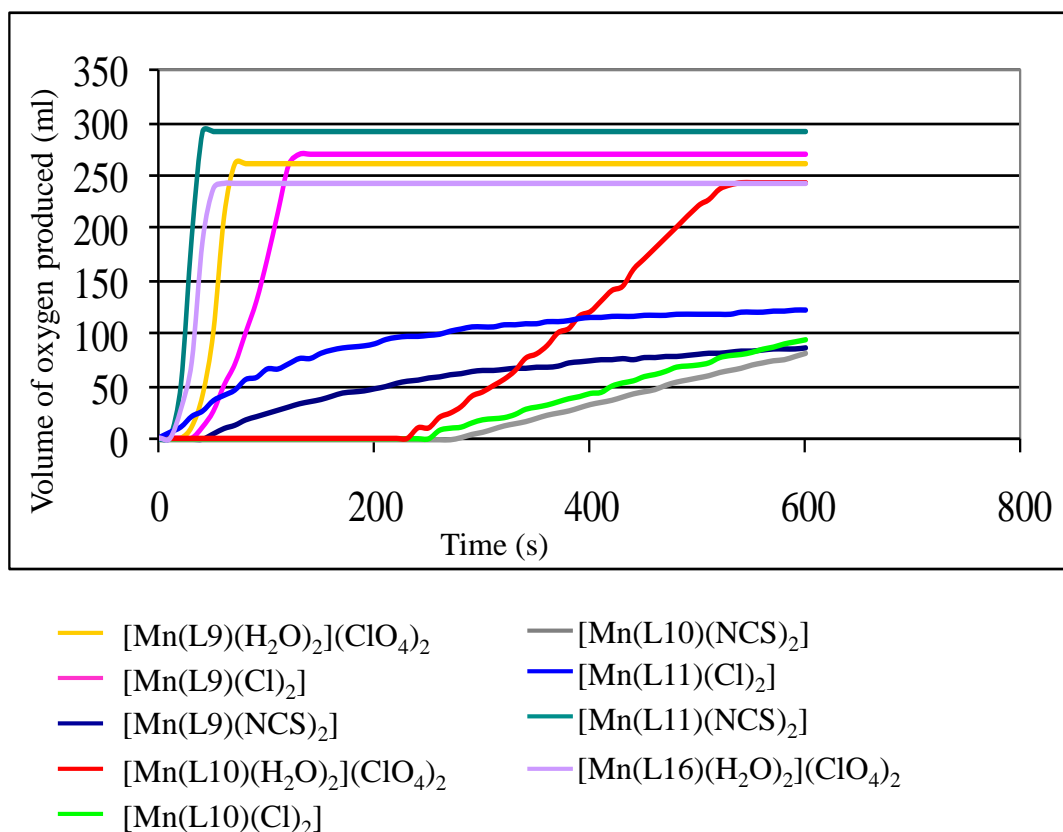


Figure 3-31 – Catalase activity for mononuclear complexes with a diacetylpyridine head unit

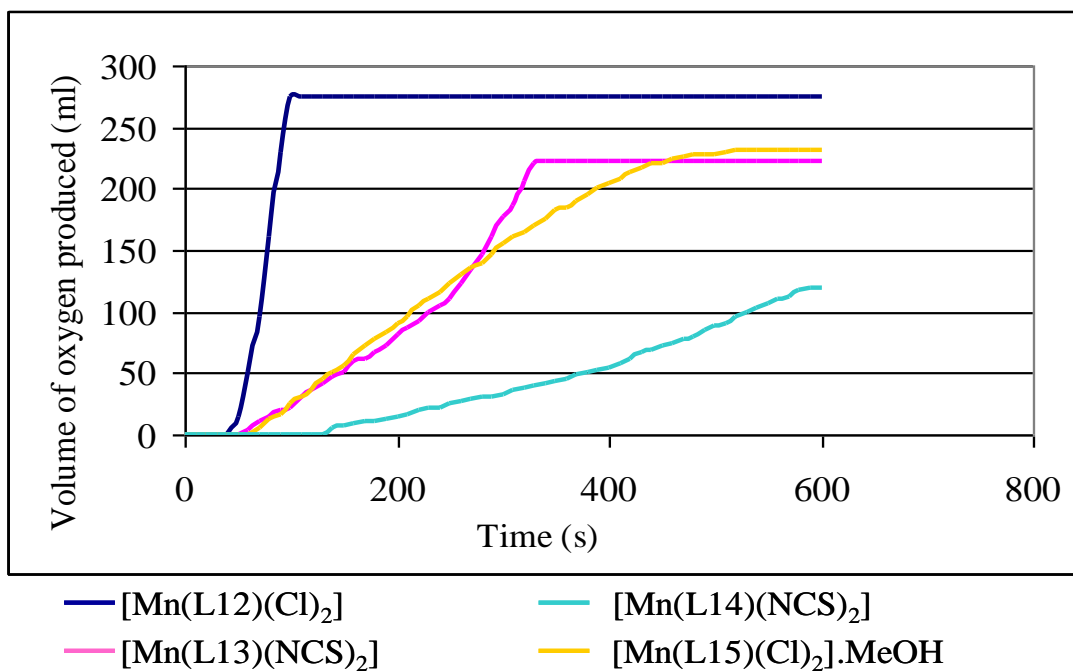


Figure 3-32 – Catalase activity for mononuclear complexes with a diformylpyridine head unit

Complex	Fastest rate (ml/s⁻¹)	Turnover Number*^a	Turnover after 60 seconds
[Mn(L9)(OH ₂) ₂](ClO ₄) ₂	7.7	181	23754
[Mn(L9)(Cl) ₂]	2.9	23	4737
[Mn(L9)(NCS) ₂]	0.3	6	687
[Mn(L10)(OH ₂) ₂](ClO ₄) ₂	0.8	27	0
[Mn(L10)(Cl) ₂]	0.3	10	0
[Mn(L10)(NCS) ₂]	0.3	13	0
[Mn(L11)(Cl) ₂]	0.7	24	1537
[Mn(L11)(NCS) ₂]	12.0	160	23659
[Mn(L12)(Cl) ₂]	5.4	20	7604
[Mn(L13)(NCS) ₂]	0.6	3	1685
[Mn(L14)(NCS) ₂]	0.18	7	416
[Mn(L15)(Cl) ₂].MeOH	0.7	8	0
[Mn(L16)(OH ₂) ₂](ClO ₄) ₂	7.5	150	9000

*Turnover number = Maximum number of molecules of hydrogen peroxide converted to oxygen per molecule of complex¹¹⁶

^a = Per second during the fastest part of the reaction

The results illustrated in Figure 3-31 and Figure 3-32 indicate that, of the mononuclear complexes tested, [Mn(L9)(OH₂)₂](ClO₄)₂ shows the highest activity with a rate of 7.7 ml/s⁻¹ during the fastest rate and approximately 24000 molecules of hydrogen peroxide broken down after one minute. The complex which showed least catalase activity was [Mn(L14)(NCS)₂] with approximately 400 molecules of hydrogen peroxide broken down per minute per molecule of complex during the fastest rate and no catalase was seen after one minute with the complex [Mn(L14)(NCS)₂].

The mononuclear complexes of L10 which possesses a more rigid structure than L9 or L11 displays less catalase activity overall. This may be due to an increased flexibility in the ligands of L9 and L11. The complexes of L10 are also more likely to be more kinetically stable than those complexes of L9 and L11. This may have

hindered the formation of a required geometry or exchange reaction of the axial ligands at the manganese centre with a hydrogen peroxide molecule that may be required for catalase activity.

The axial ligands that are bound to the manganese centre have some impact upon the observed rates. Ligands of L9 and L10 both showed that the rate of catalase activity was highest in the presence of water bound axial ligands, followed by those with chloride bound axial ligands, and finally, activity was dramatically reduced in the presence of thiocyanate axial ligands. This trend would be expected due to the strength that the axial ligand is bound to the manganese centre. An OH₂ ligand is removed with greater ease than that of a chloride and of a thiocyanate ligand, respectively.

[Mn(L9)(Cl)₂] and [Mn(L12)(Cl)₂] that share a similar structure and where the only difference is the methyl groups on the head unit show a very similar activity. However, the ligand [Mn(L12)(Cl)₂] which contains no methyl groups showed slightly faster catalase activity. This again may be related to the flexibility of the molecule, as the presence of the methyl groups would be expected to increase the rigidity of the molecule.

When the results for the more rigid complexes of L10 are compared with L13 which contains no methyl groups in the head unit, and where both L10 and L13 contain thiocyanate axial ligands, the methyl groups seemed to make more of an impact on the differences seen. The complex [Mn(L13)(NCS)₂] showed much higher activity even with the presence of the thiocyanate ligands than for each of the complexes of L10 including the OH₂ bound complex.

The complex [Mn(L15)(Cl)₂].MeOH, which has a similar structure to [Mn(L10)(Cl)₂] and [Mn(L13)(Cl)₂] but has undergone nucleophilic attack of methanol across one imine bond, displayed an activity that was similar to that of [Mn(L13)(Cl)₂] and was higher than that of [Mn(L10)(Cl)₂]. This indicates that there may only be a slight rearrangement of the ligands, however, for each of the more

rigid complexes L10, L13 and L15, there is a pronounced delay in the observed catalase activity.

The curve observed for the complexes $[\text{Mn}(\text{L9})(\text{NCS})_2]$ and $[\text{Mn}(\text{L11})(\text{Cl})_2]$ seem to show some initial catalase activity but the volume of oxygen that is given off may be levelling off at a volume of oxygen which is much lower than the expected volume for the reaction to be complete, and is lower than the volume that is shown for all of the other complexes and although it may be possible that catalase activity may continue at a very slow rate, the results may also suggest that the reaction is complete but that there is an alternative reaction occurring for the hydrogen peroxide that is present, it may be possible that the hydrogen peroxide is reacting with the manganese in the complex but that some of the hydrogen peroxide or the oxygen may become bound to the complex and not take part in a catalase reaction. It is also possible that the catalyst has altered in structure during the reaction, which has rendered the catalyst inactive part way through the testing. By altering the axial ligands that are present for these complexes, there appears to be a catalase reaction that is able to occur.

The results for catalase activity of the mononuclear complexes have been shown on a larger scale to show more clearly how the induction period differs for the various complexes and these results are shown below in Figure 3-33.

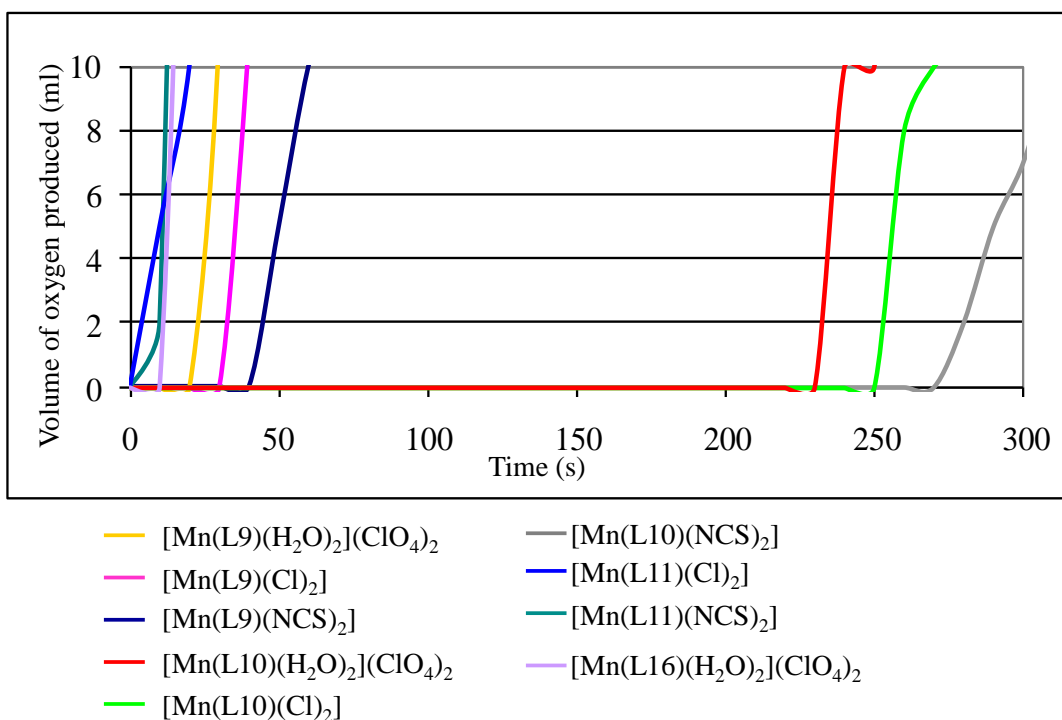


Figure 3-33 - Delay observed for catalase activity of mononuclear complexes with a diacetyl pyridine head unit

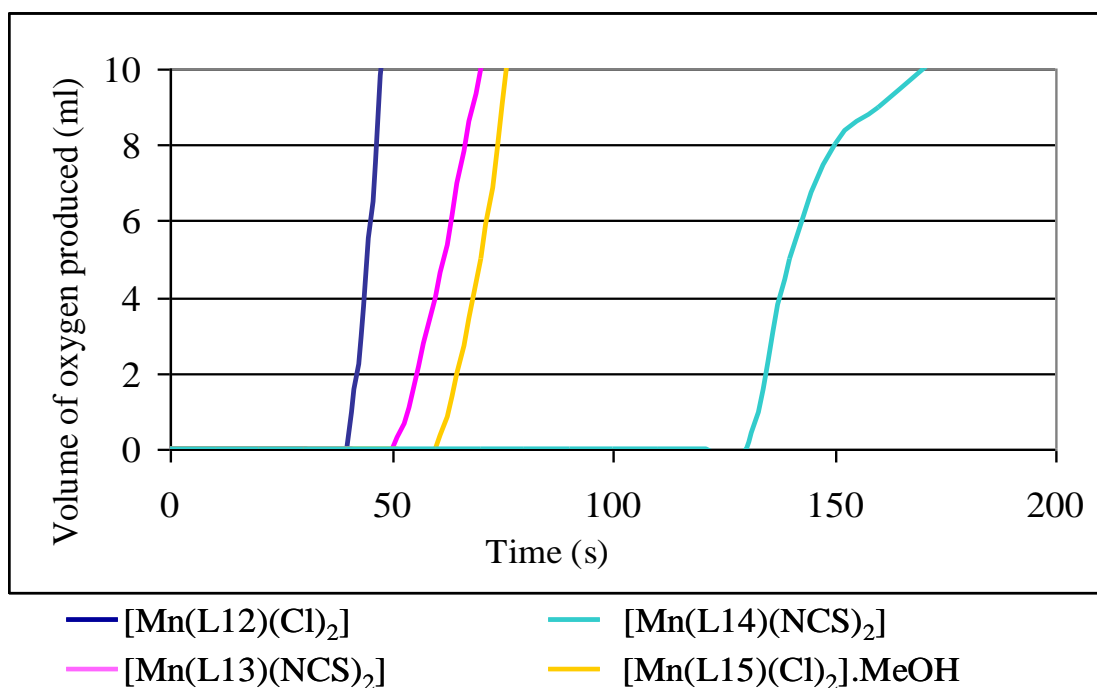


Figure 3-34 - Delay observed for catalase activity of mononuclear complexes with a diformyl pyridine head unit

The close up illustrations of the induction periods for catalase activity show that there is a clear difference for the ligands under observation. Figure 3-33 shows that the complex systems of L10 have a much longer induction period than any other ligand system. The L10 ligand system is a macrocyclic system which is expected to be more stable than the non-macrocyclic systems, so this may be preventing a rearrangement of the macrocycle which may be required for the catalase activity to begin. Complexes of L11 show catalase activity with no delay and this ligand system is non-macrocyclic and contains a single manganese centre with pentagonal bipyramidal geometry from an N_5 donor set in place of an N_3O_2 donor set, this is also true for complexes of L16 which show a slight delay, however, where two methyl groups are attached to two nitrogens of the L11 ligand system, there exists one hydrogen attached to the nitrogen in place of the methyl groups. The methyl groups that are attached in L11 may play a part in the increased activity that is observed for this ligand system.

Catalase activity of the tripodal complexes

The results illustrated in Figure 3-35 show that the catalase activity of the tripodal complexes occurs almost without delay.

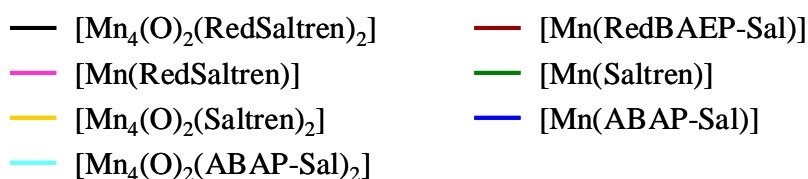
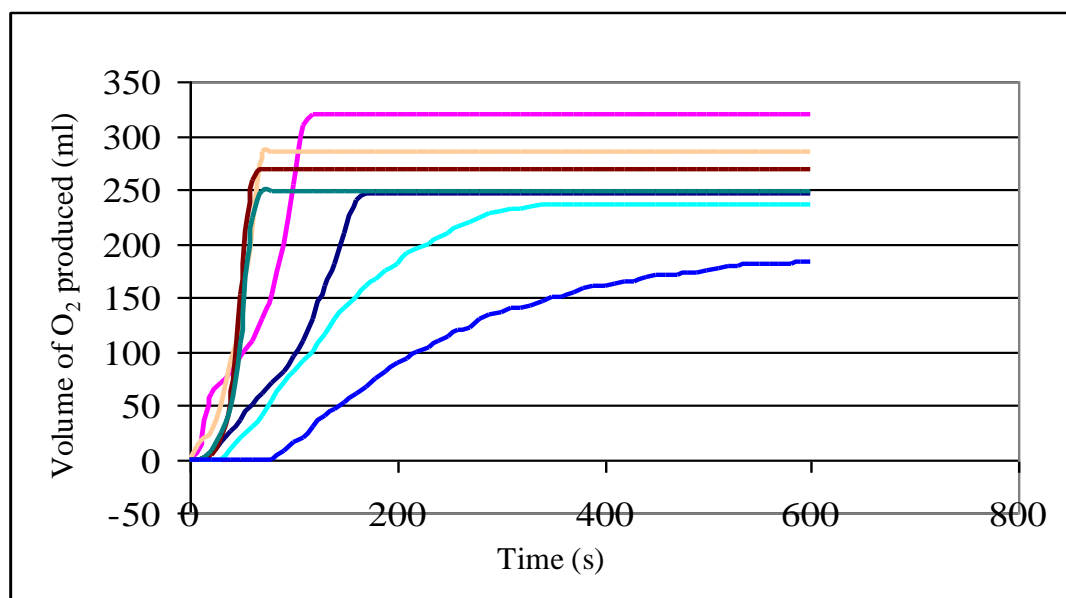


Figure 3-35 – Catalase activity of tripodal complexes

Complex	Fastest rate (ml/s ⁻¹)	Turnover Number* ^a	Turnover after 60 seconds
[Mn(RedSaltren)]	3.7	93	11372
[Mn ₄ (O) ₂ (RedSaltren) ₂]	1.2	100	8839
[Mn(Saltren)]	8.8	172	24336
[Mn ₄ (O) ₂ (Saltren) ₂]	6.0	504	50177
[Mn ₄ (O) ₂ (ABAP-Sal) ₂]	1.2	61	8372
[Mn(ABAP-Sal)]	0.5	31	0
[Mn(RedBAEP-Sal)]	10.3	262	37477

*Turnover number = Maximum number of molecules of hydrogen peroxide converted to oxygen per molecule of complex

^a = Per second during the fastest part of the reaction

The most promising complex of those tested is the tetranuclear complex $[\text{Mn}_4(\text{O})_2(\text{Saltren})_2]$ which has been calculated to break down approximately 30000 molecules of H_2O_2 per molecule of complex after one minute. Although most of the tripodal complexes did not display any delay before catalase activity was observed, there was a delay for the complexes containing the ABAP ligand, with the mononuclear complex $[\text{Mn}(\text{ABAP-Sal})]$ showing no catalase activity after one minute. We were able to reduce the delay that was observed for the mononuclear complex $[\text{Mn}(\text{ABAP-Sal})]$ by increasing the number of manganese centres present to form the complex $[\text{Mn}_4(\text{O})_2(\text{ABAP-Sal})_2]$. This indicates that an increase in the number of manganese centres is important in addition to the geometry of the metal centre.

The curve observed for the complex $[\text{Mn}(\text{ABAP-Sal})]$ seems to level off at a volume of oxygen given off which is much lower than the expected volume for the reaction to be complete. The volume was lower than that shown for all of the other complexes, and although it may be possible that catalase activity may continue at a very slow rate, the results may also suggest that the reaction is complete but that there is an alternative reaction occurring for the hydrogen peroxide that is present. It may be possible that the hydrogen peroxide is reacting with the manganese but that some of the hydrogen peroxide or the oxygen may become bound to the complex and not take part in a catalase reaction.

The highest reaction rate that was obtained for the tripodal complexes was that of complex $[\text{Mn}(\text{RedBAEP-Sal})]$ which reached a rate of 10.3 ml/s^{-1} . The reaction rate for $[\text{Mn}(\text{RedBAEP-Sal})]$ was much higher than that of the complex $[\text{Mn}(\text{RedSaltren})]$ which has a rate of 3.7 ml/s^{-1} . The difference in structure for the two complexes $[\text{Mn}(\text{RedSaltren})]$ and $[\text{Mn}(\text{RedBAEP-Sal})]$, is that $[\text{Mn}(\text{RedSaltren})]$ is a symmetrical tripod with a chain of two carbons for each arm of the tripod; $[\text{Mn}(\text{RedBAEP-Sal})]$ is an asymmetric tripod with two arms containing a 2 carbon chain and the third arm containing a three carbon chain, so the increase in one arm length causes catalase activity to be more efficient. There is a possibility of increasing the rate with the synthesis of the tetranuclear complex using the BAEP

ligand via synthesis of a 2:1 ratio of manganese to ligand. Attempts to form this complex did not produce a product with a good analysis for characterisation.

The results have also revealed that a reduction of the imine bond decreased the catalytic activity. For example, a reduction of the Saltren ligand resulted in a rate that was reduced from 6.0 ml/s^{-1} as seen for the complex $[\text{Mn}_4(\text{O})_2(\text{Saltren})_2]$, to just 1.2 ml/s^{-1} of oxygen produced for the complex $[\text{Mn}_4(\text{O})_2(\text{RedSaltren})_2]$, approximately 50000 molecules of hydrogen peroxide were broken down per molecule of complex after one minute compared with approximately 9000 molecules respectively. This difference was also observed for the mononuclear complexes $[\text{Mn}(\text{Saltren})]$ and $[\text{Mn}(\text{RedSaltren})]$ although the difference was less pronounced with rates of 8.8 ml/s^{-1} , and 3.7 ml/s^{-1} , 24000 and 11000 molecules approximately of hydrogen peroxide broken down after one minute for each molecule of complex respectively.

The results for catalase activity for the tripodal complexes are shown on a close up scale to illustrate more clearly how the induction period changes for different complex systems. These are shown below in Figure 3-36.

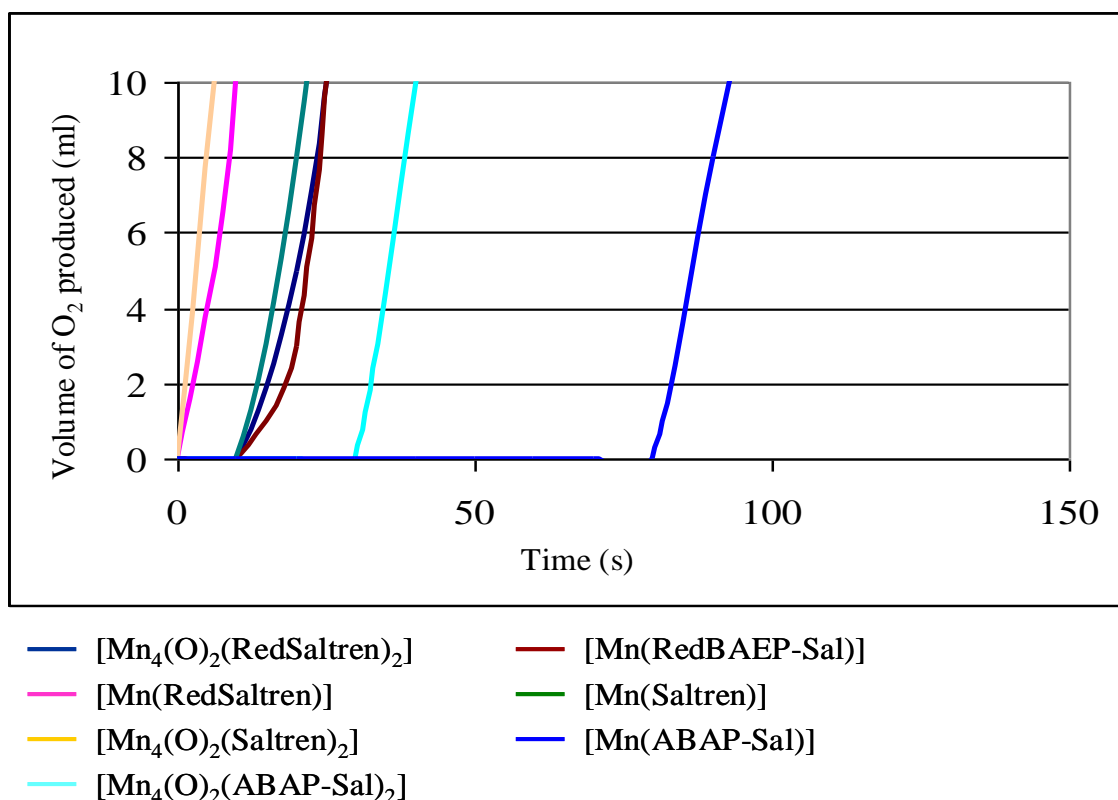


Figure 3-36 – Delay for catalase activity observed for the tripodal complexes

The graph illustrated in Figure 3-36 clearly show that there is good potential for catalase activity with no induction period observed for complexes of [Mn₄(O)₂(Saltren)₂] and [Mn(RedSaltren)]. The mononuclear complex of the Saltren ligand [Mn(Saltren)] does show a short induction period before catalase activity begins and that by reducing the imine bonds, this induction period is removed. A reduction of the imine bonds is likely to impose a slightly different geometry onto the manganese centre which may be why there is no induction period observed after reduction. However, the reverse is true for the tetranuclear system of the saltren ligands, the complex [Mn₄(O)₂(RedSaltren)₂] which has undergone a reduction shows no induction period, whereas the complex [Mn₄(O)₂(Saltren)₂] is slightly slower to show any catalase activity. The manganese centres for the tetranuclear systems contain a cubane core which may contribute to the observed catalase activity.

Expansion of Research

To extend the findings of the research as presented in this thesis, it is important firstly to find ways in which to increase the yields of the reduced complexes if they are to be used in a scale up procedure for further testing and analysis and in a commercial setting. Currently, the imine analogues of the complexes presented are very simple to prepare and can be obtained with high purity and good yields which provides an ideal situation for commercial production.

Toxicity issues must be addressed with each type of complex formed if used as a potential pharmaceutical ingredient and also, the stability of the complexes when stored in different conditions may alter greatly.

In general, many of the reduced complexes that were synthesised produced only very small crystals, which were often too small for X-ray analysis to be performed. By manipulating the different conditions for crystal growth further, it may be possible to produce larger crystals and analyse their geometry further which can lead to more comparisons to be made.

For each of the complexes that have been prepared, a range of possibilities exist as to the differing axial ligands and variations that may be introduced and which will possibly lead to an increase in the observed activity. This can only add to the catalogue of complexes prepared and aid in the understanding of a particular catalytic antioxidant activity.

The tripodal ligands that have been synthesised have not produced crystals for analysis. Perseverance with this type of complex may lead to crystals being formed with the right conditions. Some success was found with crystals that were formed for the reduced analogues however; they were not large enough for X-ray analysis to be performed. The successful synthesis of the complex $[\text{Mn}_4(\text{O})_2(\text{RedBAEP-Sal})_2]$ may lead to a complex that displays very fast catalytic activity with limited initial delay.

When the structures of the tripods can be compared and analysed, it would be interesting to observe the superoxide dismutase activity that these complexes may show. The tripodal complexes hold potentially many variations in their structure, as

the synthesis can be carried out with varying molar amounts which may lead to new complexes. A reduction of the imine analogue introduces many new forms of the complex to be analysed also. A breakthrough in the formation of a pure and neutral tripod may lead to higher yields and purity. The catalase activity of the tripodal ligand complexes seems promising and further analysis and biological testing is required in this area.

Further work must be continued on the development of a direct method for analysing superoxide dismutase activity. The reaction occurs on a millisecond timescale and lowering the reaction time may produce results that can be analysed more accurately and compared with results from the indirect modified NBT assay method used. This may require more variations in concentration for both superoxide solution and complex solution. The introduction of a microcuvette accessory will minimise the dead time for a stop-flow technique. Part of the process for developing a direct method should include the effects of variations in solvent, pH, temperature and the amount of water present to gain maximum results.

Conclusions

A wide range of simple and air stable seven coordinate manganese complexes have been successfully synthesised, producing a catalogue of complexes that display small differences in geometry around the metal centre and consequently differing biological activity. Some new complexes have been prepared with the reduction of imine bonds where possible, and a range of ring contracted species which have allowed the analysis of similar ligand structures to be compared.

A range of tripodal complexes have also been synthesised with the formation of some asymmetric examples and complexes which have been synthesised with firstly a mononuclear centre *via* 1:1 stoichiometric reaction of ligand : manganese then in a 1:2 ratio respectively to form a dimeric compound with a tetranuclear core. Their catalase activities have been measured and compared to see what helps drive the catalytic reaction.

Several of the prepared complexes were subject to indirect analysis of superoxide dismutase activity and overall, the tetranuclear complexes showed high rates of superoxide dismutase activity that are within the range reported in the literature. The complex $[\text{Mn}_2(\text{HL1})(\text{Cl})_2]_2(\text{ClO}_4)_2$ showed the highest calculated K_{McCF} value of $7.7 \times 10^6 \text{ M}^{-1} \text{ s}^{-1}$, indicating that the bridging chloride ligand is important for the observed rate of superoxide dismutase activity. A chloride ligand is expected to dissociate more readily from the manganese than other axial ligands such as acetate and thiocyanate. Thus, the results suggests that the ease of dissociation of the ligand is important and that the ligand may be substituted by the incoming superoxide molecule. The results suggested that the reaction was not a result of the complex systems falling apart and that the complexes have good stability during the catalytic reaction.

The ring contracted species showed some SOD activity even with thiocyanate axial ligands which rendered other complexes inactive and so there is potential for even higher rates to be achieved with the presence of alternative axial ligands such as the chloride ligand. These complexes do not exist as dimeric molecules and the axial ligands are not bridging so there is a lower molecular weight for these complexes

which means that a lower dosage would be required when considering it as a potential working SOD mimic.

The results for the catalase testing showed the effect that different ligands produced and how an increase in the number of manganese centres can prove to be important. The results reported in this thesis have shown that catalase activity is largely affected by the overall structure of the ligand which may be linked to differing geometries of the manganese centre and providing access to the hydrogen peroxide molecule for the reaction to occur. For the non tripodal ligands, an overall increase in activity was observed upon reduction of the imine bond and when compared to the non reduced complex which has a similar structure. In addition to the structure of the ligand being important, there were also complexes that were similar, which differed only in the type of axial ligand, suggesting that the dissociation constants may be important and maybe the axial ligand is dissociated before the hydrogen peroxide can be broken down. The complex $[\text{Mn}_5(\text{HL1})_2(\text{OAc})_2(\text{ClO}_4)_2](\text{ClO}_4)$ was shown to possess the highest rate of catalase activity and contains the acetate axial ligands, carboxyl axial ligands are present in the active site of the naturally occurring enzyme and so is an important feature in the design of a catalase active compound, this is due to the basic nature of the ligand and its binding mode may be a factor for this reaction. This complex was shown to produce a cooperative binding curve during catalase activity. The non-tripodal ligands tended to show an induction period before oxygen was evolved from the reaction, and this delay suggests that there is some rearrangement of the complex before catalase activity can begin. Reduction of the complexes appears to reduce the delay for this reaction.

The tripodal ligands showed very high rates of catalase activity, and this class of complex is different to those previously mentioned in that reduction of the imine bonds resulted in a lower rate of catalase activity. There was almost no delay for the production of oxygen in the catalase reaction with the tripodal ligands, suggesting that there is less rearrangement of the molecule required. It has also been shown that differences in the arm lengths of the tripodal complex create different rates of activity, also supporting the idea that the geometry of the complex is important for the reaction.

Of the complexes tested, all except the ring contracted species displayed both superoxide dismutase and catalase activity, and there is much scope for the development of the compounds as working antioxidants. For the ring contracted species, the fact that they do not possess catalase activity means that these compounds have the potential for use in research as anticancer compounds. In naturally occurring antioxidants, the concentration of superoxide is regulated by dismutation of the superoxide radical into hydrogen peroxide (SOD activity) which is then converted to water (peroxide activity) or dismutated to water and dioxygen (catalase activity) Both the superoxide radical and hydrogen peroxide are good regulators of cell death and in particular hydrogen peroxide is implicated as a mediator of apoptosis in cells¹²¹

The cellular damage which is caused by hydrogen peroxide is likely to be produced in part through radical production which is formed once hydrogen peroxide reacts with Fe^{2+} or Cu^{2+} . Many tumour cells have increased rates of metabolism when compared with normal cells which typically leads to an increase in the number of reactive oxygen species. MnSOD has been shown to be depleted in most cancers when compared to normal tissue and in the absence of superoxide dismutase activity, the superoxide radical can further metabolise to peroxynitrite (OONO^-) and the perhydroxyl radical ($\text{HO}_2\cdot$) which plays a role in tumour formation.⁴⁴ It has been demonstrated that by returning MnSOD enzyme activity to levels which are close to that in non-malignant cells results in the conversion of excess superoxide into hydrogen peroxide which leads to a decrease in tumour cell growth.¹²²⁻¹²⁴

4 Chapter Four - Experimental

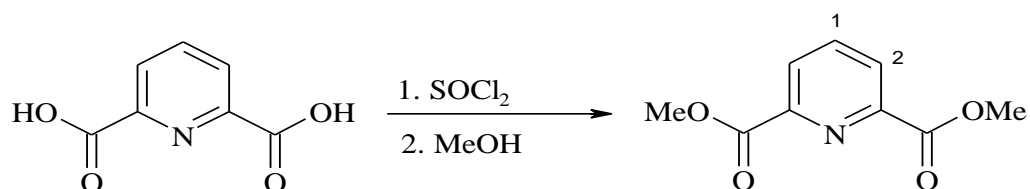
4.1 General experimental conditions

Starting materials were purchased from a commercial source and were used without further purification unless otherwise stated. The prepared compounds were characterised via IR spectroscopy, FAB, CHN analysis and in some cases by X-ray crystallography. IR spectra were performed using KBr pellets on a Perkin Elmer Paragon 1000PC. CHN analysis was performed using a CE-440 Elemental analyser by Mrs Pauline King. Mass spectra for barium macrocycles were recorded on a JEOL SX102 mass spectrometer, manganese complexes were recorded at the EPSRC National Mass Spectrometry Service Centre at Swansea University. All samples were run using Fast Atom Bombardment (FAB) and masses were calculated using average masses. UV / Vis analysis was performed on a Perkin Elmer UV / Vis Lambda 12 spectrometer. Details for X-ray crystallography, data collection: APEX2 (Bruker, 1998); ⁹⁸ cell refinement: SAINT (Bruker, 1998);⁹⁸ data reduction: SAINT; program(s) used to solve structure: SHELXS97 (Sheldrick, 1997); program(s) used to refine structure: SHELXL97 (Sheldrick, 1997); molecular graphics: SHELXTL (Sheldrick, 2001)¹²⁵ and Mercury 2.2 unless otherwise stated. Structures were also searched with use of the EPSRC's chemical database service at Daresbury.¹²⁶

4.2 Polynuclear complexes

4.2.1 2,6-Diacetylpyridine

Step 1: 2,6-Pyridinedicarboxylic acid \rightarrow 2,6-dimethylpyridine dicarboxylate¹⁰⁰



2,6-Pyridinedicarboxylic acid (31.010 g, 0.20 mol) was refluxed in thionyl chloride (200 ml) for 10 h. Most of the thionyl chloride was then removed under reduced

pressure. 2,6-Pyridinedicarboxylic acid chloride solidified out when the solution was cooled in an ice bath. Dry methanol (250 ml) was added drop wise to the cooled solid and the resulting solution was refluxed for 30 minutes. The solution was then placed onto a rotary evaporator which initiated precipitation this was then completed with the use of an ice bath to cool the solution. The white crystals were filtered and washed with ice cold methanol and dried *in vacuo*. Yield: 36.110 g, 0.18 mol, 92%.

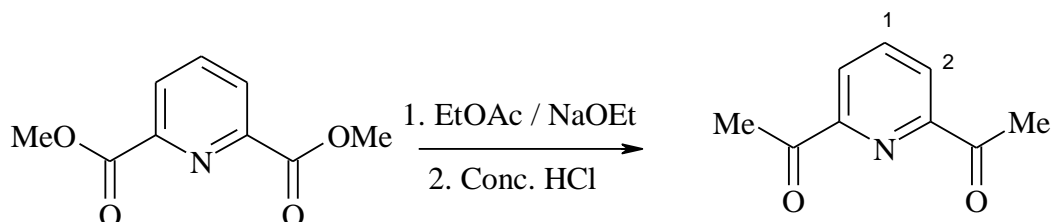
IR (KBr disc, cm^{-1}) 1740 $\nu_{(\text{RCOOR}^*)}$, 1571 $\nu_{(\text{C}=\text{C})}$, 1437, 1289, 1244, 1164, 1144, 1080, 995, 952, 852, 812, 757, 723, 697, 646, 462, 433

Anal. (%) Found C = 55.2 H = 4.8 N = 7.1

$\text{C}_9\text{H}_9\text{NO}_4$ C = 55.4 H = 4.7 N = 7.2

NMR (CDCl_3 , ppm, ^1H) 3.96 (s, 6H, CH_3), 7.98 (t, 1H, CHAr^1), 8.25 (d, 2H, CHAr^2)

Step: 2: 2,6-Dimethylpyridine dicarboxylate \rightarrow 2,6-Diacetylpyridine¹⁰⁰



Sodium ethoxide was freshly prepared by placing sodium (7.809 g) slowly into absolute ethanol (100 ml) with stirring until no sodium remained. This was then reduced to dryness using a rotary evaporator. The sodium ethoxide was placed into a 1l round-bottom flask and xylene (50 ml), 2,6-dimethylpyridine dicarboxylate (19.705 g) and ethyl acetate (32.510 g) were added. A brown/yellow colour developed on mixing. A further 110 ml of xylene was added and the suspension was refluxed for 19 h at 140 – 150 °C. The solution was then allowed to cool to room temperature and distilled water (75 ml) was added slowly, followed by concentrated hydrochloric acid (140 ml). The solution was refluxed for 30 mins at 140 – 150 °C to complete the reaction. The xylene/water azeotrope was distilled off using a Dean Stark collector, returning the aqueous phase to the reaction vessel. The solution was

white solid was collected by filtration. Washed with methanol and dried *in vacuo*.^{93, 94, 100} Yield: 7.003 g, 9.09 mmol, 70 %.

IR: (KBr disc, cm^{-1}) 3431 $\nu_{(\text{O-H})}$, 3097, 2911, 1639 $\nu_{(\text{C=N})}$, 1584 $\nu_{(\text{C=C})}$, 1451, 1430, 1380, 1365, 1273, 1242, 1188, 1099 $\nu_{(\text{ClO}_4^-)}$, 994, 932, 813, 781, 745, 715, 625 $\nu_{(\text{ClO}_4^-)}$)

Anal (%) Found C = 35.6 H = 4.3 N = 10.2
[Ba(H₂L1)(H₂O)₂](ClO₄)₂ C = 35.7 H = 4.3 N = 10.4

FAB

M/z	Rel. Abundance (%)	Fragment	Molecular weight (Calc)
671	100	[Ba(H ₂ L1)](ClO ₄) ⁺	671
571	22	[Ba(H ₂ L1)] ⁺	571

4.2.3 [Mn₂(HL1)(Cl)₂]₂(ClO₄)₂·H₂O

MnCl₂·4H₂O (1.077 g, 5.44 mmol) in methanol (50 ml) was added to a refluxing suspension of [Ba(H₂L1)(H₂O)₂](ClO₄)₂ (2.057g, 2.67 mmol) in methanol (300 ml). Refluxing was continued for 2 h. The solution was then allowed to cool and the fine orange powder product was collected *via* filtration, washed with methanol and dried *in vacuo*.^{93, 100} Yield: 1.17 g, 0.82 mmol, 66 %.

Suitable crystals were obtained for X-ray analysis by slow diffusion of ether into a solution of product dissolved in dimethylformamide. The product was found to crystallise with the formula [Mn₂(HL1)(Cl)₂]₂(ClO₄)₂·2DMF.

IR (KBr disc, cm^{-1}) 3418 $\nu_{(\text{O-H})}$, 3071, 2916, 1643 $\nu_{(\text{C=N})}$, 1582 $\nu_{(\text{C=C})}$, 1420, 1381, 1250, 1196, 1088 $\nu_{(\text{ClO}_4^-)}$, 1010, 817, 741, 625

Anal. (%) Found

C = 39.6 H = 3.8 N = 11.1

$[\text{Mn}_2(\text{HL1})(\text{Cl})_2]_2(\text{ClO}_4)_2 \cdot \text{H}_2\text{O}$

C = 39.9 H = 4.2 N = 11.6

FAB

M/z	Rel. Abundance (%)	Fragment	Molecular weight (Calc)
1327	3	$[\text{Mn}_2(\text{HL1})(\text{Cl})_2]_2(\text{ClO}_4)^+$	1327
1226	7	$[\text{Mn}_2(\text{HL1})(\text{Cl})_2]_2^+$	1226
613	4	$[\text{Mn}_2(\text{HL1})(\text{Cl})_2]^+$	613
577	100	$[\text{Mn}_2(\text{HL1})(\text{Cl})]^+$	577
540	14	$[\text{Mn}_2(\text{HL1})-\text{H}^+$	540

4.2.4 $[\text{Mn}_2(\text{HL1})(\text{N}_3)_2]_2(\text{ClO}_4)_2 \cdot \text{H}_2\text{O} \cdot \text{MeOH}$

$[\text{Ba}(\text{H}_2\text{L1})(\text{H}_2\text{O})_2](\text{ClO}_4)_2$ (0.773 g, 1.00 mmol) in methanol (250 ml) was brought to reflux. $\text{Mn}(\text{ClO}_4)_2 \cdot 6\text{H}_2\text{O}$ (0.702 g, 1.94 mmol) in methanol (20 ml) was added followed quickly by NaN_3 (0.65 g, 10 mmol) in methanol. Refluxing continued for 3 h. The orange solid was then collected by filtration, washed with methanol and dried *in vacuo*.⁹³ Yield: 0.469 g, 0.31 mmol, 31 %.

Suitable crystals were obtained for X-ray analysis by slow diffusion of ether into a solution of product dissolved in dimethylformamide. The product was found to crystallise with the formula $[\text{Mn}_2(\text{HL1})(\text{N}_3)_2]_2(\text{ClO}_4)_2 \cdot 2\text{DMF}$.

IR: (KBr disc, cm^{-1}) 3373 $\nu_{(\text{O-H})}$, 3080, 2910, 2046 $\nu_{(\text{N}_3)}$, 1653 $\nu_{(\text{C=N})}$, 1585 $\nu_{(\text{C=C})}$, 1419, 1375, 1250, 1193, 1092 $\nu_{(\text{ClO}_4^-)}$, 1013, 817, 743, 622 $\nu_{(\text{ClO}_4^-)}$

Anal. (%) Found

C = 38.9 H = 3.9 N = 22.2

$[\text{Mn}_2(\text{HL1})(\text{N}_3)_2]_2(\text{ClO}_4)_2 \cdot \text{H}_2\text{O} \cdot \text{MeOH}$

C = 39.2 H = 4.2 N = 22.4

FAB

M/z	Rel. Abundance (%)	Fragment	Molecular weight (Calc)
1367	3	$[\text{Mn}_2(\text{HL1})(\text{N}_3)]_2(\text{ClO}_4)_2$ -2H^+	1367
627	25	$[\text{Mn}_2(\text{HL1})(\text{N}_3)_2]^+$	627
584	100	$[\text{Mn}_2(\text{HL1})(\text{N}_3)]-\text{H}^+$	584
541	4	$[\text{Mn}_2(\text{HL1})]$	541

4.2.5 $[\text{Mn}_4(\text{HL1})(\text{L1})(\text{NCS})_4]\text{NCS}\cdot\text{H}_2\text{O}$

$[\text{Ba}(\text{H}_2\text{L1})(\text{H}_2\text{O})_2](\text{ClO}_4)_2$ (2.000 g, 2.60 mmol) in methanol (200 ml) was brought to reflux. $\text{Mn}(\text{ClO}_4)_2\cdot 6\text{H}_2\text{O}$ (1.800g, 4.97 mmol) in methanol (20 ml) was added followed quickly by NaNCS (1.620 g, 20.01 mmol) in methanol (80 ml). Refluxing continued overnight.¹⁰⁰ The orange solid was collected by filtration and the product washed with water and dried *in vacuo*. Yield: 0.469 g, 0.32 mmol, 28 %.

IR: (KBr disc, cm^{-1}) 3417 $\nu_{(\text{O-H})}$, 2923, 2037 $\nu_{(\text{NCS}^-)}$, 1633 $\nu_{(\text{C=N})}$, 1587 $\nu_{(\text{C=C})}$, 1457, 1421, 1376, 1252, 1199, 1090, 1015, 812

Anal. (%) Found	C = 43.3 H = 4.0 N = 14.9
$[\text{Mn}_4(\text{HL1})(\text{L1})(\text{NCS})_4]\text{NCS}\cdot\text{H}_2\text{O}$	C = 43.5 H = 4.1 N = 15.6

FAB

M/z	Rel. Abundance (%)	Fragment	Molecular weight (Calc)
1318	8	[Mn ₄ (HL1)(L1)(NCS) ₄] ⁺	1318
1258	15	[Mn ₄ (HL1)(L1)(NCS) ₃]-H ⁺	1259
1200	6	[Mn ₄ (HL1)(L1)(NCS) ₂]-H ⁺	1201
600	100	[Mn ₂ (HL1)(NCS)]-H ⁺	601
542	10	[Mn ₂ (HL1)]-H ⁺	543

4.2.6 [Mn₂(HL1)(OAc)(ClO₄)₂·2H₂O

[Ba(HL1)(H₂O)₂](ClO₄)₂ (0.501 g, 0.65 mmol) was refluxed in methanol (15 ml). Mn(OAc)·4H₂O (0.384 g, 1.6 mmol) was refluxed in methanol (15 ml) for 15 minutes, this was added to the refluxing barium solution and refluxing continued for 1 hr forming an orange solid that was collected by filtration, washed with methanol and dried *in vacuo*.^{24, 94, 127} Yield: 0.240 g, 0.17 mmol, 52 %.

IR: (KBr disc, cm⁻¹) 3427 ν_(O-H), 3087, 2924, 2883, 1658 ν_(C=N), 1565 ν_(C=C), 1408, 1374, 1362, 1277, 1243, 1195, 1092 ν_(ClO₄), 1040, 1009, 966, 890, 876, 810, 742, 735, 646, 623 ν_(ClO₄⁻), 582

Anal. % Found C = 43.1 H = 4.3 N = 11.3

[Mn₂(HL1)(OAc)(ClO₄)₂·2H₂O C = 43.4 H = 4.8 N = 11.7

FAB

M/z	Rel. Abundance (%)	Fragment	Molecular weight (Calc)
601	100	[Mn ₂ (HL1)(OAc)] ⁺	602
1301	1	[Mn ₂ (HL1)(OAc)] ₂ ⁺ ClO ₄	1303

4.2.7 [Mn₅(HL1)₂(OAc)₂(ClO₄)₂](ClO₄)₂.2MeOH

[Ba(H₂L1)(H₂O)₂](ClO₄)₂ (0.769 g, 1.00 mmol) was refluxed in methanol (15 ml). Mn(OAc).4H₂O (0.613 g, 2.50 mmol) in cold methanol (20 ml) was added and refluxing continued for 1 hr. An orange solid formed on cooling which was removed *via* filtration, washed with methanol and dried *in vacuo*.^{24, 94, 100} Yield: 0.280 g, 0.16 mmol, 33 %.

Suitable crystals were obtained for X-ray analysis by slow diffusion of ether into a solution of product dissolved in dimethylformamide. The product was found to crystallise with the formula [Mn₅(HL1)₂(OAc)₂(DMF)₂](ClO₄)₄.4DMF.

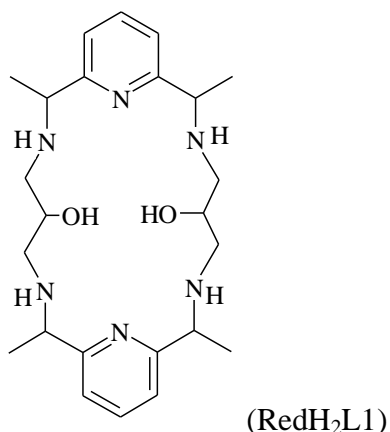
IR: (KBr disc, cm⁻¹) 3448 ν_(OH), 2921, 2880, 1642 ν_(C=N), 1577 ν_(C=C), 1417, 1379, 1249, 1198, 1099 ν_(ClO₄⁻), 1017, 896, 811, 738, 625 ν_(ClO₄⁻)

Anal. % Found C = 37.6 H = 3.9 N = 9.5
[Mn₅(HL1)₂(OAc)₂(ClO₄)₂](ClO₄)₂.2MeOH C = 37.7 H = 4.1 N = 9.8

FAB

M/z	Rel. Abundance (%)	Fragment	Molecular weight (Calc)
1556	5	[Mn ₅ (HL1) ₂ (OAc) ₂ (ClO ₄) ₂] ⁺ (ClO ₄)	1555
774	22	[Mn ₃ (HL1)(OAc) ₃] ⁺	774
655	12	[Mn ₃ (HL1)(OAc)] ⁺	655
601	100	[Mn ₂ (HL1)(OAc)] ⁺	601

RedL1 structure



The initial reduction step for ligands of RedHL1 were carried out using borohydride reduction of the barium presursor [Ba(H₂L1)(H₂O)₂](ClO₄)₂ in the following manner:

[Ba(H₂L1)(H₂O)₂](ClO₄)₂ (0.808 g, 1.05 mmol) was stirred in methanol (15 ml). Sodium tetraborate (0.200 g, 0.50 mmol) and then sodium borohydride (0.153 g, 4.00 mmol) was added slowly over 30 mins. Stirring was continued for 2 h at room temperature. The solvent was then reduced to approximately 2 ml under reduced pressure with the remaining left to evaporate at room temperature in air. Ammonium chloride in water (1.000 g, 10 ml) was added to the residue and the product extracted with dichloromethane (3 x 15 ml). The organic fractions were then combined and washed with water before drying over magnesium sulphate which was then filtered and the solvent removed under reduced pressure yielding a yellow sticky product. Yield: 0.119 g, 0.1%.

IR (KCl Plate, cm⁻¹) 3299 $\nu_{(\text{O-H})}$, 1697, 1574 $\nu_{(\text{C=C})}$, 1446, 1359, 1301, 1235, 1095 $\nu_{(\text{ClO}_4)}$, 818, 754

4.2.8 [Mn₂(RedHL1)(Cl)₂]₂[MnCl]₄.2H₂O

RedHL1 (0.108 g, 0.10 mmol) was brought to reflux in methanol (20 ml). MnCl₂.4H₂O (0.055 g, 0.28 mmol) in methanol (10 ml) was then added and refluxing

continued for 2 h. The resulting yellow solution was reduced to approximately 2 ml and a pale cream coloured solid was then removed via filtration, washed with methanol and dried *in vacuo*. Yield: 0.072 g, 0.05 mmol, 99 %.

The product was recrystallised by slow diffusion of ethanol into a solution of the product in dimethylformamide. The product was found to crystallise with the formula $[\text{Mn}_2(\text{RedHL1})(\text{Cl})_2]_2[\text{MnCl}]_4 \cdot 4\text{DMF} \cdot \text{EtOH}$.

IR: (KBr disc, cm^{-1}) 3405 $\nu_{(\text{O-H})}$, 3222, 2973, 2935, 2858, 1669, 1598 $\nu_{(\text{C=C})}$, 1577, 1383, 1309, 1248, 1167, 1131, 1096, 1078, 1012, 984, 942, 896, 837, 811, 755, 598

Anal% Found C = 39.4 H = 4.7 N = 11.1
 $[\text{Mn}_2(\text{RedHL1})(\text{Cl})_2]_2[\text{MnCl}]_4 \cdot \text{H}_2\text{O}$ C = 39.5 H = 5.2 N = 11.5

FAB

M/z	Rel. Abundance (%)	Fragment	Molecular weight (Calc)
1243	4	$[\text{Mn}_2(\text{RedHL1})(\text{Cl})_2]_2 - \text{H}^+$	1243
621	100	$[\text{Mn}_2(\text{RedHL1})(\text{Cl})_2] - \text{H}^+$	621
585	47	$[\text{Mn}_2(\text{RedHL1})(\text{Cl})]^+$	583

4.2.9 $[\text{Mn}_2(\text{RedHL1})(\text{N}_3)_2]_2(\text{ClO}_4)_2 \cdot 2\text{H}_2\text{O}$

RedHL1 (0.147 g, 0.20 mmol) was brought to reflux in methanol (20 ml). $\text{Mn}(\text{ClO}_4)_2$ (0.055 g, 0.28 mmol) in methanol (10 ml) was added followed quickly by NaN_3 (0.065 g, 1 mmol) and refluxing continued for 2 h. A white solid precipitate formed on cooling, this was collected *via* filtration, washed with methanol and dried *in vacuo*. Yield: 0.056 g, 0.04 mmol, 44 %. The product obtained did not crystallise using slow diffusion from various solvents.

IR: (KBr disc, cm^{-1}) 3365 $\nu_{(\text{O-H})}$, 3262, 2977, 2915, 2864, 2050 $\nu_{(\text{N}_3)}$, 1601, 1578 $\nu_{(\text{C=C})}$, 1465, 1383, 1323, 1275, 1261, 1169, 1099 $\nu_{(\text{ClO}_4^-)}$, 1010, 981, 947, 895, 841, 809, 757, 623 $\nu_{(\text{ClO}_4^-)}$

Anal% Found

C=38.5 H = 4.6 N = 21.6

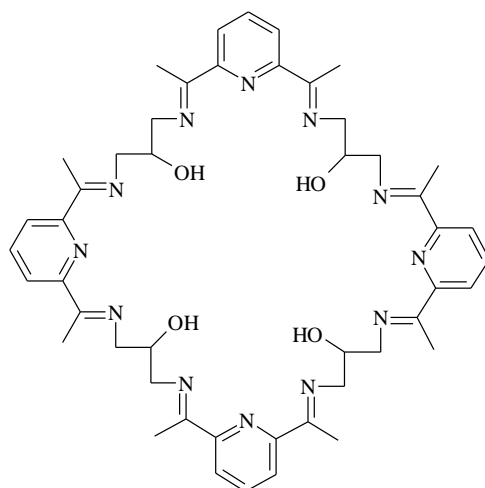
$[\text{Mn}_2(\text{RedHL1})(\text{N}_3)_2]_2(\text{ClO}_4)_2 \cdot 2\text{H}_2\text{O}$

C=38.3 H = 5.2 N = 22.3

FAB

M/z	Rel. Abundance (%)	Fragment	Molecular weight (Calc)
1229	4	$[\text{Mn}_4(\text{RedHL1})_2(\text{N}_3)_3]^+$	1228
1186	9	$[\text{Mn}_4(\text{RedHL1})_2(\text{N}_3)_2]^+$	1186
1142	13	$[\text{Mn}_4(\text{RedHL1})_2(\text{N}_3)]^+$	1144
834	100	$[\text{Mn}_2(\text{RedHL1})(\text{N}_3)_2]^+(\text{ClO}_4)_2$	834
551	23	$[\text{Mn}_2(\text{RedHL1})]^+$	551

4.2.10 $[\text{Mn}_4(\text{L2})(\text{ClO}_4)_4](\text{ClO}_4)_2 \cdot 2\text{EtOH}$



(H₄L₂)

2,6-Diacetylpyridine (0.979 g, 6.00 mmol) and $\text{Mn}(\text{ClO}_4)_2 \cdot 6\text{H}_2\text{O}$ (2.152 g, 5.95 mmol) were dissolved in methanol (100 ml) and heated to reflux. 1,3-Diamino-2-hydroxy propane (0.541 g, 6.01 mmol) was dissolved in cold methanol (40 ml) and added slowly into the refluxing solution. Refluxing was then continued overnight.

The resulting orange solid suspension was collected *via* filtration, washed with ethanol and dried *in vacuo*. a further crop was collected by reducing the solvent *in vacuo*. The solvent was again collected *via* filtration, washed with ethanol and dried *in vacuo*.^{99, 100} Yield 0.820 g, 0.47 mmol, 16 %.

IR: (KBr disc, cm⁻¹) 3421 $\nu_{\text{(OH)}}$, 3013, 1654 $\nu_{\text{(C=C)}}$, 1587 $\nu_{\text{(C=N)}}$, 1359, 1298, 1254, 1199, 1142, 1109, 1086 $\nu_{\text{(ClO}_4^-)}$, 1014, 897, 812, 746, 625 $\nu_{\text{(ClO}_4^-)}$

Anal% Found C = 35.5 H = 3.9 N = 9.8
 [Mn₄(L2)(ClO₄)₄](ClO₄)₂.2EtOH C = 35.2 H = 3.9 N = 9.5

FAB

M/z	Rel. Abundance (%)	Fragment	Molecular weight (Calc)
1381	5	[Mn ₄ (L2)(ClO ₄) ₃] ⁺	1381
1281	9	[Mn ₄ (L2)(ClO ₄) ₂] ⁺	1286
1183	5	[Mn ₄ (L2)(ClO ₄)] ⁺	1183
641	100	[Mn ₂ (L2)(ClO ₄)] ⁺ (1/2 molecule)	641

4.2.11 [Mn₄(L2)(NCS)₂](ClO₄)₂

2,5-Diacetylpyridine (0.326 g, 2.00 mmol) and Mn(ClO₄)₂.6H₂O (0.508 g, 1.40 mmol) were dissolved in methanol (30 ml) and heated to reflux. 1,3-diamino-2-hydroxy propane (0.180 g, 2.00 mmol) was dissolved in cold methanol (10 ml) and added slowly into the refluxing solution. Refluxing was then continued overnight. Sodium thiocyanate (0.649 g, 8.00 mmol) in methanol (10 ml) was added. The resulting orange solid suspension was collected by filtration, washed with methanol and dried *in vacuo*. A further crop was collected by reducing the solvent *in vacuo*. the solid was collected *via* filtration, washed with methanol and dried *in vacuo*. Yield 0.259 g, 0.19 mmol, 19 %.

IR: (KBr disc, cm^{-1}) 3426 $\nu_{(\text{OH})}$, 3078, 2901, 1643 $\nu_{(\text{C}=\text{C})}$, 1589 $\nu_{(\text{C}=\text{N})}$, 1420, 1373, 1250, 1196, 1095 $\nu_{(\text{ClO}_4^-)}$, 1011, 810, 741, 625 $\nu_{(\text{ClO}_4^-)}$

Anal. (%) Found C = 42.8 H = 4.3 N = 14.5

$[\text{Mn}_4(\text{L}2)(\text{NCS})_2](\text{ClO}_4)_2$ C = 42.9 H = 4.0 N = 14.0

FAB

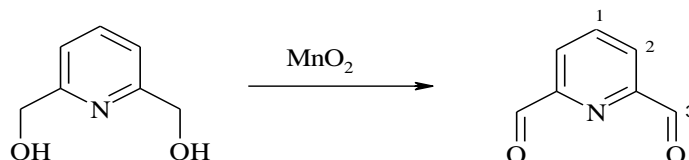
M/z	Rel. Abundance (%)	Fragment	Molecular weight (Calc)
1300	5	$[\text{Mn}_4(\text{L}2)(\text{NCS})_2]\cdot\text{NCS}^+$	1300
1258	30	$[\text{Mn}_4(\text{L}2)(\text{NCS})_2]-\text{H}^+$	1258
600	100	$[\text{Mn}_2(\text{L}2)(\text{NCS})]^+$	600

4.3 Ring contracted macrocycles

4.3.1 MnO_2

MnSO_4 (100 g) was dissolved in boiling water (125 ml). KMnO_4 (90 g) in cold water (2.5l) was added into the boiling solution slowly over 4-5 hours to form a black suspension which was collected *via* filtration. This was washed with boiling water. Active MnO_2 was obtained after drying at 110-120 °C for 48 hours.

4.3.2 2,6-Diformylpyridine



Manganese dioxide was suspended in chloroform (300 ml) and 2,6-Pyridinemethanol (4.909 g, 0.04 mol) was added. The solution was refluxed for 5 h. The remaining

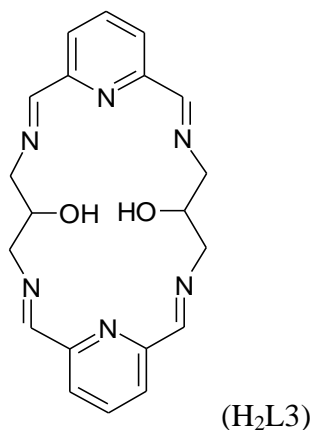
black solid was filtered and washed with ether (5 x 100 ml) the filtrate and the washings were evaporated to dryness under reduced pressure to yield a cream coloured solid. Yield: 2.256 g, 0.02mol, 50 %.

IR: (KBr disc, cm^{-1}) 3085 $\nu_{(\text{C-H})}$, 2861, 1719 $\nu_{(\text{C=O})}$, 1579 $\nu_{(\text{C=C})}$, 350, 1261, 1210, 1086, 992, 806, 786, 699, 622, 494, 414

Anal. (%) Found C = 61.7 H = 3.8 N = 10.1
C₇H₅NO₂ C = 62.2 H = 3.7 N = 10.4

NMR (CDCl₃, ppm, ¹H) 8.02 (t 1H CHAr¹), 8.13 (d 2H CHAr²), 10.11 (s 2H H³)

4.3.3 [Ba(H₂L3)(ClO₄)₂](ClO₄)₂



2,6-Diformylpyridine (1.352 g, 10.01 mmol) was dissolved in methanol (100 ml). Ba(ClO₄)₂·3H₂O (1.951 g, 5.00 mmol) in methanol (10 ml) was added. 1,3-Diamino-2-hydroxy propane (0.933 g 10.36 mmol) in methanol (10 ml) was added and stirring continued for 1 hr. The solvent was then reduced *in vacuo* to 10 ml and upon standing for several hours, large colourless crystals formed.^{1, 92} Yield: 3.251 g, 2.28 mmol, 45 %.

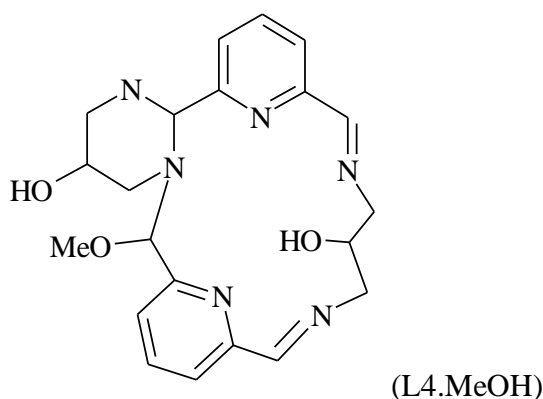
IR: (KBr disc, cm^{-1}) 3380 $\nu_{(\text{O-H})}$, 2909, 1654 $\nu_{(\text{C=N})}$, 1586 $\nu_{(\text{C=C})}$, 1458, 1397, 1354, 1324, 1265, 1092 $\nu_{(\text{ClO}_4)}$, 1046, 1000, 983, 939, 817, 804, 785, 766, 738, 661, 625 $\nu_{(\text{ClO}_4)}$, 547

Anal% Found C = 33.7 H = 3.1 N = 11.7
[Ba(H₂L3)(ClO₄)₂](ClO₄)₂ C = 33.6 H = 3.1 N = 11.8

FAB

M/z	Rel. Abundance (%)	Fragment	Molecular weight (Calc)
615	100	[Ba(H ₂ L3)] ⁺ (ClO ₄)	615
515	6	[Ba(H ₂ L3)] ⁺	516

4.3.4 [Mn(L4)(NCS)₂].MeOH



[Ba(H₂L3)(ClO₄)₂](ClO₄)₂ (0.751 g, 1.05 mmol) was dissolved in methanol (35 ml). MnCl₂·4H₂O (0.198 g, 1.00 mmol) in methanol (10 ml) was added followed by sodium thiocyanate (0.162 g, 2.00 mmol) in methanol (10 ml) and stirring continued overnight. The solvent was reduced to ~ 2ml and the resulting solid was filtered, washed with water and dried *in vacuo*. The methanol filtrate was allowed to stand yielding orange crystals which were collected via filtration and dried *in vacuo*. Yield: 0.534 g, 0.81 mmol, 77 %.

The product was recrystallised by slow diffusion of ether into a solution of the product in dimethylformamide. The product was found to crystallise with the formula $[\text{Mn}(\text{L4})(\text{NCS})_2] \cdot \text{MeOH} \cdot \text{DMF}$.

IR: (KBr disc, cm^{-1}) 3302 $\nu_{(\text{O-H})}$, 2902, 2068 $\nu_{(\text{NCS})}$, 1654 $\nu_{(\text{C=N})}$, 1587 $\nu_{(\text{C=C})}$, 1458, 1416, 1388, 1351, 1326, 1266, 1162, 1086, 1052, 1022, 1001, 957, 931, 802, 786, 738, 663, 634, 551

Anal% Found C = 47.9 H = 4.2 N = 18.8
 $[\text{Mn}(\text{L4})(\text{NCS})_2] \cdot \text{MeOH}$ C = 47.5 H = 4.5 N = 19.3.

FAB

M/z	Rel. Abundance (%)	Fragment	Molecular weight (Calc)
551	100	$[\text{Mn}(\text{L4})(\text{NCS})_2] - \text{CH}_3, -2\text{H}^+$	551
509	33	$[\text{Mn}(\text{L4})(\text{NCS})]^+$	509
450	25	$[\text{Mn}(\text{L4})]^+$	450

4.3.5 $[\text{Mn}(\text{L4})(\text{Cl})_2] \cdot \text{MeOH} \cdot 2\text{H}_2\text{O}$

$[\text{Ba}(\text{H}_2\text{L3})(\text{H}_2\text{O})_2](\text{ClO}_4)_2$ (0.814 g, 1.08 mmol) was dissolved in methanol (200ml). $\text{MnCl}_2 \cdot 4\text{H}_2\text{O}$ (0.473 g, 2.38 mmol) in methanol (20ml) was quickly added. The solution obtained was stirred overnight at room temperature, yielding a pale yellow solution. The solvent was reduced to 10ml under reduced pressure. After one night at room temperature, white crystals were obtained. Yield 0.239g. The solution was filtered and the yellow filtrate was reduced to 5ml under reduced pressure. After 2 days at room temperature, yellow crystals were observed and isolated. Yield 0.090 g. 0.06 mmol, 5.6%.

Crystals obtained were too clustered for X-ray to be performed.

IR: (KBr disc, cm^{-1}) 3331 $\nu_{(\text{O-H})}$, 2932 $\nu_{(\text{C-H})}$, 1637 $\nu_{(\text{C=N})}$, 1593 $\nu_{(\text{C=C})}$, 1381, 1274, 1149, 1072 $\nu_{(\text{ClO}_4^-)}$, 821, 678, 625 $\nu_{(\text{ClO}_4^-)}$

Anal% Found C = 43.4 H = 4.8 N = 14.5

[Mn(L4)(Cl)₂].MeOH.2H₂O C = 44.1 H = 5.3 N = 14.7

4.3.6 [Mn(L4)(N₃)₂].MeOH

[Ba(H₂L3)(ClO₄)₂](ClO₄)₂ (0.507 g, 0.7 mmol) was dissolved in methanol (40 ml) and stirred under nitrogen. Mn(ClO₄)₂.6H₂O (0.506 g, 1.4 mmol) in methanol (10 ml) followed by sodium azide (0.445 g, 7 mmol) in methanol (10 ml). Stirring continued overnight. The solvent was reduced to ~ 2ml and the resulting solid was filtered. A further crop was obtained by reducing the filtrate. Yield: 0.27 g, 0.2 mmol, 57 %.

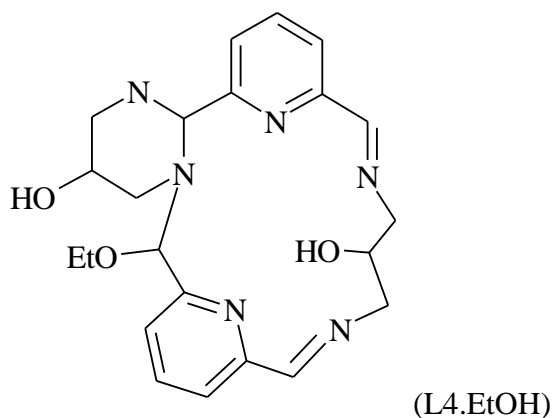
IR: (KBr disc, cm^{-1}) 3404 $\nu_{(\text{OH})}$, 2058 $\nu_{(\text{N}_3)}$, 1637 $\nu_{(\text{C=N})}$, 1592 $\nu_{(\text{C=C})}$, 1458 $\nu_{(\text{CH}_2)}$, 1087 $\nu_{(\text{ClO}_4)}$, 627 $\nu_{(\text{ClO}_4)}$

Anal% Found C = 53.8 H = 5.9 N = 18.7

[Mn(L4)(N₃)₂].MeOH C = 54.1 H = 5.8 N = 18.0

Suitable crystals of this complex did not form for X-ray analysis to be performed.

4.3.7 [Mn(L4)(NCS)₂].EtOH

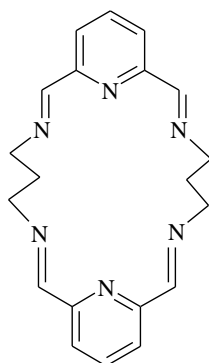


[Ba(H₂L3)(ClO₄)₂](ClO₄)₂ (0.374 g, 0.50 mmol) was stirred in ethanol (30 ml). Mn(ClO₄)₂·6H₂O (0.254 g, 0.70 mmol) was added followed with NaNCS (0.234 g, 4.00 mmol). Stirring continued in a stoppered flask for 18 h at room temperature. A white solid thought to be a barium salt was collected from the solution *via* filtration, washed with methanol and dried *in vacuo*. The yellow filtrate was allowed to stand at room temperature forming yellow crystals. Yield: 0.109 g, 0.18 mmol, 37 %.

IR: (KBr disc, cm⁻¹) 3304 ν_(O-H), 2902, 2069 ν_(NCS), 1653 ν_(C=N), 1586 ν_(C=C), 1458, 1416, 1388, 1350, 1326, 1266, 1161, 1086, 1052, 1022, 1002, 957, 930

Anal% Found	C = 48.0 H = 5.3 N = 18.7
[Mn(L4)(NCS) ₂].EtOH	C = 48.2 H = 5.1 N = 18.8

4.3.8 [Ba(L5)(ClO₄)₂(OH₂)₂]



(L5)

2,6-Diformylpyridine (1.080 g, 10 mmol) was dissolved in methanol (100 ml). Ba(ClO₄)₂·3H₂O (1.954 g, 5 mmol) was added followed by 1,3-diaminopropane (0.910 g, 10 mmol) in methanol (20 ml). Stirring was continued for 15 mins. The solvent was removed under reduced pressure to approximately 10 ml. This solution was then placed into an ice bath to form clear crystals which were filtered and dried *in vacuo*. Yield: 2.5 g, 3.5 mmol, 70 %.

IR: (KBr disc, cm⁻¹) 2927, 2863, 1642 ν_(C=N), 1586 ν_(C=C), 1458, 1394, 1348, 1266, 1108 ν_(ClO₄⁻), 1051, 1002, 923, 813, 744, 618

Anal. (%) Found	C = 33.4 H = 3.6 N = 11.3
[Ba(L5)(ClO ₄) ₂ (H ₂ O) ₂]	C = 33.4 H = 3.6 N = 11.7

4.3.9 [Mn(L5)(NCS)₂].MeOH.H₂O

MnCl₂.4H₂O (0.504 g, 3.0 mmol) in methanol (25 ml) was added to a refluxing methanolic (150 ml) suspension of [Ba(L5)](ClO₄)₂ (1.000 g, 1.37 mmol) and reflux continued for 2 h forming a yellow solution. The solution was then allowed to cool. A solid did not form and therefore sodium thiocyanate was added in excess to form a neutral complex allowing yellow crystals to form.¹⁰⁰ The crystals were collected *via* filtration and dried *in vacuo*. The crystals were too clustered for X-ray analysis and attempts to re-crystallise the products were made by slow diffusion of ether into an acetonitrile solution of the product. The crystals formed were not suitable for single crystal X-ray diffraction analysis. Yield: 0.68 g, 0.85 mmol, 62 %.

IR: (KBr disc, cm⁻¹) 3400 $\nu_{\text{(OH)}}$, 3287, 2919, 2864, 2066 $\nu_{\text{(NCS)}}$, 1646 $\nu_{\text{(C=N)}}$, 1592 $\nu_{\text{(C=C)}}$, 1458, 1384, 1354, 1276, 1156, 1133, 1104, 1072, 1009, 960, 917, 877, 826, 772, 670, 655

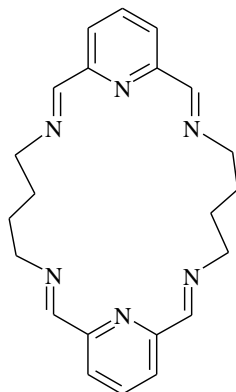
Anal. (%) Found C = 48.7 H = 4.4 N = 19.6
[Mn(L5)(NCS)₂].MeOH.H₂O C = 48.6 H = 5.1 N = 19.7

FAB

M/z	Rel. Abundance (%)	Fraction	Molecular weight (Calc)
554	8	[Mn(L5)(NCS) ₂].MeOH+4H ⁺	554
491	100	[Mn(L5)(NCS)].MeOH+H ⁺	491
401	12	[Mn(L5)(NCS)]+H ⁺	401

4.4 Dinuclear complexes

4.4.1 [Ba(L6)(ClO₄)₂]



(L6)

DFP (0.026 g, 0.20 mmol) was stirred in methanol (10 ml). Ba(ClO₄)₂·3H₂O (0.039 g, 0.09 mmol) in methanol (10 ml) was added. 1,4-Diaminobutane (0.018 g, 0.20 mmol) was added in methanol (10 ml) stirring continued overnight. The solvent was then reduced to 5 ml under reduced pressure. Large clear crystals formed on standing, these were collected via filtration and dried *in vacuo*. Yield: 0.057 g, 0.08 mmol, 80 %.

IR: (KBr disc, cm⁻¹) 2934, 1652 $\nu_{(C=N)}$, 1587 $\nu_{(C=C)}$, 1455, 1395, 1262, 1113 $\nu_{(ClO_4^-)}$, 1055, 1034, 923, 814, 742, 621 $\nu_{(ClO_4^-)}$

Anal. (%) Found C = 37.8 H = 3.8 N = 11.9
[Ba(L6)(ClO₄)₂] C = 37.2 H = 3.7 N = 11.8

FAB

M/z	Rel. Abundance (%)	Fraction	Molecular weight (Calc)
610	100	[Ba(L6)(ClO ₄) ₂] ⁺	611
512	31	[Ba(L6)] ⁺	512

4.4.2 [Mn₂(L6)(NCS)₄].MeOH

[Ba(L6)(ClO₄)₂] (0.036 g, 0.05 mmol) was stirred in methanol (10 ml). Mn(ClO₄)₂.6H₂O (0.025 g, 0.07 mmol) was added in methanol (10 ml) followed by NaNCS (0.022 g, 0.20 mmol). The solution was stirred overnight and the orange solid was collected *via* filtration, washed with methanol and dried *in vacuo*. Yield: 0.022 g, 0.03 mmol, 59 %.

The product was recrystallised by slow diffusion of ether into a solution of the product in dimethylformamide. The product was found to crystallise with the formula [Mn₂(L6)(NCS)₄].2DMF.

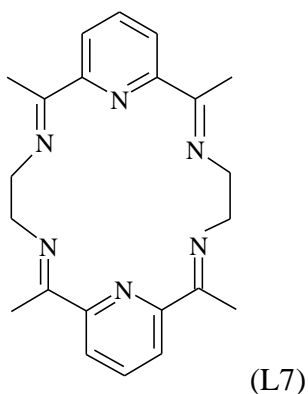
IR: (KBr disc, cm⁻¹) 2910, 2847, 2053 $\nu_{(\text{NCS})}$, 1966 $\nu_{(\text{NCS})}$, 1641 $\nu_{(\text{C}=\text{C})}$, 1586 $\nu_{(\text{C}=\text{N})}$, 1463, 1438, 1382, 1345, 1314, 1283, 1215, 1158, 1097, 1085, 1046, 1017, 982, 959, 925, 901, 809, 742, 666, 645, 624

Anal. (%) Found C = 43.6 H = 3.6 N = 18.4
[Mn₂(L6)(NCS)₄].MeOH C = 43.3 H = 4.0 N = 18.7

FAB

M/z	Rel. Abundance (%)	Fraction	Molecular weight (Calc)
658	100	[Mn(L6)(NCS) ₃] ⁺	658

4.4.3 [Ba(L7)(ClO₄)₂].H₂O



Ba(ClO₄)₂.6H₂O (1.171 g, 2.64 mmol) was added to a solution of DAP (0.979 g, 6.00 mmol) in ethanol (200 ml). The solution was brought to reflux and ethylenediamine (0.361 g, 6.00 mmol) was added and refluxing continued for 2.5 h. A white solid formed after 1h. The solid product was then filtered, washed with ethanol and dried *in vacuo*. Yield: 1.879 g, 2.58 mmol, 99 %.

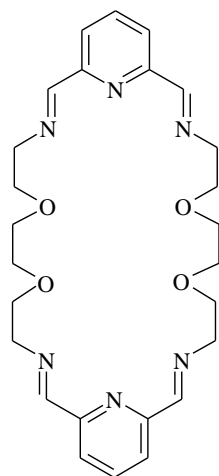
IR: (KBr disc, cm⁻¹) 3090, 2934, 1697, 1632 $\nu_{(C=N)}$, 1582 $\nu_{(C=C)}$, 1420, 1375, 1289, 1240, 1192, 1103 $\nu_{(ClO_4^-)}$, 1000, 923, 812, 749, 716, 620 $\nu_{(ClO_4^-)}$

Anal. (%) Found C = 36.7 H = 3.6 N = 11.2
[Ba(L7)(ClO₄)₂].H₂O C = 36.2 H = 3.9 N = 11.5

FAB

M/z	Rel. Abundance (%)	Fraction	Molecular weight (Calc)
611	100	[Ba(L7)(ClO ₄) ₂] ⁺	611
511	19	[Ba(L7)] ⁺	512

4.4.4 [Pb₂(L8)(NCS)₄]



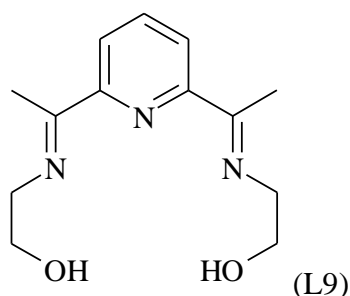
(L8)

2,6-Diformylpyridine (1.003 g, 7.42 mmol) was dissolved in dry ethanol (100 ml) at 60 °C. Pb(NCS)₂ (2.388 g, 7.38 mmol) and 2,2'-(ethylenedioxy)bis-ethylamine (1.098 g, 7.41 mmol) were added. Stirring continued for 1 hr. On standing, crystals formed in the solution these were collected *via* filtration and dried *in vacuo*.^{17, 19, 128} Yield 2.355 g, 1.07 mmol, 14 %.

IR: (KBr disc, cm⁻¹) 3419 $\nu_{(\text{O-H})}$, 2867, 2031 $\nu_{(\text{NCS})}$, 2010 $\nu_{(\text{NCS})}$, 1654 $\nu_{(\text{C=N})}$, 1588 $\nu_{(\text{C=C})}$, 1461, 1443, 1347, 1278, 1202, 1163, 1106, 1072, 1018, 814, 632, 592

4.5 Mononuclear complexes

4.5.1 [Mn(L9)(Cl)₂].H₂O



Ethanolamine (0.381 g, 6.20 mmol) in methanol (4 ml) was added to a refluxing methanolic solution (35 ml) of 2,6-diacetylpyridine (0.504 g, 3.10 mmol). This was followed by the addition of MnCl₂.4H₂O (0.616 g, 3.10 mmol) in methanol (15 ml). Refluxing was then continued for 1 hr and the brown solution left to stand overnight. The solvent was evaporated under reduced pressure until approximately 5 ml remained. Ethanol (5 ml) was then added and the solvent was removed under reduced pressure until approximately 5 ml remained. The solid product was collected *via* filtration, washed with methanol and dried *in vacuo*. Orange crystals formed in the filtrate on standing, these were collected *via* filtration, washed with ethanol and dried *in vacuo*.¹⁸ Yield: 0.590g, 1.50 mmol, 48 %.

Crystals of the product gave the formula [Mn(L9)(Cl)₂].

IR: (KBr disc, cm⁻¹) 3471 ν_(O-H), 2939, 2888, 1648 ν_(C=N), 1587 ν_(C=C), 1458, 1423, 1376, 1264, 1202, 1071, 1049, 1012, 912, 872, 833, 756, 725, 686, 647, 552

Anal% Found	C = 39.9 H = 5.5 N = 10.7
[Mn(L9)(Cl) ₂].H ₂ O	C = 39.7 H = 5.4 N = 10.7

FAB

M/z	Rel. Abundance (%)	Fraction	Molecular weight (Calc)
339	100	$[\text{Mn}(\text{L9})\text{Cl}]^+$	339
302	32	$[\text{Mn}(\text{L9})]^+$	302

4.5.2 $[\text{Mn}(\text{L9})(\text{OH}_2)_2](\text{ClO}_4)_2 \cdot \text{MeOH}$

Ethanolamine (0.240 g, 3.93 mmol) in methanol (4 ml) was added to a refluxing methanolic solution (30 ml) of 2,6-diacetylpyridine (0.328 g, 2.00 mmol). This was followed by the addition of $\text{Mn}(\text{ClO}_4)_2 \cdot 6\text{H}_2\text{O}$ (0.730 g, 2.02 mmol) in methanol (15 ml). The solution turned yellow on addition of $\text{Mn}(\text{ClO}_4)_2 \cdot 6\text{H}_2\text{O}$. Refluxing was then continued for 1 h. The orange/brown solution was allowed to cool and the solvent was evaporated under reduced pressure to approximately 5 ml. Ethanol (5 ml) was then added and the solvent was removed under reduced pressure until approximately 5 ml remained. The solid was then collected *via* filtration, washed with ethanol and dried *in vacuo*. Yield: 0.590g, 1.03 mmol, 52 %.

Crystals of the product were formed by slow diffusion of ether into a solution of the product dissolved in methanol, this method produced crystals with the formula $[\text{Mn}(\text{L9})(\text{OH}_2)_2](\text{ClO}_4)_2$.

IR: (KBr disc, cm^{-1}) 3329 $\nu_{(\text{O-H})}$, 2954, 1654 $\nu_{(\text{C=N})}$, 1593 $\nu_{(\text{C=C})}$, 1459, 1370, 1313, 1264, 1192, 1088 $\nu_{(\text{ClO}_4^-)}$, 1045, 1013, 909, 873, 819, 744, 723, 649, 626 $\nu_{(\text{ClO}_4^-)}$, 537

Anal% Found

C = 29.6 H = 4.4 N = 7.7

$[\text{Mn}(\text{L9})(\text{OH}_2)_2](\text{ClO}_4)_2 \cdot \text{MeOH}$

C = 29.4 H = 4.8 N = 7.4

FAB

M/z	Rel. Abundance (%)	Fraction	Molecular weight (Calc)
403	100	[Mn(L9)]+(ClO ₄)	403
338	32	[Mn(L9)(H ₂ O) ₂] ⁺	338
303	59	[Mn(L9)] ⁺	302

4.5.3 [Mn(L9)(NCS)₂]

This reaction was carried out as for [Mn(L9)Cl₂]. Quantities used: 2,6-diacetylpyridine (0.493 g, 3.02 mmol), ethanolamine (0.180 g, 6 mmol) and MnCl₂ (0.593 g, 3 mmol). Once the reaction was complete a brown solution was formed, to which excess potassium thiocyanate was added forming a yellow solid which was collected *via* filtration and washed with water to remove excess KCl and dried *in vacuo*. Yield: 0.250 g, 0.60 mmol, 20 %.

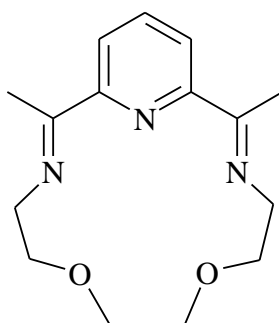
IR: (KBr disc, cm⁻¹) 3374 $\nu_{(O-H)}$, 3066, 2952, 2019 $\nu_{(NCS)}$, 1690, 1648 $\nu_{(C=N)}$, 1589 $\nu_{(C=C)}$, 1420, 1364, 1305, 1202, 1070, 1047, 1012, 910, 870, 820, 644

Anal% Found C = 43.1 H = 4.4 N = 15.9
[Mn(L9)(NCS)₂] C = 42.9 H = 4.6 N = 16.7

FAB

M/z	Rel. Abundance (%)	Fraction	Molecular weight (Calc)
362	100	[Mn(L9)(NCS)] ⁺	362
303	28	[Mn(L9)] ⁺	304

4.5.4 [Mn(L10)(Cl)₂].3H₂O



(L10)

2,2'-Ethylenedioxybis(ethylamine) (0.552 g, 3.73 mmol) in methanol (4 ml) was added to a refluxing solution of 2,6-Diacetylpyridine (0.502 g, 3.08 mmol) in methanol (35 ml). This was followed by the addition of MnCl₂.4H₂O (0.611 g, 3.09 mmol) in methanol (15 ml), refluxing was continued for 1 hr. A pink precipitate formed on mixing but dissolved during the hour of refluxing. The cooled brown solution was left to stand overnight and the solvent was then reduced down to 5 ml using a rotary evaporator. The solid that formed was then filtered and washed with ethanol and dried *in vacuo*. Further crops were obtained.¹⁸ Yield: 1.001 g, 2.20 mmol, 71 %.

IR: (KBr disc, cm⁻¹) 3508, 3405, 3145, 3062, 2921, 2879, 1645 $\nu_{(C=N)}$, 1586 $\nu_{(C=C)}$, 1473, 1417, 1375, 1355, 1313, 1269, 1241, 1205, 1109, 1087, 1073, 1038, 1018, 935, 893, 832, 825, 753, 735, 654, 546, 469

Anal% Found C = 40.0 H = 5.5 N = 9.1

[Mn(L10)(Cl)₂].3H₂O C = 39.6 H = 6.0 N = 9.2

FAB

M/z	Rel. Abundance (%)	Fraction	Molecular weight (Calc)
365	100	[Mn(L10)Cl] ⁺	365
330	5	[Mn(L10)] ⁺	330

4.5.5 [Mn(L10)(OH₂)₂](ClO₄)₂

This reaction was carried out as for [Mn(L9)(H₂O)₂](ClO₄)₂, replacing ethanolamine with 2,2'-ethylenedioxybis(ethylamine). Quantities used: 2,6-diacetylpyridine (0.490 g, 3.01 mmol), 2,2'-ethylenedioxybis(ethylamine) (0.451 g, 3.04 mmol) and Mn(ClO₄)₂·6H₂O (1.095 g, 3.03 mmol). An orange solution formed once the reaction was complete. The solvent was reduced to approximately 10ml and the orange solid was collected *via* filtration, washed with ethanol and dried *in vacuo*. Further crops were obtained by removal of solvent under reduced pressure to approximately 5 ml. Yield: 1.530 g, 2.71 mmol, 90 %.

Crystals of the product were formed by slow diffusion of ether into a solution of the product dissolved in methanol, this produced crystals with the formula [Mn(L10)(OH₂)₂](ClO₄)₂.

IR: (KBr disc, cm⁻¹) 3416 $\nu_{(\text{O-H})}$, 2928, 2881, 1648 $\nu_{(\text{C=N})}$, 1586 $\nu_{(\text{C=C})}$, 1459, 1420, 1380, 1355, 1310, 1270, 1253, 1201, 1086 $\nu_{(\text{ClO}_4^-)}$, 1018, 946, 891, 819, 727, 654, 625 $\nu_{(\text{ClO}_4^-)}$, 544, 432

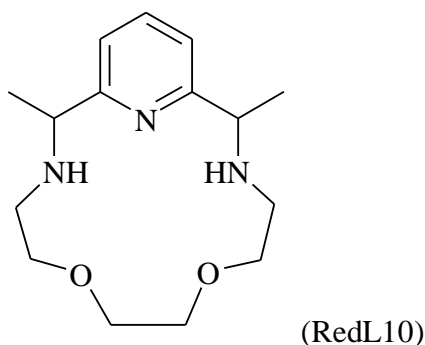
Anal% Found C = 31.5 H = 4.5 N = 7.4

[Mn(L10)(OH₂)₂](ClO₄)₂ C = 31.9 H = 4.5 N = 7.4

FAB

M/z	Rel. Abundance (%)	Fraction	Molecular weight (Calc)
429	100	[Mn(L10)(ClO ₄)] ⁺	429
330	20	[Mn(L10)] ⁺	330

4.5.6 [Mn(RedL10)(OH₂)₂](Cl)₂



[MnL10(Cl)₂] (0.804 g, 1.75 mmol) was dissolved in ethanol (40 ml). The flask was then flushed with nitrogen, before NaBH₄ (0.545g, 14.33 mmol) was added in one portion. Stirring was continued at room temperature for 2 h then the temperature was raised to 50 °C. Stirring continued for 4 h. The solvent was then removed and a solution of LiCl in methanol (0.2 M, 20 ml) was added to the residue and stirred for 30 mins. The solvent was removed under reduced pressure and water (30 ml) was added and stirred for 24 h. NaCl was added in excess and the solution extracted with dichloromethane (3 x 30 ml). The organic fractions were then dried over MgSO₄ and filtered. A sticky orange product remained on removal of the solvent under reduced pressure.³⁹ Crystallisation was set up by slow diffusion of ether into a DMF solution of the product yielding a small amount of crystals which gave the formula [Mn(RedL10)(OH₂)₂](Cl)₂.

4.5.7 [Mn(L10)(NCS)₂].H₂O

This reaction was carried out as for [Mn(L10)Cl₂]. Quantities used: 2,6-diacetylpyridine (0.494 g, 3.03 mmol) 2,2'-(ethylenedioxy)bis(ethylamine) (0.448 g, 3.02 mmol) and MnCl₂.4H₂O (0.593 g, 3.00 mmol). Once the reaction was complete, the solvent was reduced to approximately 15 ml and excess potassium thiocyanate was added forming an orange precipitate which was collected *via* filtration and washed with water to remove excess KCl. The product was dried *in vacuo*. Yield: 0.772 g, 1.66 mmol, 55 %.

Crystals of the product were formed by slow diffusion of ether into a solution of the product dissolved in methanol, this produced crystals with the formula $[\text{Mn}(\text{L10})(\text{NCS})_2]$.

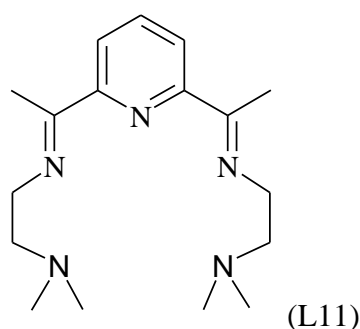
IR: (KBr disc, cm^{-1}) 3377 $\nu_{(\text{O-H})}$, 3064, 2922, 2876, 2044 $\nu_{(\text{NCS})}$, 1645 $\nu_{(\text{C=N})}$, 1585 $\nu_{(\text{C=C})}$, 1458, 1418, 1376, 1350, 1306, 1266, 1249, 1202, 1103, 1088, 1065, 1029, 1018, 958, 942, 930, 886, 827, 728, 654, 539

Anal% Found C = 44.1 H = 4.5 N = 14.8
 $[\text{Mn}(\text{L10})(\text{NCS})_2] \cdot \text{H}_2\text{O}$ C = 44.0 H = 4.9 N = 15.1

FAB

M/z	Rel. Abundance (%)	Fraction	Molecular weight (Calc)
446	2	$[\text{Mn}(\text{L10})(\text{NCS})_2]^+$	446
388	100	$[\text{Mn}(\text{L10})(\text{NCS})]^+$	388
330	20	$[\text{Mn}(\text{L10})]^+$	330

4.5.8 $[\text{Mn}(\text{L11})(\text{Cl})_2]$



N,N-Dimethylethylenediamine (0.568 g, 6.44 mmol) in methanol (4 ml) was added to a refluxing solution of 2,6-diacetylpyridine (0.508 g, 3.11 mmol). This was followed by the addition of $\text{MnCl}_2 \cdot 4\text{H}_2\text{O}$ (0.611 g, 3.11 mmol) in methanol (15 ml). A pink solid precipitated on mixing. Refluxing was continued for 1 hr and the cooled

solution was allowed to stand overnight. The volume of the solution was then reduced to approximately 5 ml under reduced pressure, and ethanol (5 ml) was added. The solvent was reduced down to 5 ml leaving a yellow solid that was collected by filtration washed with ethanol and dried *in vacuo*.¹⁸ Yield: 0.720 g, 1.68 mmol, 54 %.

Crystals of the product were formed by slow diffusion of ether into a solution of the product dissolved in methanol.

IR: (KBr disc, cm^{-1}) 3482, 3265, 3065, 2966, 2822, 2782, 1643 $\nu_{(\text{C}=\text{N})}$, 1587 $\nu_{(\text{C}=\text{C})}$, 1467, 1445, 1375, 1354, 1305, 1290, 1260, 1203, 1161, 1100, 1089, 1044, 1026, 949, 900, 830, 816, 782, 725, 654, 544

Anal% Found C = 47.3 H = 6.6 N = 16.0
[Mn(L11)(Cl)₂] C = 47.5 H = 6.8 N = 16.3

FAB

M/z	Rel. Abundance (%)	Fraction	Molecular weight (Calc)
429	7	[Mn(L11)(Cl ₂)] ⁺	428
393	100	[Mn(L11)(Cl)] ⁺	393
358	10	[Mn(L11)] ⁺	358

4.5.9 [Mn(L11)(OH₂)₂](ClO₄)₂·H₂O

This reaction was carried out as for [Mn(L9)(H₂O)₂](ClO₄)₂, replacing ethanolamine with N,N-dimethylenediamine. Quantities used: 2, 6-diacetylpyridine (0.325 g, 1.99 mmol), N,N-dimethylenediamine (0.388 g, 4.40 mmol) and Mn(ClO₄)₂·6H₂O (0.720 g, 1.99 mmol). A dark orange solution formed once the reaction was complete. After removal of the solvent under reduced pressure to approximately 5 ml. Orange crystals formed and were collected *via* filtration washed with ethanol and dried *in vacuo*. Yield: 0.720 g, 1.2 mmol, 58 %.

IR: (KBr disc, cm^{-1}) 3421 $\nu_{(\text{OH})}$, 2966, 2838, 1686, 1637 $\nu_{(\text{C}=\text{N})}$, 1592 $\nu_{(\text{C}=\text{C})}$, 1466, 1376, 1259, 1088 $\nu_{(\text{ClO}_4^-)}$, 941, 815, 778, 626 $\nu_{(\text{ClO}_4)}$

Anal. (%) Found C = 33.5 H = 5.0 N = 10.9
[Mn(L11)(H₂O)₂](ClO₄)₂·(OH₂) C = 33.4 H = 5.7 N = 11.4

FAB

M/z	Rel. Abundance (%)	Fraction	Molecular weight (Calc)
457	55	[Mn(L11)] ⁺ (ClO ₄)	457
422	100	[Mn(L11)(MeOH) ₂] ⁺	422

4.5.10 [Mn(L11)(NCS)₂].2H₂O

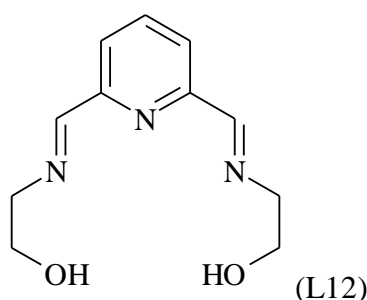
This reaction was carried out as for [Mn(L11)Cl₂]. Quantities used: 2,6-diacetylpyridine (0.493 g, 3 mmol) N,N-dimethylethylenediamine (0.525 g, 6 mmol) and MnCl₂·4H₂O (0.595 g, 3 mmol). Once the reaction was complete, the solvent was reduced to approximately 15 ml and excess potassium thiocyanate was added forming a yellow precipitate which was collected by filtration, washed with water to remove excess KCl and dried *in vacuo*. Yield: 1.28 g, 2.7 mmol, 90 %.

IR: (KBr disc, cm^{-1}) 3422, 3069, 2861, 2827, 2039 $\nu_{(\text{NCS})}$, 1643 $\nu_{(\text{C}=\text{N})}$, 1586 $\nu_{(\text{C}=\text{C})}$, 1458, 1373, 1352, 1287, 1257, 1200, 1168, 1099, 1083, 1042, 1023, 1009, 944, 902, 815, 792, 781, 724, 653, 579, 564, 537

Anal. (%) Found C = 45.2 H = 6.2 N = 20.0
[Mn(L11)(NCS)₂].2H₂O C = 44.7 H = 6.5 N = 19.2

FAB

M/z	Rel. Abundance (%)	Fraction	Molecular weight (Calc)
474	3	$[\text{Mn}(\text{L11})(\text{NCS})_2]^+$	474
416	100	$[\text{Mn}(\text{L11})(\text{NCS})]^+$	416
358	18	$[\text{Mn}(\text{L11})]^+$	358

4.5.11 $[\text{Mn}(\text{L12})(\text{OH}_2)(\text{Cl})](\text{ClO}_4)$ 

$\text{MnCl}_2 \cdot 4\text{H}_2\text{O}$ (0.596g, 3.01mmol) was dissolved in methanol (20ml) and a solution of ethanolamine (0.366g, 6.00mmol) and 2, 6-diformylpyridine (0.407g, 3.01mmol) in methanol (20ml) were added. The solution obtained was stirred at room temperature for 2 hours. The solvent was then reduced to 10ml under reduced pressure. After one night at room temperature, no crystals were formed, therefore methanol (5 ml) was added to the remaining solution and NaClO_4 was added in excess. The mixture was filtered and the solvent was reduced under reduced pressure until approximately 5ml remained. After one night at room temperature, orange crystals with the formula $[\text{Mn}(\text{L12})(\text{OH}_2)(\text{Cl})](\text{ClO}_4)$ were observed and collected *via* filtration and dried *in vacuo*. Yield 0.290g, 0.46 mmol, 15 %.

IR: (KBr disc, cm^{-1}) 3416 $\nu_{(\text{O-H})}$, 2950 $\nu_{(\text{C-H})}$, 1653 $\nu_{(\text{C=N})}$, 1592 $\nu_{(\text{C=C})}$, 1374, 1465, 1204 $\nu_{(\text{C-N})}$, 810

FAB

M/z	Rel. Abundance (%)	Fraction	Molecular weight (Calc)
545	100	$[\text{Mn}(\text{L12})(\text{Cl})_2]^+(\text{ClO}_4)_2$	474

4.5.12 $[\text{Mn}(\text{L12})(\text{OH}_2)_2](\text{ClO}_4)_2$

$\text{Mn}(\text{ClO}_4)_2 \cdot 6\text{H}_2\text{O}$ (0.804 g, 2.22 mmol) was dissolved in methanol (30ml). A solution of 2,6-diformylpyridine (0.299 g, 2.21 mmol) in methanol (20ml) and ethanolamine (0.266 g, 4.36 mmol) was added. The mixture obtained was stirred at room temperature for 2 hours, yielding a brown solution. The solvent was reduced to 10ml under reduced pressure. After one night at room temperature no crystals were formed, therefore methanol (5 ml) was added to the remaining solution and NaClO_4 was added in excess. The mixture was filtered and the solvent was removed under reduced pressure until approximately 5ml remained. Yellow crystals were obtained on standing in solution at room temperature overnight, these were collected *via* filtration, washed with ethanol and dried *in vacuo*. Yield 0.128 g, 0.25 mmol, 11 %.

IR: (KBr disc, cm^{-1}) 3414 $\nu_{(\text{O-H})}$, 1655 $\nu_{(\text{C=N})}$, 1592 $\nu_{(\text{C=C})}$, 1370, 1263, 1090 $\nu_{(\text{ClO}_4^-)}$ 813, 626 $\nu_{(\text{ClO}_4^-)}$

Anal. (%) Found

C = 25.7 H = 3.4 N = 7.6

$[\text{Mn}(\text{L12})(\text{H}_2\text{O})_2](\text{ClO}_4)_2$

C = 25.9 H = 3.8 N = 8.2

FAB

M/z	Rel. Abundance (%)	Fraction	Molecular weight (Calc)
375	45	$[\text{Mn}(\text{L12})(\text{ClO}_4)]^+$	375
275	100	$[\text{Mn}(\text{L12})-\text{H}^+$	275

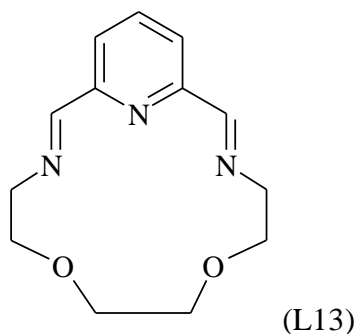
4.5.13 [Mn(L12)(Cl)₂].H₂O

MnCl₂·4H₂O (0.596 g, 3.01 mmol) was dissolved in methanol (20ml) containing ethanolamine (0.366 g, 6 mmol) and a solution of 2,6-diformylpyridine (0.407 g, 3.01 mmol) in methanol (20ml) was added. The solution obtained was stirred at room temperature for 2 hours. The solvent was reduced to approximately 10 ml under reduced pressure. After one night at room temperature no crystals were formed so methanol (5 ml) was added to the remaining solution and NaClO₄ was added in excess. The mixture was filtered and the solvent was reduced under reduced pressure to approximately 5ml. The orange solid was collected *via* filtration and dried *in vacuo*. Yield 0.290 g, 0.79 mmol, 26 %.

IR: (KBr disc, cm⁻¹) 3529, 3406 ν_(OH), 3358, 3096, 2934, 2893, 2018, 1676, 1636 ν_(C=N), 1590 ν_(C=C), 1458, 1430, 1377, 1309, 1253, 1201, 1090 ν_(ClO₄⁻), 1020, 970, 930, 866, 814, 744, 625 ν_(ClO₄⁻)

Anal. (%) Found	C = 36.9 H = 4.3 N = 11.6
[Mn(L12)(Cl) ₂].H ₂ O	C = 36.2 H = 4.7 N = 11.5

4.5.14 [Mn(L13)(OH)₂]₂(ClO₄)₂·2H₂O



Mn(ClO₄)₂·6H₂O (0.874 g, 2.41 mmol) was dissolved in methanol (10ml). A solution of 2,6-diformylpyridine (0.302 g, 2.23 mmol) in methanol (10ml) and 2,2-ethylenedioxy bis(ethylamine) (0.354 g, 2.39 mmol) were added. The mixture obtained was stirred at room temperature for 2 hours, yielding an orange solution.

The solvent was reduced to 10 ml under reduced pressure. After one night at room temperature no crystals were obtained, therefore NaClO₄ was added in excess. The mixture obtained was filtered and the solvent was reduced under reduced pressure to approximately 5ml. The solid product was collected *via* filtration, washed with ethanol and dried *in vacuo*. After one day at room temperature, yellow crystals were obtained from the filtrate with the formula [Mn(L13)(OH₂)₂](ClO₄)₂, these were isolated *via* filtration and dried *in vacuo*. Yield 0.141 g, 0.26 mmol, 12 %.

IR: (KBr disc, cm⁻¹) 3415 $\nu_{(\text{OH})}$, 2056, 1637 $\nu_{(\text{C}=\text{N})}$, 1618 $\nu_{(\text{C}=\text{C})}$, 1090 $\nu_{(\text{ClO}_4^-)}$, 625 $\nu_{(\text{ClO}_4^-)}$

Anal.(%) Found	C = 27.2 H = 3.3 N = 6.6
[Mn(L13)(OH) ₂](ClO ₄) ₂ .2H ₂ O	C = 27.2 H = 4.4 N = 7.2

4.5.15[Mn(L13)(Cl)₂]

MnCl₂·4H₂O (0.799 g, 4.04 mmol) was dissolved in methanol (30ml). A solution of 2,6-diformylpyridine (0.546 g, 4.04 mmol) in methanol (20ml) and 2,2'-ethylenedioxi-bis(ethylamine) (0.669 g, 4.52 mmol) was added. The mixture obtained was stirred at room temperature for 2 hours, yielding a brown solution. The solvent was reduced to approximately 10ml under reduced pressure. After one night at room temperature no crystals were obtained, therefore methanol (5 ml) was added to the remaining solution and excess NaClO₄ was added. the solvent was reduced under pressure until approximately 5ml remained. The solid product was then collected *via* filtration and washed with ethanol and dried *in vacuo*.. Yield 0.540 g. 0.94 mmol, 23 %.

IR: (KBr disc, cm⁻¹) 3406 $\nu_{(\text{O-H})}$, 2928cm⁻¹, 2876, 1647 $\nu_{(\text{C}=\text{N})}$, 1589 $\nu_{(\text{C}=\text{C})}$, 1370, 1284, 1086 $\nu_{(\text{ClO}_4^-)}$, 819, 626 $\nu_{(\text{ClO}_4^-)}$

Anal.(%) Found	C = 26.9 H = 3.9 N = 7.2
[Mn(L13)(Cl) ₂]	C = 26.5 H = 3.6 N = 7.1

FAB

M/z	Rel. Abundance (%)	Fraction	Molecular weight (Calc)
337	5	$[\text{Mn}(\text{L13})(\text{Cl})]^+$	337
301	100	$[\text{Mn}(\text{L13})]-\text{H}^+$	301

4.5.16[Mn(L13)(NCS)₂].MeOH.H₂O

MnCl₂.4H₂O (0.807 g, 4.08 mmol) was dissolved in methanol (10ml). A solution of 2,6-diformylpyridine (0.55 g, 4.07 mmol), NaNCS (0.674 g, 8.31 mmol) and 2,2'-ethylenedioxy-bis(ethylamine) (0.600 g, 4.04 mmol) in methanol (20ml) was added. The mixture was stirred at room temperature for 2 hours, yielding a yellow solution. The solvent was reduced to approximately 10ml under reduced pressure. After one night at room temperature, a yellow solid was obtained and collected *via* filtration then washed with water before drying *in vacuo*. Yield 1.616 g, 3.38 mmol, 83 %.

Crystals of the complex were obtained by slow diffusion of ether into a DMF solution of the product which gave the crystallised product with the formula [Mn(L13)(NCS)₂].

IR: (KBr disc, cm⁻¹) 3243, 2924, 2874, 2057 $\nu_{(\text{NCS})}$, 1646 $\nu_{(\text{C}=\text{N})}$, 1592 $\nu_{(\text{C}=\text{C})}$, 1459, 1451, 1358, 1343, 1279, 1266, 1247, 1185, 1153, 1104, 1071, 1057, 1034, 1011, 961, 939, 929, 811, 790

Anal. (%) Found

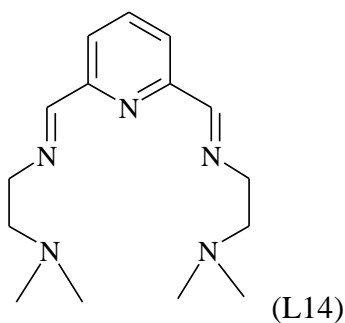
C = 40.8 H = 4.3 N = 14.9

[Mn(L13)(NCS)₂].MeOH.H₂O

C = 41.0 H = 5.0 N = 15.0

FAB

M/z	Rel. Abundance (%)	Fraction	Molecular weight (Calc)
360	45	[Mn(L13)(NCS)] ⁺	360
301	100	[Mn(L13)]-H ⁺	301

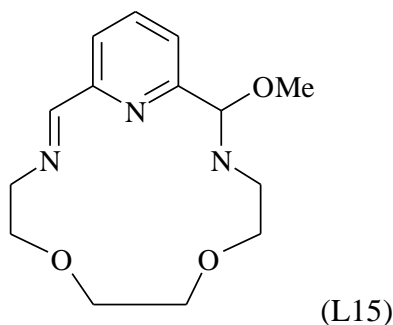
4.5.17[Mn(L14)(NCS)₂]

MnCl₂·4H₂O (0.805 g, 4.07 mmol) was dissolved in methanol (10ml). A solution of N,N-dimethylethylenediamine (0.720 g, 8.16 mmol), 2,6-diformylpyridine (0.561 g, 4.15 mmol) and NaNCS (0.664 g, 8.18 mmol) in methanol (20ml) was added. The mixture obtained was stirred at room temperature for 2 hours, yielding a yellow solution. The solvent was reduced to approximately 10ml under reduced pressure. After one night at room temperature a yellow solid was observed and isolated then washed with water and dried under vacuum. Yield 1.043 g, 2.07 mmol, 51 %.

IR: (KBr disc, cm⁻¹) 3426, 2830, 2040 ν_(NCS), 1653 ν_(C=N), 1588 ν_(C=C), 1464, 1289, 1017, 943, 777

Anal. (%) Found C = 41.1 H = 5.3 N = 19.3
[Mn(L14)(NCS)₂] C = 40.4 H = 5.0 N = 19.4

4.5.18[Mn(L15)(Cl)₂].MeOH.H₂O

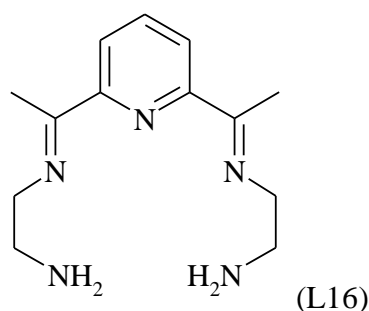


2,6-Diformylpyridine (0.135 g, 1.00 mmol) was stirred in methanol (50 ml). MnCl₂.4H₂O (0.198 g, 1.00 mmol) in methanol (10 ml), was added, followed by 2,2'-ethylenedioxy-bis(ethylamine) (0.148 g, 1.00 mmol). The solution turned yellow on addition of the amine. Stirring was continued for 30 mins. The solvent was then reduced under pressure to approximately 10 ml. The orange solid product was collected *via* filtration and dried *in vacuo*. Crystals of the product were formed by slow diffusion of ether into a solution of product dissolved in DMF which yielded crystals of the formula [Mn(L15)(Cl)₂].MeOH. Yield: 0.295 g, 0.65 mmol, 65 %.

IR: (KBr disc, cm⁻¹) 3371, 3202, 3213, 2922, 2878, 2053, 1966, 1629 $\nu_{(C=N)}$, 1589 $\nu_{(C=C)}$, 1464, 1379, 1343, 1332, 1282, 1157, 1089, 1057, 1018, 963, 927, 821, 812, 739

Anal. (%) Found	C = 39.7 H = 5.3 N = 9.9
[Mn(L15)(Cl) ₂].MeOH.H ₂ O	C = 39.8 H = 5.3 N = 10.0

4.5.19[Mn(L16)(OH₂)₂](ClO₄)₂



[Ba(L7)(ClO₄)₂] (0.379 g, 0.53 mmol) was refluxed in methanol (100 ml). Mn(ClO₄)₂·6H₂O (0.254 g, 0.70 mmol) in methanol (10 ml) was added and refluxing continued for 1 hr. The yellow/orange solution was then reduced to approximately 10 ml and the orange solid was collected via filtration. Crystals were obtained by slow diffusion of ether into a methanol solution of the product. Yield: 0.073 g, 0.14 mmol, 27 %.

IR: (KBr disc, cm⁻¹) 3443 $\nu_{(O-H)}$, 3090, 2934, 1628 $\nu_{(C=N)}$, 1583 $\nu_{(C=C)}$, 1452, 1437, 1424, 1375, 1355, 1286, 1240, 1193, 1147, 1109 $\nu_{(ClO_4)}$, 1041, 1000, 922, 749, 716, 620

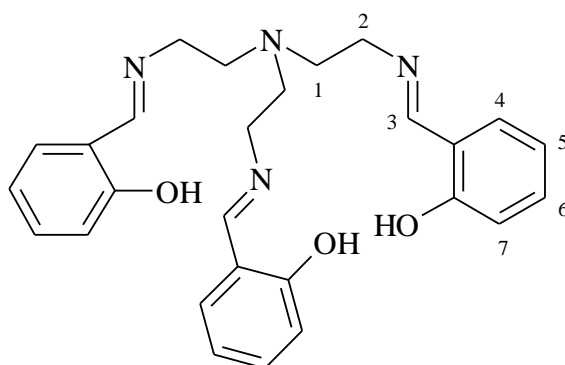
Anal. (%) Found	C = 28.7 H = 3.8 N = 12.4
[Mn(L16)(OH ₂) ₂](ClO ₄) ₂	C = 29.2 H = 4.3 N = 13.1

4.6 Tripodal ligands

Tren is a commonly used commercially available tripodal amine and was used without further purification in the synthesis of a Schiff base manganese complex. The synthesis of asymmetric tripodal amines was attempted using the methods outlined by Blackman *et al.*³⁰ by varying the arm lengths of the tripod. The synthesis of the products have been carried out with varying molar amounts of MnCl₂·4H₂O to ligand. Initially attempts were made to prepare a mononuclear complex however,

some of the analysis indicated that a μ -oxo tetranuclear complex may be forming as outlined by McKee *et al.*^{36, 37} synthesis was then carried out with excess $\text{MnCl}_2 \cdot 4\text{H}_2\text{O}$ in attempts to prepare a tetranuclear system. Suitable crystals did not form for X-ray crystallography to be performed.

4.6.1 Saltren



Tris-(2-aminoethyl)-amine (0.298 g, 2.04 mmol) was mixed with water (1 ml) and stirred. Salicylaldehyde (0.732 g, 6.00 mmol) in methanol (5 ml) was added to the solution and stirring continued for 15 minutes. On addition of salicylaldehyde, a bright yellow precipitate was formed.³⁰ The product was allowed to air dry overnight. Yield: 0.900 g, 1.96 mmol, 96 %.

IR (KBr disc, cm^{-1}) 3447 $\nu_{\text{(OH)}}$, 3054, 2939 $\nu_{\text{(CH}_2\text{)}}$, 1892, 2816, 1634 $\nu_{\text{(C=N)}}$, 1610, 1581, 1498, 1458, 1430, 1278, 1248, 1197, 1166, 1148, 1115, 1068, 1042, 1025, 944, 925, 903, 877, 854, 774, 755, 638

Anal. (%). Found C = 70.1 H = 6.7 N = 12.4

$\text{C}_{27}\text{H}_{30}\text{N}_4\text{O}_3$ C = 70.7 H = 6.6 N = 12.2

NMR (CDCl_3 , ppm, ^1H) 2.76 (t, 6H CH_2^1), 3.45 (t 6H CH_2^2), 5.95 (d 3H CH^4), 6.51 (t 3H CH^5), 6.87 (d 3H CH^7), 7.19 (t 3H CH^6), 7.72 (s 3H CH^3), 13.74 (s, 3H OH)

4.6.2 [Mn(Saltren)](Cl)₂.2H₂O

Saltren (0.439 g, 0.96 mmol) was dissolved in methanol (20 ml), MnCl₂.4H₂O (0.198 g, 1.00 mmol) was separately dissolved into methanol (20 ml). The two solutions were added together with stirring. The initial orange solution turned green over 10 minutes. The green solid was then collected on a frit, washed with methanol and dried *in vacuo*. Yield: 0.503 g, 0.811 mmol, 84 %.

IR: (KBr disc, cm⁻¹) 3374 $\nu_{(\text{O-H})}$, 3062, 2946, 2852, 1642 $\nu_{(\text{C=N})}$, 1610, 1599 $\nu_{(\text{C=C})}$, 1546, 1534, 1487, 1470, 1446, 1400, 1297, 1279, 1200, 1150, 878, 757

Anal. (%) Found C = 52.3 H = 5.0 N = 9.6
[Mn(Saltren)](Cl)₂.2H₂O C = 52.4 H = 5.2 N = 9.1

FAB

M/z	Rel. Abundance (%)	Fragment	Molecular weight (Calc)
512	100	[Mn(Saltren)]-H ⁺	512

4.6.3 $[\text{Mn}_4(\text{O})_2(\text{Saltren})_2](\text{MnCl}_4)_2$

Saltren (0.458 g, 1.00 mmol) was placed into methanol (20 ml). $\text{MnCl}_2 \cdot 4\text{H}_2\text{O}$ (0.396 g, 2.00 mmol) was placed into methanol (20 ml). The two solutions were added together with stirring. The initial orange solution turned dark green over 10 minutes. The solvent was allowed to evaporate and the green solid was then collected *via* filtration, washed with ether and dried *in vacuo*. Yield: 0.591 g, 0.59 mmol, 59 %.

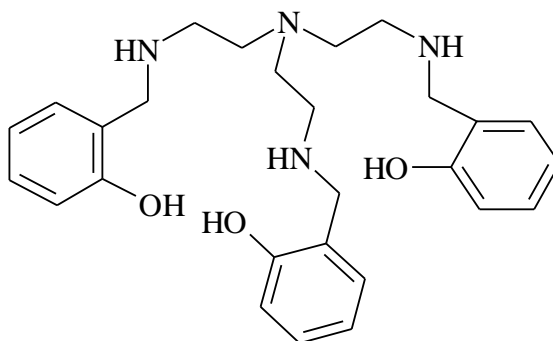
IR: (KBr disc, cm^{-1}) 3410 $\nu_{(\text{O-H})}$, 1636 $\nu_{(\text{C=N})}$, 1613, 1535, 1481, 1404, 1296, 1201, 756

Anal. (%) Found C = 41.4 H = 4.4 N = 7.7
 $[\text{Mn}_4(\text{O})_2(\text{Saltren})_2](\text{MnCl}_4)_2$ C = 41.5 H = 3.9 N = 7.2

FAB

M/z	Rel. Abundance (%)	Fragment	Molecular weight (Calc)
1584	1	$[\text{Mn}_4(\text{O})_2(\text{Saltren})_2](\text{MnCl}_4)_2 + \text{Na}^+$	1585
513	12	$[\text{Mn}(\text{Saltren})]^+$	513
407	100	$[\text{Mn}(\text{Saltren})]^+ - (\text{C}_7\text{H}_6\text{O})$	407

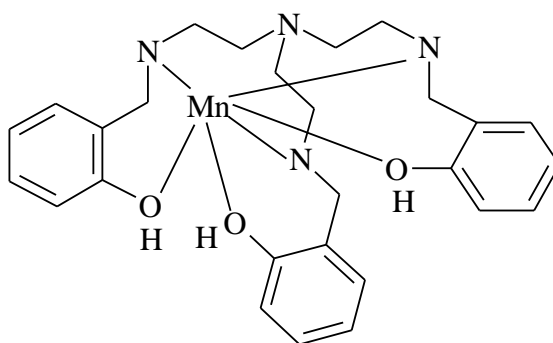
4.6.4 Reduced saltren



Saltren (0.458 g, 1.00 mmol) was placed into methanol (15 ml). Sodium tetraborate (0.200 g, 0.50 mmol) and then sodium borohydride (0.151 g, 4.00 mmol) was added slowly over 30 minutes. Stirring was continued at room temperature for 2 hours. The solvent was then evaporated under reduced pressure and ammonium chloride (1 g, in water 10 ml) was added to the residue. The resulting mixture was extracted with chloroform (3 x 15 ml) and the organic fractions combined and washed with water. This was then dried over magnesium sulphate, filtered and chloroform was removed under reduced pressure leaving a yellow oily residue, this was stored in vacuo overnight. Yield: 0.430 g, 92 %.

IR (KBr disc, cm^{-1}) 2845 $\nu_{(\text{C-H})}$, 2363, 1590 $\nu_{(\text{C}=\text{C})}$, 1458, 1258, 1152, 1104, 842, 755

4.6.5 $[\text{Mn}(\text{RedSaltren})](\text{Cl})_2 \cdot 2\text{H}_2\text{O}$



$\text{MnCl}_2 \cdot 4\text{H}_2\text{O}$ (0.078 g, 0.39 mmol) was dissolved in methanol (5 ml). Reduced saltren (0.201 g, 0.43 mmol) was dissolved in methanol (3 ml) to give a yellow solution. The saltren solution was gently heated and upon mixing the two solutions, the mixture turned dark green / black in colour. Gentle heating was continued for 15 minutes and the solution was left to evaporate in air yielding a dark green solid. Yield: 0.240 g, 0.38 mmol, 91 %.

IR (KBr disc, cm^{-1}) 3060 $\nu_{(\text{O-H})}$, 1595, 1570 $\nu_{(\text{C}=\text{C})}$, 1479, 1457, 1279, 1260, 1151, 1107, 1041, 877, 756, 619

Anal (%) Found

C = 52.3 H = 5.8 N = 8.7

[Mn(RedSaltren)](Cl)₂.2H₂O

C = 51.8 H = 6.4 N = 9.0

FAB

M/z	Rel. Abundance (%)	Fraction	Molecular weight (Calc)
517	100	[Mn(RedSaltren)] ⁺	516
461	47	(RedSaltren) ⁺	461

4.6.6 [Mn₄(O)₂(RedSaltren)₂](MnCl₄)₂.H₂O

RedSaltren (0.284 g, 0.61 mmol) was placed into methanol (20 ml) MnCl₂.4H₂O (0.241 g, 1.22 mmol) was placed into methanol (20 ml). The two solutions were added together with stirring. The initial orange solution turned green over 10 minutes. The solution was allowed to evaporate and the remaining green solid was then collected *via* filtration, washed with ether and dried *in vacuo*. Yield: 0.510 g, 0.51 mmol, 84%.

IR: (KBr disc, cm⁻¹) $\nu_{(O-H)}$ 3060 cm⁻¹, $\nu_{(C=C)}$ 1595 cm⁻¹, 1479 cm⁻¹, 1456 cm⁻¹, 1259 cm⁻¹, 876 cm⁻¹, 756 cm⁻¹

Anal. (%) Found

C = 40.4 H = 4.7 N = 7.0

[Mn₄(O)₂(RedSaltren)₂](MnCl₄)₂.H₂O

C = 40.7 H = 4.7 N = 7.0

FAB

M/z	Rel. Abundance (%)	Fraction	Molecular weight (Calc)
1088	6	[Mn ₃ (RedSaltren) ₂]-5H ⁺	1088
518	59	[Mn(RedSaltren)]-H ⁺	518
465	100	(RedSaltren)-H ⁺	465

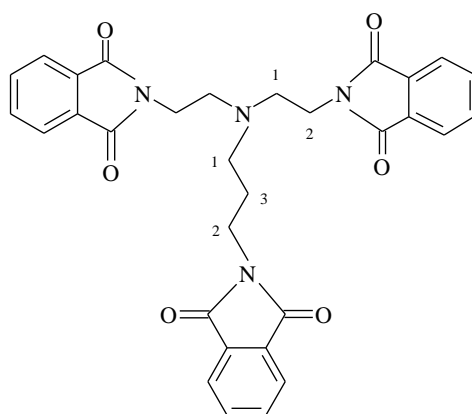
Phthalic anhydride (7.422 g, 50.00 mmol) was melted in a beaker using an oil bath at 170 °C. Diethylenetriamine (2.597 g, 25.19 mmol) was added drop wise over 15 minutes with vigorous stirring to produce a brown glassy solid on cooling. This was crushed using a pestle and mortar to give a fine pale yellow coloured powder. Yield: 8.234 g, 22.68 mmol, 90 %.

IR (KBr disc, cm^{-1}) 3461 $\nu_{(\text{N-H})}$, 3059, 2941 $\nu_{(\text{CH}_2)}$, 2834, 1773, 1708 $\nu_{(\text{C=O})}$, 1637, 1560, 1467, 1432, 1396, 1189, 1086, 1038, 872, 793, 717, 605, 530

Anal. (%) Found C = 67.1 H = 5.6 N = 10.8
C₂₀H₁₇N₃O₄ C = 67.5 H = 5.4 N = 10.7

NMR (CDCl_3 , ppm, ^1H) 3.03 (t, 4H, CH_2NH) 3.85 (t, 4H, CH_2N) 7.76 (m, 8H, CHAr)

4.6.9 2,2',3-Triphthalimidoethylpropylamine



2,2'-Diphthalimidoethylamine (0.726 g, 2.00 mmol) was melted in a beaker in an oil bath at 170 °C. N-(2-bromopropyl)phthalimide (0.536 g, 1.99 mmol) was added slowly over 10 minutes. On cooling, a dark brown glassy solid was formed. The aforementioned solid was ground, using a pestle and mortar, to give a finely divided, orange powder. Yield: 1.012 g, 1.61 mmol, 81 %.

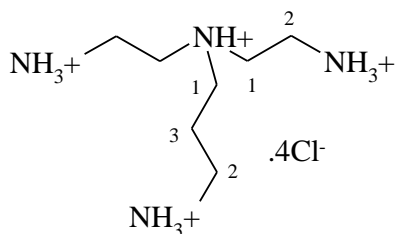
IR (KBr disc, cm^{-1}) 3463, 2945 $\nu_{(\text{CH}_2)}$, 2775, 2695, 1773, 1708 $\nu_{(\text{C}=\text{O})}$, 1612, 1467, 1432, 1396, 1189, 1172, 1087, 1033, 1013, 872, 794, 719, 530

Anal. (%) Found C = 59.0 H = 3.9 N = 8.6

$\text{C}_{31}\text{H}_{24}\text{N}_4\text{O}_6(\text{HBr})$ C = 59.1 H = 4.0 N = 8.9

NMR (CDCl_3 , ppm, ^1H) 2.21 (q, 2H, CH_2^3), 3.37 (t, 6H, CH_2^1) 3.77 (t, 6H, CH_2^2)
7.68 (m, 12H, CHAr)

4.6.10 - BAEP.6HCl



2,2',3-Triphthalimidoethylpropylamine (0.552 g, 1 mmol) was mixed with hydrochloric acid (60 ml, 8 M). The mixture was heated under reflux for 19 hours. The solid phthalic acid which formed on cooling was removed by filtration and the solvent removed under reduced pressure leaving a white residue. The residue was dissolved in water (10 ml) and a white precipitate formed on addition of ethanol (150 ml). The solution was stored in a fridge overnight, and the resulting white solid collected *via* filtration. Yield: 0.107g, 0.3 mmol, 28 %.

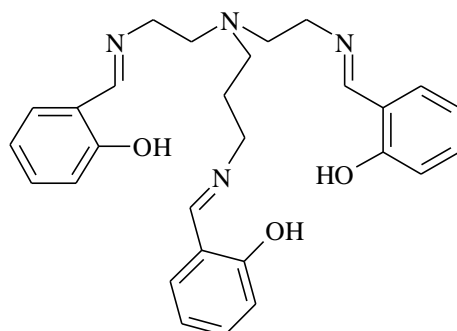
IR: (KBr disc, cm^{-1}) 2979 $\nu_{(\text{N-H})}$, 2362, 1687, 1585, 1497, 1404, 1282, 1271, 1153, 1140, 1071, 1005, 974, 908, 829, 797, 734, 674, 556

Anal. (%) Found C = 23.6 H = 7.0 N = 14.1

BAEP.6HCl C = 22.2 H = 6.9 N = 14.8

NMR (D_2O , ppm, ^1H) 1.87 (q 2H CH_2^3), 2.81 (t 6H CH_2^1) 3.56 (t 6H CH_2^2)

4.6.11 - BAEP-Sal.6H₂O



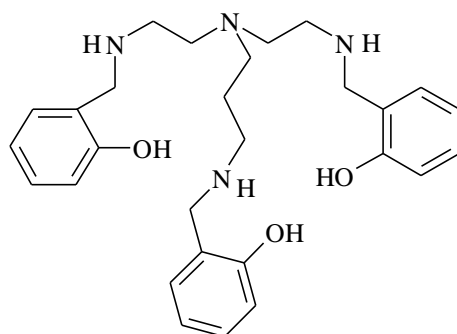
(BAEP-Sal)

BAEP.4HCl (0.155 g, 0.5 mmol) was placed into ethanol (20 ml). Salicylaldehyde (0.183 g, 1.5 mmol) was added followed with triethylamine (0.152 g, 1.5 mmol). The solution turned yellow and stirring continued for 30 mins. The solvent was then removed under reduced pressure. Yield: 0.143 g, 0.3 mmol, 61 %.

IR(KBr disc, cm⁻¹) 3447 ν (OH), 2976, 2940 ν (CH₂), 2801, 2760, 2739, 2677, 2492, 1636 ν (C=N), 1578, 1478, 1458, 1394, 1279, 1189, 1173, 1150, 1117, 1072, 1038, 966, 851, 806, 756, 638

Anal. (%) Found	C = 58.2 H = 8.7 N = 10.7
BAEP-Sal.6H ₂ O	C = 57.9 H = 7.6 N = 9.7

4.6.12 - [Mn(RedBAEP-Sal)(Cl)₂].4H₂O



(RedBAEP-Sal)

Reduction of the BAEP-Sal ligand was carried out as for the Saltren ligand previously described. The reduced ligand (0.109 g, 0.2 mmol) was placed into methanol (3ml) and the $\text{MnCl}_2 \cdot 4\text{H}_2\text{O}$ (0.040 g, 0.2 mmol) was dissolved in ethanol (15 ml) the two two solutions were mixed together and stirred with gentle heat for 15 mins, during which time, the solution turned dark green. The solvent was left to evaporate yielding a green solid. Yield: 0.119 g, 0.17 mmol, 88 %.

IR: (KBr disc, cm^{-1}) 3107 $\nu_{(\text{O-H})}$, 1624, 1595 $\nu_{(\text{C=C})}$, 1477, 1457, 1262, 878, 758

Anal. (%) Found C = 49.4 H = 5.9 N = 8.4
 $[\text{Mn}(\text{RedBAEP-Sal})](\text{Cl})_2 \cdot 4\text{H}_2\text{O}$ C = 49.7 H = 6.9 N = 8.3

FAB

M/z	Rel. Abundance (%)	Fragment	Molecular weight (Calc)
531	67	$[\text{Mn}(\text{RedBAEP-Sal})]^+$	531
479	50	$(\text{RedBAEP-Sal})\text{-H}^+$	479
460	100	$(\text{RedBAEP-Sal})\text{-OH}$	460

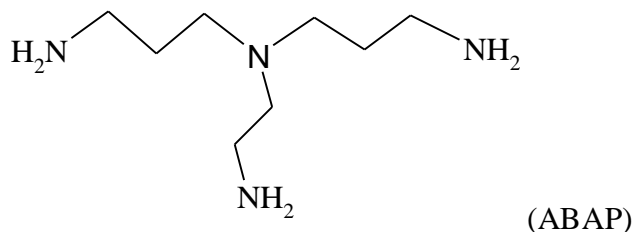
4.6.13 - 3,3',2-Triphthalimidopropylethylamine.2H₂O

3,3'-Diphthalimidopropylamine (1.957 g, 5 mmol) as purchased, was melted and stirred in a beaker. 2-Bromoethylphthalimide (2.791 g, 5 mmol) was added and both reactants were melted together. Stirring was continued for one hour. A brown glassy solid formed on cooling which was crushed into a fine powder. Yield: 2.92 g, 5.0 mmol, 86 %.

IR: (KBr disc, cm^{-1}) 3538, 3460 $\nu_{(\text{O-H})}$, 2943, 1770 $\nu_{(\text{C=O})}$, 1708, 1613, 1173, 1034, 1022, 891, 721, 528

Anal. (%) Found C = 56.7 H = 4.3 N = 7.9
 3,3'2-Triphthalimidopropylethylamine.2H₂O C = 56.4 H = 4.9 N = 8.2

4.6.14 - ABAP.4HCl.H₂O



3,3',2-Triphthalimidopropylethylamine (1.694 g, 3 mmol) refluxed in hydrochloric acid (60 ml, 8 M) for 19 hours. The solid phthalic acid which formed on cooling was removed by filtration and the solvent was reduced to approximately 2 ml and a white precipitate formed on addition of ethanol (20 ml). The resulting white solid was collected *via* filtration, washed with ethanol and dried *in vacuo*. Yield: 0.597 g, 1.9 mmol, 53 %.

IR: (KBr disc, cm⁻¹), 3426, 2951 $\nu_{(N-H)}$, 2600, 2542, 1605, 1508, 1466, 1404, 1165, 1134, 968, 930, 772

Anal. (%) Found	C = 25.3 H = 7.4 N = 14.3
ABAP.4HCl.H ₂ O	C = 25.6 H = 7.8 N = 15.0

4.6.15 - [Mn(ABAP-Sal)](ClO₄).3H₂O

ABAP.4HCl (0.253 g, 0.5 mmol) was placed into methanol (20 ml) followed with salicylaldehyde (0.366 g, 3.0 mmol) and triethylamine (0.405 g, 4.0 mmol). The solution was refluxed for 10 mins. Mn(ClO₄)₂.6H₂O (0.254 g, 1.0 mmol) was added and the solution refluxed for 2.5 h. On cooling, excess NaClO₄ in methanol (10 ml) was added and the dark brown solid was collected *via* filtration, washed with ether and dried *in vacuo*. Yield: 0.092 g, 0.13 mol, 27 %.

IR: (KBr disc, cm^{-1}) 3422 $\nu_{(\text{O-H})}$, 2928, 2857, 1618 $\nu_{(\text{C=N})}$, 1599, 1543, 1465, 1400, 1292, 1207, 1150, 1121, 1088 $\nu_{(\text{ClO}_4)}$, 907, 814, 762, 637

Anal. (%) Found

C = 51.4 H = 4.9 N = 8.3

$[\text{Mn}(\text{ABAP-Sal})](\text{ClO}_4) \cdot 3\text{H}_2\text{O}$

C = 51.4 H = 5.7 N = 8.3

FAB

M/z	Rel. Abundance (%)	Fragment	Molecular weight (Calc)
539	47	$[\text{Mn}(\text{ABAP-Sal})]-2\text{H}^+$	539
392	100	$[\text{Mn}(3,3'\text{-Sal})]-\text{H}^+$	393

4.6.16 - $[\text{Mn}_4(\text{O})_2(\text{ABAP-Sal})][\text{MnCl}_4]_2$

ABAP-Sal ligand (0.167 g, 0.34 mmol) was dissolved in ethanol (40 ml) and upon the addition of $\text{MnCl}_2 \cdot 4\text{H}_2\text{O}$ (0.336 g, 1.70 mmol) in ethanol (10 ml) a bright yellow precipitate formed. Stirring continued for 30 mins, during which time the solution and solid turned dark green. On filtering, The solution was allowed to evaporate to dryness at room temperature to yield a dark green solid. The solid removed from solution was washed with ether and gave the following analysis, Yield: 0.474 g, 0.30 mmol, 87 %.

IR: (KBr disc, cm^{-1}) 3423 $\nu_{(\text{O-H})}$, 2982, 1653 $\nu_{(\text{C=N})}$, 1610, 1599, 1542, 1474, 1301, 1204, 1152, 1126, 1030, 900, 814, 765

Anal. (%) Found

C = 43.5 H = 4.8 N = 7.4

$[\text{Mn}_4(\text{O})_2(\text{ABAP-Sal})_2][\text{MnCl}_4]_2$

C = 43.0 H = 4.2 N = 6.9

FAB

M/z	Rel. Abundance (%)	Fragment	Molecular weight (Calc)
1113	1	$[\text{Mn}(\text{ABAP-Sal})\text{O}]_2\text{-H}^+$	1113
1095	1	$[\text{Mn}_2(\text{ABAP-Sal})_2\text{O}]\text{-3H}^+$	1095
539	100	$[\text{Mn}(\text{ABAP-Sal})]\text{-2H}^+$	539
392	32	$[\text{Mn}(3,3'\text{-Sal})]\text{-H}^+$	393

Appendix 1
Single Crystal X-ray Data Tables.

Table 23 - Crystal data and structure refinement for**[Mn₂(HL1)(Cl)₂]₂(ClO₄)₂·2DMF**

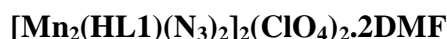
Identification code	LJP1/testsq	
Chemical formula	C ₅₄ H ₇₂ Cl ₆ Mn ₄ N ₁₄ O ₁₄	
Formula weight	1573.72	
Temperature	150(2) K	
Radiation, wavelength	MoK α , 0.71073 Å	
Crystal system, space group	Orthorhombic, <i>Pbcn</i>	
Unit cell parameters	a = 14.7345(6) Å	$\alpha = 90^\circ$
	b = 22.6943(9) Å	$\beta = 90^\circ$
	c = 21.3326(8) Å	$\gamma = 90^\circ$
Cell volume	7133.4(5) Å ³	
Z	4	
Calculated density	1.465 g/cm ³	
Absorption coefficient μ	0.984 mm ⁻¹	
F(000)	3232	
Crystal colour and size	orange, 0.54 × 0.18 × 0.17 mm ³	
Reflections for cell refinement	9845 (θ range 2.36 to 28.32°)	
Data collection method	Bruker APEX 2 CCD diffractometer ω rotation with narrow frames	
θ range for data collection	1.65 to 26.00°	
Index ranges	h -18 to 18, k -27 to 27, l -26 to 26	
Completeness to $\theta = 26.00^\circ$	100.0 %	
Intensity decay	0%	
Reflections collected	59801	
Independent reflections	7014 (Rint = 0.0334)	
Reflections with F ₂ >2 σ	5780	
Absorption correction	semi-empirical from equivalents	
Min. and max. transmission	0.6187 and 0.8506	
Structure solution	direct methods	
Refinement method	Full-matrix least-squares on F ²	
Weighting parameters a, b	0.0654, 2.1138	
Data / restraints / parameters	7014 / 46 / 449	
Final R indices [F ₂ >2 σ]	R1 = 0.0375, wR2 = 0.1093	
R indices (all data)	R1 = 0.0460, wR2 = 0.1142	
Goodness-of-fit on F ²	1.128	
Largest and mean shift/su	0.476 and 0.028	
Largest diff. peak and hole	0.621 and -0.452 e Å ⁻³	

Hydrogen atoms were inserted at calculated positions except H2o which was found and its position and temperature factor fixed. This hydrogen was formed on the second oxygen within the same macrocycle due to a two fold axis of the molecule.

One perchlorate ion remains uncoordinated to the macrocycle with disorder modelled with 75% occupancy and 25% occupancy over the two positions

The data were refined using the programme SQUEEZE¹²⁹ due to disordered solvent. There are 4 molecules per cell. SQUEEZE located 4 voids, two of which are of 191.8 Å³ and two of which are 191.6 Å³ in the cell with 40 electrons each, which was assigned as 1 molecule of DMF per cell each with the formula C₃H₇NO. There also remained one ordered DMF molecule within the cell

Table 24 - Crystal data and structure refinement for



Identification code	ljp80
Chemical formula	C ₆₀ H ₈₀ Cl ₂ Mn ₄ N ₂₈ O ₁₆
Formula weight	1740.18
Temperature	296(2) K
Radiation, wavelength	MoK α , 0.71073 Å
Crystal system, space group	monoclinic, <i>P</i> 2 ₁ / <i>c</i>
Unit cell parameters	a = 13.8095(6) Å $\alpha = 90^\circ$ b = 20.9281(9) Å $\beta = 105.3810(10)^\circ$ c = 13.4256(6) Å $\gamma = 90^\circ$
Cell volume	3741.1(3) Å ³
Z	2
Calculated density	1.545 g/cm ³
Absorption coefficient μ	0.815 mm ⁻¹
F(000)	1796
Crystal colour and size	Orange, 0.52 × 0.34 × 0.29 mm ³
Reflections for cell refinement	9851 (θ range 2.48 to 31.38°)
Data collection method	Bruker APEX 2 CCD diffractometer ω rotation with narrow frames
θ range for data collection	1.81 to 31.87°
Index ranges	h -19 to 20, k -29 to 31, l -19 to 19
Completeness to $\theta = 31.87^\circ$	91.3 %
Intensity decay	0%
Reflections collected	30101
Independent reflections	11726 (R _{int} = 0.0204)
Reflections with F ₂ >2 σ	9585
Absorption correction	semi-empirical from equivalents
Min. and max. transmission	0.6766 and 0.7980
Structure solution	direct methods
Refinement method	Full-matrix least-squares on F ²
Weighting parameters a, b	0.0700, 1.5422
Data / restraints / parameters	11726 / 0 / 507
Final R indices [F ₂ >2 σ]	R ₁ = 0.0399, wR ₂ = 0.1132
R indices (all data)	R ₁ = 0.0503, wR ₂ = 0.1205
Goodness-of-fit on F ₂	1.031
Largest and mean shift/su	0.004 and 0.000
Largest diff. peak and hole	0.845 and -0.552 e Å ⁻³

Hydrogen atoms were inserted at calculated positions except H1 which was found and its position and temperature factor fixed. This hydrogen was formed on the same oxygen of the second macrocycle due to the centrosymmetry of the molecule.

Table 25 - Crystal data and structure refinement for

Identification code	lj93
Chemical formula	C ₇₀ H ₁₀₄ Cl ₄ Mn ₅ N ₁₈ O ₃₀
Formula weight	2094.21
Temperature	150(2) K
Radiation, wavelength	MoK α , 0.71073 Å
Crystal system, space group	triclinic, P $\bar{1}$
Unit cell parameters	a = 10.7755(15) Å α = 90.871(2)° b = 13.8331(19) Å β = 109.424(2)° c = 16.136(2) Å γ = 94.217(2)°
Cell volume	2260.1(5) Å ³
Z	1
Calculated density	1.539 g/cm ³
Absorption coefficient μ	0.885 mm ⁻¹
F(000)	1083
Crystal colour and size	Orange, 0.35 × 0.18 × 0.15 mm ³
Data collection method	Bruker APEX 2 CCD diffractometer ω rotation with narrow frames
θ range for data collection	2.01 to 20.05°
Index ranges	h -10 to 10, k -13 to 13, l -15 to 15
Completeness to $\theta = 20.05^\circ$	99.5 %
Intensity decay	0%
Reflections collected	10777
Independent reflections	4241 (Rint = 0.0326)
Reflections with F ₂ >2 σ	3362
Absorption correction	semi-empirical from equivalents
Min. and max. transmission	0.7469 and 0.8787
Structure solution	direct methods
Refinement method	Full-matrix least-squares on F ²
Weighting parameters a, b	0.1263, 11.1395
Data / restraints / parameters	4241 / 770 / 630
Final R indices [F ₂ >2 σ]	R1 = 0.0679, wR2 = 0.1821
R indices (all data)	R1 = 0.0839, wR2 = 0.1968
Goodness-of-fit on F ²	1.003
Largest and mean shift/su	1.474 and 0.016
Largest diff. peak and hole	1.104 and -0.536 e Å ⁻³

All hydrogen atoms were inserted at calculated positions

One perchlorate ion remains uncoordinated to the macrocycle with disorder modelled with 70% occupancy and 30% occupancy over the two positions

Table 26 - Crystal data and structure refinement for

Identification code	ljp75sq
Chemical formula	C _{25.50} H _{39.50} Cl ₄ Mn _{2.50} N _{6.50} O _{2.50}
Formula weight	756.29
Temperature	150(2) K
0.69420 Å	
Crystal system, space group	triclinic, P $\bar{1}$
Unit cell parameters	a = 14.6329(13) Å α = 84.4870(10)° b = 15.5155(13) Å β = 79.3940(10)° c = 17.9810(16) Å γ = 67.6880(10)°
Cell volume	3710.6(6) Å ³
Z	4
Calculated density	1.354 g/cm ³
Absorption coefficient μ	1.163 mm ⁻¹
F(000)	1554
Crystal colour and size	colourless, 0.25 × 0.18 × 0.10 mm ³
Data collection method	Bruker APEX 2 CCD diffractometer ω rotation with narrow frames
θ range for data collection	1.39 to 25.00°
Index ranges	h -17 to 17, k -18 to 18, l -21 to 21
Completeness to $\theta = 25.00^\circ$	99.5 %
Intensity decay	0%
Reflections collected	30369
Independent reflections	13965 (R _{int} = 0.0408)
Reflections with F ₂ >2 σ	8794
Absorption correction	none
Min. and max. transmission	0.7597 and 0.8926
Structure solution	direct methods
Refinement method	Full-matrix least-squares on F ²
Weighting parameters a, b	0.1367, 0.0000
Data / restraints / parameters	13965 / 1047 / 869
Final R indices [F ₂ >2 σ]	R1 = 0.0659, wR2 = 0.1984
R indices (all data)	R1 = 0.0973, wR2 = 0.2193
Goodness-of-fit on F ²	0.987
Largest and mean shift/su	1.840 and 0.020
Largest diff. peak and hole	0.903 and -0.604 e Å ⁻³

Hydrogen atoms were inserted at calculated positions except H2o which was found and its position and temperature factor fixed. This hydrogen was formed on the same oxygen on the second macrocycle due to the centrosymmetry of the molecule.

The data were refined using the programme SQUEEZE¹²⁹ due to disordered solvent. SQUEEZE located 1 void of 250 Å³ per cell with 27 electrons each, which was assigned as 1 molecule of EtOH per cell with the formula C₂H₅OH.

Table 27 - Crystal data and structure refinement for [Ba(H₂L3)(ClO₄)₂](ClO₄)₂.

Identification code	lj227
Chemical formula	C ₂₀ H ₂₂ BaCl ₂ N ₆ O ₁₀
Formula weight	714.68
Temperature	150(2) K
Radiation, wavelength	MoK α , 0.71073 Å
Crystal system, space group	triclinic, P $\bar{1}$
Unit cell parameters	a = 8.4509(7) Å α = 79.7780(10)° b = 8.7341(7) Å β = 88.7820(10)° c = 17.7724(14) Å γ = 83.0790(10)°
Cell volume	1281.57(18) Å ³
Z	2
Calculated density	1.852 g/cm ³
Absorption coefficient μ	1.825 mm ⁻¹
F(000)	708
Crystal colour and size	clear, 0.57 × 0.35 × 0.12 mm ³
Reflections for cell refinement	7639 (θ range 2.39 to 31.32°)
Data collection method	Bruker APEX 2 CCD diffractometer ω rotation with narrow frames
θ range for data collection	2.33 to 31.67°
Index ranges	h -12 to 11, k -12 to 12, l -26 to 25
Completeness to $\theta = 31.67^\circ$	90.0 %
Intensity decay	0%
Reflections collected	15173
Independent reflections	7785 ($R_{\text{int}} = 0.0221$)
Reflections with $F^2 > 2\sigma$	7094
Absorption correction	semi-empirical from equivalents
Min. and max. transmission	0.4227 and 0.8108
Structure solution	direct methods
Refinement method	Full-matrix least-squares on F^2
Weighting parameters a, b	0.0360, 2.9976
Data / restraints / parameters	7785 / 10 / 405
Final R indices [$F^2 > 2\sigma$]	R1 = 0.0374, wR2 = 0.0905
R indices (all data)	R1 = 0.0427, wR2 = 0.0929
Goodness-of-fit on F^2	1.127
Largest and mean shift/su	0.081 and 0.005
Largest diff. peak and hole	1.781 and -1.005 e Å ⁻³

All hydrogen atoms were inserted at calculated positions

One perchlorate ion remains uncoordinated to the macrocycle with disorder modelled with 70% occupancy and 30% occupancy over the two positions

**Table 28 - Crystal data and structure refinement for
[Mn(L4)(NCS)₂].MeOH.DMF**

Identification code	sora1
Chemical formula	C _{24.50} H _{30.50} MnN _{8.50} O _{3.50} S ₂
Formula weight	619.13
Temperature	150(2) K
0.68840 Å	
Crystal system, space group	triclinic, P $\bar{1}$
Unit cell parameters	a = 13.1104(16) Å α = 99.367(2)° b = 14.9066(18) Å β = 97.5600(10)° c = 14.9514(18) Å γ = 101.8730(10)°
Cell volume	2779.8(6) Å ³
Z	4
Calculated density	1.479 g/cm ³
Absorption coefficient μ	0.671 mm ⁻¹
F(000)	1288
Crystal colour and size	orange, 0.52 × 0.19 × 0.18 mm ³
Reflections for cell refinement	4095 (θ range 2.71 to 25.06°)
Data collection method	Bruker SMART 1K CCD diffractometer ω rotation with narrow frames
θ range for data collection	1.36 to 30.75°
Index ranges	h -17 to 18, k -21 to 22, l -22 to 14
Completeness to $\theta = 30.75^\circ$	81.9 %
Intensity decay	0%
Reflections collected	21514
Independent reflections	15633 (R _{int} = 0.0416)
Reflections with F ₂ >2 σ	7215
Absorption correction	semi-empirical from equivalents
Min. and max. transmission	0.7216 and 0.8887
Structure solution	direct methods
Refinement method	Full-matrix least-squares on F ²
Weighting parameters a, b	0.0609, 0.0000
Data / restraints / parameters	15633 / 0 / 720
Final R indices [F ₂ >2 σ]	R1 = 0.0564, wR2 = 0.1193
R indices (all data)	R1 = 0.1486, wR2 = 0.1543
Goodness-of-fit on F ²	0.930
Largest and mean shift/su	0.001 and 0.000
Largest diff. peak and hole	0.849 and -0.598 e Å ⁻³

All hydrogen atoms were inserted at calculated positions

Table 29 - Crystal data and structure refinement for [Ba(L5)(ClO₄)₂(H₂O)₂]

Identification code	reb1
Empirical formula	C ₂₀ H ₂₆ BaCl ₂ N ₆ O ₁₀
Formula weight	718.71
Temperature	150(2) K
Wavelength	0.71073 Å
Crystal system	Monoclinic
Space group	C2/c
Unit cell dimensions	a = 14.5247(8) Å α = 90°. b = 12.0634(6) Å β = 104.1570(10)°. c = 15.8698(8) Å γ = 90°.
Volume	2696.2(2) Å ³
Z	4
Density (calculated)	1.771 Mg/m ³
Absorption coefficient	1.735 mm ⁻¹
F(000)	1432
Crystal size	0.51 x 0.31 x 0.13 mm ³
Crystal description	colourless triangular prism
Theta range for data collection	2.22 to 31.92°.
Index ranges	-21 ≤ h ≤ 21, -17 ≤ k ≤ 17, -23 ≤ l ≤ 23
Reflections collected	16000
Independent reflections	4334 [R(int) = 0.0184]
Completeness to theta =	26.00° 100.0 %
Absorption correction	Semi-empirical from equivalents
Max. and min. transmission	0.8059 and 0.4715
Refinement method	Full-matrix least-squares on F ²
Data / restraints / parameters	4334 / 3 / 213
Goodness-of-fit on F ²	1.194
Final R indices [I > 2σ(I)]	R1 = 0.0227, wR2 = 0.0565
R indices (all data)	R1 = 0.0244, wR2 = 0.0572
Largest diff. peak and hole	0.693 and -0.634 e.Å ⁻³

All hydrogen atoms were inserted at calculated positions

Table 30 - Crystal data and structure refinement for [Mn₂(L6)(NCS)₄].2DMF

Identification code	LJ238 - vicksq
Chemical formula	C ₃₂ H ₄₀ Mn ₂ N ₁₂ O ₂ S ₄
Formula weight	862.88
Temperature	150(2) K
Radiation, wavelength	MoK α , 0.71073 Å
Crystal system, space group	triclinic, P $\bar{1}$
Unit cell parameters	a = 8.8404(18) Å α = 72.539(3)° b = 11.311(2) Å β = 83.003(3)° c = 12.051(2) Å γ = 67.261(3)°
Cell volume	1060.1(4) Å ³
Z	1
Calculated density	1.352 g/cm ³
Absorption coefficient μ	0.836 mm ⁻¹
F(000)	446
Crystal colour and size	Orange, 0.17 × 0.15 × 0.14 mm ³
Reflections for cell refinement	1806 (θ range 2.50 to 23.02°)
Data collection method	Bruker APEX 2 CCD diffractometer ω rotation with narrow frames
θ range for data collection	1.77 to 15.00°
Index ranges	h -6 to 6, k -8 to 8, l -8 to 8
Completeness to $\theta = 15.00^\circ$	100.0 %
Intensity decay	0%
Reflections collected	2360
Independent reflections	860 (Rint = 0.0240)
Reflections with F ₂ >2 σ	758
Absorption correction	semi-empirical from equivalents
Min. and max. transmission	0.8709 and 0.8919
Structure solution	direct methods
Refinement method	Full-matrix least-squares on F ²
Weighting parameters a, b	0.0405, 1.9282
Data / restraints / parameters	860 / 0 / 237
Final R indices [F ₂ >2 σ]	R1 = 0.0320, wR2 = 0.0783
R indices (all data)	R1 = 0.0367, wR2 = 0.0807
Goodness-of-fit on F ₂	1.120
Largest and mean shift/su	0.000 and 0.000
Largest diff. peak and hole	0.162 and -0.193 e Å ⁻³

The data were refined using the programme SQUEEZE¹²⁹ due to disordered solvent. SQUEEZE located 1 void, of 111 Å³ with 40 electrons, which was assigned as 1 molecule of DMF with the formula C₃H₇NO. There also remained one ordered DMF molecule within the cell

Table 31 - Crystal data and structure refinement for [Pb(L8)(NCS)₄]

Identification code	rd6f
Chemical formula	C ₃₀ H ₃₄ N ₁₀ O ₄ Pb ₂ S ₄
Formula weight	1141.29
Temperature	150(2) K
Radiation, wavelength	MoK α , 0.71073 Å
Crystal system, space group	orthorhombic, <i>pbcn</i>
Unit cell parameters	a = 10.0670(4) Å $\alpha = 90^\circ$ b = 13.7259(5) Å $\beta = 90^\circ$ c = 26.6928(10) Å $\gamma = 90^\circ$
Cell volume	3688.4(2) Å ³
Z	4
Calculated density	2.055 g/cm ³
Absorption coefficient μ	9.394 mm ⁻¹
F(000)	2176
Crystal colour and size	yellow, 0.22 × 0.17 × 0.14 mm ³
Reflections for cell refinement	8489 (θ range 2.51 to 29.77°)
Data collection method	Bruker APEX 2 CCD diffractometer ω rotation with narrow frames
θ range for data collection	2.51 to 31.78°
Index ranges	h -14 to 14, k -19 to 19, l -38 to 38
Completeness to $\theta = 31.78^\circ$	96.2 %
Intensity decay	0%
Reflections collected	42101
Independent reflections	6055 (Rint = 0.0497)
Reflections with F ₂ >2 σ	4443
Absorption correction	semi-empirical from equivalents
Min. and max. transmission	0.2317 and 0.3530
Structure solution	direct methods
Refinement method	Full-matrix least-squares on F ²
Weighting parameters a, b	0.0300, 1.8848
Data / restraints / parameters	6055 / 0 / 226
Final R indices [F ₂ >2 σ]	R1 = 0.0276, wR2 = 0.0581
R indices (all data)	R1 = 0.0483, wR2 = 0.0648
Goodness-of-fit on F ²	1.007
Largest and mean shift/su	0.004 and 0.000
Largest diff. peak and hole	1.436 and -0.992 e Å ⁻³

All hydrogen atoms were inserted at calculated positions

Table 32 - Crystal data and structure refinement for [Mn(L9)(OH₂)₂](ClO₄)₂

Identification code	ljp55
Chemical formula	C ₁₃ H ₂₃ Cl ₂ MnN ₃ O ₁₂
Formula weight	539.18
Temperature	150(2) K
Radiation, wavelength	MoK α , 0.71073 Å
Crystal system, space group	monoclinic, C2/c
Unit cell parameters	a = 15.9542(7) Å α = 90° b = 12.0846(6) Å β = 94.3920(10)° c = 10.9334(5) Å γ = 90°
Cell volume	2101.77(17) Å ³
Z	4
Calculated density	1.704 g/cm ³
Absorption coefficient μ	0.949 mm ⁻¹
F(000)	1108
Crystal colour and size	Yellow, 0.37 × 0.10 × 0.10 mm ³
Reflections for cell refinement	5682 (θ range 2.56 to 31.28°)
Data collection method	Bruker APEX 2 CCD diffractometer ω rotation with narrow frames
θ range for data collection	2.12 to 31.87°
Index ranges	h -23 to 23, k -17 to 17, l -15 to 16
Completeness to $\theta = 31.87^\circ$	94.3 %
Intensity decay	0%
Reflections collected	12616
Independent reflections	3406 (Rint = 0.0204)
Reflections with F ₂ >2 σ	3006
Absorption correction	semi-empirical from equivalents
Min. and max. transmission	0.7202 and 0.9110
Structure solution	direct methods
Refinement method	Full-matrix least-squares on F ²
Weighting parameters a, b	0.0519, 2.1627
Data / restraints / parameters	3406 / 0 / 155
Final R indices [F ₂ >2 σ]	R1 = 0.0343, wR2 = 0.0935
R indices (all data)	R1 = 0.0390, wR2 = 0.0966
Goodness-of-fit on F ²	1.059
Largest and mean shift/su	0.005 and 0.000
Largest diff. peak and hole	0.632 and -0.469 e Å ⁻³

All hydrogen atoms were inserted at calculated positions

Table 33 - Crystal data and structure refinement for [Mn(L9)(Cl)₂]

Identification code	MnLJP7 → <i>sad</i> C2/c
Chemical formula	C ₁₃ H ₁₇ Cl ₂ MnN ₃ O ₂
Formula weight	373.14
Temperature	150(2) K
Radiation, wavelength	MoK α , 0.71073 Å
Crystal system, space group	Monoclinic, I2/a
Unit cell parameters	a = 17.472 Å $\alpha = 90^\circ$ b = 9.811 Å $\beta = 121.98^\circ$ c = 11.383 Å $\gamma = 90^\circ$
Cell volume	1655.1 Å ³
Z	4
Calculated density	1.497 g/cm ³
Absorption coefficient μ	1.126 mm ⁻¹
F(000)	764
Crystal colour and size	translucent, 0.40 × 0.38 × 0.32 mm ³
Reflections for cell refinement	4965 (θ range 2.49 to 31.62°)
Data collection method	CCD area detector phi and omega scans
θ range for data collection	2.49 to 31.98°
Index ranges	h -25 to 25, k -14 to 14, l -16 to 16
Completeness to $\theta = 31.98^\circ$	93.7 %
Reflections collected	9800
Independent reflections	2687 (R _{int} = 0.0208)
Reflections with F ₂ >2 σ	2472
Absorption correction	semi-empirical from equivalents
Min. and max. transmission	0.6615 and 0.7145
Structure solution	direct methods
Refinement method	Full-matrix least-squares on F ²
Weighting parameters a, b	0.0382, 1.6419
Data / restraints / parameters	2687 / 0 / 98
Final R indices [F ₂ >2 σ]	R ₁ = 0.0273, wR ₂ = 0.0758
R indices (all data)	R ₁ = 0.0301, wR ₂ = 0.0773
Goodness-of-fit on F ²	1.076
Largest and mean shift/su	0.097 and 0.002
Largest diff. peak and hole	0.921 and -0.341 e Å ⁻³

All hydrogen atoms were inserted at calculated positions

Table 34 - Crystal data and structure refinement for [Mn(L10)(OH₂)₂](ClO₄)₂

Identification code	ljp71 → ljp71b
Chemical formula	C ₁₅ H ₂₅ Cl ₂ MnN ₃ O ₁₂
Formula weight	565.22
Temperature	150(2) K
Radiation, wavelength	MoK α , 0.71073 Å
Crystal system, space group	monoclinic, C2/c
Unit cell parameters	a = 15.926 Å $\alpha = 90^\circ$ b = 13.540 Å $\beta = 98.03^\circ$ c = 10.880 Å $\gamma = 90^\circ$
Cell volume	2323.2 Å ³
Z	4
Calculated density	1.616 g/cm ³
Absorption coefficient μ	0.863 mm ⁻¹
F(000)	1164
Crystal colour and size	Clear, 0.40 × 0.17 × 0.16 mm ³
Reflections for cell refinement	4810 (θ range 2.58 to 29.72°)
Data collection method	CCD area detector phi and omega scans
θ range for data collection	1.98 to 26.00°
Index ranges	h -19 to 19, k -16 to 16, l -13 to 13
Completeness to $\theta = 26.00^\circ$	100.0 %
Intensity decay	0%
Reflections collected	9876
Independent reflections	2289 (Rint = 0.0236)
Reflections with F ₂ >2 σ	2041
Absorption correction	semi-empirical from equivalents
Min. and max. transmission	0.7240 and 0.8743
Structure solution	direct methods
Refinement method	Full-matrix least-squares on F ²
Weighting parameters a, b	0.0510, 2.9962
Data / restraints / parameters	2289 / 0 / 156
Final R indices [F ₂ >2 σ]	R1 = 0.0320, wR2 = 0.0865
R indices (all data)	R1 = 0.0369, wR2 = 0.0902
Goodness-of-fit on F ²	1.057
Largest and mean shift/su	0.120 and 0.003
Largest diff. peak and hole	0.794 and -0.321 e Å ⁻³

All hydrogen atoms were inserted at calculated positions

Table 35 - Crystal data and structure refinement for [Mn(RedL10)(OH₂)₂].2Cl

Identification code	lj175 → lj175a
Chemical formula	C ₁₅ H ₂₉ Cl ₂ MnN ₃ O ₄
Formula weight	441.25
Temperature	150(2) K
Radiation, wavelength	MoK α , 0.71073 Å
Crystal system, space group	monoclinic, <i>P21/c</i>
Unit cell parameters	$a = 16.036(12)$ Å $\alpha = 90^\circ$ $b = 12.838(9)$ Å $\beta = 96.285(10)^\circ$ $c = 9.743(7)$ Å $\gamma = 90^\circ$
Cell volume	1994(2) Å ³
Z	4
Calculated density	1.470 g/cm ³
Absorption coefficient μ	0.954 mm ⁻¹
F(000)	924
Crystal colour and size	Clear, 0.17 × 0.12 × 0.05 mm ³
Reflections for cell refinement	741 (θ range 2.56 to 14.38°)
Data collection method	Bruker APEX 2 CCD diffractometer ω rotation with narrow frames
θ range for data collection	1.28 to 20.00°
Index ranges	$h -15$ to 15, $k -12$ to 12, $l -9$ to 9
Completeness to $\theta = 20.00^\circ$	99.9 %
Intensity decay	0%
Reflections collected	7899
Independent reflections	1868 ($R_{int} = 0.0805$)
Reflections with $F_2 > 2\sigma$	1400
Absorption correction	semi-empirical from equivalents
Min. and max. transmission	0.8546 and 0.9538
Structure solution	direct methods
Refinement method	Full-matrix least-squares on F ²
Weighting parameters a, b	0.0902, 3.1929
Data / restraints / parameters	1868 / 0 / 244
Final R indices [$F_2 > 2\sigma$]	$R_1 = 0.0599$, $wR_2 = 0.1464$
R indices (all data)	$R_1 = 0.0863$, $wR_2 = 0.1670$
Goodness-of-fit on F ²	1.101
Largest and mean shift/su	0.097 and 0.000
Largest diff. peak and hole	1.073 and -0.382 e Å ⁻³

All hydrogen atoms were inserted at calculated positions

Table 36 - Crystal data and structure refinement for [Mn(L10)(NCS)₂]

Identification code	LJP77 → vick
Chemical formula	C _{18.5} H _{24.5} MnN _{5.5} O _{2.5} S ₂
Formula weight	483.00
Temperature	150(2) K
Radiation, wavelength	MoK α , 0.71073 Å
Crystal system, space group	triclinic, P1
Unit cell parameters	a = 7.368(8) Å α = 86.952(12)° b = 10.462(11) Å β = 82.181(12)° c = 14.368(15) Å γ = 81.586(13)°
Cell volume	1085(2) Å ³
Z	2
Calculated density	1.479 g/cm ³
Absorption coefficient μ	0.830 mm ⁻¹
F(000)	502
Crystal colour and size	Orange, 0.59 × 0.18 × 0.16 mm ³
Reflections for cell refinement	1951 (θ range 0.00 to 0.00°)
Data collection method	Bruker APEX 2 CCD diffractometer ω rotation with narrow frames
θ range for data collection	1.43 to 26.00°
Index ranges	h -9 to 9, k -12 to 12, l -17 to 17
Completeness to $\theta = 26.00^\circ$	98.8 %
Intensity decay	0%
Reflections collected	8390
Independent reflections	4207 (Rint = 0.0581)
Reflections with F ₂ >2 σ	2772
Absorption correction	semi-empirical from equivalents
Structure solution	direct methods
Refinement method	Full-matrix least-squares on F ²
Weighting parameters a, b	0.0670, 0.0000
Data / restraints / parameters	4207 / 42 / 290
Final R indices [F ₂ >2 σ]	R1 = 0.0509, wR2 = 0.1141
R indices (all data)	R1 = 0.0886, wR2 = 0.1290
Goodness-of-fit on F ²	0.961
Largest and mean shift/su	0.000 and 0.000
Largest diff. peak and hole	0.477 and -0.641 e Å ⁻³

All hydrogen atoms were inserted at calculated positions

Table 37 - Crystal data and structure refinement for [Mn(L11)(Cl)₂]

Identification code	mnljp15
Chemical formula	C ₁₇ H ₂₉ Cl ₂ MnN ₅
Formula weight	429.29
Temperature	150(2) K
Radiation, wavelength	MoK α , 0.71073 Å
Crystal system, space group	monoclinic, C2/c
Unit cell parameters	a = 16.5279(15) Å α = 90° b = 17.1546(16) Å β = 112.8150(10)° c = 7.7470(7) Å γ = 90°
Cell volume	2024.7(3) Å ³
Z	4
Calculated density	1.408 g/cm ³
Absorption coefficient μ	0.926 mm ⁻¹
F(000)	900
Crystal colour and size	yellow, 0.46 × 0.09 × 0.04 mm ³
Reflections for cell refinement	2638 (θ range 2.37 to 29.25°)
Data collection method	Bruker APEX 2 CCD diffractometer ω rotation with narrow frames
θ range for data collection	1.79 to 30.52°
Index ranges	h -23 to 23, k -24 to 24, l -11 to 11
Completeness to $\theta = 30.52^\circ$	99.6 %
Intensity decay	0%
Reflections collected	11818
Independent reflections	3083 (Rint = 0.0427)
Reflections with F ₂ >2 σ	2212
Absorption correction	semi-empirical from equivalents
Min. and max. transmission	0.6753 and 0.9639
Structure solution	direct methods
Refinement method	Full-matrix least-squares on F ²
Weighting parameters a, b	0.0478, 0.3793
Data / restraints / parameters	3083 / 0 / 118
Final R indices [F ₂ >2 σ]	R1 = 0.0363, wR2 = 0.0843
R indices (all data)	R1 = 0.0612, wR2 = 0.0952
Goodness-of-fit on F ²	1.007
Largest and mean shift/su	0.000 and 0.000
Largest diff. peak and hole	0.434 and -0.464 e Å ⁻³

All hydrogen atoms were inserted at calculated positions

Table 38 - Crystal data and structure refinement for [Mn(L12)(OH₂)(Cl)]ClO₄

Identification code	Sora4 → vsad
Chemical formula	C ₁₁ H ₁₇ Cl ₂ MnN ₃ O ₇
Formula weight	429.12
Temperature	150(2) K
Radiation, wavelength	MoK α , 0.71073 Å
Crystal system, space group	triclinic, P $\bar{1}$
Unit cell parameters	a = 6.886(5) Å α = 98.427(9)° b = 10.010(7) Å β = 92.073(9)° c = 12.507(8) Å γ = 102.800(9)°
Cell volume	829.5(10) Å ³
Z	2
Calculated density	1.718 g/cm ³
Absorption coefficient μ	1.157 mm ⁻¹
F(000)	438
Crystal colour and size	Orange, 0.46 × 0.17 × 0.15 mm ³
Reflections for cell refinement	1108 (θ range 2.88 to 18.69°)
Data collection method	Bruker APEX 2 CCD diffractometer
θ range for data collection	1.65 to 18.75°
Index ranges	h -6 to 6, k -9 to 9, l -11 to 11
Completeness to $\theta = 18.75^\circ$	99.1 %
Reflections collected	2742
Independent reflections	1269 (Rint = 0.0373)
Reflections with F ₂ >2 σ	1027
Absorption correction	semi-empirical from equivalents
Min. and max. transmission	0.6181 and 0.8456
Structure solution	direct methods
Refinement method	Full-matrix least-squares on F ²
Weighting parameters a, b	0.0947, 0.8878
Data / restraints / parameters	1269 / 200 / 217
Final R indices [F ₂ >2 σ]	R1 = 0.0480, wR2 = 0.1284
R indices (all data)	R1 = 0.0623, wR2 = 0.1401
Goodness-of-fit on F ²	1.078
Largest and mean shift/su	0.000 and 0.000
Largest diff. peak and hole	0.579 and -0.597 e Å ⁻³

All hydrogen atoms were inserted at calculated positions

Table 39 - Crystal data and structure refinement for [Mn(L12)(OH₂)₂](ClO₄)₂

Identification code	sora3
Chemical formula	C ₁₁ H ₁₉ Cl ₂ MnN ₃ O ₁₂
Formula weight	511.13
Temperature	150(2) K
Radiation, wavelength	MoK α , 0.71073 Å
Crystal system, space group	Monoclinic, C2/c
Unit cell parameters	a = 15.9263(8) Å $\alpha = 90^\circ$ b = 12.1372(6) Å $\beta = 90.2870(10)^\circ$ c = 10.1134(5) Å $\gamma = 90^\circ$
Cell volume	1954.90(17) Å ³
Z	4
Calculated density	1.737 g/cm ³
Absorption coefficient μ	1.016 mm ⁻¹
F(000)	1044
Crystal colour and size	orange, 0.25 × 0.18 × 0.10 mm ³
Reflections for cell refinement	5333 (θ range 2.56 to 30.88°)
Data collection method	CCD area detector phi and omega scans
θ range for data collection	2.11 to 31.77°
Index ranges	h -23 to 22, k -17 to 17, l -15 to 14
Completeness to $\theta = 31.77^\circ$	94.0 %
Reflections collected	11581
Independent reflections	3130 (Rint = 0.0238)
Reflections with F ₂ >2 σ	2771
Absorption correction	semi-empirical from equivalents
Min. and max. transmission	0.7854 and 0.9053
Structure solution	direct methods
Refinement method	Full-matrix least-squares on F ²
Weighting parameters a, b	0.0560, 3.0764
Data / restraints / parameters	3130 / 0 / 138
Final R indices [F ₂ >2 σ]	R1 = 0.0407, wR2 = 0.1078
R indices (all data)	R1 = 0.0460, wR2 = 0.1117
Goodness-of-fit on F ²	1.038
Largest and mean shift/su	0.001 and 0.000
Largest diff. peak and hole	0.707 and -0.691 e Å ⁻³

All hydrogen atoms were inserted at calculated positions

Table 40 - Crystal data and structure refinement for [Mn(L13)(OH₂)₂](ClO₄)₂

Identification code	Sora2 → vsad
Chemical formula	C ₁₃ H ₂₁ Cl ₂ MnN ₃ O ₁₂
Formula weight	537.17
Temperature	150(2) K
Radiation, wavelength	MoK α , 0.71073 Å
Crystal system, space group	Monoclinic, <i>P</i> 21/ <i>c</i>
Unit cell parameters	$a = 9.857(7)$ Å $\alpha = 90^\circ$ $b = 16.864(11)$ Å $\beta = 106.267(9)^\circ$ $c = 13.626(9)$ Å $\gamma = 90^\circ$
Cell volume	2174(2) Å ³
Z	4
Calculated density	1.641 g/cm ³
Absorption coefficient μ	0.918 mm ⁻¹
F(000)	1100
Crystal colour and size	orange, 0.43 × 0.17 × 0.15 mm ³
Reflections for cell refinement	2792 (θ range 2.42 to 20.55°)
Data collection method	CCD area detector phi and omega scans
θ range for data collection	1.97 to 20.58°
Index ranges	$h -9$ to 9, $k -16$ to 16, $l -13$ to 13
Completeness to $\theta = 20.58^\circ$	99.8 %
Intensity decay	0%
Reflections collected	10364
Independent reflections	2203 ($R_{int} = 0.0615$)
Reflections with $F_2 > 2\sigma$	1647
Absorption correction	semi-empirical from equivalents
Min. and max. transmission	0.6937 and 0.8746
Structure solution	direct methods
Refinement method	Full-matrix least-squares on F ²
Weighting parameters a, b	0.1051, 8.0987
Data / restraints / parameters	2203 / 0 / 347
Final R indices [$F_2 > 2\sigma$]	$R_1 = 0.0677$, $wR_2 = 0.1767$
R indices (all data)	$R_1 = 0.0908$, $wR_2 = 0.1967$
Goodness-of-fit on F ²	1.046
Largest and mean shift/su	0.000 and 0.000
Largest diff. peak and hole	0.816 and -0.460 e Å ⁻³

All hydrogen atoms were inserted at calculated positions

One perchlorate ion remains uncoordinated to the macrocycle with disorder modelled with 50% occupancy and 50% occupancy over the two positions

Table 41 - Crystal data and structure refinement for [Mn(L13)(NCS)₂]

Identification code	lj330n	
Chemical formula	C ₁₅ H ₁₇ MnN ₅ O ₂ S ₂	
Formula weight	418.40	
Temperature	150(2) K	
Radiation, wavelength	MoK α , 0.71073 Å	
Crystal system, space group	monoclinic, <i>P</i> 21/ <i>c</i>	
Unit cell parameters	a = 16.5321(19) Å	$\alpha = 90^\circ$
	b = 27.395(3) Å	$\beta = 102.129(2)^\circ$
	c = 12.5836(14) Å	$\gamma = 90^\circ$
Cell volume	5571.9(11) Å ³	
Z	12	
Calculated density	1.496 g/cm ³	
Absorption coefficient μ	0.954 mm ⁻¹	
F(000)	2580	
Crystal colour and size	Orange, 0.21 × 0.08 × 0.07 mm ³	
Reflections for cell refinement	3481 (θ range 2.23 to 21.48°)	
Data collection method	Bruker APEX 2 CCD diffractometer ω rotation with narrow frames	
θ range for data collection	1.49 to 17.50°	
Index ranges	h -13 to 13, k -23 to 23, l -10 to 10	
Completeness to $\theta = 17.50^\circ$	99.9 %	
Intensity decay	0%	
Reflections collected	18855	
Independent reflections	3526 (R _{int} = 0.0636)	
Reflections with F ₂ >2 σ	2726	
Absorption correction	semi-empirical from equivalents	
Min. and max. transmission	0.8248 and 0.9362	
Structure solution	direct methods	
Refinement method	Full-matrix least-squares on F ²	
Weighting parameters a, b	0.0297, 13.4307	
Data / restraints / parameters	3526 / 0 / 676	
Final R indices [F ₂ >2 σ]	R ₁ = 0.0368, wR ₂ = 0.0794	
R indices (all data)	R ₁ = 0.0561, wR ₂ = 0.0903	
Goodness-of-fit on F ²	1.046	
Largest and mean shift/su	0.034 and 0.003	
Largest diff. peak and hole	0.555 and -0.207 e Å ⁻³	

All hydrogen atoms were inserted at calculated positions

Table 42 - Crystal data and structure refinement for [Mn(L15)(Cl)₂].MeOH

Identification code	lj330
Chemical formula	C ₁₄ H ₂₁ Cl ₂ MnN ₃ O ₃
Formula weight	405.18
Temperature	150(2) K
Radiation, wavelength	MoK α , 0.71073 Å
Crystal system, space group	triclinic, $P\bar{1}$
Unit cell parameters	a = 10.2254(12) Å α = 112.504(2)° b = 12.1091(15) Å β = 103.901(2)° c = 15.3886(19) Å γ = 92.031(2)°
Cell volume	1691.4(4) Å ³
Z	4
Calculated density	1.591 g/cm ³
Absorption coefficient μ	1.113 mm ⁻¹
F(000)	836
Crystal colour and size	Orange, 0.23 × 0.19 × 0.12 mm ³
Reflections for cell refinement	5406 (θ range 2.57 to 26.41°)
Data collection method	Bruker APEX 2 CCD diffractometer ω rotation with narrow frames
θ range for data collection	1.84 to 26.41°
Index ranges	h -12 to 12, k -15 to 15, l -19 to 19
Completeness to $\theta = 26.41^\circ$	99.2 %
Intensity decay	0%
Reflections collected	14887
Independent reflections	6892 (Rint = 0.0268)
Reflections with F ₂ >2 σ	5361
Absorption correction	semi-empirical from equivalents
Min. and max. transmission	0.7839 and 0.8780
Structure solution	direct methods
Refinement method	Full-matrix least-squares on F ²
Weighting parameters a, b	0.0598, 0.4790
Data / restraints / parameters	6892 / 0 / 417
Final R indices [F ₂ >2 σ]	R1 = 0.0394, wR2 = 0.1024
R indices (all data)	R1 = 0.0545, wR2 = 0.1109
Goodness-of-fit on F ²	1.049
Largest and mean shift/su	0.004 and 0.000
Largest diff. peak and hole	0.568 and -0.486 e Å ⁻³

All hydrogen atoms were inserted at calculated positions

Appendix 2

List of Publications and Poster Presentations.

Publications

- R. Dennett, L. James and V. McKee, *Acta Cryst*, 2007, **E63**, 1720. Title: Aqua[7,11:19,23-dinitrilo-1,5,13,17-tetraazacyclotetracos-1(24),5,7,9,12,17,20,22-octaene]bis(perchlorate- κ^2 O,O')barium(II)monohydrate
- L.James, G.E.M. Maguire, B.S.Martincigh, V.McKee and N. Ndlovu, *Acta Cryst*, 2007, **E63**, o153. Title: 3-Phenyl,-1,5-di-2-pyridylpentane-1,5-dione

Poster Presentations

December 2007 - RSC UK Macrocycles and Supramolecular Chemistry Group Meeting, University of Manchester Biological Activity of seven coordinate Mn(II)

March 2008 - RSC Dalton Discussion group, Warwick University – Title: Biological Activity of seven coordinate Mn(II)

April 2009 - British Crystallographic Association Spring meeting, Loughborough University. Title: The design and synthesis of seven-coordinate Mn(II) complexes.

June 2009 - Coordination Chemistry Discussion Group Meeting. Leeds University. Title: Effect of geometry on SOD and Catalase activity for seven-coordinate Mn(II)

Professional development courses

Nov 06 - Keeping Research Up-to-Date

Dec 06 - Teaching Skills

Dec 06 -Supervising Practical Activities

Jan 07 - Reading for Research

Jan 07 - Finding Research Information

Feb 07 - Word: Large Documents

Feb 07 - RefWorks - Advanced Techniques

May 07 - Report Writing

References

- 1 C. Harding, D. McDowell, J. Nelson, S. Raghunathan, C. Stevenson, M. G. B. Drew and P. C. Yates, *J. Chem. Soc. Dalton Trans.*, 1990, , 2521.
- 2 M. G. B. Drew, A. H. B. Othman, S. G. McFall, P. D. A. McIlroy and S. M. Nelson, *J. Chem. Soc. Dalton Trans.*, 1977, 1173-1180.
- 3 L. F. Lindoy, *The Chemistry of Macrocyclic Ligand Complexes*, Press Syndicate of the University of Cambridge, Cambridge, 1989.
- 4 E. C. Constable, *Coordination Chemistry of Macrocyclic compounds*, Oxford University Press, New York, 1999.
- 5 K. B. Yatsimirskii, *Theoretical and Experimental Chemistry*, 1980, **16**, 28.
- 6 F. P. Hinz and D. W. Margerum, *Inorg. Chem.*, 1974, **13**, 2941-2949.
- 7 C. E. Housecroft and A. G. Sharpe, *Inorganic Chemistry*, Pearson Education Limited, England, 2001.
- 8 D. F. Shriver and P. W. Atkins, *Inorganic Chemistry. 3rd edition*, Oxford university press, oxford, 2001.
- 9 G. Ferguson, R. McCrindle and M. Parvez, *Acta Cryst*, 1984, **C40**, 354-356.
- 10 V. Alexander, *Chem. Rev.*, 1995, **95**, 273-342.
- 11 N. E. Borisova, M. D. Reshetova and Y. A. Ustynyuk, *Chem. Rev.*, 2007, **107**, 46-79.
- 12 Z. L. Chu, W. Huang, L. Wang and S. H. Gou, *Polyhedron*, 2008, **27**, 1079-1092.
- 13 S. M. Nelson, *Pure & Appl. Chem.*, 1980, **52**, 2461-2476.
- 14 S. R. Collinson and D. E. Fenton, *Coord. Chem. Rev.*, 1996, **148**, 19-40.
- 15 P. Guerriero, S. Tarnburini and P. A. Vigato, *Coord. Chem. Rev.*, 1995, **139**, 17-243.
- 16 W. Radecka-Paryzek, V. Patroniak and J. Lisowski, *Coord. Chem. Rev.*, 2005, **249**, 2156-2175.
- 17 D. H. Cook, D. E. Fenton, M. G. B. Drew, A. Rodgers, M. McCann and S. M. Nelson, *J. Chem. Soc. Dalton Trans.*, 1979, , 414-419.
- 18 S. Brooker and V. McKee, *J. Chem. Soc. Dalton Trans.*, 1990, 2397-2401.
- 19 M. G. B. Drew, A. Rodgers, M. McCann and S. M. Nelson, *J. Chem. Soc. Chem. Commun.*, 1978, , 415.
- 20 J. W. Steed and J. L. Atwood, *Supramolecular Chemistry*, John Wiley and Sons, UK, 2009.
- 21 S. Brooker and V. McKee, *J. Chem. Soc. Dalton Trans.*, 1990, , 3183-3188.
- 22 M. G. B. Drew, J. Nelson, F. Esho, V. McKee and S. M. Nelson, *J. Chem. Soc. , Dalton Trans.*, 1982, , 1837-1843.
- 23 S. M. Nelson, C. V. Knox, M. McCann and M. G. B. Drew, *J. Chem. Soc., Dalton Trans.*, 1981, **8**, 1669-1677.
- 24 J. E. Metcalfe, MSc, university of Canterbury, 1993.
- 25 M. G. B. Drew, J. Nelson and S. M. Nelson, *J. Chem. Soc. Dalton Trans.*, 1981, 1678-1684.
- 26 H. Adams, N. A. Bailey, D. E. Fenton, P. D. Hempstead and G. P. Westwood, *J. Includ. Phenom. Mol*, 1991, **11**, 63-69.
- 27 Z. Pan, Q. Luo, C. Duan and M. Shen, *Polyhedron*, 2001, **20**, 2945-2950.

- 28 H. Adams, N. A. Bailey, P. Bertrand, S. R. Collinson, D. E. Fenton and S. J. Kitchen, *J. Chem. Soc., Dalton Trans.*, 1996, **6**, 1181-1183.
- 29 J. Chakraborty, B. Samanta, G. Pilet and S. Mitra, *Inorg. Chem. Commun.*, 2007, **10**, 40-44.
- 30 A. G. Blackman, *Polyhedron.*, 2005, **24**, 1-39.
- 31 N. J. Lundin, G. Hamilton and A. G. Blackman, *Polyhedron.*, 2004/1/1, **23**, 97-102.
- 32 A. E. Martell, R. D. Hancock and R. J. Motekaitis, *Coord. Chem. Rev.*, 1994, **133**, 39-65.
- 33 A. E. Martell and R. D. Hancock, in *Coordination Chemistry*, ed. G. B. Kauffman, American chemical society, Washington DC, 1994, p. 240-254.
- 34 H. Keypour, S. Salehzadeh and R. V. Parish, *Molecules*, 2002, **7**, 140-144.
- 35 J. Costes, A. Dupuis, G. Commenges, S. Lagrave and J. Laurent, *Inorg. Chim. Acta.*, 1999, **285**, 49-54.
- 36 C. Gedye, C. Harding, V. McKee, J. Nelson and J. Patterson, *J. Chem. Soc. Chem. Commun.*, 1992, 392.
- 37 M. G. B. Drew, C. J. Harding, V. McKee, G. G. Morgan and J. Nelson, *J. Chem. Soc., Chem. Commun.*, 1995, 1035-1038.
- 38 N. A. Law, M. Tyler Claude and V. L. Pecoraro, in *Advances in Inorganic Chemistry*, ed. A. G. Sykes, Academic Press, 1998, p. 305.
- 39 K. Aston, N. Rath, A. Naik, U. Slomczynska, O. F. Schall and D. P. Riley, *Inorg. Chem.*, 2001, **40**, 1779.
- 40 K. Kahlos, *The expression and possible role of manganese superoxide dismutase in malignant pleural mesothelioma*, University of Oulu, Oulu University Library, 1999. (web access)
- 41 A. Dees, A. Zahl, R. Puchta, N. J. R. V. E. Hommes, F. W. Heinemann and I. Ivanovic-Burmazovic, *Inorg. Chem.*, 2007, **46**, 2459-2470.
- 42 M. Devereux, M. McCann, D. O'Shea, M. O'Connor, E. Kiely, V. McKee, D. Naughton, A. Fisher, A. Kellett, M. Walsh, D. Egan and C. Deegan, *Bioinorg. Chem. Appl.*, 2006, 1.
- 43 D. W. Christianson, *Prog. Biophys. Molec. Biol.*, 1997, **67**, 217.
- 44 C. Muscoli, S. Cuzzocrea, D. P. Riley, J. L. Zweier, C. Thiemermann, Z. Wang and D. Salvemini, *Br. J. Pharmacol.*, 2003, **140**, 460.
- 45 M. Kaneko, T. Takahashi, Y. Niinuma and Y. Nomura, *Biol. Pharm. Bull.*, 2004, **27**, 1202-1206.
- 46 E. G. Tzortzaki, M. Tsoumakidou, D. Makris and N. M. Sifakas, *Clin. Chim. Acta.*, 2006, **364**, 124-138.
- 47 F. Fucassi, J. E. Lowe, K. D. Pavey, S. Shah, R. G. A. Faragher, M. H. L. Green, F. Paul, D. O'Hare and P. J. Cragg, *J. Inorg. Biochem.*, 2007, **101**, 225.
- 48 E. A. Lewis, H. H. Khodr, R. C. Hider, J. R. L. Smith and P. H. Walton, *J. Chem. Soc., Dalton Trans.*, 2004, 187-188.
- 49 J. C. Vites and M. M. Lynam, *Coord. Chem. Rev.*, 1995, **138**, 1-25.
- 50 J. W. Whittaker, *Biochem. Soc. Trans.*, 2003, **31**, 1318-1321.
- 51 Z. J. Guo and P. J. Sadler, *Angew. Chem. Int. Ed. Engl.*, 1999, **38**, 1513-1531.
- 52 I. Fridovich, *Annu. Rev. Biochem.*, 1995, **64**, 97-112.
- 53 M. J. Horsburgh, S. J. Wharton, M. Karavolos and S. J. Foster, *Trends Microbiol.*, 2002, **10**, 496-501.
- 54 R. Kachadourian, I. Batinic-Haberle and I. Fridovich, *Inorg. Chem.*, 1999, **38**, 391-396.

- 55 D. P. Riley, W. J. Rivers and R. H. Weiss, *Anal. Biochem.*, 1991, **196**, 344-349.
- 56 G. F. Liu, M. Filipovic, F. W. Heinemann and I. Ivanovic-Burmazovic, *Inorg. Chem.*, 2007, **46**, 8825-8835.
- 57 S. Cuzzocrea, D. P. Riley, A. P. Caputi and D. Salvemini, *Pharmacol Rev.*, 2001, **53**, 135-159.
- 58 P. Quint, R. Reutzel, R. Mikulski, R. McKenna and D. N. Silverman, *Free Rad. Biol. Med.*, 2006, **40**, 453-458.
- 59 I. A. Abreu and D. E. Cabelli, *Biochimica et Biophysica Acta (BBA) - Proteins & Proteomics.*, 2010, **1804**, 263-274.
- 60 M. Pick, J. Rabani, F. Yost and I. Fridovic, *J. Am. Chem. Soc.*, 1974, **96**, 7329.
- 61 C. Bull, E. C. Niederhoffer, T. Yoshida, J. A. Fee and F. Abanda, *J. Am. Chem. Soc.*, 1991, **113**, 4069.
- 62 B. Douglas, D. H. McDaniel and J. J. Alexander, *Concepts and models of inorganic chemistry*, John Wiley and sons, Inc, Canada, 1983.
- 63 D. P. Riley and R. H. Weiss, *J. Am. Chem. Soc.*, 1994, **116**, 387-388.
- 64 D. P. Riley and O. F. Schall, *Adv. Inorg. Chem*, 2007, **59**, 233-263.
- 65 M. R. Filipovic, A. C. W. Koh, S. Arbault, V. Niketic, A. Debus, U. Schleicher, C. Bogdan, M. Guille, F. Lemaitre, C. Amatore and I. Ivanovic-Burmazovic, *Angewandte Chemie-International Edition*, 2010, **49**, 4228-4232.
- 66 D. P. Riley, P. J. Lennon, W. L. Neumann and R. H. Weiss, *J. Am. Chem. Soc.*, 1997, **119**, 6522-6528.
- 67 A. Maroz, G. F. Kelso, R. A. J. Smith, D. C. Ware and R. F. Anderson, *J Phys Chem A.*, 2008, **112**, 4929-4935.
- 68 D. Salvemini, C. Muscoli, D. P. Riley and S. Cuzzocrea, *Pulm. Pharmacol. Ther.*, 2002, **15**, 439-447.
- 69 R. M. Roat-Malone, *Bioinorganic Chemistry - A Short Course*, John Wiley and sons, Inc., New Jersey, 2002.
- 70 M. Devereux, D. O'Shea, M. O'Connor, H. Grehan, G. Connor, M. McCann, G. Rosair, F. Lyng, A. Kellett, M. Walsh, D. Egan and B. Thati, *Polyhedron.*, 2007, **26**, 4073-4084.
- 71 J. M. McCord and I. Fridovic, *J. Biol. Chem.*, 1969, **244**, 6049-&.
- 72 S. Goldstein and G. Czapski, *Free Radic. Res. Commun.*, 1991, **12-3**, 5-10.
- 73 S. Goldstein and G. Czapski, in *Free Radicals: A practical approach*, ed. N. A. punchard and F. J. Kelly, Oxford University Press, 1996, p. 241.
- 74 N. Farrell, in , ed. nonymous , RSC, Great Britain, 1999, p. 79.
- 75 D. P. Riley, *Chem. Rev.*, 1999, **99**, 2573-2587.
- 76 Y. Kono and I. Fridovich, *J. Biol. Chem.*, 1983, **258**, 6015-6019.
- 77 V. V. Barynin, M. M. Whittaker, S. V. Antonyuk, V. S. Lamzin, P. M. Harrison, P. J. Artymiuk and J. W. Whittaker, *Structure*, 2001, **9**, 725-738.
- 78 J. W. De Boer, W. R. Browne, B. L. Feringa and R. Hage, *C. R. Chimie*, 2007, **10**, 341.
- 79 A. J. Wu, J. E. Penner-Hahn and V. L. Pecoraro, *Chem. Rev.*, 2004, **104**, 903-938.
- 80 S. McCann, M. McCann, M. T. Casey, M. Jackman, M. Devereux and V. McKee, *Inorg. Chim. Acta*, 1998, **279**, 24-29.
- 81 X. J. Jiang, H. Liu, B. Zheng and J. Y. Zhang, *Dalton Transactions*, 2009, 8714-8723.

- 82 V. L. Pecoraro, M. J. Baldwin and A. Gelasco, *Chem. Rev.*, 1994, **94**, 807-826.
- 83 M. Devereux, M. McCann, M. T. Casey, M. Curran, G. Ferguson, C. Cardin, M. Convery and V. Quillet, *J. Chem. Soc., Dalton Trans.*, 1995, **5**, 771-776.
- 84 J. Kaizer, T. Csay, P. Kovari, G. Speier and L. Parkanyi, *J. Mol. Catal A-Chem*, 2008, **280**, 203-209.
- 85 M. Devereux, M. Curran, M. McCann, M. T. Casey and V. McKee, *Polyhedron*, 1996, **15**, 2029-2033.
- 86 Y. G. Abashkin and S. K. Burt, *Inorg. Chem.*, 2005, **44**, 1425-1432.
- 87 H. B. Dunford, *Coord. Chem. Rev.*, 2002, **233-234**, 311-318.
- 88 A. E. M. Boelrijk and G. C. Dismukes, *Inorg. Chem.*, 2000, **39**, 3020-3028.
- 89 M. M. Whittaker, V. V. Barynin, S. V. Antonyuk and J. Whittaker, *Biochemistry (N. Y.)*, 1999, **38**, 9126-9136.
- 90 Y. Naruta, M. Sasayama and T. Sasaki, *Angewandte Chemie-International Edition in English*, 1994, **33**, 1839-1841.
- 91 H. Adams, N. A. Bailey, D. E. Fenton, R. J. Good, R. Moody and C. O. Rodriguez-Barbarin, *J. Chem. Soc., Dalton Trans.*, 1987, , 207.
- 92 R. Dennett, L. James and V. McKee, *Acta Cryst*, -2007, **-E63**, -1720.
- 93 S. Brooker and V. McKee, *J. Chem. Soc. Chem. Commun.*, 1989, 619-620.
- 94 S. Brooker, V. McKee and T. Metcalfe, *Inorg. Chim. Acta.*, 1996, **246**, 171-179.
- 95 G. B. Deacon and R. J. Phillips, *Coord. Chem. Rev.*, 1980, **33**, 227-250.
- 96 X. M. Chen and T. C. W. Mak, *Inorg. Chim. Acta.*, 1991, **189**, 3-5.
- 97 T. N. Sorrell, *Organic chemistry second edition*, University Science Books, California, USA, 2006.
- 98 A. I. Bruker, *APEX2 software for CCD diffractometers*, Madison, USA, 1998.
- 99 S. Brooker, V. McKee, W. B. Shepard and L. K. Pannell, *J. Chem. Soc. Dalton Trans.*, 1987, 2555-2562.
- 100 S. A. Brooker, Ph.D., University of Canterbury, 1989.
- 101 S. Raghunathan, C. Stevenson, J. Nelson and V. McKee, *Journal of the Chemical Society-Chemical Communications*, 1989, 5-7.
- 102 S. Brooker and V. McKee, *Acta Cryst.*, 1993, **C49**, 441-445.
- 103 A. M. Bond, *Broadening Electrochemical Horizons - Principles and illustration of voltammetric and related techniques*, Oxford Science Publications, Oxford UK, 2002.
- 104 A. M. Bond, E. A. McLennan, R. S. Stojanovic and F. G. Thomas, *Anal. Chem.*, 1987, **59**, 2853-2860.
- 105 D. F. Shriver, P. W. Atkins and C. H. Langford, *Inorganic Chemistry - Second edition*, Oxford University Press, Walton Street, Oxford, UK, 1994.
- 106 K. M. Rosso and M. Dupuis, *Theoretical Chemistry Accounts*, 2006, **116**, 124-136.
- 107 S. Durot, C. Policar, F. Cisnetti, F. Lambert, J. P. Renault, G. Pelosi, G. Blain, H. Korri-Youssoufi and J. P. Mahy, *Eur. J. Inorg. Chem.*, 2005, **17**, 3513-3523.
- 108 F. Cisnetti, A. S. Lefevre, R. Guillot, F. Lambert, G. Blain, E. Anxolabehere-Mallart and C. Policar, *Eur. J. Inorg. Chem.*, 2007, **28**, 4472-4480.
- 109 I. Kani, C. Darak, O. Sahin and O. Buyukgungor, *Polyhedron.*, 2008, **27**, 1238-1247.

- 110 D. Salvemini, Z. Q. Wang, J. L. Zweier, A. Samouilov, H. Macarthur, T. P. Misko, M. G. Currie, S. Cuzzocrea, J. A. Sikorski and D. P. Riley, *Science.*, 1999, **286**, 304-306.
- 111 V. Daier, D. Moreno, C. Duhayon, J. P. Tuchagues and S. Signorella, *Eur. J. Inorg. Chem.*, 2010, **6**, 965.
- 112 D. Klugroth, Fridovic.i and J. Rabani, *J. Am. Chem. Soc.*, 1973, **95**, 2786-2790.
- 113 I. B. Afanas'ev, *Superoxide ion: Chemistry and biological implications*, CRC press, USA, 1989.
- 114 R. H. Liu, S. Y. Fu, H. Y. Zhan and L. A. Lucia, *Ind Eng Chem Res.*, 2009, **48**, 9331-9334.
- 115 L. Dubois, J. Pecaut, M. F. Charlot, C. Baffert, M. N. Collomb, A. Deronzier and J. M. Latour, *Chem-Eur. J.*, 2008, **14**, 3013-3025.
- 116 R. H. Garrett and C. M. Grisham, *Biochemistry*, Mary Finch, USA, 2010.
- 117 M. Shank, V. Barynin and G. C. Dismukes, *Biochemistry (N. Y.)*, 1994, **33**, 15433-15436.
- 118 J. Ricard and A. Cornishbowden, *Eur. J. Biochem.*, 1987, **166**, 255-272.
- 119 C. Ciaccio, A. Coletta, G. De Saneti, S. Marini and M. Coletta, *IUBMB Life*, 2008, **60**, 112-123.
- 120 S. A. Kuby, *A study of enzymes*, CRC press, Florida, 1991.
- 121 M. Matés, *Toxicology*, 2000, **153**, 83-104
- 122 C. J. Weydert, T. A. Waugh, J. M. Ritchie, K. S. Iyer, J. L. Smith, L. Li, D. R. Spitz and L. W. Oberley, *Free Radic. Biol. Med.*, 2006, **41**, 226-237.
- 123 C. J. Darby Weydert, B. B. Smith, L. Xu, K. C. Kregel, J. M. Ritchie, C. S. Davis and L. W. Oberley, *Free Radic. Biol. Med.*, 2003, **34**, 316-29.
- 124 E. W. N. Lam, R. Zwacka, J. F. Engelhardt, B. L. Davidson, F. E. Domann, T. Yan and L. W. Oberley, *Cancer Res.*, 1997, **57**, 5550-5556.
- 125 A. I. Bruker, *SHELXTL user manual*, Madison, USA, 2001.
- 126 D. A. Fletcher, R. F. McMeeking and D. Parkin, *Chem. Inf. Comput. Sci.*, 1996, **36**, 746.
- 127 J. McCrea, V. McKee, T. Metcalfe, S. S. Tandon and J. Wikaira, *Inorg. Chim. Acta.*, 2000, **297**, 220-230.
- 128 J. Nelson, B. P. Murphy, M. G. B. Drew, P. C. Yates and S. M. Nelson, *J. Chem. Soc. Dalton Trans.*, 1988, **4**, 1001-1010.
- 129 P. Sluis and A. L. Spek, *Acta Cryst.*, 1990, **A46**, 194.